Manipulating elastic wave propagation in non-linear flexible materials via external stimuli

Pavel I. Galich

Manipulating elastic wave propagation in non-linear flexible materials via external stimuli

Research thesis

In Partial Fulfillment of the Requirements for the Degree of Doctor of Philosophy

Pavel I. Galich

Submitted to the Senate of the Technion - Israel Institute of Technology

Elul 5778, August 2018, Haifa

The Research Thesis Was Done
Under the Supervision of Stephan Rudykh
in the Faculty of Aerospace Engineering

Acknowledgements

The generous financial help of Technion – Israel Institute of Technology and The Irwin and Joan Jacobs Scholarship is gratefully acknowledged.

I am deeply thankful to Stephan Rudykh for his professional guidance, for sharing his knowledge and experience with me, and for his dedicated support through my Doctorate studies.

I thank Viacheslav (Slava) Slesarenko, Jian Li and Artemii Goshkoderia for useful discussions of my PhD research.

I wish to express my gratitude to the Israel Science Foundation for the financial support of my research.

Contents

Abstract

Understanding of wave propagation phenomena in solids is pivotal for numerous engineering applications in healthcare, petroleum, military, and aerospace industries. Among them nondestructive material testing, vibration protection of sensitive electronics, unwanted noise mitigation, earthquake forecasting, and medical ultrasound diagnostics. The ability of flexible materials to sustain large deformations opens rich prospects for manipulating elastic wave characteristics by deformation. Moreover, elastic waves can be tuned through designing micro- or macrostructures, which can be further actively controlled by external stimuli, such as mechanical loading, electric or magnetic fields. Understanding of how large deformations affect relatively simple isotropic and more complex anisotropic materials is essential for this task. Therefore, in my thesis, I investigated the acoustic properties of the relatively simple initially isotropic non-linear materials and then proceeded with the periodic layered and fiber composites made of these materials. Firstly, I studied the influence of the deformation induced stiffening (intrinsic feature of most soft materials) on the propagation of small-amplitude elastic plane waves. Secondly, I showed that electroelastic isotropic materials (i.e. dielectric elastomers) can be utilized to achieve acoustic functionalities such as decoupling of pressure and shear waves by application of an electric field. Thirdly, I analyzed wave propagation in non-linear elastic and electroelastic laminates. In particular, I derived the long wave estimates of the phase and group velocities for the waves propagating in the laminates subject to external mechanical or electrical stimuli. Moreover, I found the material compositions and loading conditions producing wide complete

band gaps (frequency ranges where neither pressure nor shear waves can propagate) at desired low frequency ranges. Finally, I investigated the anisotropy of elastic wave propagation in finitely deformed fiber composites (FCs). Specifically, by employing rigorous analytical methods of non-linear mechanics, I derived long wave estimates for phase and group velocities of shear waves propagating in non-linear FCs. Next, by utilizing Bloch-Floquet approach in a finite element code, I calculated dispersion relations for shear waves propagating along the fibers in FCs with square arrays of fibers.

List of abbreviations

FC – Fiber composite

P-wave – Pressure (longitudinal) wave

S-wave – Shear (transversal) wave

BG – Band gap

SBG – Shear wave band gap

PBG – Pressure wave band gap

DE – Dielectric elastomer

RVE – Representative Volume Element

Chapter 1

Preamble

Lightweight composite materials with excellent mechanical properties are of immense importance for aerospace engineering [8]; however, in aerospace structures, undesirable vibrations and noise propagate from the source, e.g., an engine, to other parts; this phenomenon requires control, reduction, or even elimination. Therefore, new lightweight materials allowing tunable noise and vibration reduction need to be developed, while maintaining mechanical properties such as stiffness, toughness, and damage tolerance. Moreover, better understanding of wave propagation phenomena in flexible materials can benefit nondestructive material testing in composite aerospace structures. Motivated by these requirements for aerospace structural materials, in my PhD research I explored the general field of elastic wave propagation in non-linear isotropic elastic [21] and electroelastic [22] materials and then in layered [19, 23] and fibrous [25] composites made of these materials.

1.1 Wave propagation in non-linear elastic materials

1.1.1 Finitely deformed isotropic materials

Small amplitude elastic wave propagation in finitely deformed homogeneous isotropic materials was pioneered by Biot [5]. Boulanger and Hayes [6] considered wave propagation in finitely deformed incompressible Mooney-Rivlin materials and derived explicit relations for wave velocities. Boulanger et al. [7] extended this work to a broader class of finitely deformed compressible Hadamard materials and first obtained the explicit expressions for the phase velocities of longitudinal (pressure) and transversal (shear) waves. Recently, Destrade and Ogden [15] have revised and generalized the problem of an infinitesimal wave propagation in the finitely deformed hyperelastic materials by application of the invariant theory. More recently, I have investigated infinitesimal (linear) wave propagation in finitely deformed compressible Gent materials, exhibiting pronounced stiffening effects, and obtained closed form expressions for the phase velocities of longitudinal and transversal waves [21]. It is worth mentioning that deformation can be utilized not only for the changing of phase and group velocities of elastic waves but also for decoupling of P- and S-waves in these relatively simple originally isotropic non-linear materials [9, 20].

1.1.2 Finitely deformed laminates

Small amplitude (linear) elastic wave propagation in linear bi-laminates made of isotropic materials was pioneered by by Rytov [43]. He derived explicit disper-

sion relations for steady-state P- and S-waves propagating perpendicular and parallel to the layers. Recently, problem of wave propagation in periodic laminates has been revived in a framework of elastic metamaterials [53, 59]. Hence, I extended classical result of Rytov [43] for non-linear bi-laminates made of hyperelastic isotropic materials, namely neo-Hookean and Gent materials [19]. This allowed me to investigate influence of finite deformations on S- and P-wave band gaps in these laminates. In particular, I found that S-wave band gaps (SBGs) in laminates with compressible neo-Hookean layers are not influenced by deformation, because deformation-induced changes in geometry and effective material properties fully compensate each other. Thus, I corrected a misconception that had prevailed in the literature [47], namely that SBGs could be tuned by application of elastic deformation in compressible neo-Hookean laminates – I rigorously showed, through exact analytical solution, that they could not [19]. However, contraction or extension of the laminate with Gent layers (exhibiting strong stiffening effects) widens and shifts up SBGs towards higher frequencies due to the stronger effect of deformation-induced change in the layer properties as compared to the change in the layer thicknesses. Moreover, I derived closed-form expressions for the phase and group velocities of long S-waves propagating in any direction in the finitely deformed laminates with incompressible neo-Hookean layers. For the case of wave propagation perpendicular to the layers, I also obtained long wave estimates for the velocities of P- and S-waves propagating in laminates with compressible neo-Hookean or Gent layers [19]. More recently, Li et al. [32] studied oblique S-wave propagation in finitely deformed laminates and showed that SBGs closes immediately when the wave inclines from the normal (i.e., perpendicular to the

layers) direction of propagation. Additionally, Li et al. [33] investigated influence of compressibility on BGs in buckled bi-laminates. Slesarenko et al. [50] found that shear waves of lowest frequencies in marginally stable bi-laminates (i.e., deformed close to the instability point) have negative (anti-parallel to the phase velocity) group velocities for certain wavenumbers, which foreshadow onset of elastic instability. Very recently, Demcenko et al. [13, 14] extended my analysis [19] and investigated propagation of finite amplitude elastic waves in hyperelastic laminates.

1.1.3 Finitely deformed fiber-reinforced composites

By employing the nonlinear elastic theory [57] and a phenomenological approach, Scott and Hayes [46] considered small amplitude plane waves superimposed on a homogeneous deformation in the so-called idealized fiber-reinforced materials (with an incompressible matrix and inextensible fibers). The infinitesimal elastic wave propagation in nearly incompressible and nearly inextensible fiber-reinforced materials with unidirectional fibers was examined by Rogerson and Scott [38]. Later, Ogden and Singh [37] revisited the problem of infinitesimal wave propagation in an incompressible transversely isotropic elastic solid in the presence of an initial stress. In particular, they exploited the phenomenological theory of invariants and presented a more general and transparent formulation of the theory for small amplitude waves propagating in a deformed transversely isotropic hyperelastic solid.

In my work [25], I employed a *micromechanics* based approach [11] accounting

for the phase properties and their spatial distribution to analyze the wave propagation in finitely deformed 3D FCs, as opposite to previous works that employed phenomenological approach [46, 44, 45, 38, 37], or numerically modeled the composites in 2D settings [3], or did not consider finite deformations [1, 30]. I derived explicit closed-form expressions for phase and group velocities of the S-waves for any direction of propagation in finitely deformed 3D FCs with neo-Hookean phases. These explicit expressions provide essential information on the S-wave propagation in the long wave limit. To account for the interaction of the S-waves with the composite microstructure, I implemented the Bloch-Floquet analysis [1, 3] in the finite element code (COMSOL), allowing me to analyze small amplitude motions superimposed on finite macroscopically applied homogeneous deformation. Moreover, I compared the micromechanics-based homogenization approach and the numerical Bloch-Floquet analysis and showed the equivalence of these distinct approaches for the large wavelengths [25]. More recently, I studied influence of fiber arrangement on shear waves and elastic instabilities in finitely deformed FCs [24]. In particular, I showed that elastic instabilities and S-waves propagating along the fibers in uniaxially deformed FCs can be tuned through the choice of the periodicity (or periodic unit cell aspect ratio b/a) of FCs. It worth mentioning that my numerical results on elastic instabilities in FCs with rectangular arrays of fibers were validated by Li et al. [31] on 3D-printed FCs.

1.2 Wave propagation in non-linear electroelastic materials

Another part of my PhD research deals with problems of elastic wave propagation in dielectric elastomers (DEs) materials that can significantly deform when subject to an electric field (Pelrine et al., 1998). Investigation of this problem opens new possibilities for improving small length-scale devices, e.g., micro-electromechanical systems in aerospace structures, where electric field is the preferred control parameter. Remarkably, even isotropic DEs allow to tune elastic wave propagation by an electric field, e.g. one can decouple P- and S-waves propagating in DE via application of a specific electric field [22]. However, for achieving more sophisticated wave phenomena, such as band gaps, structured materials must be introduced [61, 28].

Following the work of Toupin [56], the theory of nonlinear electroelasticity for homogeneous isotropic hyperelastic media has been revised recently by Dorfmann and Ogden [16], McMeeking and Landis [36], and Suo et al. [54]. More recently, Cohen et al. [10] proposed a model based on considerations of polymer networks under electromechanical loadings. Motivated by potential enhancement of electromechanical coupling, which is typically rather weak in DEs, microstructured DEs have been explored [12, 55, 42] showing significant potential of this approach. However, one needs to account for electromechanical instabilities [40, 4, 27] when dealing with composite DEs.

The analysis of small amplitude wave propagation in finitely deformed nonlinear electroelastic materials in the presence of an electric field in the frame of the

quasi-electrostatic approximation was presented by Dorfmann and Ogden [17]. This paper has been followed by a number of works on elastic wave propagation in finitely deformed homogenous and composite DEs [26, 48, 22, 60]. Note that layered DEs are of specific importance since they may be realized through various layer-by-layer material fabrication techniques which already allow manufacturing of deformable layered materials [39, 29].

During my PhD I revisited the problem of S-wave propagation perpendicularly to the layers in the laminates made of ideal (neo-Hookean) dielectric elastomers and corrected a misconception that had prevailed in the literature [48, 49], namely that SBGs could be shifted via application of an electric field I rigorously demonstrated, through exact analytical solution, that they could not [23]. My results were recently confirmed by Jandron and Henann [28].

Chapter 2

Research methods

2.1 Non-linear elasticity

Consider a continuum body and identify each point in the reference configuration with vector $\mathbf{X}$. In the current configuration, the new location of the corresponding points is defined by vector $\mathbf{x} = \mathbf{x}(\mathbf{X}, t)$. Then, the deformation gradient is $\mathbf{F} = \partial\mathbf{x}/\partial\mathbf{X}$, and $J \equiv \det \mathbf{F} > 0$. For a hyperelastic compressible material with a strain energy function $\psi(\mathbf{F})$, the first Piola-Kirchhoff stress tensor can be calculated as follows

$$\mathbf{P} = \frac{\partial \psi(\mathbf{F})}{\partial \mathbf{F}}. \tag{2.1}$$

For an incompressible material, $J = 1$ and Eq. (2.1) modifies as

$$\mathbf{P} = \frac{\partial \psi(\mathbf{F})}{\partial \mathbf{F}} - p\mathbf{F}^{-T}, \tag{2.2}$$

where p represents an unknown Lagrange multiplier. The corresponding Cauchy stress tensor is related to the first Piola-Kirchhoff stress tensor via the relation $\sigma = J^{-1}\mathbf{P} \cdot \mathbf{F}^T$.

In the absence of body forces the equations of motion can be written in the undeformed configuration as

$$\mathrm{Div}\mathbf{P} = \rho_0 \frac{D^2\boldsymbol{\chi}}{Dt^2}, \tag{2.3}$$

where ρ_0 is the initial density of the material and the operator $D^2(\bullet)/Dt^2$ represents the material time derivative. If the deformation is applied quasi-statically, the right hand part of (2.3) can be assumed to be zero, and the equilibrium equation reads as

$$\mathrm{Div}\mathbf{P} = \mathbf{0}. \tag{2.4}$$

Consider next infinitesimal motions superimposed on the equilibrium state. The equations of the incremental motions are

$$\mathrm{Div}\dot{\mathbf{P}} = \rho_0 \frac{D^2\mathbf{u}}{Dt^2}, \tag{2.5}$$

where $\dot{\mathbf{P}}$ is the incremental change in the first Piola-Kirchhoff stress tensor and $\mathbf{u}$ is the incremental displacement.

The linearized constitutive law can be written as

$$\dot{P}_{ij} = \mathcal{A}_{0ijkl}\dot{F}_{kl}, \tag{2.6}$$

where $\dot{\mathbf{F}} = \mathrm{Grad}\,\mathbf{u}$ is the incremental change in the deformation gradient, and the tensor of elastic moduli is defined as $\mathcal{A}_{0i\alpha k\beta} = \partial^2\psi/\partial F_{i\alpha}\partial F_{k\beta}$. Under substitution of (2.6) into (2.5) the incremental motion equation takes the form

$$\mathcal{A}_{0ijkl}u_{k,lj} = \rho_0 \frac{D^2u_i}{Dt^2}. \tag{2.7}$$

2.1.1 Small amplitude motions superimposed on large deformations

To analyze small amplitude motions superimposed on a finite deformation, we present equation of motion (2.7) in the updated Lagrangian formulation

$$\mathcal{A}_{ijkl} u_{k,lj} = \rho \frac{\partial^2 u_i}{\partial t^2}, \tag{2.8}$$

where $\mathcal{A}_{iqkp} = J^{-1} \mathcal{A}_{0ijkl} F_{pl} F_{qj}$ is the updated tensor of elastic moduli and $\rho = J^{-1} \rho_0$ is the density of the deformed material.

We seek a solution for equation (2.8) in the form of plane waves with constant polarization

$$\mathbf{u} = \mathbf{g} h(\mathbf{n} \cdot \mathbf{x} - ct), \tag{2.9}$$

where h is a twice continuously differentiable function and unit vector $\mathbf{g}$ denotes the polarization; the unit vector $\mathbf{n}$ defines the direction of wave propagation, and c is the phase velocity of the wave.

Substituting (2.9) into (2.8), we obtain

$$\mathbf{Q}(\mathbf{n}) \cdot \mathbf{g} = \rho c^2 \mathbf{g}, \tag{2.10}$$

where

$$Q_{ik} = \mathcal{A}_{ijkl} n_j n_l \tag{2.11}$$

is the acoustic tensor defining the condition of propagation of the infinitesimal plane waves. Thus, for a real wave to exist acoustic tensor has to be positively defined for any non-zero vectors $\mathbf{n}$ and $\mathbf{g}$

$$\mathbf{g} \cdot \mathbf{Q}(\mathbf{n}) \cdot \mathbf{g} = \mathcal{A}_{ijkl} n_j n_l g_i g_k = \rho c^2 > 0. \tag{2.12}$$

Recall that the inequality

$$\mathcal{A}_{ijkl} n_j n_l g_i g_k > 0 \tag{2.13}$$

is called the strong ellipticity condition [57]. This inequality also arises in the stability theory of elastic and elasto-plastic solids. Thus, if the inequality (2.13) does not hold true in any point of the body for the applied boundary conditions, the body is unstable in this state. In a similar vein, the body becomes unstable if the velocity of at least one wave with any polarization and any propagation direction in the body becomes zero. It is worth noting that loss of strong ellipticity analysis is widely used for finding macroscopic instabilities in homogenizable composites [34, 35, 2, 41].

For incompressible materials Eq. (2.8) modifies as

$$\mathcal{A}_{ijkl} \mathbf{u}_{k,lj} + \dot{p}_{,i} = \rho \frac{\partial^2 v_i}{\partial t^2}, \tag{2.14}$$

together with the incompressibility constraint

$$u_{i,i} = 0. \tag{2.15}$$

Substitution of (2.9) and $\dot{p} = p_0 h'(\mathbf{n} \cdot \mathbf{x} - ct)$, where p_0 is a scalar, into (2.14) and (2.15) yields

$$\hat{\mathbf{Q}}(\mathbf{n}) \cdot \mathbf{g} = \rho c^2 \mathbf{g} \quad \text{and} \quad \mathbf{g} \cdot \mathbf{n} = 0, \tag{2.16}$$

where $\hat{\mathbf{Q}} = \hat{\mathbf{I}} \cdot \mathbf{Q} \cdot \hat{\mathbf{I}}$ and $\hat{\mathbf{I}} = \mathbf{I} - \mathbf{n} \otimes \mathbf{n}$ is the projection onto the plane normal to $\mathbf{n}$. Thus, in the incompressible case, the strong ellipticity condition (2.13) subject to the restriction $\mathbf{g} \cdot \mathbf{n} = 0$. The readers, who are not familiar with non-linear elasticity, are referred to the book by Volokh [58] for comprehensible discussion and derivations of the material presented above.

2.2 Bloch-Floquet approach for periodic composites

To analyze elastic wave propagation in finitely deformed periodic composites, I superimpose small amplitude (linear) motions on a finitely deformed state [3]. Recall that in a periodic structure plane waves can be described by the Bloch function [30]. To perform the analysis, I utilize the finite element method with the help of COMSOL.

2.2.1 Static finite deformation

Firstly, the solution for the finitely deformed periodic composite is obtained. The macroscopic deformation gradient $\bar{\mathbf{F}} = 1/\Omega \int_\Omega \mathbf{F} dV$ is applied through periodic boundary conditions imposed on the displacements of the representative volume element (RVE) faces such that

$$\mathbf{U}_B - \mathbf{U}_A = (\bar{\mathbf{F}} - \mathbf{I}) \cdot (\mathbf{X}_B - \mathbf{X}_A), \tag{2.17}$$

where A and B are the nodes on the opposite faces of the RVE boundary and $\mathbf{U} = \mathbf{x}(\mathbf{X}) - \mathbf{X}$ is the displacement field; RVE occupies a domain Ω in the undeformed configuration. The macroscopic first Piola-Kirchhoff stress tensor and the corresponding Cauchy stress tensor are calculated as $\bar{\mathbf{P}} = 1/\Omega \int_\Omega \mathbf{P} dV$ and $\bar{\sigma} = 1/\Omega \int_\Omega \sigma dV$, respectively. Rigid body motions are prevented by fixing the displacements of a single node, i.e. $\mathbf{U}_A = \mathbf{0}$.

2.2.2 Small-amplitude motions superimposed on a deformed state

Secondly, the Bloch-Floquet periodicity conditions are superimposed on the deformed state. The corresponding incremental change in the displacement and the first Piola-Kirchhoff stress tensor are

$$\mathbf{u}\left(\mathbf{X},t\right)=\mathcal{U}\left(\mathbf{X}\right)e^{-i\omega t}\quad\text{and}\quad\dot{\mathbf{P}}\left(\mathbf{X},t\right)=\mathcal{P}\left(\mathbf{X}\right)e^{-i\omega t},\tag{2.18}$$

where ω is the angular frequency. Substitution of (2.18) in (2.5) yields

$$\mathrm{Div}\mathcal{P}+\rho_0\omega^2\mathcal{U}=\mathbf{0}.\tag{2.19}$$

Next, according to the Floquet theorem

$$\mathcal{U}\left(\mathbf{X}+\mathbf{R}\right)=\mathcal{U}\left(\mathbf{X}\right)e^{-i\mathbf{K}\cdot\mathbf{R}}\quad\text{and}\quad\mathcal{P}\left(\mathbf{X}+\mathbf{R}\right)=\mathcal{P}\left(\mathbf{X}\right)e^{-i\mathbf{K}\cdot\mathbf{R}},\tag{2.20}$$

where $\mathbf{R}$ defines the distance between the nodes on the opposite faces of the RVE in the reference configuration, and $\mathbf{K}$ is the wavevector in the reference configuration. The periodicity conditions (2.20) are imposed in the finite element code through the corresponding boundary conditions for the displacements of the opposite faces [3, 51]. The dispersion relations are obtained by solving the eigenvalue problem stemming from Eq. (2.18), (2.19) and (2.20) for a range of the wavevectors $\mathbf{K}$. Recall that the corresponding wavevector in the deformed configuration can be found via relation $\mathbf{k}=\mathbf{F}^{-T}\cdot\mathbf{K}$.

2.3 Non-linear electroelasticity

In this section, a brief description of non-linear electroelastic theory is presented. For a full story, the readers are referred to the book by Dorfmann and Ogden [18]

and references therein.

2.3.1 Electrostatics

Here, the so-called quasi-electrostatic approximation assuming the absence of magnetic fields and neglecting electromagnetic interactions is adopted. Thus, in the absence of free body charges and currents, the equations of electrostatics in the current configuration read as

$$\text{div}\mathbf{D} = 0 \text{ and } \text{curl}\mathbf{E} = \mathbf{0}, \tag{2.21}$$

where $\mathbf{D}$ and $\mathbf{E}$ denote electric displacement and electric field applied in the current configuration, respectively. Here and thereafter, the differential operators with the first low-case letter refer to the current configuration, while the differential operators with the first upper-case letter refer to the reference configuration.

In the reference configuration, the equations of electrostatics read as

$$\text{Div}\mathbf{D}_L = 0 \text{ and } \text{Curl}\mathbf{E}_L = \mathbf{0}, \tag{2.22}$$

where

$$\mathbf{D}_L = J\mathbf{F}^{-1} \cdot \mathbf{D} \text{ and } \mathbf{E}_L = \mathbf{F}^T \cdot \mathbf{E} \tag{2.23}$$

are the Lagrangian counterparts of $\mathbf{D}$ and $\mathbf{E}$, respectively.

2.3.2 Mechanical balance laws

In the absence of body forces, the linear and angular momentum balance for an electroelastic material are

$$\text{div}\boldsymbol{\tau} = \rho\mathbf{x}_{,tt} \text{ and } \boldsymbol{\tau} = \boldsymbol{\tau}^T, \tag{2.24}$$

where $\boldsymbol{\tau}$ represents the *total* Cauchy stress tensor (current configuration).

In Lagrangian description the balance equations (2.24) read as

$$\text{Div}\mathbf{P} = \rho_0 \mathbf{x}_{,tt} \text{ and } \mathbf{P} \cdot \mathbf{F}^T = \mathbf{F} \cdot \mathbf{P}^T, \tag{2.25}$$

where

$$\mathbf{P} = J\boldsymbol{\tau} \cdot \mathbf{F}^{-T} \tag{2.26}$$

is the first Piola-Kirchhoff *total* stress tensor (reference configuration).

2.3.3 Constitutive equations

To model non-linear behavior of DEs, an energy potential $\psi(\mathbf{F}, \mathbf{D}_L)$, as introduced in Dorfmann and Ogden [16], is considered. The strain energy-density potential is a function of deformation gradient $\mathbf{F}$ and Lagrangian counterpart of electric displacement $\mathbf{D}_L$. Then, for an electroelastic material, the first Piola-Kirchhoff total stress tensor and Lagrangian counterpart of electric field are given by

$$\mathbf{P} = \frac{\partial \psi}{\partial \mathbf{F}} \quad \text{and} \quad \mathbf{E}_L = \frac{\partial \psi}{\partial \mathbf{D}_L}. \tag{2.27}$$

For an incompressible material, $J = 1$, and the constitutive equations (2.27) modify as

$$\mathbf{P} = \frac{\partial \psi}{\partial \mathbf{F}} - p\mathbf{F}^{-T} \quad \text{and} \quad \mathbf{E}_L = \frac{\partial \psi}{\partial \mathbf{D}_L}. \tag{2.28}$$

2.3.4 Incremental equations

For an electroelastic material, the incremental constitutive equations for the first Piola-Kirchhoff stress and Lagrangian electric field read as

$$\dot{\mathbf{P}} = \mathbb{C}_0 : \dot{\mathbf{F}} + \mathcal{M}_0 \cdot \dot{\mathbf{D}}_L \quad \text{and} \quad \dot{\mathbf{E}}_L = \dot{\mathbf{F}} : \mathcal{M}_0 + \mathbf{K}_0 \cdot \dot{\mathbf{D}}_L, \tag{2.29}$$

respectively. Here, the superposed dot represent incremental changes in the corresponding variables; $\mathbb{C}_0$, $\mathcal{M}_0$, and $\mathbf{K}_0$ are the tensors of electroelastic moduli defined as

$$\mathbb{C}_0 = \frac{\partial^2 \psi}{\partial \mathbf{F} \partial \mathbf{F}}, \quad \mathcal{M}_0 = \frac{\partial^2 \psi}{\partial \mathbf{F} \partial \mathbf{D}_L} \quad \text{and} \quad \mathbf{K}_0 = \frac{\partial^2 \psi}{\partial \mathbf{D}_L \partial \mathbf{D}_L}. \tag{2.30}$$

For an incompressible material, the incremental equations (2.29) read as

$$\dot{\mathbf{P}} = \mathbb{C}_0 : \dot{\mathbf{F}} + p\mathbf{F}^{-T} \cdot \dot{\mathbf{F}}^T \cdot \mathbf{F}^{-T} - \dot{p}\mathbf{F}^{-T} + \mathcal{M}_0 \cdot \dot{\mathbf{D}}_L \quad \text{and} \quad \dot{\mathbf{E}}_L = \dot{\mathbf{F}} : \mathcal{M}_0 + \mathbf{K}_0 \cdot \dot{\mathbf{D}}_L. \tag{2.31}$$

2.3.5 Incremental motions superimposed on finite deformation in the presence of an electric field

In a framework of the updated Lagrangian formulation, the incremental forms of the governing Eqs. (2.22) and $(2.25)_1$, describing small motions superimposed on finite deformation, transform to

$$\text{div}\dot{\mathbf{D}}_{L\star} = 0, \ \text{curl}\dot{\mathbf{E}}_{L\star} = \mathbf{0}, \ \text{and} \ \text{div}\dot{\mathbf{P}}_\star = \rho \dot{\mathbf{x}}_{,tt}, \tag{2.32}$$

where

$$\dot{\mathbf{D}}_{L\star} = J^{-1}\mathbf{F} \cdot \dot{\mathbf{D}}_L, \ \dot{\mathbf{E}}_{L\star} = \mathbf{F}^{-T} \cdot \dot{\mathbf{E}}_L, \ \text{and} \ \dot{\mathbf{P}}_\star = J^{-1}\dot{\mathbf{P}} \cdot \mathbf{F}^T \tag{2.33}$$

are the so-called push-forward versions of $\dot{\mathbf{D}}_L$, $\dot{\mathbf{E}}_L$, and $\dot{\mathbf{P}}$, respectively. Identifying the field of incremental displacements as $\mathbf{u} = \dot{\mathbf{x}}$ and then displacement gradient as $\mathbf{H} = \text{grad}\mathbf{u} = \dot{\mathbf{F}} \cdot \mathbf{F}^{-1}$, the following updated incremental relations (2.29) are obtained

$$\dot{\mathbf{P}}_\star = \mathbb{C} : \mathbf{H} + \mathcal{M} \cdot \dot{\mathbf{D}}_{L\star} \quad \text{and} \quad \dot{\mathbf{E}}_{L\star} = \mathbf{H} : \mathcal{M} + \mathbf{K} \cdot \dot{\mathbf{D}}_{L\star}, \tag{2.34}$$

where

$$\mathbb{C}_{irks} = J^{-1}\mathbb{C}_{0ijkl}F_{rj}F_{sl}, \quad \mathcal{M}_{irk} = \mathcal{M}_{0ijm}F_{rj}F^{-1}_{mk} \quad \text{and} \quad \mathbf{K} = J\mathbf{F}^{-T}\cdot\mathbf{K}_0\cdot\mathbf{F}^{-1} \tag{2.35}$$

are the updated tensors of electroelastic moduli, enjoying the following symmetries

$$\mathbb{C}_{irks} = \mathbb{C}_{ksir}, \quad \mathcal{M}_{irk} = \mathcal{M}_{rik}, \quad \text{and} \quad \mathbf{K} = \mathbf{K}^T. \tag{2.36}$$

For an incompressible material, the incremental equations (2.34) read as

$$\dot{\mathbf{P}}_\star = \mathbb{C} : \mathbf{H} + p\mathbf{H}^T - \dot{p}\mathbf{I} + \mathcal{M}\cdot\dot{\mathbf{D}}_{L\star} \quad \text{and} \quad \dot{\mathbf{E}}_{L\star} = \mathbf{H} : \mathcal{M} + \mathbf{K}\cdot\dot{\mathbf{D}}_{L\star}; \tag{2.37}$$

moreover, the incompressibility assumption implies

$$\text{tr}\mathbf{H} \equiv \text{div}\mathbf{u} = 0. \tag{2.38}$$

2.3.6 Plane waves in incompressible DEs subjected to electromechanical loading

The solution of Eqs. (2.32) is sought in the form of plane waves with constant polarizations [17]

$$\mathbf{u} = \mathbf{g}f(\mathbf{n}\cdot\mathbf{x} - ct), \ \dot{\mathbf{D}}_{L\star} = \mathbf{d}g(\mathbf{n}\cdot\mathbf{x} - ct), \text{ and } \dot{p} = \Pi(\mathbf{n}\cdot\mathbf{x} - ct), \tag{2.39}$$

where f, g, and Π are arbitrary twice continuously differentiable, continuously differentiable, and continuous functions, respectively; as before, the unit vectors $\mathbf{g}$ and $\mathbf{d}$ represent polarization vectors of mechanical and electrical displacements, respectively; the unit vector $\mathbf{n}$ denotes the direction of wave propagation, and c is the phase velocity of the wave.

Substitution of (2.37) and (2.39) into (2.32) and (2.38) yields

$$\hat{\mathbf{A}} \cdot \mathbf{g} = \rho c^2 \mathbf{g} \quad \text{and} \quad \mathbf{g} \cdot \mathbf{n} = 0, \tag{2.40}$$

where $\hat{\mathbf{A}}$ is the so-called generalized acoustic tensor defining the condition of propagation of plane elastic waves in an incompressible electroelastic solid. The generalized acoustic tensor for an electroelastic material with an arbitrary energy potential $\psi(\mathbf{F}, \mathbf{D}_L)$ can be calculated as follows [52]

$$\hat{\mathbf{A}} = \hat{\mathbf{Q}} - \frac{2}{(\mathrm{tr}\hat{\mathbf{K}})^2 - \mathrm{tr}\hat{\mathbf{K}}^2} \hat{\mathbf{R}} \cdot \left((\mathrm{tr}\hat{\mathbf{K}})\hat{\mathbf{I}} - \hat{\mathbf{K}} \right) \cdot \hat{\mathbf{R}}^T, \tag{2.41}$$

where $\hat{\mathbf{K}} = \hat{\mathbf{I}} \cdot \mathbf{K} \cdot \hat{\mathbf{I}}$, $\hat{\mathbf{Q}} = \hat{\mathbf{I}} \cdot \mathbf{Q} \cdot \hat{\mathbf{I}}$, $\hat{\mathbf{R}} = \hat{\mathbf{I}} \cdot \mathbf{R} \cdot \hat{\mathbf{I}}$, and

$$Q_{ik} = \mathbb{C}_{ijkl} n_j n_l \quad \text{and} \quad \mathbf{R} = \mathbf{n} \cdot \mathcal{M}. \tag{2.42}$$

The generalized acoustic tensor $\hat{\mathbf{A}}$ is symmetric. Recall that an incompressible electroelastic material is strongly elliptic (stable), if its generalized acoustic tensor $\hat{\mathbf{A}}$ is positively defined, i.e. $\mathbf{g} \cdot \hat{\mathbf{A}} \cdot \mathbf{g} > 0$ for any unit vectors $\mathbf{n}$ and $\mathbf{g}$ satisfying the incompressibility constraint ($J = 1$) $\mathbf{n} \cdot \mathbf{g} = 0$ along an electromechanical loading path defined through a combination of $\mathbf{D}_L$ and $\mathbf{F}$.

Chapter 3

Findings

This chapter contains the findings of the research conducted to fulfill the requirements of the Graduate School of the Technion – Israel Institute of Technology. The thesis submitted as a collection of papers, which were published in peer-reviewed scientific journals. The list of published papers is cited below.

List of published papers:

1. P. I. Galich and S. Rudykh, Influence of stiffening on elastic wave propagation in extremely deformed soft matter: from nearly incompressible to auxetic materials. Extreme Mech. Lett., 4, 156-161 (2015).

2. P. I. Galich and S. Rudykh, Manipulating pressure and shear waves in dielectric elastomers via external electric stimuli. Int. J. Solids Struct., 91, 18-25 (2016).

3. P. I. Galich, N. X. Fang, M. C. Boyce, and S. Rudykh, Elastic wave propagation in finitely deformed layered materials. J. Mech. Phys. Solids, 98, 390-410

(2017).

4. P. I. Galich and S. Rudykh, Shear wave propagation and band gaps in finitely deformed dielectric elastomer laminates: long wave estimates and exact solution. J. Appl. Mech., 84(9), 91002 (2017).

5. P. I. Galich, V. Slesarenko, and S. Rudykh, Shear wave propagation in finitely deformed 3D fiber-reinforced composites. Int. J. Solids Struct., 110-111, 294-304 (2017).

Extreme Mechanics Letters 4 (2015) 156–161

Contents lists available at ScienceDirect

Extreme Mechanics Letters

journal homepage: www.elsevier.com/locate/eml

Influence of stiffening on elastic wave propagation in extremely deformed soft matter: from nearly incompressible to auxetic materials

Pavel I. Galich, Stephan Rudykh *

Department of Aerospace Engineering, Technion - Israel Institute of Technology, Haifa 32000, Israel

ARTICLE INFO

Article history:
Received 5 April 2015
Received in revised form 9 June 2015
Accepted 10 June 2015
Available online 14 June 2015

Keywords:
Elastic waves
Finite deformations
Soft materials
Compressible materials
Stiffening
Auxetics

ABSTRACT

We analyse the propagation of elastic waves in soft materials subjected to finite deformations. We derive explicit phase velocity relations for matter with pronounced stiffening effect, namely Gent model, and apply these results to study elastic wave propagation in (a) nearly incompressible materials such as biological tissues and polymers, (b) highly compressible and (c) negative Poisson's ratio or auxetic materials. We find, that for nearly incompressible materials transverse wave velocities exhibit strong dependence on the direction of propagation and initial strain state, whereas the longitudinal wave velocity is not affected significantly until extreme levels of deformation are attained. For highly compressible materials, we show that both longitudinal and transversal wave velocities depend strongly on deformation and direction of propagation. Moreover, the dependence becomes stronger when stiffening effects increase. When compression is applied, the longitudinal wave velocity decreases regardless the direction of wave propagation in highly compressible materials, and increases for most of the directions in materials with negative Poisson's ratio behaviour. We demonstrate that finite deformations can influence elastic wave propagation through combinations of induced effective compressibility and stiffness.

1. Introduction

The propagation of elastic waves has been investigated intensively [1–16] because the understanding of the phenomenon is vital for a large variety of applications from non-invasive material testing and medical imaging for health care to petroleum exploration. Recently, the field of acoustic or phononic metamaterials has attracted considerable attention. The peculiarity of these metamaterials originates in their microstructure [17,18], which can be tailored to give rise to various effects such as local resonances [19], band-gaps [12] and cloaking [20]. Furthermore, *soft* metamaterials, due to their capability to sustain large deformations, open promising opportunities of manipulating acoustic characteristics via deformation [21–23].

In this work, we derive explicit phase velocity relations for *finitely deformed* materials, which stiffen when stretched/compressed. Our analysis is based on the theory first developed by Hadamard [2], which was recently revised by Destrade and Ogden [11]. We specify the theory for the class of Gent materials, and obtain compact explicit expressions of phase velocities for any finite deformation and direction of propagation. The availability of explicit relations for phase velocity is important for designing *mechanotunable* acoustic metamaterials. Moreover, the information may benefit non-invasive medical diagnostic techniques by providing important information on the dependence of elastic wave propagation on pre-stress/pre-strain conditions, which are common in biological

* Corresponding author.
E-mail address: rudykh@technion.ac.il (S. Rudykh).

http://dx.doi.org/10.1016/j.eml.2015.06.003
2352-4316/

tissues. By application of the derived explicit expressions, we show the role of deformation and significant influence of stiffening effects on wave propagation in soft media undergoing finite deformations. Moreover, we extend the analysis to a class of exotic metamaterials characterized by negative Poisson's ratio (NPR) behaviour. Examples of NPR materials, also known as *auxetics*, include living bone tissue [24], skin [25], blood vessels [26], certain rocks and minerals [25], and artificial materials [27]. As we shall show, elastic wave propagation in these materials is significantly affected by deformation. In our analysis, we treat the materials as continuous media; their overall homogenized behaviour is characterized by effective elastic moduli. These material properties may originate in sophisticatedly engineered microstructures that give rise to remarkable overall properties (for example, negative Poisson's ratio or/and bulk modulus). The information on elastic wave propagation in terms of the effective properties can guide the design of new tunable metamaterials. Moreover, this information can shed light on the distinct roles of geometrical changes and material non-linearities occurring in tunable metamaterials due to large deformations [28]. Furthermore, even simple homogeneous materials can behave like smart metamaterials when finitely deformed. For example, they can be used to disentangle shear and pressure waves [23,29].

2. Analysis

To analyse the finitely deformed state, we introduce the deformation gradient $\mathbf{F}(\mathbf{X}, t) = \nabla_{\mathbf{X}} \otimes \mathbf{x}(\mathbf{X}, t)$, where $\mathbf{X}$ and $\mathbf{x}$ are position vectors in the reference and current configurations, respectively. To take into account the nonlinear effects of the finite deformation as well as material non-linearity, we analyse the wave propagation in terms of infinitesimal plane waves *superimposed* on a finitely deformed state [2,4]. To account for the stiffening effects (due to, for example, finite extensibility of polymer chains, or due to collective straightening of collagen fibres in biological tissues) in finitely deformed media, we make use of the strain–energy density function corresponding to an approximation of the Arruda–Boyce model [30], namely the Gent model [31,32] which is given in Eq. (1).

$$\psi(\mathbf{F}) = -\frac{\mu J_m}{2} \ln\left(1 - \frac{I_1 - 3}{J_m}\right) - \mu \ln J + \left(\frac{K}{2} - \frac{\mu}{3} - \frac{\mu}{J_m}\right)(J-1)^2, \tag{1}$$

where μ is the initial shear modulus, K is the initial bulk modulus, $I_1 = \operatorname{tr} \mathbf{B}$ is the first invariant of the left Cauchy–Green tensor $\mathbf{B} = \mathbf{F} \cdot \mathbf{F}^T$, and $J = \det \mathbf{F}$. The model neatly covers the stiffening of the material with the deformation; as the first strain invariant approaches $I_1 = 3 + J_m$, the energy function becomes unbounded and a dramatic increase in stress occurs. Consequently, J_m is a locking parameter. Clearly, when $J_m \to \infty$, the strain–energy function (1) reduces to

$$\psi(\mathbf{F}) = \frac{\mu}{2}(I_1 - 3) - \mu \ln J + (K/2 - \mu/3)(J-1)^2, \tag{2}$$

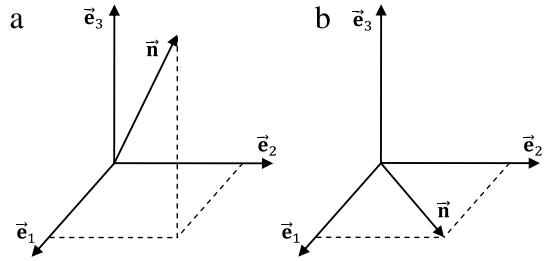

Fig. 1. Direction of propagation $\mathbf{n}$ relating to principal directions in general case (a) and when $\mathbf{n}$ lies in one of the planes of orthotropy (b). Here $(\mathbf{e}_1, \mathbf{e}_2, \mathbf{e}_3)$ is orthonormal basis of eigenvectors of left Cauchy–Green tensor $\mathbf{B}$.

which is a compressible extension of the neo-Hookean strain–energy function [33].

Recall the definition of an acoustic tensor [2,4] which defines the condition of propagation of plane waves

$$\mathbf{Q}(\mathbf{n}) = \mathcal{A}^{(1324)} : \mathbf{n} \otimes \mathbf{n}, \tag{3}$$

where the unit vector $\mathbf{n}$ defines the direction of propagation of the wave; $\mathcal{A} = J^{-1}\left(\mathbf{F} \cdot \mathcal{A}_0^{(2134)}\right)^{(2134)} \cdot \mathbf{F}^T$ and $\mathcal{A}_0 = \frac{\partial^2 \psi}{\partial \mathbf{F} \partial \mathbf{F}}$ are tensors of elastic moduli in current and reference configuration respectively; superscripts (1324) and (2134) denote isomers of the fourth-rank tensors [34,35], as detailed in Appendix A.

Strong stiffening. Acoustic tensor for finitely deformed Gent material (1) takes the form

$$\mathbf{Q}(\mathbf{n}) = \frac{\mu}{J}\left(1 + \left(\frac{K}{\mu} - \frac{2}{3} - \frac{2}{J_m}\right)J^2\right)\mathbf{n} \otimes \mathbf{n} + \frac{\mu J_m}{J\xi^2}\left(\xi(\mathbf{n} \cdot \mathbf{B} \cdot \mathbf{n})\mathbf{I} + 2\mathbf{n} \otimes \mathbf{n} : \mathbf{B} \otimes \mathbf{B}^{(1324)}\right), \tag{4}$$

where $\xi = 3 + J_m - I_1$, $\mathbf{I}$ is the identity tensor, and $\mathbf{B} \otimes \mathbf{B}^{(1324)}$ is the fourth-rank tensor isomer (see Appendices A and B).

General case. One can conclude from (4) that in general case (when $\mathbf{n}$ does not lie in any plane of orthotropy (Fig. 1(a)) and deformations are different along each principal axis, i.e. all eigenvalues of tensor $\mathbf{B}$ are different) the waves are neither purely longitudinal nor purely transversal (for details see Appendix B).

Case 1. If wave vector $\mathbf{n}$ lies in one of the planes of orthotropy (Fig. 1(b)) then we always have one purely transversal wave with the velocity

$$c_{tr} = \sqrt{\mu(\mathbf{n} \cdot \mathbf{B} \cdot \mathbf{n})J_m/(\rho_0 \xi)}, \tag{5}$$

where ρ_0 is the density of the undeformed material. Any finite deformation $\mathbf{F}$ at a homogeneous state can be represented as

$$\mathbf{F} = \lambda_1 \mathbf{e}_1 \otimes \mathbf{e}_1 + \lambda_2 \mathbf{e}_2 \otimes \mathbf{e}_2 + \lambda_3 \mathbf{e}_3 \otimes \mathbf{e}_3, \tag{6}$$

where $\lambda_{1,2,3}$ are stretch ratios along principal directions. Thus, expression (5) holds true for any combination of λ_1, λ_2 and λ_3.

Case 2. When wave vector $\mathbf{n}$ lies in one of the planes of orthotropy (for example in $\mathbf{e}_1 - \mathbf{e}_2$) and stretch ratios in this plane are equal ($\lambda_1 = \lambda_2 = \hat{\lambda}$) then we have

one longitudinal and two transversal polarizations with following velocities

$$c_l = \sqrt{\mu\left(1+\eta J^2 + J_m\xi^{-2}\left(\xi+2\hat{\lambda}^2\right)\hat{\lambda}^2\right)/\rho_0} \tag{7}$$

and

$$c_{tr} = \hat{\lambda}\sqrt{\mu J_m/(\rho_0\xi)} \tag{8}$$

respectively, with $\eta = K/\mu - 2/3 - 2/J_m$.

Case 3. For waves propagating along the principal direction ($\mathbf{n} = \mathbf{e}_i$), the velocities of longitudinal and transversal waves are

$$c_l = \sqrt{\mu\left(1+\eta J^2 + J_m\xi^{-2}\left(\xi+2\lambda_i^2\right)\lambda_i^2\right)/\rho_0} \tag{9}$$

and

$$c_{tr} = \lambda_i\sqrt{\mu J_m/(\rho_0\xi)}. \tag{10}$$

Case 4. When materials undergo so-called uniform dilatation or compaction ($\lambda_1 = \lambda_2 = \lambda_3$ or $\mathbf{F} = q\mathbf{I}$), then we have only pure modes with the velocities given by

$$c_l = \sqrt{\mu\left(1+\left(\eta q^4 + J_m\xi^{-2}\left(\xi+2q^2\right)\right)q^2\right)/\rho_0} \tag{11}$$

and

$$c_{tr} = q\sqrt{\mu J_m/(\rho_0\xi)}. \tag{12}$$

Weak stiffening. In case of a weak stiffening effect, namely, $J_m \to \infty$, the acoustic tensor (4) reduces to the well-known expression [9]

$$\mathbf{Q}(\mathbf{n}) = a_1\mathbf{n}\otimes\mathbf{n} + a_2(\mathbf{I} - \mathbf{n}\otimes\mathbf{n}), \tag{13}$$

where $\mathbf{n}\otimes\mathbf{n}$ is the projection on the direction $\mathbf{n}$; $(\mathbf{I}-\mathbf{n}\otimes\mathbf{n})$ is the projection on the plane normal to $\mathbf{n}$; $a_1 = (K - 2\mu/3)J + \mu J^{-1}(1 + \mathbf{n}\cdot\mathbf{B}\cdot\mathbf{n})$ and $a_2 = \mu J^{-1}(\mathbf{n}\cdot\mathbf{B}\cdot\mathbf{n})$. Consequently, there always exist one longitudinal and two transverse waves for any direction of propagation $\mathbf{n}$. Phase velocities of these waves can be calculated as [13] $c_l = \sqrt{a_1 J/\rho_0}$ and $c_{tr} = \sqrt{a_2 J/\rho_0}$. In the small deformation limit these formulae reduce to $c_l = \sqrt{(K+4\mu/3)/\rho_0}$ and $c_{tr} = \sqrt{\mu/\rho_0}$. It is worth mentioning that Boulanger and Hayes [13,16] presented explicit phase velocity expressions for wide classes of Hadamard and Mooney–Rivlin materials; however, the Gent material model, considered here, does not belong to these classes of hyperelastic materials.

3. Examples

To illustrate the dependence of wave propagation on the deformation and direction of propagation, we consider the case of uniaxial tension

$$\mathbf{F} = \lambda\mathbf{e}_1\otimes\mathbf{e}_1 + \tilde{\lambda}(\mathbf{I} - \mathbf{e}_1\otimes\mathbf{e}_1), \tag{14}$$

where λ is the applied stretch ratio and $\tilde{\lambda} = \tilde{\lambda}(\lambda, K/\mu)$ is defined through λ and the compressibility of the material. Remind that the compressibility of the material is defined by the ratio K/μ. In the linear elastic limit the elastic moduli are related through

$$\frac{K}{\mu} = \frac{2(1+\nu)}{3(1-2\nu)}, \tag{15}$$

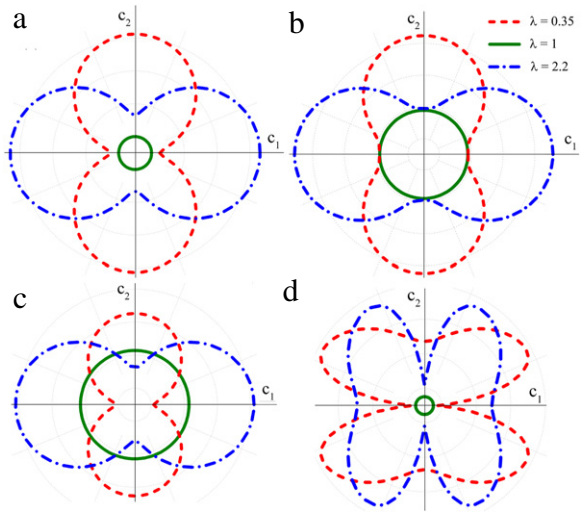

Fig. 2. Polar diagrams of the phase velocities in nearly incompressible materials: for the purely transversal (a), quasi-longitudinal (b), quasi-transversal (d) waves in Gent material with $J_m = 3$ and $K/\mu = 300$; and for the purely transversal (c) wave in neo-Hookean material with $K/\mu = 300$.

where ν is Poisson's ratio. Thus, $-1/3 < K/\mu < \infty$ with $\mu > 0$. Note that for $-1/3 < K/\mu < 0$ the material is stable only if constrained [34,36,37]. It follows from (15) that matter exhibits auxetic behaviour when $-1/3 < K/\mu < 2/3$.

Nearly incompressible materials. For nearly incompressible materials ($K/\mu \gg 1$ and $\tilde{\lambda} \simeq \lambda^{-1/2}$) the dependence of the longitudinal wave velocity on the direction of propagation and initial stress state is relatively weak unless extreme levels of deformation are attained. Fig. 2 shows the polar diagrams of the phase velocities for the nearly incompressible Gent and neo-Hookean materials under extreme levels of deformation. Here and thereafter the velocities are normalized by their value in the undeformed state; c_1 and c_2 are phase velocities along principal directions $\mathbf{e}_1$ and $\mathbf{e}_2$, correspondingly; more details on phase velocity or slowness surfaces can be found in the textbooks of Auld [38] or Nayfeh [39]. At the extreme levels of deformations, the stiffening effect manifests in a significant increase of the effective shear modulus, which becomes comparable with the bulk modulus (see Eq. (9)). Fig. 2(b) shows that velocity of longitudinal wave increases in both compressed and stretched materials. Moreover, stiffening of the material gives rise to the dramatic dependence of transversal wave velocities on the direction of propagation and deformation as compared to the materials with weak stiffening effect (compare Fig. 2(a) and (d) vs (c)). Besides, we observe that the dependence of the phase velocities on deformation and propagation direction increases when the locking parameter J_m decreases (which corresponds to an earlier stiffening of the material with deformation). Comparing the quasi-transversal wave velocity profiles with the purely transversal ones on the Fig. 2, we observe that the velocity of quasi-transversal wave has maxima for the non-principal directions (Fig. 2(d)). Note

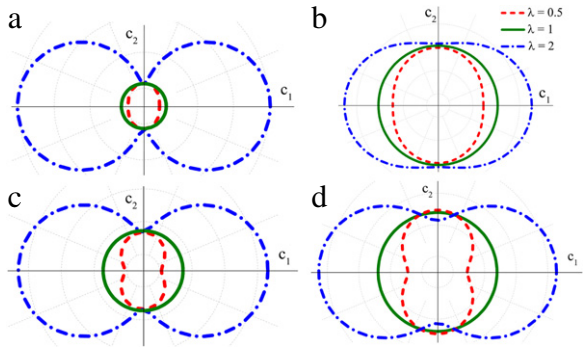

Fig. 3. Polar diagrams of the phase velocities in highly compressible materials: for the quasi-longitudinal (a) and purely transversal (c) waves in Gent material with $J_m = 3$ and $K/\mu = 1$; for the purely longitudinal (b) and transversal (d) waves in neo-Hookean material with $K/\mu = 1$.

that this phenomenon is not observed in Hadamard materials [40,41].

Highly compressible materials. In contrast to nearly incompressible materials, for highly compressible matter, the velocity of longitudinal wave depends strongly on the direction of propagation and initial deformation state even for moderate levels of deformation. More specifically Fig. 3(a) and (b) show that the velocity of pressure wave increases when material is stretched and decreases when it is compressed. Propagation of shear waves in highly compressible media differs significantly from the one in nearly incompressible materials. In particular, under compression the velocities of shear waves decrease in any direction if $K/\mu \leq 1$ (Fig. 3(c)), while it can either decrease or increase depending on the propagation direction in the nearly incompressible case (Fig. 2(a) and (c)). It should be noted that the deformation induced stiffening has a significant influence on both modes (compare Fig. 3(a), (c) vs (b), (d)), in particular when material is stretched. This is due to an increase in the effective shear modulus (the term $\mu J_m/\xi^2$ in Eq. (9) and $\mu J_m/\xi$ in Eq. (10)). The polar diagram of the phase velocity for the quasi-transversal wave in Gent material with $J_m = 3$ and $K/\mu = 1$ is similar to one plotted in Fig. 3(c), and it is not presented here.

Auxetic materials. Next, we consider auxetic materials characterized by NPR behaviour. Yet can such materials exist? Would they be stable? How can they be constructed? These questions have recently arisen in many papers [19,27,36,37,42–45] and still the topic is open for discussion. Wang and Lakes in their article [36] report that bulk modulus can be varied within the range $-\frac{4\mu}{3} < K < \infty$. Based on this and the previous estimations (Eq. (15)), we examine the material behaviour when $-1/3 < K/\mu < 0$. To illustrate the auxetic materials behaviour, we present the dependence of $\tilde{\lambda}$ and Poisson's ratio on the applied stretch λ for different ratios of K/μ.

Fig. 4 show that NPR behaviour is more pronounced in materials with negative bulk modulus. Note that the material becomes locally non-auxetic when certain level of deformation is reached. Furthermore, this level depends on stiffening of the material. In particular, materials with pronounced stiffening effect become locally non-auxetic faster than materials with weak stiffening effect. For

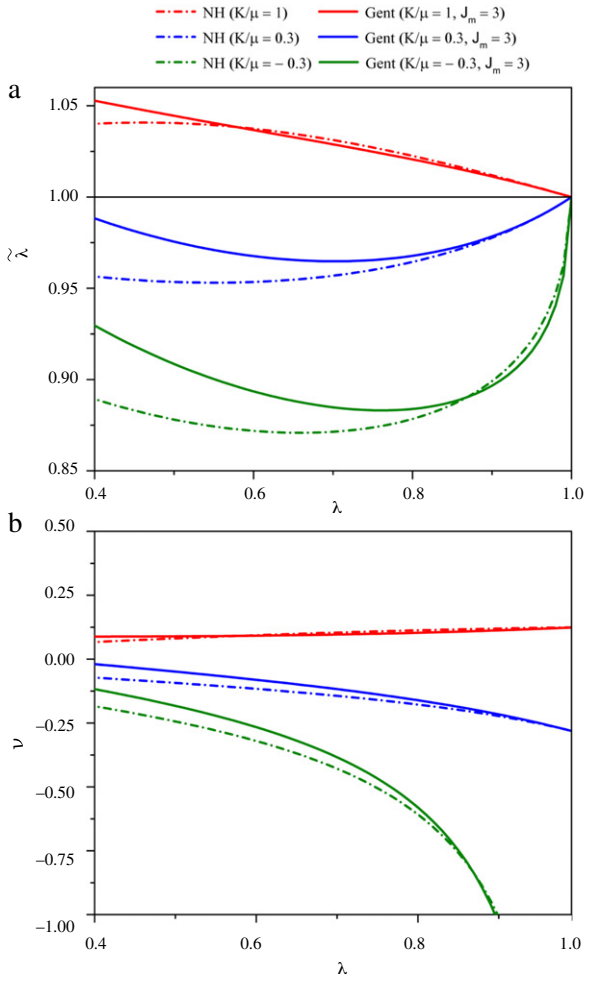

Fig. 4. Dependence of $\tilde{\lambda}$ (a) and Poisson's ratio ν (b) on applied stretch λ for Gent and neo-Hookean materials with different ratios K/μ.

example, $\lambda_{cr} \approx 0.66$ for neo-Hookean material with $K/\mu = -0.3$, and $\lambda_{cr} \approx 0.76$ for Gent material with $K/\mu = -0.3$ and $J_m = 3$.

An example of wave velocities for auxetic materials is shown in Fig. 5. We observe that the velocity of the longitudinal wave increases in any direction of propagation **n** when the material undergoes compression (Fig. 5(b)). This is in contrast to the case of highly compressible matter (see Fig. 3(a) and (b)). Moreover, the velocity of the longitudinal wave increases and reaches the maximum when wave vector **n** lies in the plane of transverse isotropy. However, for materials with strong stiffening effect the velocity of longitudinal wave decreases in some direction of propagation (see Fig. 5(a)). Fig. 5(c) and (d) show that velocities of transversal waves decrease considerably for all directions of propagations **n** in contrast to the effect of deformation observed in the nearly incompressible materials (Fig. 5(a), (c) and (d)). The influence of stiffening on elastic wave propagation is rather weak in the case of auxetics as compared to nearly incompressible and highly compressible materials; yet it can be observed. In particular, phase velocity of transversal wave decreases more under compression when stiffening effect is pronounced (compare

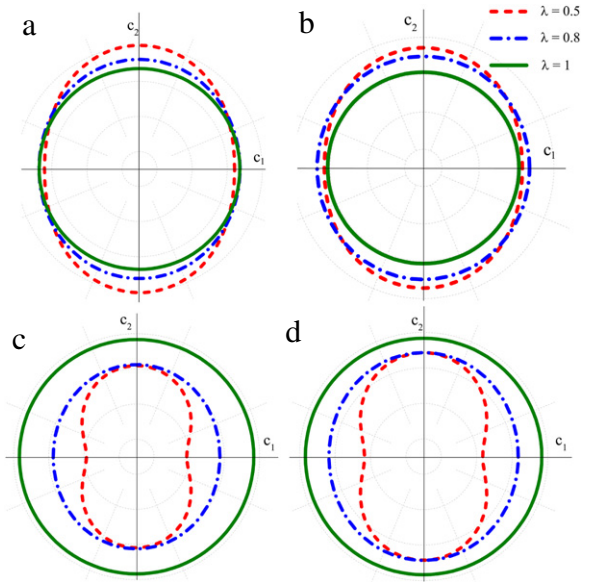

Fig. 5. Polar diagrams of the phase velocities in auxetics: for the quasi-longitudinal (a) and purely transversal (c) waves in Gent material with $J_m = 3$ and $K/\mu = -0.3$; for the purely longitudinal (b) and transversal (d) waves in neo-Hookean material with $K/\mu = -0.3$.

Fig. 5(c) vs (d)). The polar diagram of the phase velocity for the quasi-transversal wave in Gent material with $J_m = 3$ and $K/\mu = -0.3$ is similar to one plotted in Fig. 5(c), and is not shown here.

4. Concluding remarks

We derived explicit expressions for phase velocity for finitely deformed materials with pronounced stiffening effect and demonstrated the significant role of the deformation on elastic wave propagation on examples for nearly incompressible, highly compressible and extreme auxetic materials. Furthermore, we demonstrated how direction of wave propagation influences on the phase velocities of elastic waves. These findings may guide further design of mechanotunable acoustic metamaterials and phononic crystals with a large range of constituent properties. The local strain field in these engineered materials could be used to induce regions with extremely varied phononic properties to give rise to various acoustic effects. This opens a very rich and broad research avenue for designing tunable acoustic/phononic metamaterials.

Appendix A. Isomers of a fourth-rank tensor

Here we follow the notation of isomer firstly introduced by Ryzhak [34,35]. Let $\mathcal{M}$ be a fourth-rank tensor with the following representation as the sum of a certain number of tetrads:

$$\mathcal{M} = \mathbf{a}_1 \otimes \mathbf{a}_2 \otimes \mathbf{a}_3 \otimes \mathbf{a}_4 + \mathbf{b}_1 \otimes \mathbf{b}_2 \otimes \mathbf{b}_3 \otimes \mathbf{b}_4 + \cdots. \quad (A.1)$$

Let $(ijks)$ be some permutation of the numbers (1234). Then the isomer $\mathcal{M}^{(ijks)}$ is defined to be the fourth-rank tensor determined by the relation

$$\mathcal{M} = \mathbf{a}_i \otimes \mathbf{a}_j \otimes \mathbf{a}_k \otimes \mathbf{a}_s + \mathbf{b}_i \otimes \mathbf{b}_j \otimes \mathbf{b}_k \otimes \mathbf{b}_s + \cdots. \quad (A.2)$$

The fact that the isomer is independent of the choice of the polyadic representation of the original tensor can be readily proved by using well-known isomorphism between tensors and multilinear forms of the same rank.

Appendix B. Proof of absence of pure modes in general case in deformed Gent material

For clarity sake let us write an expanded form of tensor $\mathbf{n} \otimes \mathbf{n} : \mathbf{B} \otimes \mathbf{B}^{(1324)}$ and its scalar product on $\mathbf{n}$. First, let us write $\mathbf{B}$ and $\mathbf{B} \otimes \mathbf{B}$:

$$\mathbf{B} = \mathbf{F} \cdot \mathbf{F}^T = \lambda_1^2 \mathbf{e}_1 \otimes \mathbf{e}_1 + \lambda_2^2 \mathbf{e}_2 \otimes \mathbf{e}_2 + \lambda_3^2 \mathbf{e}_3 \otimes \mathbf{e}_3 \quad (B.1)$$

$$\begin{aligned}\mathbf{B} \otimes \mathbf{B} = {} & \lambda_1^4 \mathbf{e}_1 \otimes \mathbf{e}_1 \otimes \mathbf{e}_1 \otimes \mathbf{e}_1 + \lambda_2^4 \mathbf{e}_2 \otimes \mathbf{e}_2 \otimes \mathbf{e}_2 \otimes \mathbf{e}_2 \\ & + \lambda_3^4 \mathbf{e}_3 \otimes \mathbf{e}_3 \otimes \mathbf{e}_3 \otimes \mathbf{e}_3 \\ & + \lambda_1^2 \lambda_2^2 (\mathbf{e}_1 \otimes \mathbf{e}_1 \otimes \mathbf{e}_2 \otimes \mathbf{e}_2 + \mathbf{e}_2 \otimes \mathbf{e}_2 \otimes \mathbf{e}_1 \otimes \mathbf{e}_1) \\ & + \lambda_1^2 \lambda_3^2 (\mathbf{e}_1 \otimes \mathbf{e}_1 \otimes \mathbf{e}_3 \otimes \mathbf{e}_3 + \mathbf{e}_3 \otimes \mathbf{e}_3 \otimes \mathbf{e}_1 \otimes \mathbf{e}_1) \\ & + \lambda_2^2 \lambda_3^2 (\mathbf{e}_2 \otimes \mathbf{e}_2 \otimes \mathbf{e}_3 \otimes \mathbf{e}_3 + \mathbf{e}_3 \otimes \mathbf{e}_3 \otimes \mathbf{e}_2 \otimes \mathbf{e}_2). \end{aligned} \quad (B.2)$$

Now we can write the isomer (1324) of fourth-rank tensor $\mathbf{B} \otimes \mathbf{B}$ as

$$\begin{aligned}\mathbf{B} \otimes \mathbf{B}^{(1324)} = {} & \lambda_1^4 \mathbf{e}_1 \otimes \mathbf{e}_1 \otimes \mathbf{e}_1 \otimes \mathbf{e}_1 \\ & + \lambda_2^4 \mathbf{e}_2 \otimes \mathbf{e}_2 \otimes \mathbf{e}_2 \otimes \mathbf{e}_2 + \lambda_3^4 \mathbf{e}_3 \otimes \mathbf{e}_3 \otimes \mathbf{e}_3 \otimes \mathbf{e}_3 \\ & + \lambda_1^2 \lambda_2^2 (\mathbf{e}_1 \otimes \mathbf{e}_2 \otimes \mathbf{e}_1 \otimes \mathbf{e}_2 + \mathbf{e}_2 \otimes \mathbf{e}_1 \otimes \mathbf{e}_2 \otimes \mathbf{e}_1) \\ & + \lambda_1^2 \lambda_3^2 (\mathbf{e}_1 \otimes \mathbf{e}_3 \otimes \mathbf{e}_1 \otimes \mathbf{e}_3 + \mathbf{e}_3 \otimes \mathbf{e}_1 \otimes \mathbf{e}_3 \otimes \mathbf{e}_1) \\ & + \lambda_2^2 \lambda_3^2 (\mathbf{e}_2 \otimes \mathbf{e}_3 \otimes \mathbf{e}_2 \otimes \mathbf{e}_3 + \mathbf{e}_3 \otimes \mathbf{e}_2 \otimes \mathbf{e}_3 \otimes \mathbf{e}_2). \end{aligned} \quad (B.3)$$

Resolving $\mathbf{n}$ on the orthonormal basis $\mathbf{n} = n_1\mathbf{e}_1 + n_2\mathbf{e}_2 + n_3\mathbf{e}_3$, we obtain

$$\begin{aligned}\mathbf{n} \otimes \mathbf{n} : \mathbf{B} \otimes \mathbf{B}^{(1324)} = {} & \lambda_1^4 n_1^2 \mathbf{e}_1 \otimes \mathbf{e}_1 + \lambda_2^4 n_2^2 \mathbf{e}_2 \otimes \mathbf{e}_2 \\ & + \lambda_3^4 n_3^2 \mathbf{e}_3 \otimes \mathbf{e}_3 + \lambda_1^2 \lambda_2^2 n_1 n_2 (\mathbf{e}_1 \otimes \mathbf{e}_2 + \mathbf{e}_2 \otimes \mathbf{e}_1) \\ & + \lambda_1^2 \lambda_3^2 n_1 n_3 (\mathbf{e}_1 \otimes \mathbf{e}_3 + \mathbf{e}_3 \otimes \mathbf{e}_1) \\ & + \lambda_2^2 \lambda_3^2 n_2 n_3 (\mathbf{e}_2 \otimes \mathbf{e}_3 + \mathbf{e}_3 \otimes \mathbf{e}_2) \end{aligned} \quad (B.4)$$

and

$$\begin{aligned}\mathbf{n} \otimes \mathbf{n} : \mathbf{B} \otimes \mathbf{B}^{(1324)} \cdot \mathbf{n} = {} & \left(\lambda_1^2 n_1^2 + \lambda_2^2 n_2^2 + \lambda_3^2 n_3^2\right) \\ & \times \left(\lambda_1^2 n_1 \mathbf{e}_1 + \lambda_2^2 n_2 \mathbf{e}_2 + \lambda_3^2 n_3 \mathbf{e}_3\right). \end{aligned} \quad (B.5)$$

Now, let $\mathbf{g}$ be a polarization vector, hence if $\mathbf{g} \parallel \mathbf{n}$ we have longitudinal polarization and if $\mathbf{g} \perp \mathbf{n}$ we have transversal polarization. Firstly, assume that $\mathbf{g} \parallel \mathbf{n}$ then expression (4) yields

$$\begin{aligned}\mathbf{Q}(\mathbf{n}) \cdot \mathbf{n} = {} & (\alpha + \beta\xi(\mathbf{n} \cdot \mathbf{B} \cdot \mathbf{n}))\,\mathbf{n} \\ & + 2\beta\left(\mathbf{n} \otimes \mathbf{n} : \mathbf{B} \otimes \mathbf{B}^{(1324)}\right) \cdot \mathbf{n}, \end{aligned} \quad (B.6)$$

where for convenience we denoted $\alpha = \frac{\mu}{J}\left(1 + \left(\frac{K}{\mu} - \frac{2}{3} - \frac{2}{J_m}\right)J^2\right)$ and $\beta = \frac{\mu J_m}{J\xi^2}$. Since in general case vector $\left(\mathbf{n} \otimes \mathbf{n} : \mathbf{B} \otimes \mathbf{B}^{(1324)} \cdot \mathbf{n}\right)$ is not collinear to $\mathbf{n}$ (see Eq. (B.5)), therefore vector $\mathbf{g} = \mathbf{n}$ is not an eigenvector of acoustic tensor, i.e. longitudinal polarization is absent, *q.e.d.*

Now let us assume that $\mathbf{g} \perp \mathbf{n}$ then (4) yields

$$\begin{aligned}\mathbf{Q}(\mathbf{n}) \cdot \mathbf{g} = {} & \beta\xi(\mathbf{n} \cdot \mathbf{B} \cdot \mathbf{n})\mathbf{g} \\ & + 2\beta\left(\mathbf{n} \otimes \mathbf{n} : \mathbf{B} \otimes \mathbf{B}^{(1324)}\right) \cdot \mathbf{g}, \end{aligned} \quad (B.7)$$

Suppose that $\mathbf{g}$ is an eigenvector of acoustic tensor then

$$\beta\xi(\mathbf{n}\cdot\mathbf{B}\cdot\mathbf{n})\mathbf{g}+2\beta\left(\mathbf{n}\otimes\mathbf{n}:\mathbf{B}\otimes\mathbf{B}^{(1324)}\right)\cdot\mathbf{g}=\theta\mathbf{g}. \quad \text{(B.8)}$$

Scalar multiplication of the last equation by $\mathbf{n}$ yields

$$\mathbf{n}\cdot\left(\mathbf{n}\otimes\mathbf{n}:\mathbf{B}\otimes\mathbf{B}^{(1324)}\right)\cdot\mathbf{g}=0$$

$$\text{or}\quad \left(\lambda_1^2 n_1\mathbf{e}_1+\lambda_2^2 n_2\mathbf{e}_2+\lambda_3^2 n_3\mathbf{e}_3\right)\cdot\mathbf{g}=0. \quad \text{(B.9)}$$

Yet last expression does not hold true in the general case. Consequently, $\mathbf{g}\perp\mathbf{n}$ is not an eigenvector of acoustic tensor, *q.e.d.*

References

[1] M. Biot, The influence of initial stress on elastic waves, J. Appl. Phys. 11 (1940) 522.
[2] C. Truesdell, W. Noll, in: S.S. Antman (Ed.), The Non-Linear Field Theories of Mechanics, third ed., Springer, 1965.
[3] A. Norris, Propagation of plane waves in a pre-stressed elastic medium, J. Acoust. Soc. Am. 74 (1983) 1642.
[4] R. Ogden, Non-Linear Elastic Deformations, Dover Publications, 1984.
[5] F. John, Plane elastic waves of finite amplitude. Hadamard materials and harmonic materials, Comm. Pure Appl. Math. 19 (1966) 309–341.
[6] M.S. Kushwaha, P. Halevi, L. Dobrzynski, B. Djafari-Rouhani, Acoustic band structure of periodic elastic composites, Phys. Rev. Lett. 71 (1993) 2022.
[7] V.K. Ignatovich, L.T.N. Phan, Those wonderful elastic waves, Amer. J. Phys. 77 (2009) 1162.
[8] R. Ogden, B. Sighn, Propagation of waves in an incompressible transversally isotripic elastic solid with initial stress: Biot revisited, J. Mech. Mater. Struct. 6 (2011) 453–477.
[9] M. Shams, M. Destrade, R. Ogden, Initial stresses in elastic solids: Constitutive laws and acoustoelasticity, Wave Motion 48 (2011) 552–567.
[10] W. Parnell, A.N. Norris, T. Shearer, Employing pre-stress to generate finite cloaks for antiplane elastic waves, Appl. Phys. Lett. 100 (2012) 171907.
[11] M. Destrade, R.W. Ogden, On stress-dependent elastic moduli and wave speeds, J. of Appl. Math. 78 (2013) 965–997.
[12] M. Hussein, M. Leamy, M. Ruzzene, Dynamics of phononic materials and structures: Historical origins, recent progress and future outlook, Appl. Mech. Rev. 66 (2014) 040802.
[13] P. Boulanger, M. Hayes, C. Trimarco, Finite-amplitude plane waves in deformed hadamard elastic materials, Geophys. J. Int. 118 (1994) 447–458.
[14] S. Shan, S.H. Kang, P. Wang, C. Qu, S. Shian, E.R. Chen, K. Bertoldi, Harnessing multiple folding mechanisms in soft periodic structures for tunable control of elastic waves, Adv. Funct. Mater. 24 (2014) 4935–4942.
[15] A. Bergamini, T. Delpero, L.D. Simoni, L.D. Lillo, M. Ruzzene, P. Ermanni, Phononic crystal with adaptive connectivity, Adv. Mater 26 (2014) 1343–1347.
[16] P. Boulanger, M. Hayes, Finite-amplitude waves in deformed mooney-rivlin materials, Q. J. Mech. Appl. Math. 45 (1992) 575–593.
[17] X. Zhuang, Y. Mai, D. Wu, F. Zhang, X. Feng, Two-dimensional soft nanomaterials: A fascinating world of materials, Adv. Mater. 27 (2015) 403–427.
[18] Y. Li, N. Kaynia, S. Rudykh, M. Boyce, Wrinkling of interfacial layers in stratified composites, Adv. Energy Mater. 15 (2013) 921–926.
[19] P. Wang, F. Casadei, S. Shan, J.C. Weaver, K. Bertoldi, Harnessing buckling to design tunable locally resonant acoustic metamaterials, Phys. Rev. Lett. 113 (2014) 014301.
[20] S. Zhang, C. Xia, N. Fang, Broadband acoustic cloak for ultrasound waves, Phys. Rev. Lett. 106 (2011) 024301.
[21] K. Bertoldi, M.C. Boyce, Wave propagation and instabilities in monolithic and periodically structured elastomeric materials undergoing large deformations, Phys. Rev. B 78 (2008) 184107.
[22] S. Rudykh, M. Boyce, Transforming wave propagation in layered media via instability-induced interfacial wrinkling, Phys. Rev. Lett. 112 (2014) 034301.
[23] Z. Chang, H.-Y. Guo, B. Li, X.-Q. Feng, Disentangling longitudinal and shear elastic waves by neo-hookean soft devices, Appl. Phys. Lett. 106 (2015) 161903.
[24] J.L. Williams, J.L. Lewis, Properties and an anisotropic model of cancellous bone from the proximal tibial epiphysis, Trans. ASME, J. Biomech. Eng. 104 (1982) 5–56.
[25] K.E. Evans, K.L. Alderson, Auxetic materials: the positive side of being negative, Eng. Sci. Educ. J. 9 (2000) 148–154.
[26] B.D. Caddock, K.E. Evans, Negative Poisson ratios and strain-dependent mechanical properties in arterial prostheses, Biomaterials 16 (1995) 1109–1115.
[27] S. Babaee, J. Shim, J. Weaver, E. Chen, N. Patel, K. Bertoldi, 3d soft metamaterials with negative Poisson ratio, Adv. Mater. 25 (2013) 5044–5049.
[28] P. Wang, J. Shim, K. Bertoldi, Effects of geometric and material nonlinearities on the tunable response of phononic crystals, Phys. Rev. B 88 (2013) 014304.
[29] P.I. Galich, S. Rudykh, Comment on "Disentangling longitudinal and shear elastic waves by neo-hookean soft devices", 2015.
[30] E. Arruda, M. Boyce, A three-dimensional constitutive model for the large stretch behavior of rubber elastic materials, J. Mech. Phys. Solids 41 (1993) 389–412.
[31] A.N. Gent, A new constitutive relation for rubber, Rubber Chem. Technol. 69 (1996) 59–61.
[32] C. Horgan, The remarkable gent constitutive model for hyperelastic materials, Int. J. Non-Linear Mech. 68 (2015) 9–16.
[33] M. Boyce, E. Arruda, Constitutive models of rubber elasticity: A review, Rubber Chem. Technol. 73 (2000) 504–523.
[34] E. Ryzhak, On stable deformation of unstable materials in a rigid triaxial testing mashine, J. Mech. Phys. Solids 41 (1993) 1345–1356.
[35] L. Nikitin, E. Ryzhak, On stability and instability of a compressed block pressed to a smooth basement, Mech. Solids 43 (2008) 558–570.
[36] Y. Wang, R. Lakes, Composites with inclusions of negative bulk modulus: Extreme damping and negative Poisson ratio, J. Compos. Mater. 39 (2005) 1645–1657.
[37] N. Gaspar, C.W. Smith, K.E. Evans, Effect of heterogeneity on the elastic properties of auxetic materials, J. Appl. Phys. 94 (2003) 6143.
[38] B. Auld, Acoustic Fields and Waves in Solids, Krieger publishing company, 1990.
[39] A. Nayfeh, Wave Propagation in Layered Anisotropic Media with Applications to Composites, Elsevier Science, 1995.
[40] N. Scott, The slowness surfaces of incompressible and nearly incompressible elastic materials, J. Elasticity 16 (1986) 239–250.
[41] G. Rogerson, N. Scott, Wave propagation in singly-constrained and nearly-constrained elastic materials, Q. J. Mech. Appl. Math. 45 (1992) 77–99.
[42] L. Chen, C. Liu, J. Wang, W. Zhang, C. Hu, S. Fan, Auxetic materials with large negative Poisson ratios based on highly oriented carbon nanotube structures, Appl. Phys. Lett. 94 (2009) 253111.
[43] K. Bertoldi, P. Reis, S. Willshaw, T. Mullin, Negative Poisson ratio behavior induced by an elastic instability, Adv. Mater. 22 (2010) 361–366.
[44] T. Still, M. Oudich, G.K. Auerhammer, D. Vlassopoulos, B. Djafari-Rouhani, G. Fytas, P. Sheng, Soft silicone rubber in phononic structures: Correct elastic moduli, Phys. Rev. B 88 (2013) 094102.
[45] P.J. Beltramo, D. Schneider, G. Fytas, E.M. Furst, Anisotropic hypersonic phonon propagation in films of aligned ellipsoids, Phys. Rev. Lett. 113 (2014) 205503.

International Journal of Solids and Structures 91 (2016) 18–25

Contents lists available at ScienceDirect

International Journal of Solids and Structures

journal homepage: www.elsevier.com/locate/ijsolstr

Manipulating pressure and shear waves in dielectric elastomers via external electric stimuli

Pavel I. Galich, Stephan Rudykh*

Department of Aerospace Engineering, Technion – Israel Institute of Technology, Haifa 32000, Israel

ARTICLE INFO

Article history:
Received 31 December 2015
Revised 19 April 2016
Available online 3 May 2016

Keywords:
Elastic waves
Non-linear electroelasticity
Dielectric elastomers
Finite deformation

ABSTRACT

We investigate elastic wave propagation in finitely deformed dielectric elastomers in the presence of an electrostatic field. To analyze the propagation of both longitudinal (P-) and transverse (S-) waves, we utilize *compressible* material models. We derive explicit expressions for the generalized acoustic tensor and phase velocities of elastic waves for ideal and enriched dielectric elastomer models. We analyze the slowness curves of elastic wave propagation, and find the P-S-mode disentangling phenomenon. In particular, P-and S-waves can be separated by applying an electric field. The divergence angle between P-and S-waves strongly depends on the applied electrostatic excitation. The influence of an electric field depends on the choice of a material model. In the case of the ideal dielectric model, the in-plane shear wave velocity increases with an increase in electric field, while for the enriched model the velocity may decrease depending on material constants. The divergence angle also gradually increases with an increase in electric field, while for the enriched model the angle variation may be limited. Material compressibility affects the P-wave velocity, and for relatively compressible materials the slowness curve of the P-wave evolves from circular to elliptical shape manifesting in an increase in the refraction angle of the P-wave. As a result, the divergence angle decreases with an increase in material compressibility.

1. Introduction

Dielectric elastomers (DEs) are soft responsive materials that can change their form and shape when subjected to an electric stimulus (Pelrine et al., 2000; Bar-Cohen, 2002). DEs have attracted considerable attention due to a large variety of possible applications ranging from artificial muscles and soft robotics to energy conversion and noise canceling devices (O'Halloran et al., 2008; Brochu and Pei, 2010; Carpi et al., 2011; Rudykh et al., 2012; Kornbluh et al., 2012; Rogers, 2013). The theoretical framework of the non-linear electroelasticity is based on a theory first developed by Toupin (1956; 1963), which was recently revisited by Dorfmann and Ogden (2005; 2010) and Suo et al. (2008); Suo (2010). This followed by a series of works on modeling DEs (Volokh, 2012; Itskov and Khiêm, 2014; Keip et al., 2014; Cohen and deBotton, 2014; Jabareen, 2015; Miehe et al., 2015; Aboudi, 2015; Hossain et al., 2015; Cohen et al., 2016), to name a few recent contributions. The electromechanical coupling in typical DEs is rather weak, and, therefore, DEs need to operate at the edge of instabilities and breakthrough voltages to achieve meaningful actuation (Zhao et al., 2007; Zhao and Suo, 2008; 2010; Rudykh and deBotton, 2011; Rudykh et al., 2014; Rudykh and Bertoldi, 2013; Gei et al., 2014; Siboni et al., 2014; Bortot et al., 2016). Potentially, the need for the high voltage can be reduced through architectured microstructures of DEs increasing the electromechanical coupling (Huang et al., 2004; Rudykh et al., 2013; Cao and Zhao, 2013; Galipeau et al., 2014; Chatzigeorgiou et al., 2015). Moreover, synthesis of new soft dielectric materials seems to be another promising approach (Madsen et al., 2014). The effective electromechanical properties of DEs can be actively controlled by external electric stimuli. The dominant factor is the finite deformations induced by an electric excitation. Since in purely elastic materials wave propagation strongly depends on the mechanical properties of the media and deformation fields (Rudykh and Boyce, 2014; Galich and Rudykh, 2015b; 2015a), this opens an opportunity to manipulate wave propagation in DEs by applying an electric field.

In this work, we focus on elastic wave propagation in finitely deformed DEs in the presence of a uniform electric field. To explore the elastic wave propagation in DEs, we follow the widely used approach for the analysis of small-amplitude motions superimposed on the finite deformations (Ogden, 1997) induced by an external stimulus (Dorfmann and Ogden, 2010; Destrade and Ogden, 2011). To allow for the consideration of the longitudinal wave propagation (differently from the recent works (Gei et al., 2011; Shmuel et al., 2012; Chen and Dai, 2012), where incompressible

* Corresponding author. Tel.: +972 48292547.
E-mail address: rudykh@technion.ac.il (S. Rudykh).

http://dx.doi.org/10.1016/j.ijsolstr.2016.04.032
0020-7683/

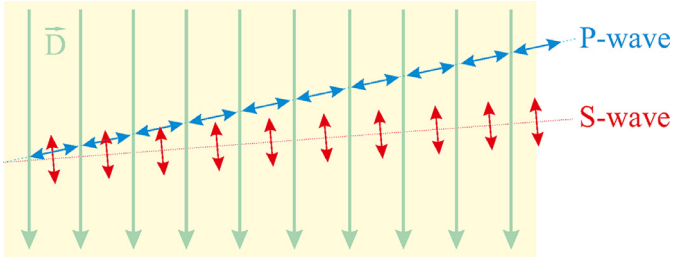

Fig. 1. Schematics of the splitting of pressure (P-) and shear (S-) elastic waves in a nearly incompressible neo-Hookean DE. P-wave does not refract from the initial direction of propagation, while S-wave refracts at a certain angle.

materials were considered), we utilize *compressible* electroactive material models, namely the ideal (Zhao et al., 2007) and enriched DE models. By application of wave propagation analysis to the compressible DE models, we derive explicit expressions for the generalized acoustic tensor and phase velocities for both longitudinal and transverse waves. We find that electrostatically induced changes in the key characteristics of shear (S-) and pressure (P-) waves lead to a disentangling phenomenon, where P-and S-waves travel in different directions. Fig. 1 schematically illustrates the P-and S-wave splitting phenomenon. The divergence angle strongly depends on the external field, the induced deformation, and material compressibility. P-and S-waves possess diverse properties and, thus, can be used for different purposes. For example, the S-wave serves as a virtual "finger" to probe elasticity of internal regions of the body in shear wave elasticity imaging (Sarvazyan et al., 1998). Longitudinal and transversal elastic waves can be separated at the interface between dissimilar materials; however, this may cause a loss of energy or/and a wave-mode conversion at the interface (Achenbach, 1973). Alternatively, we can use dielectric elastomers to split P-and S-elastic waves by applying a bias electric field. This feature can be employed, for example, in small-scale micro-electromechanical systems, where it is convenient to use an electric field to control the performance. Moreover, due to mathematical similarities between electro- and magneto-active materials, this splitting phenomenon can be utilized in magnetorheological elastomers controlled by an external magnetic field.

2. Analysis

To analyze the finitely deformed state, we introduce the deformation gradient $\mathbf{F}(\vec{X},t)=\nabla_{\vec{X}}\otimes\vec{x}(\vec{X},t)$, where $\vec{X}$ and $\vec{x}$ are position vectors in the reference and current configurations, respectively. In order to model a non-linear electroelastic material behavior, we consider an energy function $\psi(\mathbf{F},\vec{D}_0)$, which is a function of deformation gradient $\mathbf{F}$ and electric displacement vector $\vec{D}_0$ in the reference configuration. The corresponding electric displacement in the current configuration is given by $\vec{D}=J^{-1}\mathbf{F}\cdot\vec{D}_0$, where $J\equiv\det\mathbf{F}>0$. The first Piola–Kirchhoff stress tensor and electric field in the reference configuration are given by

$$\mathbf{P}_0=\frac{\partial\psi}{\partial\mathbf{F}}\quad\text{and}\quad\vec{E}_0=\frac{\partial\psi}{\partial\vec{D}_0},\tag{1}$$

the corresponding counterparts in the current configuration are

$$\mathbf{T}=J^{-1}\mathbf{P}_0\cdot\mathbf{F}^T\quad\text{and}\quad\vec{E}=\mathbf{F}^{-T}\cdot\vec{E}_0.\tag{2}$$

Linearized constitutive Eqs. (1) read as

$$\delta\mathbf{P}_0=\mathbb{C}_0:\delta\mathbf{F}+\mathcal{M}_0\cdot\delta\vec{D}_0\quad\text{and}\quad\delta\vec{E}_0=\delta\mathbf{F}:\mathcal{M}_0+\mathbf{K}_0\cdot\delta\vec{D}_0,\tag{3}$$

where δ denotes an incremental change; $\mathbb{C}_0,\mathcal{M}_0$ and $\mathbf{K}_0$ are the so-called tensors of electroelastic moduli (Dorfmann and Ogden, 2010) defined as

$$\mathbb{C}_0=\frac{\partial^2\psi}{\partial\mathbf{F}\partial\mathbf{F}},\quad\mathcal{M}_0=\frac{\partial^2\psi}{\partial\mathbf{F}\partial\vec{D}_0}\quad\text{and}\quad\mathbf{K}_0=\frac{\partial^2\psi}{\partial\vec{D}_0\partial\vec{D}_0}.\tag{4}$$

Note that $\mathbb{C}_0=\mathbb{C}_0^{(3412)}$ and $\mathbf{K}_0=\mathbf{K}_0^T$; here the superscript (3412) denotes an isomer of the fourth-rank tensor (Galich and Rudykh, 2015b; Ryzhak, 1993; Nikitin and Ryzhak, 2008) as detailed in Appendix A.

Next, we consider the small-amplitude motions superimposed on finite deformations; hence, we present the incremental constitutive Eqs. (3) in the frame of the updated reference configuration

$$\delta\mathbf{P}=\mathbb{C}:\delta\mathbf{H}+\mathcal{M}\cdot\delta\vec{D}_{01}\quad\text{and}\quad\delta\vec{E}_{01}=\delta\mathbf{H}:\mathcal{M}+\mathbf{K}\cdot\delta\vec{D}_{01},\tag{5}$$

where $\delta\mathbf{P}=J^{-1}\delta\mathbf{P}_0\cdot\mathbf{F}^T$, $\delta\vec{D}_{01}=J^{-1}\mathbf{F}\cdot\delta\vec{D}_0$, $\delta\vec{E}_{01}=\mathbf{F}^{-T}\cdot\delta\vec{E}_0$, $\delta\mathbf{H}=\delta\mathbf{F}\cdot\mathbf{F}^{-1}$,

$$\mathbb{C}=J^{-1}\left(\mathbf{F}\cdot\mathbb{C}_0^{(2134)}\cdot\mathbf{F}^T\right)^{(2134)},\quad\mathcal{M}=\mathbf{F}\cdot\mathcal{M}_0^{(213)}\cdot\mathbf{F}^{-1}\text{ and }\mathbf{K}=J\mathbf{F}^{-T}\cdot\mathbf{K}_0\cdot\mathbf{F}^{-1}.\tag{6}$$

Note that $\mathbb{C}=\mathbb{C}^{(3412)}$, $\mathcal{M}^{(213)}=\mathcal{M}$ and $\mathbf{K}=\mathbf{K}^T$. The linearized equation of motion and Maxwell's equations in Eulerian form are

$$\nabla_{\vec{x}}\cdot\delta\mathbf{P}=\rho\frac{\partial^2\vec{u}}{\partial t^2},\quad\nabla_{\vec{x}}\times\delta\vec{E}_{01}=0\quad\text{and}\quad\nabla_{\vec{x}}\cdot\delta\vec{D}_{01}=0,\tag{7}$$

where $\vec{u}$ is the incremental displacement; $\rho=\rho_0/J$ is the density of the deformed material and ρ_0 is the initial density of the material. We assume the absence of free body charges and currents. Note that we use the so called quasi-electrostatic approximation (Dorfmann and Ogden, 2010; Maugin, 1985); more specifically, the interactions between electric and magnetic fields are neglected. This is the non-relativistic approximation corresponding to the case where the mechanical velocity is significantly smaller than the light velocity (Dorfmann and Ogden, 2010).

We seek for a solution for Eqs. (7) in the form of plane waves with constant polarizations

$$\vec{u}=\vec{m}f(\vec{n}\cdot\vec{x}-ct)\quad\text{and}\quad\delta\vec{D}_{01}=\vec{d}g(\vec{n}\cdot\vec{x}-ct),\tag{8}$$

where f is a twice continuously differentiable function and g is a continuously differentiable function; unit vectors $\vec{m}$ and $\vec{d}$ are polarization vectors of mechanical and electrical displacements, respectively; the unit vector $\vec{n}$ defines the direction of wave propagation, and c is the phase velocity of the wave.

Substituting (5) and (8) into (7), we obtain

$$\mathbf{A}\cdot\vec{m}=\rho c^2\vec{m},\tag{9}$$

where $\mathbf{A}$ is the so-called "generalized" acoustic tensor defining the condition of propagation of elastic plane waves in non-linear electroelastic materials. The generalized acoustic tensor of electroelastic materials with an arbitrary strain energy function $\psi(\mathbf{F},\vec{D}_0)$, has the following form (Destrade and Ogden, 2011; Spinelli and Lopez-Pamies, 2015)

$$\mathbf{A}=\mathbf{Q}-\frac{2}{(\mathrm{tr}\hat{\mathbf{K}})^2-\mathrm{tr}\hat{\mathbf{K}}^2}\mathbf{R}\cdot\left((\mathrm{tr}\hat{\mathbf{K}})\hat{\mathbf{I}}-\hat{\mathbf{K}}\right)\cdot\mathbf{R}^T,\tag{10}$$

where

$$\hat{\mathbf{I}}=\mathbf{I}-\vec{n}\otimes\vec{n}\tag{11}$$

is the projection on the plane normal to $\vec{n}$, $\hat{\mathbf{K}}=\hat{\mathbf{I}}\cdot\mathbf{K}\cdot\hat{\mathbf{I}}$, and

$$\mathbf{Q}=\mathbb{C}^{(1324)}:\vec{n}\otimes\vec{n}\quad\text{and}\quad\mathbf{R}=\vec{n}\cdot\mathcal{M}.\tag{12}$$

Note that the generalized acoustic tensor $\mathbf{A}$ and the purely elastic acoustic tensor $\mathbf{Q}$ are symmetric. Recall that for DE to be stable, the generalized acoustic tensor $\mathbf{A}$ has to be positively defined. Note that an analogue of the generalized acoustic tensor (10) was derived by Destrade and Ogden (2011) for incompressible magnetoelastic materials.

A detailed description of the non-linear electroelastic theory for DEs can be found in publications of Dorfmann and Ogden (2005; 2010), and Suo et al. (2008), Suo (2010).

It is well known that incompressible materials do not support longitudinal waves. Therefore, to analyze both transversal and longitudinal waves, we consider the energy function $\psi(\mathbf{F}, \vec{D}_0)$ for the *compressible* electroelastic material in the following form:

$$\psi(\mathbf{F}, \vec{D}_0) = \psi_{elas}(\mathbf{F}) + \frac{1}{2\epsilon J}(\gamma_0 I_{4e} + \gamma_1 I_{5e} + \gamma_2 I_{6e}), \tag{13}$$

where $\psi_{elas}(\mathbf{F})$ is a purely elastic energy function (for example, neo-Hookean, Mooney–Rivlin, Gent, etc. (Ogden, 1997)), ϵ is the material permittivity in the undeformed state ($\mathbf{F} = \mathbf{I}$) and γ_i are dimensionless parameters, moreover $\gamma_0 + \gamma_1 + \gamma_2 = 1$, and

$$I_{4e} = \vec{D}_0 \cdot \vec{D}_0, \quad I_{5e} = \vec{D}_0 \cdot \mathbf{C} \cdot \vec{D}_0 \quad \text{and} \quad I_{6e} = \vec{D}_0 \cdot \mathbf{C}^2 \cdot \vec{D}_0 \tag{14}$$

are invariants depending on the electric displacement $\vec{D}_0$ and right Cauchy-Green tensor $\mathbf{C} = \mathbf{F}^T \cdot \mathbf{F}$.

For the energy function (13) the relation between the electric field and displacement is

$$\vec{E} = \frac{1}{\epsilon}\left(\gamma_0 \mathbf{B}^{-1} + \gamma_1 \mathbf{I} + \gamma_2 \mathbf{B}\right) \cdot \vec{D}, \tag{15}$$

where $\mathbf{B} = \mathbf{F} \cdot \mathbf{F}^T$ is the left Cauchy–Green tensor. The corresponding tensors of electroelastic moduli are

$$\mathbb{C} = \mathbb{C}_{elas} + \frac{1}{2\epsilon}\left(\gamma_0 \mathbb{C}_{4e} + \gamma_1 \mathbb{C}_{5e} + \gamma_2 \mathbb{C}_{6e}\right),$$

$$\mathcal{M} = \frac{1}{2\epsilon}\left(\gamma_0 \mathcal{M}_{4e} + \gamma_1 \mathcal{M}_{5e} + \gamma_2 \mathcal{M}_{6e}\right) \quad \text{and}$$

$$\mathbf{K} = \frac{1}{\epsilon}\left(\gamma_0 \mathbf{B}^{-1} + \gamma_1 \mathbf{I} + \gamma_2 \mathbf{B}\right), \tag{16}$$

where $\mathbb{C}_{elas}$ is derived from the purely elastic part $\psi_{elas}(\mathbf{F})$ of the energy function in accordance to (4) and (6); and the explicit expressions for the other tensors are given in Appendix B.

Finally, the corresponding generalized acoustic tensor takes the following form

$$\mathbf{A} = \mathbf{Q}_{elas} + \frac{1}{2\epsilon}\left(\gamma_0 \mathbf{Q}_{4e} + \gamma_1 \mathbf{Q}_{5e} + \gamma_2 \mathbf{Q}_{6e} - \frac{4}{\eta}\mathbf{A}_e\right), \tag{17}$$

where $\mathbf{Q}_{elas}$ is calculated by applying of Eqs. (4), (6) and (12) to the purely elastic part $\psi_{elas}(\mathbf{F})$ of the energy function; the explicit expressions for η, and tensors $\mathbf{Q}_{4e}$, $\mathbf{Q}_{5e}$, $\mathbf{Q}_{6e}$ and $\mathbf{A}_e$ are given in the Appendix B. Remarkably, in the particular case of $\mathbf{F} = \lambda_1 \vec{e}_1 \otimes \vec{e}_1 + \lambda_2 \vec{e}_2 \otimes \vec{e}_2 + \lambda_3 \vec{e}_3 \otimes \vec{e}_3$, $\vec{n} = \vec{e}_1$ and $\vec{D}_0 = D_2 \vec{e}_2$, the generalized acoustic tensor (17) reduces to

$$\mathbf{A} = \mathbf{Q}_{elas} + \frac{\gamma_2 D_2^2}{\epsilon \lambda_3^2} \vec{e}_2 \otimes \vec{e}_2, \tag{18}$$

here the set of $(\vec{e}_1, \vec{e}_2, \vec{e}_3)$ defines the orthonormal basis.

Let us consider the influence of an electric field on the P-and S-waves propagation. Important characteristics of elastic waves can be deduced from the consideration of slowness curves. Fig. 2 (a) schematically shows the slowness curves for P-and S-waves propagating in a DE subjected to an electric field. P-and S-waves refract differently from the initial direction of propagation, thus, the P-and S-waves can be split in such media. The normals to the slowness curves can be defined by the corresponding angle θ (see Fig. 2 (a))

$$\tan\theta_{p,s} = \frac{s_{p,s}\sin\varphi - (ds_{p,s}/d\varphi)\cos\varphi}{s_{p,s}\cos\varphi + (ds_{p,s}/d\varphi)\sin\varphi}, \tag{19}$$

where φ is the incident angle and $s_{p,s}(\varphi) = c_{p,s}^{-1}(\varphi)$ are slownesses of P-and S-waves, respectively. Consequently, the divergence angle between P-and S-wave can be calculated as $\Delta\theta = \theta_p - \theta_s$.

3. Results

3.1. Ideal dielectric elastomer model

First, we consider an ideal dielectric elastomer model (Zhao et al., 2007), namely $\gamma_0 = \gamma_2 = 0$ and $\gamma_1 = 1$ in (13). For the elastic part of the energy function (13), here and thereafter, we utilize a model of a compressible neo-Hookean material (Ogden, 1997)

$$\psi_{elas}(\mathbf{F}) = \frac{\mu}{2}(I_1 - 3) - \mu \ln J + \left(\frac{K}{2} - \frac{\mu}{3}\right)(J-1)^2, \tag{20}$$

where $I_1 = \mathrm{tr}\,\mathbf{C}$ is the first invariant of the right Cauchy-Green tensor, μ is the shear modulus and K is the bulk modulus.

For the ideal DE, the generalized acoustic tensor takes the form

$$\mathbf{A} = a_1^* \vec{n} \otimes \vec{n} + a_2^* \hat{\mathbf{I}}, \tag{21}$$

where $\vec{n} \otimes \vec{n}$ is the projection on the direction $\vec{n}$ and $\hat{\mathbf{I}}$ is given in (11),

$$a_1^* = (K - 2\mu/3)J + \mu J^{-1}(1 + \vec{n} \cdot \mathbf{B} \cdot \vec{n}) \tag{22}$$

$$\text{and} \quad a_2^* = \mu J^{-1}(\vec{n} \cdot \mathbf{B} \cdot \vec{n}). \tag{23}$$

Consequently, there always exist one pressure and two shear waves for any direction of propagation $\vec{n}$, finite deformation $\mathbf{F}$ and electric displacement $\vec{D}$. The phase velocities of these waves can be calculated as

$$c_p = \sqrt{a_1^* J/\rho_0} \quad \text{and} \quad c_s = \sqrt{a_2^* J/\rho_0}. \tag{24}$$

Remarkably, while the electroelastic moduli (16) explicitly depend on the electric field, the phase velocities of elastic waves do not explicitly depend on the electric field. The dependence of the velocities on an electric field is introduced through the electrostatically induced deformation. Let us consider the case when $\vec{D}_0 = D\sqrt{\mu\epsilon}\vec{e}_2$, DE can freely expand in plane $\vec{e}_1 - \vec{e}_3$, and the deformation gradient can be expressed as

$$\mathbf{F} = \lambda(D)\vec{e}_2 \otimes \vec{e}_2 + \tilde{\lambda}(D)(\mathbf{I} - \vec{e}_2 \otimes \vec{e}_2). \tag{25}$$

For an incompressible ideal DE (Zhao et al., 2007), the stretch ratios can be expressed as $\lambda = (1 + D^2)^{-1/3}$ and $\tilde{\lambda} = \lambda^{-1/2}$. It should be noted that these relations approximately hold even for very compressible materials with $K/\mu \sim 1$ for the range of deformations and electric fields considered here. Recall that neo-Hookean DE is stable for $D \leqslant \sqrt{3}$ (Zhao et al., 2007) and it will thin down without any limit when the electric field is further increased. Note that in the absence of an electric field, expressions (24) reduce to $c_p = \sqrt{(K + 4\mu/3)/\rho_0}$ and $c_s = \sqrt{\mu/\rho_0}$.

For the nearly incompressible DE, the phase velocities of P-and S-waves can be calculated as

$$c_p = \sqrt{\left((K + \mu/3 + \frac{\mu\left(1 + D^2\cos^2\varphi\right)}{\left(1 + D^2\right)^{2/3}}\right)/\rho_0} \tag{26}$$

and

$$c_s = \sqrt{\left(1 + D^2\cos^2\varphi\right)\left(1 + D^2\right)^{-2/3}\mu/\rho_0}, \tag{27}$$

where the propagation direction is defined as $\vec{n} = (\cos\varphi, \sin\varphi, 0)$. Hence, refraction angles of P-and S-waves are

$$\tan\theta_p = \frac{\left(K + \mu/3 + \mu\left(1 + D^2\right)^{-2/3}\right)\tan\varphi}{K + \mu/3 + \mu\left(1 + D^2\right)^{1/3}} \tag{28}$$

and

$$\tan\theta_s = \frac{\tan\varphi}{1 + D^2}. \tag{29}$$

Remarkably, relations (26), (27), (28) and (29) approximately hold even for very compressible materials with $K/\mu \sim 1$ for the range of deformations and electric fields considered here. By making use of relations (26) and (27), the slowness curves of P-and S-waves for the ideal DE can be constructed. Fig. 2 (b) shows an example

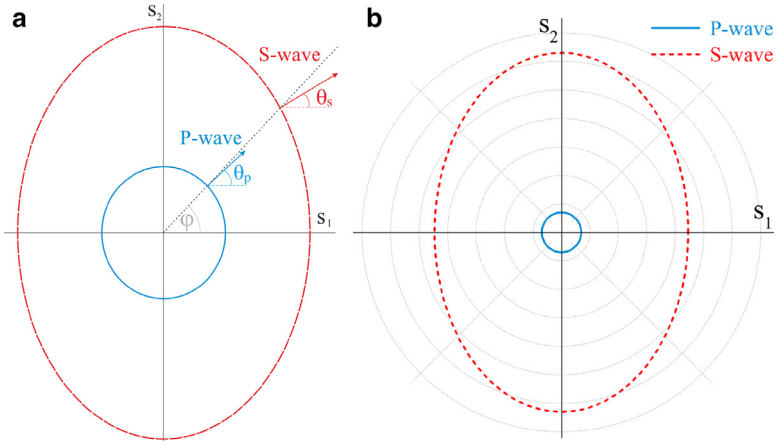

Fig. 2. (a) Schematic illustration of slowness curves for P-and S-waves in the DE subjected to an electric field. (b) Slowness curves of P-and S-waves for the ideal DE with $K/\mu = 50$ subjected to the electric excitation of $D = 1$. Slowness curves are constructed by using (26) and (27). Scale is 0.2 per division, and slowness curves are normalized by $\sqrt{\mu/\rho_0}$.

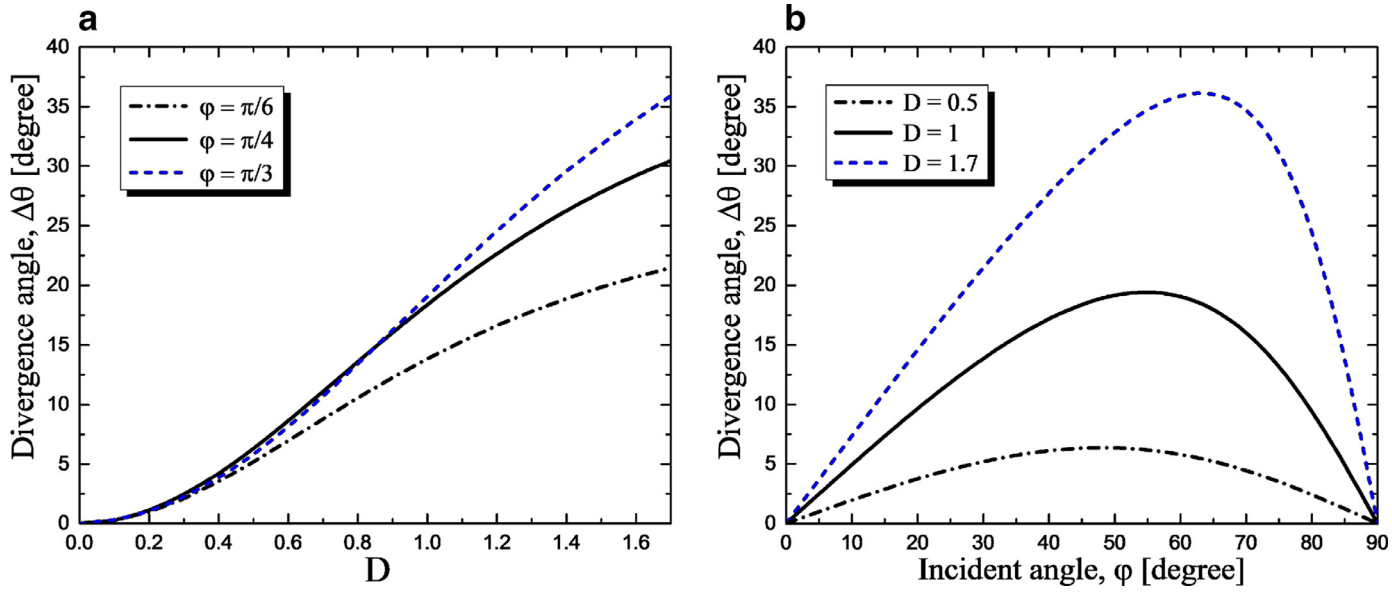

Fig. 3. Divergence angle as function of non-dimensional electric displacement – (a), and incident angle – (b) for the nearly incompressible neo-Hookean DE with $K/\mu = 300$.

of the slowness curves for an ideal DE with $K/\mu = 50$ subjected to the electric excitation of $D = 1$.

Fig. 3(a) shows that the divergence angle $\Delta\theta$ significantly depends on the value of an applied electric field. In particular, the divergence angle increases monotonically with an increase in the electric field until the limiting value of the electric field is reached ($D = \sqrt{3}$). Fig. 3(b) shows the dependence of the divergence angle $\Delta\theta$ on the incident angle φ. We observe that the divergence angle $\Delta\theta$ has a maximum for a certain incident angle φ_0 depending on the applied electric field. The incident angle φ_0 corresponding to the maximal divergence angle is given by

$$\tan\varphi_0 = \sqrt{\frac{\alpha\left(\alpha\mu^3(\alpha+27)+3D^2\alpha_1\mu(\alpha_1-3\mu)+\zeta\right)}{\mu^3\left(\alpha^2+27\right)+\zeta}}, \qquad (30)$$

where $\alpha = 1 + D^2$, $\alpha_1 = \alpha^{2/3}(3K + \mu)$ and $\zeta = 9K\alpha^2\left(\mu^2 + 3K(K+\mu)\right)$. The maximal angle, φ_0, monotonically increases with an increase in the electric field. Note that for $\mu/K \ll 1$, $\varphi_0 = \arccos\left(2+D^2\right)^{-1/2}$.

Next we consider the influence of the material compressibility on the elastic wave propagation in DEs. It has been recently shown that for highly compressible material (in the absence of an electric field) the phase velocity of the longitudinal wave depends significantly on the direction of wave propagation and applied deformation (Galich and Rudykh, 2015b). Here, we also observe a strong dependence of the P-wave velocity on the direction of wave propagation and the deformation induced by an electric field. An increase in the material compressibility parameter μ/K results in a more pronounced influence of electrostatically induced deformation on elastic waves. In particular, the slowness curves of P-wave evolve from circle to ellipse shape with an increase in electric field. Thus, refraction angle of P-wave differs from the incident angle, namely P-wave refracts along with S-wave. Fig. 4 schematically illustrates the phenomenon in compressible materials. The dependence of the divergence angle on compressibility for different values of the electrostatic excitation is presented in Fig. 5. Clearly, an increase in material compressibility weakens the disentangling phenomenon.

3.2. Enriched electroactive material model

Motivated by the experimental observations (Wissler and Mazza, 2007; Li et al., 2011), in this section we investigate elastic wave propagation in DEs described by an enriched electroactive material model (13). The model is similar to that considered by

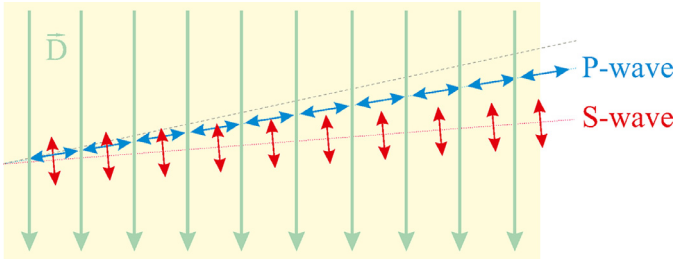

Fig. 4. Schematics of the splitting of P-and S-waves in the compressible neo-Hookean DE. P-and S-waves unidirectionally refract from the initial direction of propagation, however, their refraction angles are different.

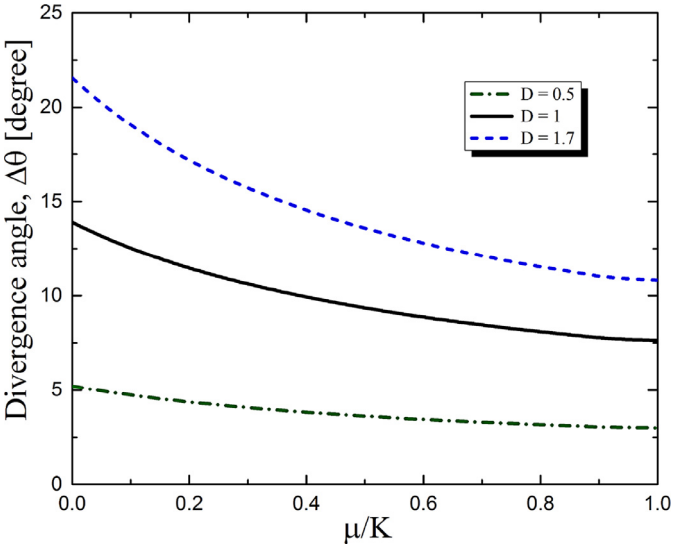

Fig. 5. Divergence angle as function of material compressibility for the ideal neo-Hookean DE subjected to different levels of electrostatic excitation, $\varphi = \pi/6$.

Table 1
Material constants of DE model (13).

Reference	γ_0	γ_1	γ_2
Ideal DE (Zhao et al., 2007)	0	1	0
Wissler and Mazza (2007)	0.00104	1.14904	−0.15008
Li et al. (2011)	0.00458	1.3298	−0.33438

Gei et al. (2014). To allow for the investigation of pressure waves, we extend the model to capture the compressibility effects. Table 1 summarizes the parameters of the material model (13) for different experimental data (Wissler and Mazza, 2007; Li et al., 2011).

In the case when $\gamma_0 \neq 0$, $\gamma_2 \neq 0$, and the deformation gradient identical to (25), and $\vec{n} = \vec{e}_1$, the expressions for phase velocities take the following form

$$c_p = \sqrt{\left((K - 2\mu/3)\lambda^2\tilde{\lambda}^4 + \left(1 + \tilde{\lambda}^2\right)\mu\right)/\rho_0} \quad (\vec{m} = \vec{e}_1), \tag{31}$$

$$c_s = \sqrt{\left(\gamma_2 D^2\lambda + \tilde{\lambda}^2\right)\mu/\rho_0} \quad (\vec{m} = \vec{e}_2) \tag{32}$$

and

$$c_s = \tilde{\lambda}\sqrt{\mu/\rho_0} \quad (\vec{m} = \vec{e}_3). \tag{33}$$

For incompressible materials $\tilde{\lambda} = \lambda^{-1/2}$, and the stretch ratio λ can be determined by solving the following polynomial equation

$$\lambda^3\left(1 + D^2\left(\gamma_1 + 2\gamma_2\lambda^2\right)\right) = 1. \tag{34}$$

Hence, the phase velocity of the in-plane shear wave (with polarization $\vec{m} = \vec{e}_2$) explicitly depends on the electric field in contrast to the result $(24)_2$ for the ideal DE model. Fig. 6 shows the

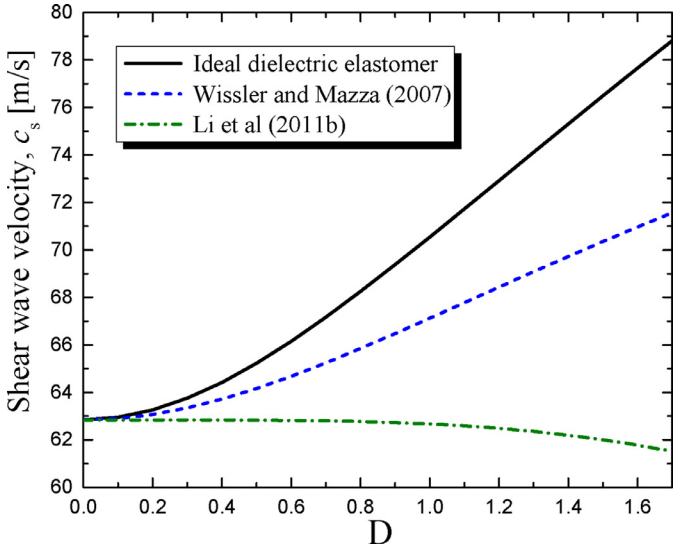

Fig. 6. Phase velocity of in-plane shear wave as functions of non-dimensional electric displacement for ideal and enriched DE models, $\varphi = 0$.

phase velocity of the in-plane shear wave as a function of the non-dimensional electrostatic excitation for the ideal and enriched DE models. One can see that the consideration of the I_{4e} and I_{6e} invariants strongly influences the in-plane shear wave velocity. In particular, the increase in phase velocity of the in-plane shear wave is less prominent (dashed blue curve in Fig. 6) as compared with the ideal DE model result; moreover, the velocity may even decrease with an increase in the electric field (see the example for the particular material denoted by the dot-dashed green curve in Fig. 6), while for the ideal DE model the velocity always increases. These differences indeed affect the splitting mechanism and, thus, different results are produced by these material models. Fig. 7 illustrates the difference in the divergence angles for the ideal and enriched DE models. In particular, Fig. 7(a) shows that the divergence angle $\Delta\theta$ is smaller than it is predicted by the ideal DE model. Moreover, for Li et al. experimental data, the divergence angle $\Delta\theta$ decreases with an increase in the electric field after a certain level of the applied voltage is reached. Fig. 7(b) shows that the divergence angle $\Delta\theta$ has a maximum for a certain incident angle φ_1. Moreover, the incident angle φ_1, producing the maximum divergence angle, varies for different materials.

Although in this work we perform a fully electromechanical coupling analysis, it is possible to employ only a purely mechanical analysis of wave propagation in non-linear electroelastic solids. In that case the contribution of the electroelastic moduli tensors $\mathcal{M}$ and $\mathbf{K}$ is neglected, and only terms of the tensor $\mathbb{C}$ contribute to the generalized acoustic tensor. Remarkably, this approximation yields very close results for the phase velocity of pressure wave as the fully electromechanically coupled analysis; moreover, the resulting expressions for the phase velocities of the shear waves are identical in both analyzes. For example, for the deformation gradient (25), $\vec{n} = \vec{e}_1$ and $\vec{D}_0 = D\sqrt{\mu\epsilon}\vec{e}_2$, the *classic* acoustic tensor takes the form

$$\mathbf{Q} = \mathbf{Q}_{elas} + \mu D^2(\gamma_0 J^{-2} + \gamma_1\tilde{\lambda}^{-4} + \gamma_2\lambda^2\tilde{\lambda}^{-4})\vec{e}_1 \otimes \vec{e}_1 + \mu\gamma_2 D^2\tilde{\lambda}^{-2}\vec{e}_2 \otimes \vec{e}_2. \tag{35}$$

It is easy to see that the resulting expressions for the phase velocities of S-waves are the same as given by expressions (32) and (33), and the corresponding expression for the phase velocity of P-wave has the form

$$c_p = \sqrt{\mu\left(1 + \tilde{\lambda}^2 + (K/\mu - 2/3)\lambda^2\tilde{\lambda}^4 + D^2(\gamma_0\lambda^{-2} + \gamma_1 + \gamma_2\lambda^2)\tilde{\lambda}^{-4}\right)/\rho_0}. \tag{36}$$

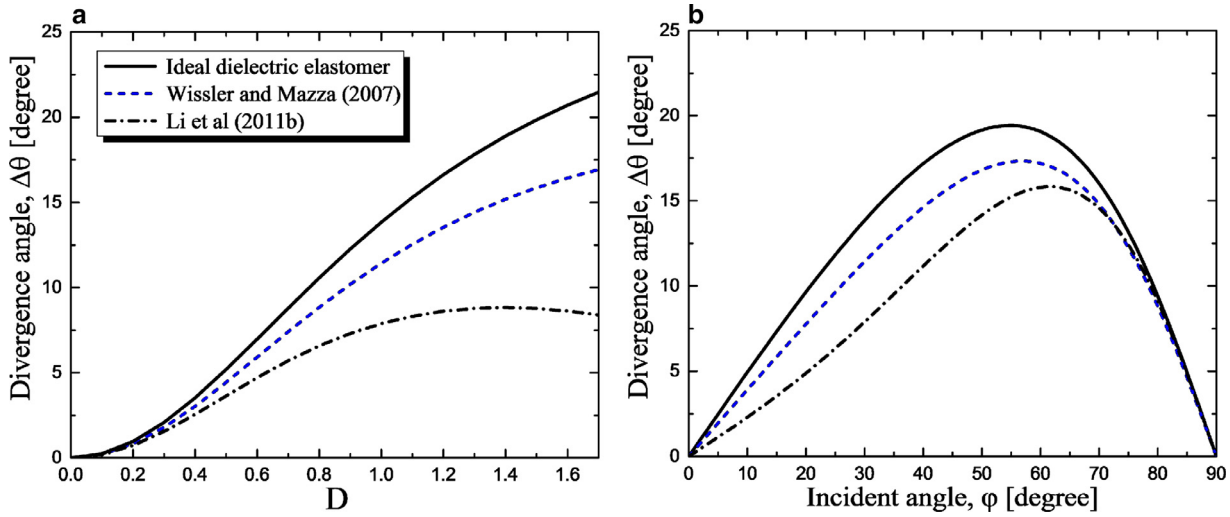

Fig. 7. Divergence angle as function of non-dimensional electric displacement for $\varphi = \pi/6$ (a) and incident angle for $D = 1$ (b) in the nearly incompressible neo-Hookean DE with $K/\mu = 300$.

Expression (36) for the P-wave velocity differs from (31) by the additional term containing the electric displacement magnitude. However, according to our observations for $K/\mu \gtrsim 100$, this term can be neglected for small and moderate levels of electric displacement.

4. Concluding remarks

In this paper, we considered pressure (P-) and shear (S-) elastic waves propagating in soft DEs subjected to finite deformations in the presence of an electric field. To allow for the consideration of P-wave propagation, we utilized the ideal and enriched material models accounting for the *compressibility* effects. Explicit expressions for the generalized acoustic tensor and phase velocities of elastic waves for DEs subjected to an electric field were presented. We found that, for the ideal DE model, the elastic wave propagation is explicitly independent of an applied electric field, while it is influenced through the deformation induced via bias electric field; this is despite the fact that all electroelastic moduli tensors explicitly depend on the applied electric field. However, for the enriched material model, including all three electroelastic invariants I_{4e}, I_{5e} and I_{6e}, elastic wave propagation explicitly depends on the applied electric field; in particular, the phase velocity of the in-plane shear wave decreases when an electric field is applied.

These findings were applied to explore the phenomenon of disentangling P-and S-elastic waves in DEs by an electric field. We showed that the divergence angle between P-and S-waves strongly depends on the value of the applied electric field and direction of wave propagation. Moreover, we found that an increase in the material compressibility weakens the separation of P-and S-waves. This is due to the fact that the P-wave also refracts (in the same direction as the S-wave) from the initial direction of wave propagation, while for nearly incompressible materials the change in the P-wave direction is negligible. The phenomenon can be used to manipulate elastic waves by a bias electrostatic field; this can be beneficial for applications in small length-scale devices, such as micro-electromechanical systems, where an electric field is the preferred control parameter. Thanks to the mathematical similarities in the description of electro- and magneto-active materials, the disentangling phenomenon can be utilized to control P-and S-waves in magnetorheological elastomers by applying an external magnetic field.

Acknowledgments

This research was supported by the ISRAEL SCIENCE FOUNDATION (grants 1550/15 and 1973/15). SR gratefully acknowledges the support of Taub Foundation through the Horev Fellowship – Leaders in Science and Technology.

Appendix A. Notation of tensor isomers

To achieve a more compact representation of the results, we have used the notation of isomers firstly introduced by Ryzhak (1993); Nikitin and Ryzhak (2008). Let $\mathcal{S}$ be a third-rank tensor with the following representation as the sum of a certain number of triads:

$$\mathcal{S} = \vec{a}_1 \otimes \vec{a}_2 \otimes \vec{a}_3 + \vec{b}_1 \otimes \vec{b}_2 \otimes \vec{b}_3 + \cdots \tag{A.1}$$

Let (ikj) be some permutation of the set (123). Then the isomer $\mathcal{S}^{(ikj)}$ is defined to be the third-rank tensor determined by the relation

$$\mathcal{S}^{(ikj)} = \vec{a}_i \otimes \vec{a}_k \otimes \vec{a}_j + \vec{b}_i \otimes \vec{b}_k \otimes \vec{b}_j + \cdots \tag{A.2}$$

Analogously, we can define isomers for higher-rank tensors. For example, if $\mathcal{S} = \vec{b} \otimes \mathbf{I}$, where $\vec{b}$ is an arbitrary vector and $\mathbf{I}$ is the unit tensor, then $\mathcal{S}^{(231)} = \mathcal{S}^{(321)} = \mathbf{I} \otimes \vec{b}$ and $\mathcal{S}^{(132)} = \mathcal{S}$. If $\mathbb{S} = \mathbf{M} \otimes \mathbf{N}$, where $\mathbf{N}$ and $\mathbf{M}$ are arbitrary second-rank tensors, then $\mathbb{S}^{(3412)} = \mathbf{N} \otimes \mathbf{M}$.

Appendix B. Components of the electroelastic moduli and generalized acoustic tensors

Here we introduce the following notations

$$\begin{aligned}
&L_{ab} = \vec{a} \cdot \mathbf{L} \cdot \vec{b}, L_{ab}^{(2)} = \vec{a} \cdot \mathbf{L}^2 \cdot \vec{b}, \mathbf{L}^2 = \mathbf{L} \cdot \mathbf{L},\\
&L_{ab}^{(-1)} = \vec{a} \cdot \mathbf{L}^{-1} \cdot \vec{b}, L_{ab}^{(-2)} = \vec{a} \cdot \mathbf{L}^{-2} \cdot \vec{b}, \mathbf{L}^{-2} = \mathbf{L}^{-1} \cdot \mathbf{L}^{-1},\\
&L_{ab}^{(3)} = \vec{a} \cdot \mathbf{L}^3 \cdot \vec{b}, \mathbf{L}^3 = \mathbf{L}^2 \cdot \mathbf{L}, L_{ab}^{(-3)} = \vec{a} \cdot \mathbf{L}^{-3} \cdot \vec{b},\\
&\mathbf{L}^{-3} = \mathbf{L}^{-2} \cdot \mathbf{L}^{-1}, \vec{a} \otimes \vec{b}^s = \frac{1}{2}\left(\vec{a} \otimes \vec{b} + \vec{b} \otimes \vec{a}\right),\\
&a_b = \vec{a} \cdot \vec{b}, a_b^2 = (a_b)^2,
\end{aligned} \tag{B.1}$$

where $\mathbf{L}$ is an arbitrary second-rank tensor, $\vec{a}$ and $\vec{b}$ are arbitrary vectors.

$$\begin{aligned}
\mathbb{C}_{4e} &= B_{DD}^{-1}(\mathbf{I} \otimes \mathbf{I} + \mathbf{I} \otimes \mathbf{I}^{(1342)}),\\
\mathbb{C}_{5e} &= 2(\vec{D} \otimes \mathbf{I} \otimes \vec{D}^{(2134)} - \vec{D} \otimes \vec{D} \otimes \mathbf{I} - \mathbf{I} \otimes \vec{D} \otimes \vec{D})
\end{aligned}$$

$$
\begin{aligned}
&+D_D(\mathbf{I}\otimes\mathbf{I}+\mathbf{I}\otimes\mathbf{I}^{(1342)}),\\
\mathbb{C}_{6e} = \;& 2(\vec{D}\otimes\mathbf{I}\otimes(\mathbf{B}\cdot\vec{D})^{(2134)}+\mathbf{B}\otimes\vec{D}\otimes\vec{D}^{(1432)}\\
&+\vec{D}\otimes\mathbf{B}\otimes\vec{D}^{(2134)}+(\mathbf{B}\cdot\vec{D})\otimes\mathbf{I}\otimes\vec{D}^{(2134)}\\
&+\vec{D}\otimes\vec{D}\otimes\mathbf{B}^{(1324)}+\vec{D}\otimes\mathbf{B}\otimes\vec{D}\\
&-\mathbf{I}\otimes(\mathbf{B}\cdot\vec{D})\otimes\vec{D}-\mathbf{I}\otimes\vec{D}\otimes(\mathbf{B}\cdot\vec{D})\\
&-\vec{D}\otimes(\mathbf{B}\cdot\vec{D})\otimes\mathbf{I}-(\mathbf{B}\cdot\vec{D})\otimes\vec{D}\otimes\mathbf{I})\\
&+B_{DD}(\mathbf{I}\otimes\mathbf{I}+\mathbf{I}\otimes\mathbf{I}^{(1342)}).
\end{aligned}
\tag{B.2}
$$

$$
\begin{aligned}
\mathbf{Q}_{4e} = \;& 2\,B_{DD}^{(-1)}\vec{n}\otimes\vec{n},\\
\mathbf{Q}_{5e} = \;& 2((D_D+D_n^2)\vec{n}\otimes\vec{n}+D_n^2\hat{\mathbf{I}}-2D_n\vec{D}\otimes\vec{n}^s),\\
\mathbf{Q}_{6e} = \;& 2((2B_{Dn}D_n+B_{DD})\vec{n}\otimes\vec{n}+2B_{Dn}D_n\hat{\mathbf{I}}\\
&-2B_{Dn}\vec{D}\otimes\vec{n}^s+D_n^2\mathbf{B}+2D_n(\mathbf{B}\cdot\vec{n})\otimes\vec{D}^s\\
&-2D_n(\mathbf{B}\cdot\vec{D})\otimes\vec{n}^s+B_{nn}\vec{D}\otimes\vec{D}).
\end{aligned}
\tag{B.3}
$$

$$
\begin{aligned}
\mathcal{M}_{4e} = \;& -2\mathbf{I}\otimes(\mathbf{B}^{-1}\cdot\vec{D}),\\
\mathcal{M}_{5e} = \;& 2(\vec{D}\otimes\mathbf{I}+\vec{D}\otimes\mathbf{I}^{(213)}-\mathbf{I}\otimes\vec{D}),\\
\mathcal{M}_{6e} = \;& 2(\vec{D}\otimes\mathbf{B}+\vec{D}\otimes\mathbf{B}^{(213)}+(\mathbf{B}\cdot\vec{D})\otimes\mathbf{I}\\
&+(\mathbf{B}\cdot\vec{D})\otimes\mathbf{I}^{(213)}-\mathbf{I}\otimes(\mathbf{B}\cdot\vec{D})).
\end{aligned}
\tag{B.4}
$$

$$
\begin{aligned}
\mathbf{R}_{4e} = \;& -2\vec{n}\otimes(\mathbf{B}^{-1}\cdot\vec{D}),\\
\mathbf{R}_{5e} = \;& 2(D_n\mathbf{I}+\vec{D}\otimes\vec{n}-\vec{n}\otimes\vec{D}),\\
\mathbf{R}_{6e} = \;& 2(D_n\mathbf{B}+\vec{D}\otimes(\mathbf{B}\cdot\vec{n})+B_{Dn}\mathbf{I}\\
&+(\mathbf{B}\cdot\vec{D})\otimes\vec{n}-\vec{n}\otimes(\mathbf{B}\cdot\vec{D})).
\end{aligned}
\tag{B.5}
$$

$$
\begin{aligned}
\eta = \;& \gamma_0^2\left(2B_{nn}^{(-2)}-\mathbf{B}^{-1}:\mathbf{B}^{-1}-(B_{nn}^{(-1)})^2\right)\\
&+\gamma_2^2\left(2B_{nn}^{(2)}-\mathbf{B}:\mathbf{B}-(B_{nn})^2\right)\\
&+\left(\gamma_0\left(\mathbf{I}:\mathbf{B}^{-1}-B_{nn}^{(-1)}\right)+\gamma_1\right)^2+(\gamma_2\beta+\gamma_1)^2\\
&+2\gamma_0\gamma_2\left((\mathbf{I}:\mathbf{B}^{-1})\beta-I_1B_{nn}^{(-1)}-1\right)
\end{aligned}
\tag{B.6}
$$

$$
\begin{aligned}
\mathbf{A}_e = \;& a_1\vec{n}\otimes\vec{n}+a_2\mathbf{I}+a_3\vec{D}\otimes\vec{D}+a_4\vec{n}\otimes\vec{D}^s+a_5\mathbf{B}+a_6(\mathbf{B}\cdot\vec{n})\otimes\vec{D}^s\\
&+a_7(\mathbf{B}\cdot\vec{D})\otimes\vec{n}^s+a_8(\mathbf{B}\cdot\vec{n})\otimes\vec{n}^s+a_9\mathbf{B}^2+a_{10}(\mathbf{B}^2\cdot\vec{n})\otimes\vec{D}^s\\
&+a_{11}(\mathbf{B}^2\cdot\vec{D})\otimes\vec{n}^s+a_{12}(\mathbf{B}^2\cdot\vec{n})\otimes\vec{n}^s+a_{13}(\mathbf{B}\cdot\vec{n})\otimes(\mathbf{B}\cdot\vec{n})\\
&+a_{14}\mathbf{B}^3+a_{15}(\mathbf{B}^3\cdot\vec{n})\otimes\vec{D}^s+a_{16}(\mathbf{B}^3\cdot\vec{D})\otimes\vec{n}^s\\
&+a_{17}(\mathbf{B}^2\cdot\vec{n})\otimes(\mathbf{B}\cdot\vec{n})^s+a_{18}\mathbf{B}^{-1}+a_{19}(\mathbf{B}^{-1}\cdot\vec{n})\otimes\vec{n}^s\\
&+a_{20}(\mathbf{B}^{-1}\cdot\vec{n})\otimes\vec{D}^s+a_{21}(\mathbf{B}^{-1}\cdot\vec{D})\otimes\vec{n}^s\\
&+a_{22}(\mathbf{B}^{-1}\cdot\vec{n})\otimes(\mathbf{B}\cdot\vec{n})^s+a_{23}(\mathbf{B}^{-2}\cdot\vec{D})\otimes\vec{n}^s,
\end{aligned}
\tag{B.7}
$$

where

$$
\begin{aligned}
a_1 = \;& \gamma_0^3\left(\left(B_{DD}^{(-2)}-(B_{Dn}^{(-1)})^2\right)\mathbf{I}:\mathbf{B}^{-1}-B_{nn}^{(-1)}B_{DD}^{(-2)}-B_{DD}^{(-3)}\right.\\
&\left.+2B_{Dn}^{(-1)}B_{Dn}^{(-2)}\right)+\gamma_1^3D_D\\
&+\gamma_2^3\left(\beta B_{DD}^{(2)}-B_{DD}^{(3)}\right)+2\gamma_0\gamma_1\gamma_2\left(\beta B_{DD}^{(-1)}+B_{Dn}B_{Dn}^{(-1)}\right.\\
&\left.+\beta_4B_{DD}-D_D\right)\\
&+\gamma_0\gamma_1^2\left(\beta_4D_D+B_{DD}^{(-1)}\right)+\gamma_0\gamma_2^2\left(\beta_4B_{DD}^{(2)}-3B_{DD}+2\beta D_D\right.\\
&\left.+2B_{Dn}^{(-1)}B_{Dn}^{(2)}\right)\\
&+\gamma_1\gamma_0^2\left(2\beta_4B_{DD}^{(-1)}-B_{DD}^{(-2)}+(B_{Dn}^{(-1)})^2\right)+\gamma_1\gamma_2^2\left(2\beta B_{DD}-B_{DD}^{(2)}\right)\\
&+\gamma_2\gamma_0^2\left(\beta B_{DD}^{(-2)}-3B_{DD}^{(-1)}+2\beta_4D_D+B_{Dn}^{(-1)}\left(2D_n-I_1B_{Dn}^{(-1)}\right)\right)\\
&+\gamma_2\gamma_1^2(\beta D_D+B_{DD}),\\
a_2 = \;& \gamma_1^3D_n^2+\gamma_2^3\beta(B_{Dn})^2+2\gamma_0\gamma_1\gamma_2D_n(\beta_4B_{Dn}-D_n)+\gamma_0\gamma_1^2\beta_4D_n^2\\
&+\gamma_0\gamma_2^2(\beta_4B_{Dn}-2D_n)B_{Dn}+\gamma_1\gamma_2^2B_{Dn}(B_{Dn}+2\beta D_n)\\
&+\gamma_2\gamma_1^2(\beta D_n+2B_{Dn})D_n,\\
a_3 = \;& \gamma_2^2\left(\gamma_2\left(I_1\left(B_{nn}^{(2)}-(B_{nn})^2\right)+B_{nn}B_{nn}^{(2)}-B_{nn}^{(3)}\right)\right.\\
&+\gamma_0\left(B_{nn}-B_{nn}^{(-1)}B_{nn}^{(2)}+(\mathbf{I}:\mathbf{B}^{-1})\left(B_{nn}^{(2)}-(B_{nn})^2\right)\right)\\
&\left.+\gamma_1\left(B_{nn}^{(2)}-(B_{nn})^2\right)\right),\\
a_4 = \;& 2\left(\gamma_0\gamma_1\gamma_2(D_n-2\beta_4B_{Dn})-\gamma_1^3D_n-\gamma_2^3\left(I_1B_{Dn}^{(2)}-B_{Dn}^{(3)}\right)\right.\\
&-\gamma_0\gamma_1^2\beta_4D_n\\
&+\gamma_0\gamma_2^2\left(3B_{Dn}-\beta_4B_{Dn}^{(2)}+I_1\left(B_{Dn}^{(-1)}B_{nn}-2D_n\right)\right.\\
&\left.+D_nB_{nn}-B_{Dn}^{(-1)}B_{nn}^{(2)}\right)+\gamma_1\gamma_2^2B_{Dn}(B_{nn}-2I_1)\\
&+\gamma_2\gamma_0^2\left(B_{nn}\left(B_{Dn}^{(-1)}(\mathbf{I}:\mathbf{B}^{-1})-B_{Dn}^{(-2)}\right)-2D_n\beta_4\right)\\
&\left.-\gamma_2\gamma_1^2(\beta D_n+2B_{Dn})\right),\\
a_5 = \;& \gamma_2\left(\gamma_2^2B_{Dn}(2D_n\beta-B_{Dn})+2\gamma_0\gamma_1\beta_4D_n^2\right.\\
&\left.+\gamma_0\gamma_2D_n(2\beta_4B_{Dn}-D_n)+2\gamma_1\gamma_2\beta D_n^2+\gamma_1^2D_n^2\right),
\end{aligned}
\tag{B.8}
$$

$$
\begin{aligned}
a_6 = \;& 2\gamma_2\left(\gamma_2^2\left(D_nB_{nn}^{(2)}+I_1(B_{Dn}-D_nB_{nn})\right)+\gamma_0\gamma_1\beta_4D_n\right.\\
&+\gamma_0\gamma_2\left((\mathbf{I}:\mathbf{B}^{-1})(B_{Dn}-D_nB_{nn})-B_{nn}^{(-1)}B_{Dn}\right)\\
&\left.+\gamma_1\gamma_2(B_{Dn}+\beta D_n)+\gamma_1^2D_n\right),\\
a_7 = \;& -2\gamma_2\left(\gamma_2^2\beta B_{Dn}+2\gamma_0\gamma_1\beta_4D_n+\gamma_0\gamma_2(\beta_4B_{Dn}-2D_n)\right.\\
&\left.+2\gamma_1\gamma_2\beta D_n+\gamma_1^2D_n\right),\\
a_8 = \;& 2\gamma_2\left(\gamma_0\gamma_2\left(B_{Dn}^{(-1)}(I_1D_n-B_{Dn})-D_n^2\right)\right.\\
&+D_n\left(\gamma_0^2\left(B_{Dn}^{(-1)}(\mathbf{I}:\mathbf{B}^{-1})-B_{Dn}^{(-2)}\right)-\gamma_2^2B_{Dn}^{(2)}\right.\\
&\left.\left.-\gamma_0\gamma_1B_{Dn}^{(-1)}-\gamma_1\gamma_2B_{Dn}\right)\right),\\
a_9 = \;& \gamma_2^2D_n(\gamma_2(\beta D_n-2B_{Dn})+D_n(\gamma_0\beta_4-\gamma_1)),\\
a_{10} = \;& 2\gamma_2^2(\gamma_2(I_1D_n-B_{Dn})+\gamma_0\beta_4D_n),\\
a_{11} = \;& 2\gamma_2^2(\gamma_2(B_{Dn}-\beta D_n)-D_n(\gamma_0\beta_4-\gamma_1)),\\
a_{12} = \;& -2\gamma_0\gamma_2^2D_nB_{Dn}^{(-1)},\\
a_{13} = \;& \gamma_2^2D_n\left(\gamma_2(2B_{Dn}-I_1D_n)+\gamma_1D_n-\gamma_0D_n(\mathbf{I}:\mathbf{B}^{-1})\right),\\
a_{14} = \;& -\gamma_2^3D_n^2,\ a_{15}=-2\gamma_2^3D_n,\ a_{16}=-a_{15},\ a_{17}=-2a_{14},\\
a_{18} = \;& -\gamma_0(\gamma_1D_n+\gamma_2B_{Dn})^2,\ a_{19}=-2\gamma_0^2B_{Dn}^{(-1)}(\gamma_1D_n+\gamma_2B_{Dn}),\\
a_{20} = \;& 2\gamma_0\gamma_2B_{nn}(\gamma_1D_n+\gamma_2B_{Dn}),\\
a_{21} = \;& 2\gamma_0(\gamma_2\gamma_0(D_n-\beta_4B_{Dn})-\gamma_2\beta(\gamma_1D_n+\gamma_2B_{Dn})-\gamma_1\gamma_0\beta_4D_n),\\
a_{22} = \;& 2\gamma_0\gamma_2D_n(\gamma_1D_n+\gamma_2B_{Dn}),\ a_{23}=2\gamma_0^2(\gamma_1D_n+\gamma_2B_{Dn}),\\
\beta = \;& I_1-B_{nn}\quad\text{and}\quad\beta_4=\mathbf{I}:\mathbf{B}^{-1}-B_{nn}^{(-1)}.
\end{aligned}
\tag{B.9}
$$

References

Aboudi, J., 2015. Micro-electromechanics of soft dielectric matrix composites. Int. J. Solids Struct. 64, 30–41.

Achenbach, J.D., 1973. Wave Propagation in Elastic Solids. Applied Mathematics and Mechanics. North-Holland Publishing Company.

Bar-Cohen, Y., 2002. Electroactive polymers as artificial muscles: A review. J. Spacecr. Rockets 39 (6), 822–827.

Bortot, E., Denzer, R., Menzel, A., Gei, M., 2016. Analysis of viscoelastic soft dielectric elastomer generators operating in an electrical circuit. Int. J. Solids Struct. 78-79, 205–215.

Brochu, P., Pei, Q., 2010. Advances in dielectric elastomers for actuators and artificial muscles. Macromol. Rapid Commun. 31 (1), 10–36.
Cao, C., Zhao, X., 2013. Tunable stiffness of electrorheological elastomers by designing mesostructures. Appl. Phys. Lett. 103, 041901.
Carpi, F., De Rossi, D., Kornbluh, R., Pelrine, R.E., Sommer-Larsen, P., 2011. Dielectric Elastomers as Electromechanical Transducers: Fundamentals, Materials, Devices, Models and Applications of an Emerging Electroactive Polymer Technology. Elsevier Science.
Chatzigeorgiou, G., Javili, A., Steinmann, P., 2015. Interface properties influence the effective dielectric constant of composites. Philos. Mag. 95 (28–30), 3402–3412.
Chen, W., Dai, H., 2012. Waves in pre-stretched incompressible soft electroactive cylinders: exact solution. Acta Mech. Solida Sinica 25 (5), 530–541.
Cohen, N., deBotton, G., 2014. Multiscale analysis of the electromechanical coupling in dielectric elastomers. Eur. J. Mech. A/Solids 48, 48–59.
Cohen, N., Menzel, A., deBotton, G., 2016. Towards a physics-based multiscale modelling of the electro-mechanical coupling in electro-active polymers. Proc. R. Soc. A 472, 20150462.
Destrade, M., Ogden, R.W., 2011. On magneto-acoustic waves in finitely deformed elastic solids. Math. Mech. Solids 16, 594–604.
Dorfmann, A., Ogden, R.W., 2005. Nonlinear electroelasticity. Acta Mech. 174, 167–183.
Dorfmann, A., Ogden, R.W., 2010. Electroelastic waves in a finitely deformed electroactive material. J. Appl. Math. 75, 603–636.
Galich, P.I., Rudykh, S., 2015a. Comment on "disentangling longitudinal and shear elastic waves by neo-hookean soft devices" [appl. phys. lett. 106, 161903 (2015)]. Appl. Phys. Lett. 107 (5), 056101.
Galich, P.I., Rudykh, S., 2015b. Influence of stiffening on elastic wave propagation in extremely deformed soft matter: from nearly incompressible to auxetic materials. Extreme Mech. Lett. 4, 156–161.
Galipeau, E., Rudykh, S., deBotton, G., Ponte Castañeda, P., 2014. Magnetoactive elastomers with periodic and random microstructures. Int. J. Solids Struct. 51, 3012–3024.
Gei, M., Colonnelli, S., Springhetti, R., 2014. The role of electrostriction on the stability of dielectric elastomer actuators. Int. J. Solids Struct. 51 (3–4), 848–860.
Gei, M., Roccabianca, S., Bacca, M., 2011. Controlling bandgap in electroactive polymer-based structures. IEEE/ASME Trans. Mechatron. 16 (1), 102–107.
Hossain, M., Vu, D.K., Steinmann, P., 2015. A comprehensive characterization of the electro-mechanically coupled properties of VHB 4910 polymer. Arch. Appl. Mech. 85 (4), 523–537.
Huang, C., Zhang, Q.M., deBotton, G., Bhattacharya, K., 2004. All-organic dielectric-percolative three-component composite materials with high electromechanical response. Appl. Phys. Lett. 84 (22), 4391–4393.
Itskov, M., Khiêm, V.N., 2014. A polyconvex anisotropic free energy function for electro-and magneto-rheological elastomers. Math. Mech. Solids 1081286514555140.
Jabareen, M., 2015. On the modeling of electromechanical coupling in electroactive polymers using the mixed finite element formulation. Procedia IUTAM 12, 105–115.
Keip, M.A., Steinmann, P., Schröder, J., 2014. Two-scale computational homogenization of electro-elasticity at finite strains. Comput. Methods Appl. Mech. Eng. 278, 62–79.
Kornbluh, R., Pelrine, R., Prahlad, H., Wong-Foy, A., McCoy, B., Kim, S., Eckerle, J., Low, T., 2012. From boots to buoys: Promises and challenges of dielectric elastomer energy harvesting. In: Lenore, R. (Ed.), Electroactivity in Polymeric Materials. Springer, US, pp. 67–93.
Li, B., Chen, H., Qiang, J., Hu, S., Zhu, Z., Wang, Y., 2011. Effect of mechanical pre-stretch on the stabilization of dielectric elastomer actuation. J. Phys. D Appl. Phys. 44 (15), 155301.
Madsen, F.B., Yu, L., Daugaard, A.E., Hvilsted, S., Skov, A.L., 2014. Silicone elastomers with high dielectric permittivity and high dielectric breakdown strength based on dipolar copolymers. Polymer 55 (24), 6212–6219.
Maugin, G.A., 1985. Nonlinear Electromechanical Effects and Applications, 1. World Scientific.
Miehe, C., Vallicotti, D., Zäh, D., 2015. Computational structural and material stability analysis in finite electro-elasto-statics of electro-active materials. Int. J. Numer. Methods Eng. 102 (10), 1605–1637.
Nikitin, L.V., Ryzhak, E.I., 2008. On stability and instability of a compressed block pressed to a smooth basement. Mech. Solids 43 (4), 558–570.
O'Halloran, A., O'Malley, F., McHugh, P., 2008. A review on dielectric elastomer actuators, technology, applications, and challenges. J. Appl. Phys. 104 (7), 071101.
Ogden, R.W., 1997. Non-Linear Elastic Deformations. Dover Publications, New York.
Pelrine, R., Kornbluh, R., Pei, Q., Joseph, J., 2000. High-speed electrically actuated elastomers with strain greater than 100. Science 287 (5454), 836–839.
Rogers, J.A., 2013. A Clear Advance in Soft Actuators. Science 341 (6149), 968–969.
Rudykh, S., Bertoldi, K., 2013. Stability of anisotropic magnetorheological elastomers in finite deformations: a micromechanical approach. J. Mech. Phys. Solids 61, 949–967.
Rudykh, S., Bhattacharya, K., deBotton, G., 2012. Snap-through actuation of thick-wall electroactive balloons. Int. J. Nonlinear Mech. 47, 206–209.
Rudykh, S., Bhattacharya, K., deBotton, G., 2014. Multiscale instabilities in soft heterogeneous dielectric elastomers. Proc. R. Soc. A 470, 20130618.
Rudykh, S., Boyce, M.C., 2014. Transforming wave propagation in layered media via instability-induced interfacial wrinkling. Phys. Rev. Lett. 112, 034301.
Rudykh, S., deBotton, G., 2011. Stability of anisotropic electroactive polymers with application to layered media. Z. Angew. Math. Phys. 62, 1131–1142.
Rudykh, S., Lewinstein, A., Uner, G., deBotton, G., 2013. Analysis of microstructural induced enhancement of electromechanical coupling in soft dielectrics. Appl. Phys. Lett. 102, 151905.
Ryzhak, E.I., 1993. On stable deformation of unstable materials in a rigid triaxial testing machine. J. Mech. Phys. Solids 41 (8), 1345–1356.
Sarvazyan, A., Rudnenko, O., Swanson, S., Fowlkes, J., Emelianov, S., 1998. Shear wave elasticity imaging: a new ultrasonic technology of medical diagnostics. Ultrasound Med. Biol. 24 (9), 1419–1435.
Shmuel, G., Gei, M., deBotton, G., 2012. The rayleigh-lamb wave propagation in dielectric elastomer layers subjected to large deformations. Int. J. Nonlinear Mech. 47 (2), 307–316.
Siboni, M.H., Avazmohammadi, R., Ponte-Castañeda, P., 2014. Electromechanical instabilities in fiber-constrained, dielectric-elastomer composites subjected to all-around dead-loading. Math. Mech. Solids 1081286514551501.
Spinelli, S.A., Lopez-Pamies, O., 2015. Some simple explicit results for the elastic dielectric properties and stability of layered composites. Int. J. Eng. Sci. 88, 15–28.
Suo, Z., 2010. Theory of dielectric elastomers. Acta Mech. Solida Sinica 23 (6), 549–578.
Suo, Z., Zhao, X., Greene, W.H., 2008. A nonlinear field theory of deformable dielectrics. J. Mech. Phys. Solids 56, 467–486.
Toupin, R.A., 1956. The elastic dielectric. J. Ration. Mech. Anal. 5, 849–915.
Toupin, R.A., 1963. A dynamical theory of elastic dielectrics. Int. J. Eng. Sci. 1, 101–126.
Volokh, K.Y., 2012. On electromechanical coupling in elastomers. J. Appl. Mech. 79 (4), 044507.
Wissler, M., Mazza, E., 2007. Electromechanical coupling in dielectric elastomer actuators. Sens. Actuators A Phys. 138 (2), 384–393.
Zhao, X., Hong, W., Suo, Z., 2007. Electromechanical hysteresis and coexistent states in dielectric elastomers. Phys. Rev. B 76, 134113.
Zhao, X., Suo, Z., 2008. Method to analyze programmable deformation of dielectric elastomer layers. Appl. Phys. Lett. 93, 251902.
Zhao, X., Suo, Z., 2010. Theory of dielectric elastomers capable of giant deformation of actuation. Phys. Rev. Lett. 104, 178302.

J. Mech. Phys. Solids 98 (2017) 390–410

Contents lists available at ScienceDirect

Journal of the Mechanics and Physics of Solids

journal homepage: www.elsevier.com/locate/jmps

Elastic wave propagation in finitely deformed layered materials

Pavel I. Galich[a], Nicholas X. Fang[b], Mary C. Boyce[c], Stephan Rudykh[a,*]

[a] Department of Aerospace Engineering, Technion – Israel Institute of Technology, Haifa 32000, Israel
[b] Department of Mechanical Engineering, Massachusetts Institute of Technology, Cambridge 02139-4307, MA, USA
[c] School of Engineering and Applied Science, Columbia University, New York 10027, USA

ARTICLE INFO

Keywords:
Layered materials
Elastic waves
Finite deformations
Band gaps
Phononic crystals

ABSTRACT

We analyze elastic wave propagation in highly deformable layered media with isotropic hyperelastic phases. Band gap structures are calculated for the periodic laminates undergoing large deformations. Compact explicit expressions for the phase and group velocities are derived for the long waves propagating in the finitely deformed composites. Elastic wave characteristics and band gaps are shown to be highly tunable by deformation. The influence of deformation on shear and pressure wave band gaps for materials with various composition and constituent properties are studied, finding advantageous compositions for producing highly tunable complete band gaps in low-frequency ranges. The shear wave band gaps are influenced through the deformation induced changes in effective material properties, whereas pressure wave band gaps are mostly influenced by deformation induced geometry changes. The wide shear wave band gaps are found in the laminates with small volume fractions of a soft phase embedded in a stiffer material; pressure wave band gaps of the low-frequency range appear in the laminates with thin highly compressible layers embedded in a nearly incompressible phase. Thus, by constructing composites with a small amount of a highly compressible phase, wide complete band gaps at the low-frequency range can be achieved; furthermore, these band gaps are shown to be highly tunable by deformation.

1. Introduction

Metamaterials have attracted considerable attention due to their unusual properties such as negative elastic moduli (Babaee et al., 2013), mass density (Brunet et al., 2013), and negative refractive index (Liu et al., 2011). *Soft* metamaterials, capable of large deformations, open promising opportunities for tuning and switching acoustic properties by deformation (Bertoldi and Boyce, 2008a; Rudykh and Boyce, 2014b; Babaee et al., 2016). Even relatively simple deformable homogeneous materials can exhibit switchable acoustic functionalities upon applied deformations (Galich and Rudykh, 2015a). Indeed, soft *microstructured* metamaterials possess even greater capability for transforming and tuning wave propagation by external stimuli, such as mechanical loading (Rudykh and Boyce, 2014b; Bertoldi and Boyce, 2008b), electric (Gei et al., 2011; Galich and Rudykh, 2016) or magnetic fields (Destrade and Ogden, 2011). Applied deformation can lead to a change in the internal geometry of a phononic crystal giving rise to formation and/or transformation of phononic band gaps (BGs) (Kushwaha et al., 1993, 1994; Tanaka et al., 2000; Hussein, 2009). Moreover, local material properties can also change as a result of inhomogeneous distribution of local deformation fields leading to local softening or stiffening (Galich and Rudykh, 2015b). In fact, these effects are of significant importance for understanding elastic wave phenomena in soft biological tissues that are frequently found in a deformed state due to growth or other

* Corresponding author.
E-mail address: rudykh@technion.ac.il (S. Rudykh).

http://dx.doi.org/10.1016/j.jmps.2016.10.002
Received 4 July 2016; Received in revised form 27 September 2016; Accepted 6 October 2016
Available online 11 October 2016

biological processes. Large deformations together with material heterogeneity may give rise to elastic instabilities (Bertoldi et al., 2008; Rudykh and deBotton, 2012; Li et al., 2013; Slesarenko and Rudykh, 2016) – a phenomenon actively used in material design by nature (Crosby, 2010). Recently, this approach has been employed to utilize instability-induced dramatic microstructure transformations and achieve remarkable tunability of acoustic metamaterials (Bertoldi and Boyce, 2008a; Rudykh and Boyce, 2014b; Babaee et al., 2016). Inspired by possible applications – such as noise reducers, acoustic mirrors and filters, waveguides, to name a few – a number of recent works were dedicated to the analysis of influence of material parameters (Zhou et al., 2009), topologies (Mousanezhad et al., 2015), deformations (Bertoldi and Boyce, 2008a), and stiffening effects (Wang et al., 2013) on elastic wave propagation and band gap structure in various phononic crystals. Nevertheless, realization of the complex microstructures remains challenging, especially, at small length-scales desirable for some applications. Recent advances in additive and layer-by-layer material manufacturing allow fabrication of highly structured layered materials ranging from sub-light-wavelength scale (Kolle et al., 2013) to meso-length-scale (Li et al., 2013; Rudykh et al., 2015). These layered materials can produce complete phononic BGs – the frequency ranges where neither pressure nor shear waves can propagate – spanning different frequency ranges depending on the characteristic microstructure size. Moreover, these BGs can be further actively controlled by deformation. In this work, we specifically focus on identifying the key parameters defining the appearance of shear wave, pressure wave, and complete BGs in finitely deformed layered composites with isotropic phases. Special attention is given to the influence of deformation on the acoustic characteristics and BGs.

The layered media exhibit both geometrical and material non-linearities when subjected to finite strains; hence, these non-linear effects need to be taken into account in the model. To this end, we first obtain the solution for the finitely deformed state of hyperelastic periodic layered materials, and then perform the wave propagation analysis in terms of the incremental small amplitude motions *superimposed* on the finitely deformed state. By utilizing an exact analytical solution for the finitely deformed incompressible laminates with alternating isotropic hyperelastic phases, we derive explicit relations for the phase and group velocities in finitely deformed incompressible laminates in the long wave limit. Moreover, based on the expressions of the phase velocities for finitely deformed compressible homogeneous materials, we estimate the phase velocities of pressure and shear waves propagating perpendicular to the layers in finitely deformed laminates comprised of *compressible* phases. Next, considering steady-state plane waves in layered media, we thoroughly analyze band gap structures for shear and pressure waves propagating perpendicular to the layers in soft laminates with nearly incompressible and highly compressible phases. We show that wide shear wave BGs at the low-frequency range can be achieved by constructing laminates with thin soft layers embedded in a stiffer matrix. Moreover, these band gaps can be further tuned by deformation through the change in the geometry and effective properties of the phases. We find that for layers with pronounced stiffening effects (such as Gent materials), the change in the material effective properties prevails over the change in the geometry. However, for the materials with weak stiffening effects (such as neo-Hookean materials) the deformation induced change in the material properties is entirely compensated by the change in the geometry. We find that wide pressure wave BGs at the low-frequency range are attainable in laminates with small amount of highly compressible phase embedded in a nearly incompressible matrix. These pressure wave BGs are highly tunable by deformation. The laminate geometry change induced by deformation is shown to be the dominant factor influencing pressure wave BGs (as compared to the influence of the change in the effective material properties). Consequently, wide *complete* BGs at low-frequency range can be achieved by including a small amount of thin highly compressible phase into a nearly incompressible matrix. Furthermore, these complete BGs can be widened and shifted via deformation.

2. Theoretical background

Consider a continuum body and identify each point in the undeformed configuration with its position vector $\mathbf{X}$. When the body is deformed, the new location of a point is defined by mapping function $\mathbf{x} = \boldsymbol{\chi}(\mathbf{X}, t)$. Thus, the deformation gradient is $\mathbf{F} = \partial\mathbf{x}/\partial\mathbf{X}$, and its determinant $J \equiv \det\mathbf{F} > 0$. For a hyperelastic material whose constitutive behavior is described in terms of a strain energy function $\psi(\mathbf{F})$, the first Piola–Kirchhoff stress tensor is given by

$$\mathbf{P} = \frac{\partial\psi(\mathbf{F})}{\partial\mathbf{F}}. \tag{1}$$

The corresponding true or Cauchy stress tensor is related to the first Piola–Kirchhoff stress tensor via the relation $\boldsymbol{\sigma} = J^{-1}\mathbf{P}\mathbf{F}^T$. In the absence of body forces the equations of motion can be written in the undeformed configuration as

$$\mathrm{Div}\,\mathbf{P} = \rho_0\frac{D^2\boldsymbol{\chi}}{Dt^2}, \tag{2}$$

where ρ_0 is the initial density of the material, and the $D^2(\bullet)/Dt^2$ operator represents the material time derivative. If the deformation is applied quasi-statically, the right hand part of Eq. (2) can be assumed to be zero, and the equilibrium equation is obtained, namely

$$\mathrm{Div}\,\mathbf{P} = 0. \tag{3}$$

2.1. Wave propagation in homogeneous media

Consider next small amplitude motions[1] superimposed on the equilibrium state. The equations of the incremental motions are

$$\text{Div}\,\mathbf{P} = \rho_0 \frac{D^2\mathbf{u}}{Dt^2}, \tag{4}$$

where $\dot{\mathbf{P}}$ is an incremental change in the first Piola–Kirchhoff stress tensor and $\mathbf{u}$ is the incremental displacement. The incremental change in the deformation gradient is $\dot{\mathbf{F}} = \text{Grad}\,\mathbf{u}$.

The linearized constitutive law can be written as

$$\dot{P}_{ij} = \mathcal{A}_{0ijkl}\dot{F}_{kl} \tag{5}$$

with the tensor of elastic moduli defined as $\mathcal{A}_{0i\alpha k\beta} = \partial^2\psi/\partial F_{i\alpha}\partial F_{k\beta}$. Under substitution of Eq. (5) into Eq. (4) the incremental motion equation takes the form of

$$\mathcal{A}_{0ijkl}u_{k,lj} = \rho_0 \frac{D^2u_i}{Dt^2}. \tag{6}$$

To analyze small amplitude motions superimposed on a finite deformation, we present (6) in the updated Lagrangian formulation

$$\mathcal{A}_{ijkl}u_{k,lj} = \rho\frac{\partial^2 u_i}{\partial t^2}, \tag{7}$$

where $\mathcal{A}_{iqkp} = J^{-1}\mathcal{A}_{0ijkl}F_{pl}F_{qj}$ and $\rho = J^{-1}\rho_0$ is the density of the deformed material.

We seek a solution for Eq. (7) in the form of the plane waves with constant polarization

$$\mathbf{u} = \mathbf{g}h(\mathbf{n}\cdot\mathbf{x} - ct), \tag{8}$$

where h is a twice continuously differentiable function and unit vector $\mathbf{g}$ is the polarization; the unit vector $\mathbf{n}$ defines the direction of propagation of the wave, and c is the phase velocity of the wave.

By substitution of (8) into (7), we obtain

$$\mathbf{Q}(\mathbf{n})\cdot\mathbf{g} = \rho c^2\mathbf{g}, \tag{9}$$

where

$$Q_{ij} = \mathcal{A}_{ijkl}n_j n_l \tag{10}$$

is the acoustic tensor which defines the condition of propagation of the infinitesimal plane waves.

For incompressible materials $J = 1$ and $\mathbf{g}\cdot\mathbf{n} = 0$, and Eq. (9) reads as

$$\widehat{\mathbf{Q}}(\mathbf{n})\cdot\mathbf{g} = \rho c^2\mathbf{g}, \tag{11}$$

where $\widehat{\mathbf{Q}} = \hat{\mathbf{I}}\cdot\mathbf{Q}\cdot\hat{\mathbf{I}}$ and $\hat{\mathbf{I}} = \mathbf{I} - \mathbf{n}\otimes\mathbf{n}$ is the projection on the plane normal to $\mathbf{n}$.

2.2. Wave propagation in periodic layered media

Consider periodic laminates constructed of two alternating phases with initial volume fractions v_a and $v_b = 1 - v_a$. Here and thereafter, the fields and parameters of the constituents are denoted by subscripts $(\bullet)_a$ and $(\bullet)_b$, respectively. Geometrically, the layers are characterized by their thicknesses $d_a^o = v_a d^o$ and $d_b^o = v_b d^o$, where d^o is the initial period of the laminate (see Fig. 1(a)).

When laminates are deformed (see Fig. 1(b)), the layer thicknesses change as follows:

$$d_a = \lambda_{1a}d_a^o, \quad d_b = \lambda_{1b}d_b^o, \quad \text{and} \quad d = \overline{\lambda}_1 d^o, \tag{12}$$

where $\overline{\lambda}_1 = v_a\lambda_{1a} + v_b\lambda_{1b}$; $\lambda_{1a,b}$ are the stretch ratios in the direction $\mathbf{e}_1$ for phases a and b, respectively.

Let us consider steady-state compression small amplitude plane waves superimposed on a finitely deformed state and propagating along the x direction orthogonal to the interface between the layers (Bedford and Drumheller, 1994) (see Fig. 1(b) and (c)). For each layer, the one-dimensional wave equation takes the form

$$\frac{\partial^2 u_\xi}{\partial t^2} = c_\xi^2\frac{\partial^2 u_\xi}{\partial x^2}, \tag{13}$$

where u_ξ denotes the displacement in x direction, and subscript ξ stands for a or b. We seek a solution within each layer in the following form[2]:

$$u_\xi = A_\xi e^{i(k_\xi x - \omega t)} + B_\xi e^{i(-k_\xi x - \omega t)}, \tag{14}$$

where ω denotes the angular frequency, and $k_\xi = \omega/c_\xi$ is the wave number. The normal stress within each layer is

[1] Note that we consider only small amplitude elastic waves (Ogden, 1997); the amplitudes of the superimposed on finite deformations displacements of the material points are assumed to be much (infinitesimally) smaller than any characteristic dimension of the composite, $|\mathbf{u}|/d \ll 1$; so that its geometry and the constitutive properties of the material (such as density and tangent elastic moduli) at each point of the composite are assumed to be unchanged by these small amplitude motions.

[2] Note that we consider only small amplitude elastic waves here, i.e. $u_\xi/d \ll 1$.

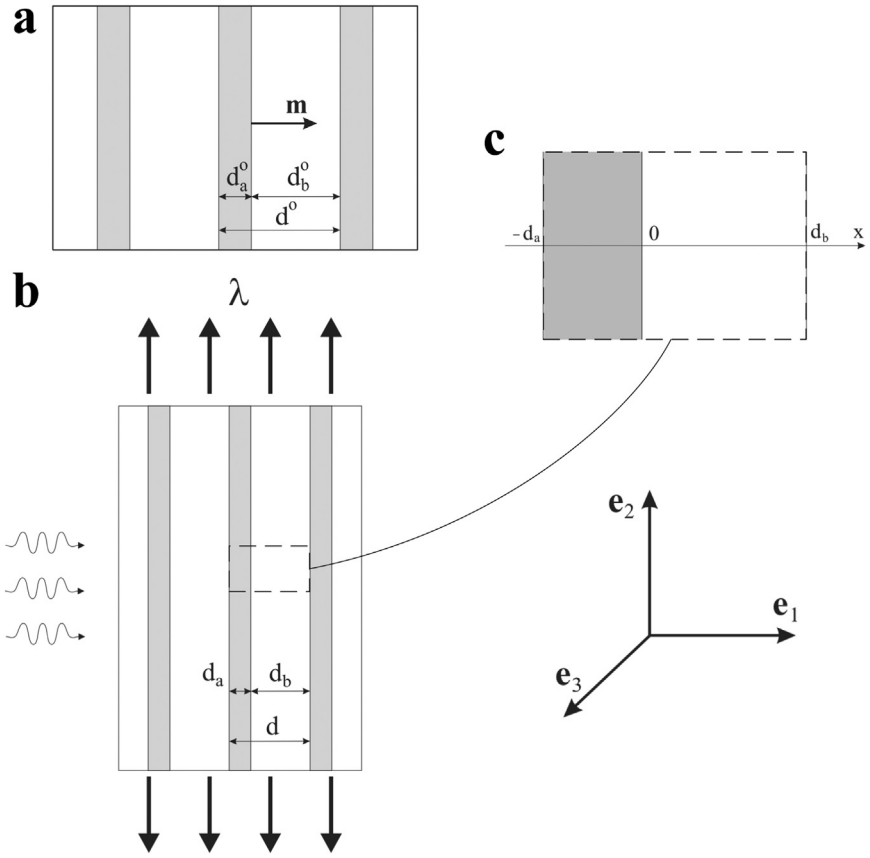

Fig. 1. Schematic representation of the undeformed (a) and deformed (b) periodic layered material with alternating phases a and b. A unit cell (c); ($\mathbf{e}_1$, $\mathbf{e}_2$, $\mathbf{e}_3$) is the orthonormal basis.

$$\sigma_\xi = \rho_\xi c_\xi^2 \frac{\partial u_\xi}{\partial x} = \frac{z_\xi^2}{\rho_\xi}\frac{\partial u_\xi}{\partial x}, \tag{15}$$

where $z_\xi = \rho_\xi c_\xi$ is the acoustic impedance.

The interface continuity condition between the layers implies

$$u_a(0,t) = u_b(0,t) \quad \text{and} \quad \sigma_a(0,t) = \sigma_b(0,t), \tag{16}$$

where we assign $x = 0$ to be the interface between the layers of the unit cell (Fig. 1(c)).

Two additional conditions are obtained from the periodicity of the material by the use of Floquet theorem. For this reason we adjust Eq. (14) to be the steady-state wave expression with the same wave number k for both materials

$$u_\xi = U_\xi(x) e^{i(kx-\omega t)}, \tag{17}$$

where

$$U_\xi(x) = A_\xi e^{iK_\xi^- x} + B_\xi e^{-iK_\xi^+ x} \quad \text{and} \quad K_\xi^\pm = k_\xi \pm k. \tag{18}$$

According to Floquet theorem, function $U_\xi(x)$ must be periodic functions of x with the period equal to the length of the unit cell, namely $d = d_a + d_b$,

$$U_a(-d_a) = U_b(d_b). \tag{19}$$

The corresponding relations for the stress are

$$\sigma_\xi = \Sigma_\xi(x) e^{i(kx-\omega t)}, \tag{20}$$

where

$$\Sigma_\xi(x) = i z_\xi \omega (A_\xi e^{iK_\xi^- x} - B_\xi e^{-iK_\xi^+ x}) \tag{21}$$

and

$$\Sigma_a(-d_a) = \Sigma_b(d_b). \tag{22}$$

Thus, Eqs. (16), (19) and (22) together with (17), (18), (20) and (21) yield the dispersion relation $\omega = \omega(k)$ for the steady-state wave (Rytov, 1956)

$$\cos kd = \cos\left(\frac{\omega d_a}{c_a}\right)\cos\left(\frac{\omega d_b}{c_b}\right) - \frac{1}{2}\left(\frac{z_a}{z_b} + \frac{z_b}{z_a}\right)\sin\left(\frac{\omega d_a}{c_a}\right)\sin\left(\frac{\omega d_b}{c_b}\right). \tag{23}$$

The dispersion relation (23) is derived for pressure waves. However, the same expression can be obtained for shear waves by considering displacements perpendicular to axis x in Eq. (13). In this case, the phase velocities of shear waves are used in (23) to obtain the dispersion relation for shear waves.

3. Results

The macroscopically applied loading is expressed in terms of the average deformation gradient

$$\overline{\mathbf{F}} = v_a\mathbf{F}_a + v_b\mathbf{F}_b, \tag{24}$$

where $\mathbf{F}_a$ and $\mathbf{F}_b$ are the corresponding deformation gradients within each phase. The displacement continuity condition along the interface between the layers yields the condition for $\mathbf{F}_a$ and $\mathbf{F}_b$

$$(\mathbf{F}_a - \mathbf{F}_b)\cdot\mathbf{q} = \mathbf{0} \tag{25}$$

and the interface stress jump condition is

$$(\mathbf{P}_a - \mathbf{P}_b)\cdot\mathbf{m} = \mathbf{0}, \tag{26}$$

where unit vector $\mathbf{m}$ denotes the initial lamination direction (see Fig. 1(a)), $\mathbf{q}$ is an arbitrary unit vector orthogonal to $\mathbf{m}$.

Loading paths. Although the analysis is general and can be applied for materials subjected to any deformation $\overline{\mathbf{F}}$, the examples are given for (i) in-plane and (ii) equibiaxial deformations. The corresponding macroscopic deformation gradients are

(i) *in-plane tension*

$$\overline{\mathbf{F}} = \overline{\lambda}_1\mathbf{e}_1 \otimes \mathbf{e}_1 + \lambda\mathbf{e}_2 \otimes \mathbf{e}_2 + \mathbf{e}_3 \otimes \mathbf{e}_3, \tag{27}$$

(ii) *equibiaxial deformation*

$$\overline{\mathbf{F}} = \overline{\lambda}_1\mathbf{e}_1 \otimes \mathbf{e}_1 + \lambda(\mathbf{I} - \mathbf{e}_1 \otimes \mathbf{e}_1), \tag{28}$$

where λ is the applied stretch in the direction of the layers (see Fig. 1), and $\overline{\lambda}_1$ is an unknown and needs to be calculated. For an incompressible laminate $\overline{\lambda}_1 = \lambda^{-1}$ and $\overline{\lambda}_1 = \lambda^{-2}$ for in-plane and equibiaxial deformations, respectively. To describe the behavior of *incompressible* phases, we utilize the neo-Hookean strain energy function (Ogden, 1997)

$$\psi_\xi^{inc} = \frac{\mu_\xi}{2}(\mathbf{F}_\xi\colon \mathbf{F}_\xi - 3), \tag{29}$$

where μ_ξ is the initial shear modulus.

The constitutive behavior of the *compressible* phases is assumed to be governed by the extended neo-Hookean strain energy function (Ogden, 1997)

$$\psi_\xi^{comp} = \frac{\mu_\xi}{2}(\mathbf{F}_\xi\colon \mathbf{F}_\xi - 3) - \mu_\xi \ln J_\xi + \frac{\Lambda_\xi}{2}(J_\xi - 1)^2, \tag{30}$$

where Λ_ξ is the first Lame's parameter. Recall that Λ relates to the bulk modulus as $K = \Lambda + 2\mu/3$.

By making use of strain energy function (30) together with (25) and (26), the unknown stretch ratios λ_{1a} and λ_{1b} are determined. In particular, the explicit expressions are

(i) *in-plane tension*

$$\lambda_{1a} = \frac{\eta_a\lambda\gamma + \sqrt{2(4 + \eta_a(4 + \eta_a)\lambda^2)(2 + \eta_b\lambda(\gamma + 2\lambda))}}{2(1 + \eta_a\lambda^2)\gamma} \quad \text{and} \quad \lambda_{1b} = \frac{\gamma}{2(1 + \eta_b\lambda^2)}, \tag{31}$$

where $\eta_a = \Lambda_a/\mu_a$, $\eta_b = \Lambda_b/\mu_b$, and $\gamma = \eta_b\lambda + \sqrt{4 + \eta_b(4 + \eta_b)\lambda^2}$;

(ii) *equibiaxial deformation*

$$\lambda_{1a} = \frac{\eta_a\lambda^2\zeta + \sqrt{2(4 + \eta_a(4 + \eta_a)\lambda^4)(2 + \eta_b\lambda^2(\zeta + 2\lambda^2))}}{2(1 + \eta_a\lambda^4)\zeta} \quad \text{and} \quad \lambda_{1b} = \frac{\zeta}{2(1 + \eta_b\lambda^4)}, \tag{32}$$

where $\zeta = \eta_b\lambda^2 + \sqrt{4 + \eta_b(4 + \eta_b)\lambda^4}$.

To account for the stiffening effects (for example, due to a finite extensibility of polymer chains) in finitely deformed incompressible laminates, we employ the strain-energy density function corresponding to an approximation of the Arruda–Boyce model (Arruda and Boyce, 1993), namely the Gent model (Gent, 1996)

$$\psi_\xi^{inc} = -\frac{\mu_\xi J_{m\xi}}{2}\ln\left(1 - \frac{\mathbf{F}_\xi\colon \mathbf{F}_\xi - 3}{J_{m\xi}}\right), \tag{33}$$

where $J_{m\xi}$ is the so-called dimensionless locking parameter defining the lock-up stretch ratio, such that in the limit $(\mathbf{F}_\xi\colon \mathbf{F}_\xi - 3) \to J_{m\xi}$, the strain energy becomes unbounded. Thus, for incompressible Gent materials under in-plane tension, the lock-up stretch ratios can be calculated as

$$\lambda_\xi^{lock} = (\sqrt{J_{m\xi} + 4} \pm \sqrt{J_{m\xi}})/2, \tag{34}$$

where "+" and "−" correspond to the extension ($\lambda > 1$) and contraction ($\lambda < 1$), respectively. Clearly, in the limit $J_m \to \infty$, the strain-energy function (33) reduces to the neo-Hookean material model (29).

The constitutive behavior of the *compressible* phases exhibiting strong stiffening is assumed to be governed by the extended Gent strain energy function (Horgan and Saccomandi, 2004; Wang et al., 2013)

$$\psi_\xi^{comp} = -\frac{\mu_\xi J_{m\xi}}{2}\ln\left(1 - \frac{\mathbf{F}_\xi\colon \mathbf{F}_\xi - 3}{J_{m\xi}}\right) - \mu_\xi \ln J_\xi + \left(\frac{\Lambda_\xi}{2} - \frac{\mu_\xi}{J_{m\xi}}\right)(J_\xi - 1)^2, \tag{35}$$

Again, in the limit $J_m \to \infty$, the strain-energy function (35) reduces to the extended neo-Hookean material model (30).

3.1. Long wave estimates for finitely deformed layered materials

3.1.1. Incompressible laminates

First, let us consider layered materials with *incompressible* phases. The incompressibility assumption allows us to obtain a closed form exact solution for finitely deformed periodic layered materials with neo-Hookean phases (deBotton, 2005; Tzianetopoulou, 2007; Rudykh and Boyce, 2014a; Spinelli and Lopez-Pamies, 2015). By utilizing the exact analytical solution, an effective strain energy function can be constructed (Spinelli and Lopez-Pamies, 2015)

$$\psi(\overline{\mathbf{F}}) = \frac{\overline{\mu}}{2}(\overline{\mathbf{F}}\colon \overline{\mathbf{F}} - 3) - \frac{\overline{\mu} - \breve{\mu}}{2}\left(\mathbf{m}\cdot\overline{\mathbf{C}}\cdot\mathbf{m} - \frac{1}{\mathbf{m}\cdot\overline{\mathbf{C}}^{-1}\cdot\mathbf{m}}\right), \tag{36}$$

where $\overline{\mathbf{C}} = \overline{\mathbf{F}}^T\cdot\overline{\mathbf{F}}$ is the average right Cauchy–Green deformation tensor, and

$$\overline{\mu} = v_a\mu_a + v_b\mu_b \quad \text{and} \quad \breve{\mu} = \left(\frac{v_a}{\mu_a} + \frac{v_b}{\mu_b}\right)^{-1}. \tag{37}$$

Note that while the solution for finitely deformed laminates is provided in deBotton (2005), Tzianetopoulou (2007), Rudykh and Boyce (2014a), Spinelli and Lopez-Pamies (2015), the strain energy function in the form of (36) is reported by Spinelli and Lopez-Pamies (2015).

The acoustic tensor (11) corresponding to the strain energy function (36), takes the form

$$\widehat{\mathbf{Q}}(\mathbf{n}, \overline{\mathbf{F}}) = q_1\hat{\mathbf{I}} + q_2(\hat{\mathbf{I}}\cdot\overline{\mathbf{F}}^{-T}\cdot\mathbf{m}) \otimes (\hat{\mathbf{I}}\cdot\overline{\mathbf{F}}^{-T}\cdot\mathbf{m}), \tag{38}$$

where

$$q_1 = \overline{\mu}(\mathbf{n}\cdot\overline{\mathbf{B}}\cdot\mathbf{n}) + (\breve{\mu} - \overline{\mu})(\mathbf{n}\cdot\overline{\mathbf{F}}\cdot\mathbf{m})^2 \quad \text{and} \quad q_2 = \frac{\overline{\mu} - \breve{\mu}}{\alpha^2}\left(\frac{4\beta^2}{\alpha} - 1\right), \tag{39}$$

where $\overline{\mathbf{B}} = \overline{\mathbf{F}}\cdot\overline{\mathbf{F}}^T$ is the average left Cauchy–Green deformation tensor, $\alpha = \mathbf{m}\cdot\overline{\mathbf{C}}^{-1}\cdot\mathbf{m}$, and $\beta = \mathbf{n}\cdot\overline{\mathbf{F}}^{-T}\cdot\mathbf{m}$. One can show that the acoustic tensor (38) has the following eigenvalues in the two-dimensional space normal to $\mathbf{n}$:

$$a_1 = q_1 \quad \text{and} \quad a_2 = q_1 + q_2(\alpha - \beta^2). \tag{40}$$

In general, we have two distinct shear waves propagating in the finitely deformed incompressible laminate. The corresponding phase velocities are

$$\overline{c}_{sw}^{(1)} = \sqrt{a_1/\overline{\rho}_0} \quad \text{and} \quad \overline{c}_{sw}^{(2)} = \sqrt{a_2/\overline{\rho}_0}, \tag{41}$$

where $\overline{\rho}_0 = v_a\rho_{0a} + v_b\rho_{0b}$ is the average initial density of the laminate.

Note that the phase velocities of shear waves (41) coincide only for special cases of applied deformation and direction of wave propagation. For instance, for wave propagating perpendicular to the layers, i.e. $\mathbf{n} = \mathbf{m} = \mathbf{e}_1$, the phase velocities of shear waves coincide:

(i) *in-plane tension*

$$\overline{c}_{sw} = \overline{c}_{sw}^{(1)} = \overline{c}_{sw}^{(2)} = \lambda^{-1}\sqrt{\breve{\mu}/\overline{\rho}_0}, \tag{42}$$

(ii) *equibiaxial deformation*

$$\overline{c}_{sw} = \overline{c}_{sw}^{(1)} = \overline{c}_{sw}^{(2)} = \lambda^{-2}\sqrt{\breve{\mu}/\overline{\rho}_0}. \tag{43}$$

However, if the wave propagates along the layers, i.e. $\mathbf{m} = \mathbf{e}_1$ and $\mathbf{n} = \mathbf{e}_2$, the phase velocities of shear waves are distinct:
(i) *in-plane tension*

$$\overline{c}_{sw}^{(1)} = \lambda\sqrt{\overline{\mu}/\overline{\rho}_0} \quad (\mathbf{g} = \mathbf{e}_3) \tag{44}$$

and

$$\overline{c}_{sw}^{(2)} = \lambda^{-1}\sqrt{(\breve{\mu} + (\lambda^4 - 1)\overline{\mu})/\overline{\rho}_0} \quad (\mathbf{g} = \mathbf{e}_1), \tag{45}$$

(ii) *equibiaxial deformation*

$$\overline{c}_{sw}^{(1)} = \lambda\sqrt{\overline{\mu}/\overline{\rho}_0} \quad (\mathbf{g} = \mathbf{e}_3) \tag{46}$$

and

$$\overline{c}_{sw}^{(2)} = \lambda^{-2}\sqrt{(\breve{\mu} + (\lambda^6 - 1)\overline{\mu})/\overline{\rho}_0} \quad (\mathbf{g} = \mathbf{e}_1). \tag{47}$$

Note that expressions (45) and (47) yield explicit expressions for the critical stretch ratios corresponding to the onset of macroscopic instability under in-plane and equibiaxial contractions:
(i) *in-plane tension*

$$\lambda_{cr}^{pt} = \left(1 - \frac{\breve{\mu}}{\overline{\mu}}\right)^{1/4}, \tag{48}$$

(ii) *equibiaxial deformation*

$$\lambda_{cr}^{bt} = \left(1 - \frac{\breve{\mu}}{\overline{\mu}}\right)^{1/6}. \tag{49}$$

It is worth mentioning that Eq. (48) agrees with the results obtained by Rosen (1965), and Triantafyllidis and Maker (1985) utilizing distinct approaches.

To illustrate the influence of the deformation and direction of wave propagation on the elastic waves in the layered materials, we construct slowness curves (which are commonly used in acoustics, Auld, 1990) by the use of the explicit relations (41). Fig. 2 shows examples of the slowness curves $\overline{s}_{sw}(\varphi) = 1/\overline{c}_{sw}(\varphi)$ for (a) out-of-plane (with polarization $\mathbf{e}_3$) and (b) in-plane (with polarization lying in plane $\mathbf{e}_1 - \mathbf{e}_2$) shear waves in layered material undergoing equibiaxial deformation, where the direction of propagation is defined as $\mathbf{n} = (\cos\varphi, \sin\varphi, 0)$. Note that the critical stretch ratio for the laminate with $\nu_a = 0.1$ and $\mu_a/\mu_b = 20$ undergoing equibiaxial contraction is $\lambda_{cr}^{bt} = 0.92$; therefore, we present slowness curves corresponding to the equibiaxially contracted laminate ($\lambda = 0.95$) in the macroscopically stable state. The slowness curves clearly indicate the significant influence of the applied deformation on the wave propagation. Specifically, an extension results in a decrease of the phase velocities of the shear waves propagating perpendicular to the layers; while the phase velocities increase for waves propagating along the layers since these directions experience extension. The phase velocity of the in-plane shear wave in the equibiaxially deformed laminate has maxima for certain directions of wave

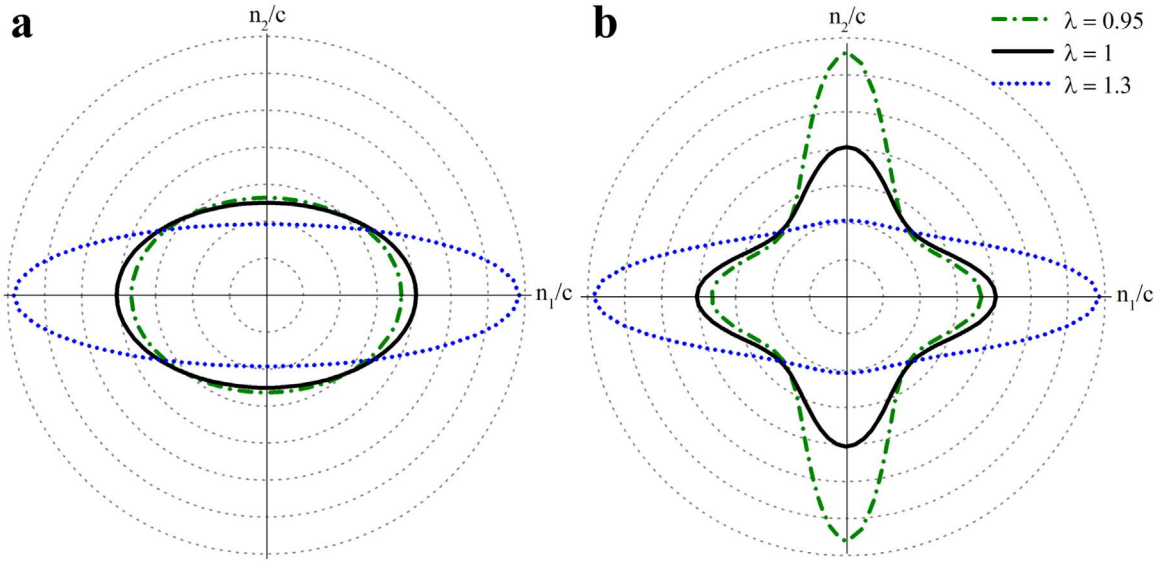

Fig. 2. Slowness curves for (a) out-of-plane and (b) in-plane shear waves propagating in the laminate with $\nu_a = 0.1$, $\mu_a/\mu_b = 20$, and $\rho_{0a}/\rho_{0b} = 1$ under equibiaxial deformation. Scale is 0.4 per division, and the slownesses are normalized by $\sqrt{\overline{\mu}/\overline{\rho}_0}$.

propagation (see Fig. 2(b)). In particular, these directions are expressed as

$$\varphi_0 = \pm\frac{1}{2}\arccos\left(\frac{1-\lambda^6}{4\left(1-\frac{\breve{\mu}}{\overline{\mu}}\right)}\right)+\pi z, \quad z=0,\,1. \tag{50}$$

In the undeformed state, $\varphi_0 = \pm\frac{\pi}{4}, \pm\frac{3\pi}{4}$. Moreover, these directions differ from the principal directions in contrast to the out-of-plane shear wave – the phase velocity of which has maxima in the directions of the principal axes. For example, in the equibiaxially deformed laminate the phase velocity of the out-of-plane shear wave is maximal for the wave propagation along the layers, i.e. for $\mathbf{n} = \pm\mathbf{e}_2$ (see Fig. 2(a)). Note that in the undeformed state the phase velocity of the in-plane shear wave is the same for wave propagation along and perpendicular to the layers, namely Eq. $(41)_2$ yields

$$\overline{c}_{sw}^{(2)} = \sqrt{\breve{\mu}/\overline{\rho}_0}\,. \tag{51}$$

The dispersion relations for long waves in the incompressible laminates are derived from (41)

$$\overline{\omega}_{sw}^{(1)} = \sqrt{b_1/\overline{\rho}_0} \quad \text{and} \quad \overline{\omega}_{sw}^{(2)} = \sqrt{b_2/\overline{\rho}_0} \tag{52}$$

where

$$b_1 = \overline{\mu}\,(\mathbf{k}\cdot\overline{\mathbf{B}}\cdot\mathbf{k}) + (\breve{\mu}-\overline{\mu})(\mathbf{k}\cdot\overline{\mathbf{F}}\cdot\mathbf{m})^2 \quad \text{and} \quad b_2 = b_1 + \frac{\overline{\mu}-\breve{\mu}}{\alpha^2}\left(\frac{4\beta_k^2}{\alpha}-k^2\right)\left(\alpha-\frac{\beta_k^2}{k^2}\right), \tag{53}$$

where $\mathbf{k}$ is the wave vector, $k = |\mathbf{k}|$ is the wave number, and $\beta_k = \mathbf{k}\cdot\overline{\mathbf{F}}^{-T}\cdot\mathbf{m}$.

Now we can find the transmission velocity of a wave packet or the group velocity (Kittel, 2004)

$$\mathbf{v}_g = \nabla_{\mathbf{k}}\,\omega. \tag{54}$$

From (52) and (54), we obtain the explicit formulae for the group velocities in homogenized laminates

$$\mathbf{v}_{sw}^{(1)} = \frac{\overline{\mu}\,\overline{\mathbf{B}}\cdot\mathbf{n} + (\breve{\mu}-\overline{\mu})(\mathbf{n}\cdot\overline{\mathbf{F}}\cdot\mathbf{m})\overline{\mathbf{F}}\cdot\mathbf{m}}{\sqrt{\overline{\rho}_0 a_1}} \tag{55}$$

and

$$\mathbf{v}_{sw}^{(2)} = \frac{1}{\sqrt{\overline{\rho}_0 a_2}}\left(\overline{\mu}\,\overline{\mathbf{B}}\cdot\mathbf{n} + (\breve{\mu}-\overline{\mu})(\mathbf{n}\cdot\overline{\mathbf{F}}\cdot\mathbf{m})\overline{\mathbf{F}}\cdot\mathbf{m} + \frac{\overline{\mu}-\breve{\mu}}{\alpha^2}\left(\beta\left(5-\frac{8\beta^2}{\alpha}\right)\overline{\mathbf{F}}^{-T}\cdot\mathbf{m} + \left(\frac{4\beta^4}{\alpha}-\alpha\right)\mathbf{n}\right)\right). \tag{56}$$

To illustrate the derived results (55) and (56), energy curves (Nayfeh, 1995) are plotted in Fig. 3. Fig. 3 shows the energy curves for (a) out-of-plane and (b) in-plane shear waves in the laminate with $\nu_a = 0.1$, $\mu_a/\mu_b = 20$, and $\rho_{0a}/\rho_{0b} = 1$ under equibiaxial deformation. Clearly, the group velocities of the both shear waves strongly depend on the applied deformation and direction of wave

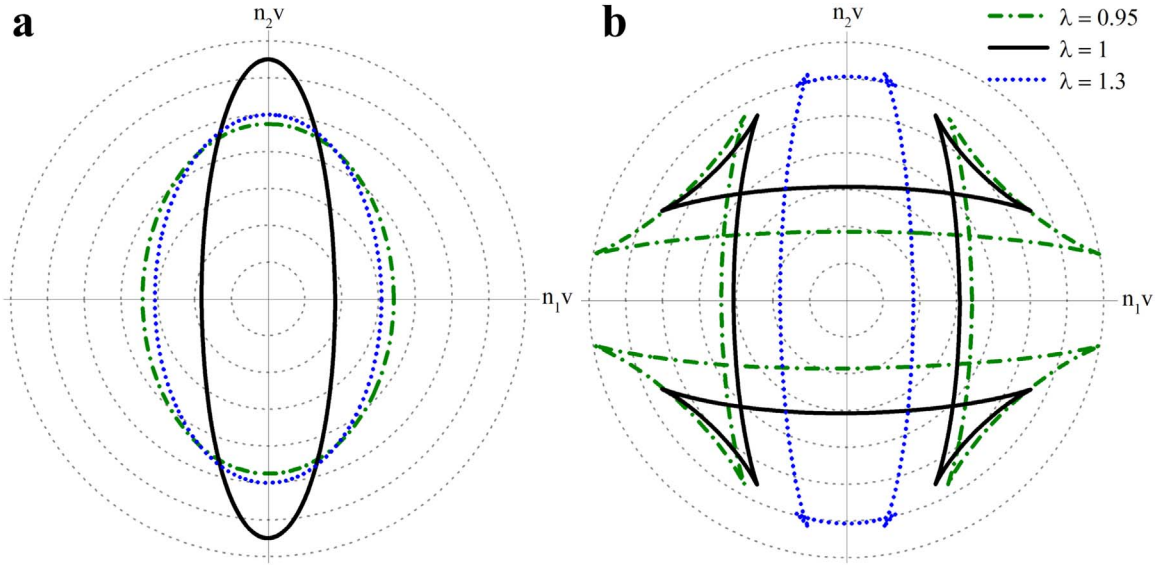

Fig. 3. Energy curves for (a) out-of-plane and (b) in-plane shear waves in the laminate under equibiaxial deformation ($\nu_a = 0.1$, $\mu_a/\mu_b = 20$, and $\rho_{0a}/\rho_{0b} = 1$). Scale is 0.2 per division, where group velocity is normalized by $\sqrt{\overline{\rho}_0/\overline{\mu}}$.

propagation. In particular, an equibiaxial extension increases the group velocity of the out-of-plane shear wave propagating perpendicular to the layers while it decreases the group velocity of the in-plane shear wave propagating in the same direction. An equibiaxial contraction increases group velocities of both the out-of-plane and the in-plane shear waves propagating perpendicular to the layers. Moreover, the energy curves of the in-plane shear waves have the cusps, and position of the cusps is highly tunable by deformation (see Fig. 3(b)). According to Nayfeh (1995) these cusps correspond to regions of null energy. However, for the out-of-plane shear wave the cusps are not observed (see Fig. 3(a)).

3.1.2. Compressible laminates

Next we present long wave estimates for the phase velocities of pressure and shear waves propagating in the direction perpendicular to the layers in the finitely deformed laminate with *compressible* neo-Hookean and Gent phases. Recall (Boulanger et al., 1994) that the phase velocities of shear and pressure waves in the finitely deformed neo-Hookean material for $\mathbf{F}_\xi = \lambda_{1\xi}\mathbf{e}_1 \otimes \mathbf{e}_1 + \lambda_{2\xi}\mathbf{e}_2 \otimes \mathbf{e}_2 + \lambda_{3\xi}\mathbf{e}_3 \otimes \mathbf{e}_3$ and $\mathbf{n} = \mathbf{e}_1$ are the following:

$$c_\xi^s = \lambda_{1\xi}\sqrt{\frac{\mu_\xi}{\rho_{0\xi}}} \quad \text{and} \quad c_\xi^p = \sqrt{\frac{\Lambda_\xi J_\xi^2 + \mu_\xi(1+\lambda_{1\xi}^2)}{\rho_{0\xi}}}. \tag{57}$$

When the wavelength is much larger than the period of the laminate, the sines can be replaced by their arguments and only second order terms are retained from the cosines in Eq. (23), namely

$$\sin\left(\frac{\omega d_\xi}{c_\xi}\right) \simeq \frac{\omega d_\xi}{c_\xi} \quad \text{and} \quad \cos\left(\frac{\omega d_\xi}{c_\xi}\right) \simeq 1 - \frac{\omega^2 d_\xi^2}{2c_\xi^2}. \tag{58}$$

Under this assumption, substitution of (12) and (57) in (23) yields expressions for the phase velocities of shear and pressure waves propagating perpendicular to the layers ($\mathbf{n} = \mathbf{m} = \mathbf{e}_1$) in the finitely deformed layered material with neo-Hookean phases:

$$\overline{c}_{sw} = \overline{\lambda}_1\sqrt{\breve{\mu}/\overline{\rho}_0} \quad \text{and} \quad \overline{c}_{pw} = \overline{\lambda}_1\sqrt{\breve{\Gamma}/\overline{\rho}_0}, \tag{59}$$

where

$$\breve{\Gamma} = (v_a/\Gamma_a + v_b/\Gamma_b)^{-1} \quad \text{and} \quad \Gamma_\xi = \Lambda_\xi(\lambda_{2\xi}\lambda_{3\xi})^2 + \mu_\xi(1+\lambda_{1\xi}^{-2}). \tag{60}$$

For the in-plane tension (27), $\lambda_{2\xi} = \lambda$ and $\lambda_{3\xi} = 1$, while for the equibiaxial deformation (28) $\lambda_{2\xi} = \lambda_{3\xi} = \lambda$.

For the Gent material model, the phase velocities of shear and pressure waves are (Galich and Rudykh, 2015b)

$$c_\xi^s = \lambda_{1\xi}\sqrt{\mu_\xi J_{m\xi}/(\theta_\xi\rho_{0\xi})} \tag{61}$$

and

$$c_\xi^p = \sqrt{\frac{\mu_\xi(1+(\eta_\xi - 2/J_{m\xi})J_\xi^2 + J_{m\xi}\theta_\xi^{-2}(\theta_\xi + 2\lambda_{1\xi}^2)\lambda_{1\xi}^2)}{\rho_{0\xi}}}, \tag{62}$$

where $\theta_\xi = 3 + J_{m\xi} - \mathbf{F}_\xi\colon\mathbf{F}_\xi$. Hence, substitution of (12), (61) and (62) in (23) together with (58) yields expressions for the phase velocities of shear and pressure waves propagating perpendicular to the layers ($\mathbf{n} = \mathbf{m} = \mathbf{e}_1$) in the finitely deformed layered material with Gent phases, namely

$$\overline{c}_{sw} = \overline{\lambda}_1\sqrt{\breve{\Theta}/\overline{\rho}_0} \quad \text{and} \quad \overline{c}_{pw} = \overline{\lambda}_1\sqrt{\breve{G}/\overline{\rho}_0}, \tag{63}$$

where

$$\breve{\Theta} = \left(\frac{v_a}{\Theta_a} + \frac{v_b}{\Theta_b}\right)^{-1} \quad \text{and} \quad \breve{G} = \left(\frac{v_a}{G_a} + \frac{v_b}{G_b}\right)^{-1}, \tag{64}$$

where $\Theta_\xi = \mu_\xi J_{m\xi}/\theta_\xi$ and

$$G_\xi = \mu_\xi\left(\lambda_{1\xi}^{-2} + \left(\eta_\xi - \frac{2}{J_{m\xi}}\right)(\lambda_{2\xi}\lambda_{3\xi})^2 + J_{m\xi}\theta_\xi^{-2}(\theta_\xi + 2\lambda_{1\xi}^2)\right). \tag{65}$$

Fig. 4 shows a comparison of the long wave estimates (59) and (63) with the exact solution (23) for the waves propagating perpendicular to the layers under equibiaxial deformation. Here and thereafter, we present the normalized frequency $f_n = fd^o\sqrt{\overline{\rho}_0/\breve{\mu}}$, where $f = \omega/(2\pi)$. Remarkably, the long wave estimates (59) and (63) are in excellent agreement with the exact solution (23) for wavelengths exceeding the effective period of the laminate, namely $l \gtrsim \pi d$. For example, for $l = 4d$ the differences in frequencies between the long wave estimates and exact solution are less than 1% for both shear and pressure waves (see Fig. 4).

3.2. Band gap structure

Band gap is a frequency range where waves cannot propagate due to, for example, Bragg scattering (Kushwaha et al., 1993) or/

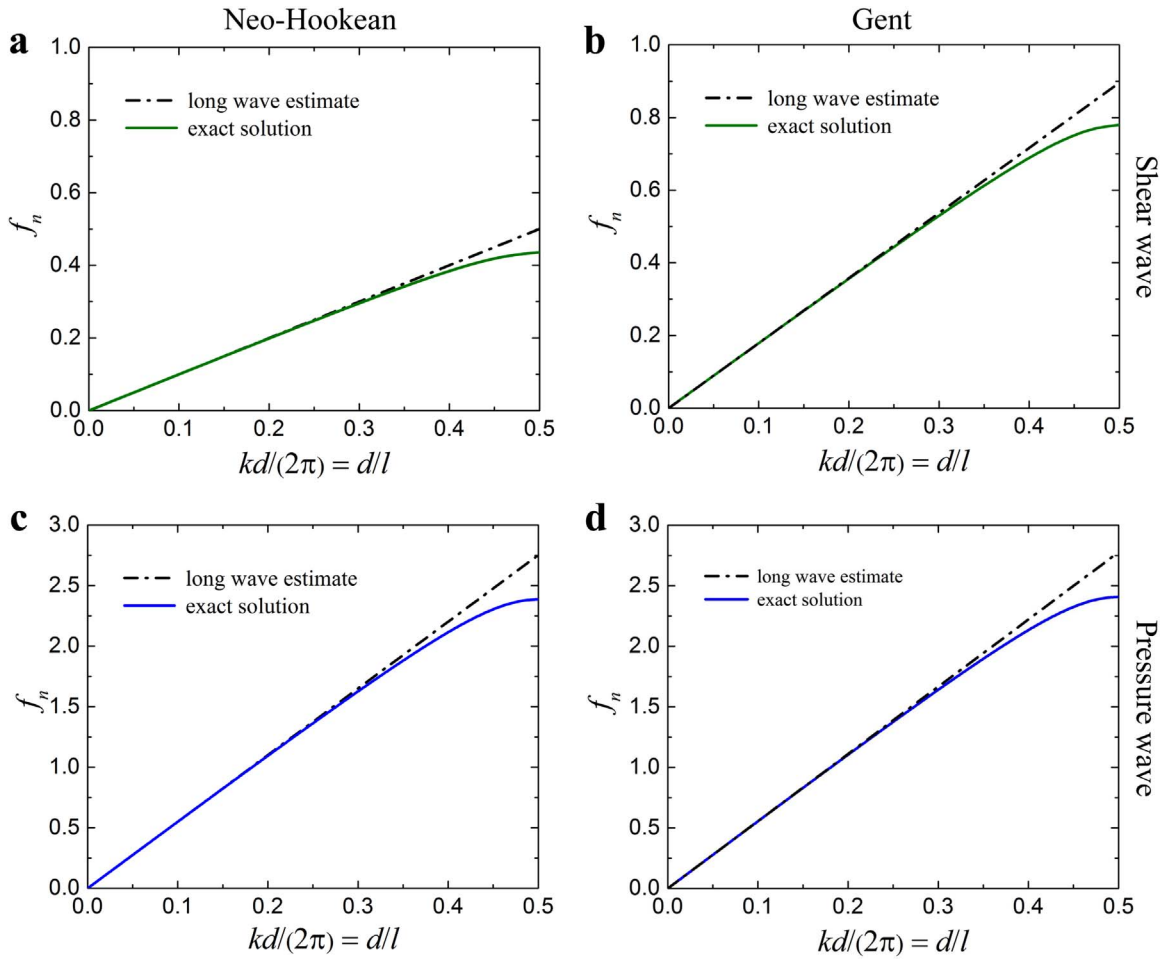

Fig. 4. Comparison of the long wave estimates (59) and (63) with the exact solution (23) for the waves propagating perpendicular to the layers in the laminates with neo-Hookean ((a) and (c)) and Gent ((b) and (d)) phases under equibiaxial deformation ($\lambda = 1.5$). $\nu_a = 0.2$, $\mu_a/\mu_b = 100$, $\rho_{0a}/\rho_{0b} = 1.5$, $\Lambda_a/\mu_a = 10$, $\Lambda_b/\mu_b = 5$, $J_{mb} = 2.5$, and $J_{ma}/J_{mb} = 2$. (a) and (b) correspond to shear waves and (c) and (d) – pressure waves.

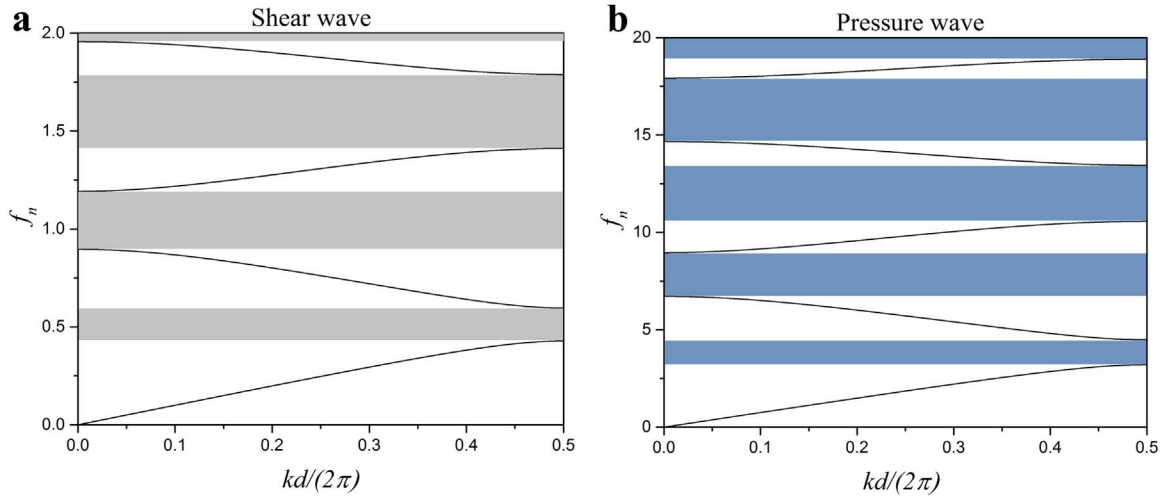

Fig. 5. Dispersion diagrams for shear (a) and pressure (b) waves in the laminate with $\nu_a = 0.3$, $\mu_a/\mu_b = 100$, $\Lambda_a/\mu_a = 100$, $\Lambda_b/\mu_b = 10$, and $\rho_{0a}/\rho_{0b} = 1$ under equibiaxial tension, $\lambda = 1.5$. The shaded areas correspond to the shear (gray) and pressure (blue) wave band gaps. Frequency is normalized as $f_n = \frac{\omega d^0}{2\pi}\sqrt{\rho_0/\tilde{\mu}}$. (For interpretation of the references to color in this figure caption, the reader is referred to the web version of this paper.)

and local resonance (Auriault and Bonnet, 1985; Auriault, 1994; Liu et al., 2000; Auriault and Boutin, 2012). In case of layered media with high contrast in the mechanical properties between the phases both Bragg scattering and inner resonance of stiffer layer (Auriault and Boutin, 2012) participate in formation of band gaps (Khelif and Adibi, 2016). Mathematically, it corresponds to the situation when wave number k becomes imaginary in the dispersion relation (23), i.e. within a band gap displacement and stress amplitudes exponentially attenuate (see Eqs. (17) and (20)). Fig. 5 illustrates the band gap structures of shear and pressure waves in the finitely deformed laminate with $\nu_a = 0.3$, $\mu_a/\mu_b = 100$, $\Lambda_a/\mu_a = 100$, $\Lambda_b/\mu_b = 10$, and with identical densities of the phases,[3] i.e. $\rho_{0a}/\rho_{0b} = 1$. The laminate is subjected to equibiaxial tension with the magnitude of the stretch ratio $\lambda = 1.5$. The shaded gray and blue areas correspond to the shear and pressure wave BGs, respectively. Clearly, the shear wave BGs appear earlier (i.e. at lower frequencies) than the pressure wave BGs (compare Fig. 5(a) and (b)); thus, to induce complete BGs at the low-frequency range, one needs to design laminates with pressure wave BGs at the low-frequency range. Next, we identify the key parameters that govern the shear and pressure wave band gaps.

3.2.1. Incompressible laminate

Here we consider the influence of (a) microstructures, (b) deformations, and (c) elastic moduli on the band gap structures in *incompressible* laminates. Recall that incompressible materials support only shear waves; consequently, only shear wave band gaps (SBGs) are considered, while pressure wave BGs (PBG) will be considered in detail in the next section.

(a) *Material geometry*. First, we investigate the influence of the material geometry on SBG structure. Fig. 6(a) presents the width of the first SBG as a function of the volume fraction of phase a. The first SBG has a maximal width for a certain volume fraction ν_a; moreover, the maximal width of SBG with corresponding volume fraction of phase a strongly depends on the contrast in shear modulus between the phases (compare Fig. 6(a) and (b)). Thus, for the contrast in shear modulus of $\mu_a/\mu_b = 10$, the maximal width of the first SBG is $\Delta f_n = 0.41$ with $\nu_a = 0.76$; while for the contrast in shear modulus of $\mu_a/\mu_b = 1000$, the SBG width significantly increases up to $\Delta f_n = 2.25$, and the corresponding volume fraction shifts to $\nu_a = 0.97$. It is clear that an increase in the shear modulus contrast widens the maximal SBG width. Thus, wide SBGs can be achieved by composing laminates with thin soft layers embedded in the stiff phase ($\nu_b = 0.03$ in Fig. 6(b)). As expected SBGs disappear when $\nu_a = 0$ or 1.

(b) *Deformation*. Next, we analyze the influence of deformation on SBGs. We start from the consideration of laminates with phases characterized by weak stiffening, which can be described by neo-Hookean model (29). Substitution of the corresponding phase velocities $(57)_1$ into the dispersion relation (23), together with the deformation induced change in geometry (12), yields

$$\cos k\bar{\lambda}_1 d^o = \cos\left(\omega d_a^o \sqrt{\frac{\rho_{0a}}{\mu_a}}\right)\cos\left(\omega d_b^o \sqrt{\frac{\rho_{0b}}{\mu_b}}\right) - \frac{1}{2}\left(\sqrt{\frac{\rho_{0a}\mu_a}{\rho_{0b}\mu_b}} + \sqrt{\frac{\rho_{0b}\mu_b}{\rho_{0a}\mu_a}}\right)\sin\left(\omega d_a^o \sqrt{\frac{\rho_{0a}}{\mu_a}}\right)\sin\left(\omega d_b^o \sqrt{\frac{\rho_{0b}}{\mu_b}}\right). \tag{66}$$

This result clearly shows that SBGs in layered materials with neo-Hookean phases do not depend on deformation. This is due to the equal contribution of two competing effects induced by deformation: (i) the change in the phase properties (i.e. $c_\xi^{nH}/c_\xi^o = \lambda_{1\xi}$, where c_ξ^{nH} and c_ξ^o are the phase velocities in the deformed and undeformed material) and (ii) change in the layer thicknesses (i.e. $d_\xi/d_\xi^o = \lambda_{1\xi}$). Clearly, any deformation induced change in the geometry is fully compensated by the change in the phase velocity.

However, for laminates with phases exhibiting stronger stiffening (such as Gent phases), the deformation induced change in the effective properties prevails over the geometry changes. The phase velocities of the shear waves in a deformed Gent material are larger than in the identically deformed neo-Hookean material (i.e. $c_\xi^G/c_\xi^{nH} = \sqrt{J_{m\xi}/\theta_\xi} > 1$) while the changes in the geometry are the same. Fig. 7 presents the relative changes in the phase velocities of the shear waves as functions of the stretch for the neo-Hookean and Gent phases under in-plane tension. Clearly, for the contraction ($\lambda < 1$), the phase velocities of the shear waves in the Gent phase increase more significantly than in the neo-Hookean phase. For the extension ($\lambda > 1$), the phase velocities of the shear waves in the Gent phase decrease in the beginning; however, the phase velocity starts to grow as the stiffening effect becomes more pronounced with an increase in deformation. Eventually, the phase velocity becomes larger than the one in the undeformed material. This corresponds to a certain stretch ratio $\lambda^* < \lambda^{lock}$ (see Fig. 7); the expressions for this stretch ratio are

$$\lambda_{pt}^* = \sqrt{1 + J_m} \tag{67}$$

for the in-plane tension and

$$\lambda_{bt}^* = \frac{1}{2}\sqrt{1 + J_m + \sqrt{9 + (10 + J_m)J_m}} \tag{68}$$

for the equibiaxial extension. Since in laminates with Gent phases the deformation induced change in material properties (i.e. $c_\xi^G/c_\xi^o = \lambda_{1\xi}\sqrt{J_{m\xi}/\theta_\xi}$) is not fully compensated by the change in the geometry (i.e. $d_\xi/d_\xi^o = \lambda_{1\xi}$), the tunability of SBGs by deformation is observed.

Fig. 8 illustrates the dependence of SBGs on in-plane ((a) and (c)) and equibiaxial ((b) and (d)) deformations for the layered materials with Gent phases. The lock-up stretches for $J_m = 2.5$ are $\lambda_-^{lock} = 0.48$ and $\lambda_+^{lock} = 2.07$ for the in-plane deformation; and $\lambda_-^{lock} = 0.68$ and $\lambda_+^{lock} = 1.64$ for the equibiaxial deformation. We observe that SBGs shift towards higher frequencies and widen as the lock-up stretch ratio is approached. In particular, for the laminate with $\nu_a = 0.3$, $\mu_a/\mu_b = 100$, $J_{ma} = 5$, and $J_{mb} = 2.5$ the first SBG widens from $\Delta f_n = 0.16$ up to $\Delta f_n = 0.49$ and its lower boundary shifts from $f_n = 0.43$ up to $f_n = 1.35$ by application of the in-plane

[3] Typical deformable polymers are characterized by low densities that change only slightly from polymer to polymer. Therefore, we present the results for laminates with similar or identical phase densities; the values of the density contrast ratio are specified in each example.

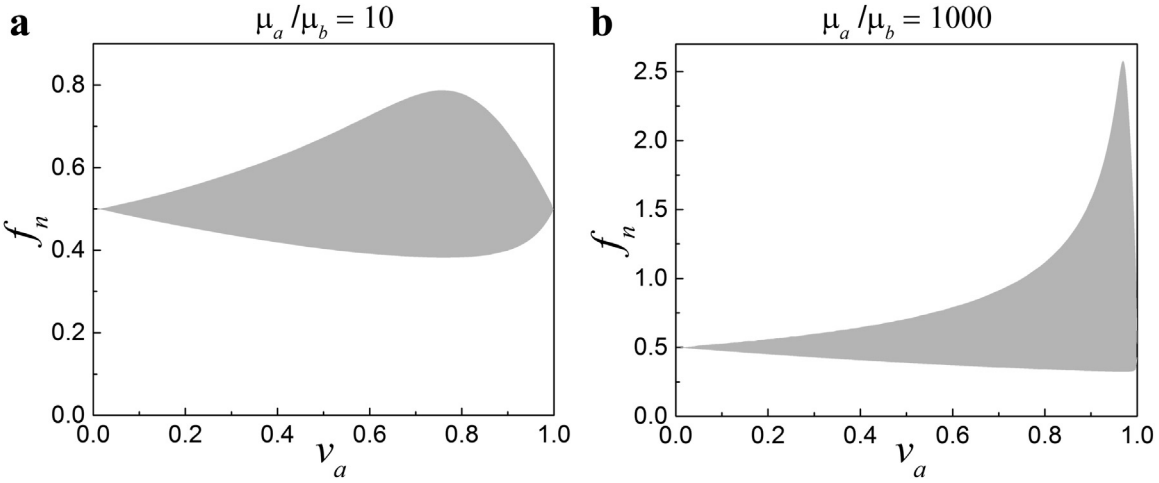

Fig. 6. First shear wave band gap vs. volume fraction of phase a for layered materials in undeformed state with (a) $\mu_a/\mu_b = 10$ and (b) $\mu_a/\mu_b = 1000$; $\rho_{0a}/\rho_{0b} = 1$.

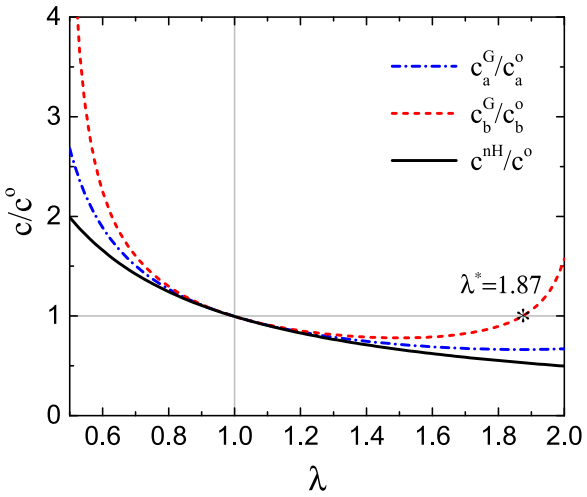

Fig. 7. Relative change in the phase velocities of shear waves as functions of in-plane tension for laminates with $\nu_a = 0.97$, $\mu_a/\mu_b = 1000$, $J_{ma} = 5$, $J_{mb} = 2.5$, and $\rho_{0a}/\rho_{0b} = 1$.

deformation of the magnitude $\lambda = 0.5$ or $\lambda = 2$ (see Fig. 8(a)). The equibiaxial deformation of magnitude $\lambda = 0.70$ or $\lambda = 1.58$ widens the first SBG from $\Delta f_n = 0.16$ up to $\Delta f_n = 0.42$ and shifts its lower boundary from $f_n = 0.43$ up to $f_n = 1.14$ (see Fig. 8(b)). Fig. 8(c) and (d) show the first SBG as a function of the stretch ratio for the in-plane (c) and equibiaxial (d) deformations for the laminate with the volume fraction producing a maximal width of the first SBG in the undeformed laminate, namely $\nu_a = 0.97$ and $\mu_a/\mu_b = 1000$. Consistent with the previous observations the first SBG widens and shifts towards higher frequencies once the lock-up stretches are attained. In particular, lower boundary of the first SBG shifts from $f_n = 0.33$ up to $f_n = 1.00$ and its width increases from $\Delta f_n = 2.25$ up to $\Delta f_n = 2.73$ in the laminate undergoing the in-plane contraction with $\lambda = 0.5$ or extension with $\lambda = 2$ (Fig. 8(c)). Clearly, equibiaxial deformation has a more pronounced effect on SBGs as compared to the in-plane deformation (compare Fig. 8(a) vs. (b) and (c) vs. (d)). Remarkably, contraction ($\lambda < 1$) and extension ($\lambda > 1$) of the laminate with Gent phases influence SBGs in similar ways, namely any homogeneous deformations considered here widen and shift up SBGs towards higher frequencies (see Fig. 8). This happens because for both contraction ($\lambda < 1$) and extension ($\lambda > 1$), the stiffening leads to an increase in the phase velocities of the Gent phases compared to the phase velocities of the neo-Hookean constituents, i.e. $c_\xi^G/c_\xi^{nH} = \sqrt{J_{m\xi}/\theta_\xi} > 1$ (see Fig. 7), whereas the deformation induced geometry changes are identical for laminates with weak and strong stiffening effects, i.e. $d_\xi/d_\xi^o = \lambda_{1\xi}$. For example, the in-plane contraction of the magnitude $\lambda = 0.5$ increases the phase velocities in the layers a and b up to $c_a^G/c_a^o = 2.7$ and $c_b^G/c_b^o = 6.3$, respectively, whereas the layer thicknesses increase up to $d/d^o = 2$ only (see Fig. 7). Again, the in-plane extension of the magnitude $\lambda = 2$ decreases the phase velocity in the layer a down to $c_a^G/c_a^o = 0.7$ and increases it up to $c_b^G/c_b^o = 1.6$ in the layer b, whereas the layer thicknesses decrease down to $d/d^o = 0.5$ (see Fig. 7). Note that for the in-plane tension of magnitude $\lambda = 0.5$ or $\lambda = 2$, the phase velocities in Gent phases increase by the same value compared to the phase velocities of the neo-Hookean phases, namely $c_a^G/c_a^{nH}|_{\lambda=0.5} = c_a^G/c_a^{nH}|_{\lambda=2} = 1.35$ and $c_b^G/c_b^{nH}|_{\lambda=0.5} = c_b^G/c_b^{nH}|_{\lambda=2} = 3.16$. This together with the identical deformation induced change in the geometry leads to the identical width and position of the SBGs for these values of the stretch ratio.

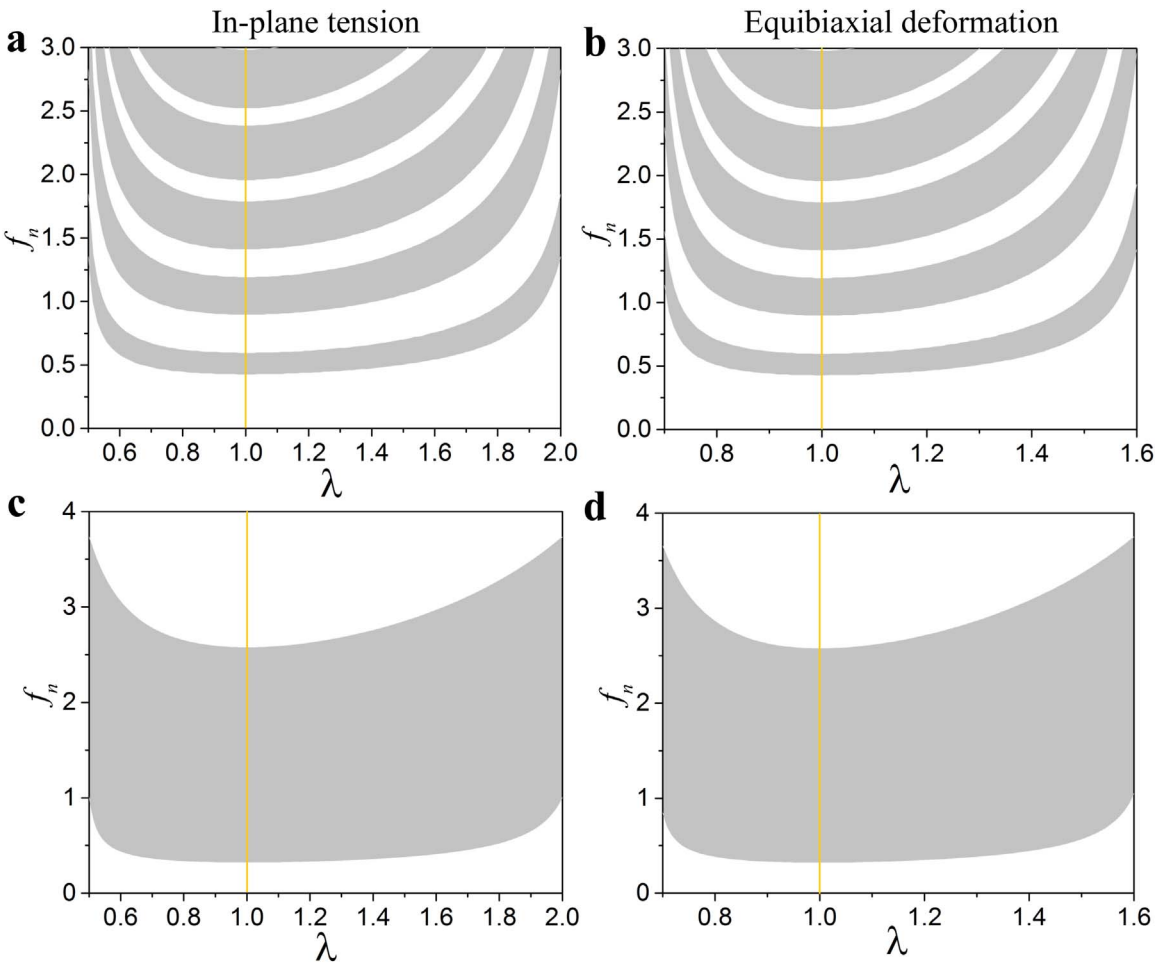

Fig. 8. Shear wave band gaps vs. in-plane ((a) and (c)) and equibiaxial ((b) and (d)) deformations for the layered materials with Gent phases, namely $\rho_{0a}/\rho_{0b} = 1$, $J_{ma} = 5$, $J_{mb} = 2.5$, $\nu_a = 0.3$, $\mu_a/\mu_b = 100$ ((a) and (b)) and $\nu_a = 0.97$, $\mu_a/\mu_b = 1000$ ((c) and (d)).

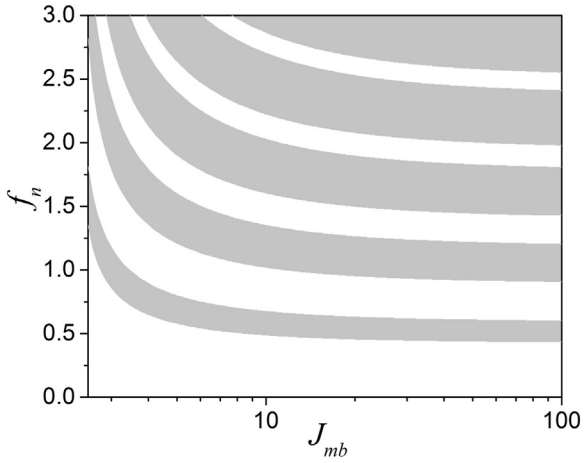

Fig. 9. Shear wave band gaps as a function of locking parameter J_{mb} for the layered material with $\nu_a = 0.3$, $J_{ma} = 100$, $\rho_{0a}/\rho_{0b} = 1$, and $\mu_a/\mu_b = 100$ subjected to the in-plane tension of the magnitude $\lambda = 2$.

To illustrate the influence of the stiffening of the laminate constituents on the SBGs, we present SBGs as functions of locking parameter J_{mb} for the layered material with $\nu_a = 0.3$, $J_{ma} = 100$, and $\mu_a/\mu_b = 100$ subjected to the in-plane tension of the magnitude $\lambda = 2$ in Fig. 9. We observe that SBGs widen and shift towards higher frequencies with a decrease in the locking parameter J_{mb}. In

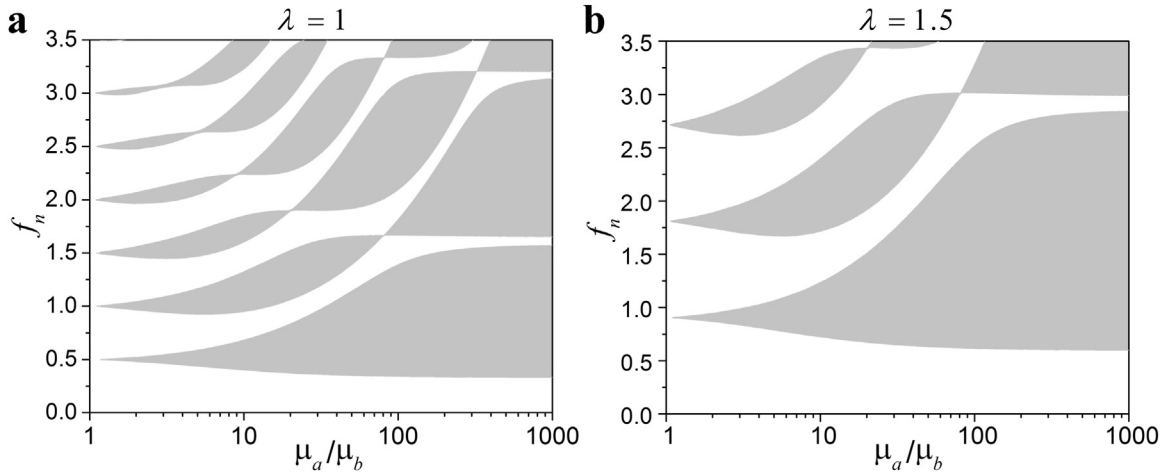

Fig. 10. Shear band gaps vs. shear modulus contrast for the layered material with $\nu_a = 0.9$, $\rho_{0a}/\rho_{0b} = 1$, and $J_{ma} = J_{mb} = 1$ in the undeformed state (a) and the one subjected to the in-plane tension with $\lambda = 1.5$ (b).

particular, the lower boundary of the first SBG shifts from $f_n = 0.44$ up to $f_n = 1.35$ and its width increases from $\Delta f_n = 0.16$ up to $\Delta f_n = 0.46$ when locking parameter of phase b decreases from $J_{mb} = 100$ down to $J_{mb} = 2.5$. This happens because the lock-up stretch ratio (34) decreases together with J_{mb}, leading to the significant increase in the phase velocity of shear wave in the phase b (see Eq. (61)).

(c) *Shear modulus contrast*. To illustrate the influence of the shear modulus contrast of the phases on SBGs, we present SBGs as functions of the shear modulus contrast for the laminates with $\nu_a = 0.9$ and $J_{m\tilde{\xi}} = 1$ in Fig. 10. The corresponding lock-up stretch ratio is $\lambda = 1.62$. The SBGs of the undeformed ($\lambda = 1$) laminate and the one subjected to the in-plane tension with $\lambda = 1.5$ are presented in Fig. 10(a) and (b), respectively. Fig. 10(a) shows that the first SBG rapidly widens with an increase in the contrast from 1 to ~100, after that the upper boundary flattens, and the SBG width changes slowly with further increase in the shear modulus contrast. The second and the following SBGs close at certain values of the shear modulus contrast. For example, the third SBG closes when $\mu_a/\mu_b = 20$ and $\mu_a/\mu_b = 322$; however, the SBG reopens again if the shear modulus contrast increases. For laminates with phases exhibiting strong stiffening (such as Gent phases), these BGs shift towards higher frequencies for any shear modulus contrast with application of deformation. In particular, the first SBG widens from $\Delta f_n = 0.79$ up to $\Delta f_n = 1.44$ and its lower boundary shifts from $f_n = 0.35$ up to $f_n = 0.63$ in the laminate with $\mu_a/\mu_b = 50$ subjected to the in-plane extension of the magnitude $\lambda = 1.5$ (Fig. 10(b)).

3.2.2. *Compressible laminates*

To analyze the pressure wave BGs (PBGs), we consider periodic layered materials with *compressible* phases to ensure the existence of pressure waves. Fig. 11 shows pressure and shear wave BGs as functions of the volume fraction of phase a in the undeformed and deformed laminates. Here and thereafter, gray, blue, and black colors correspond to the shear wave, pressure wave,

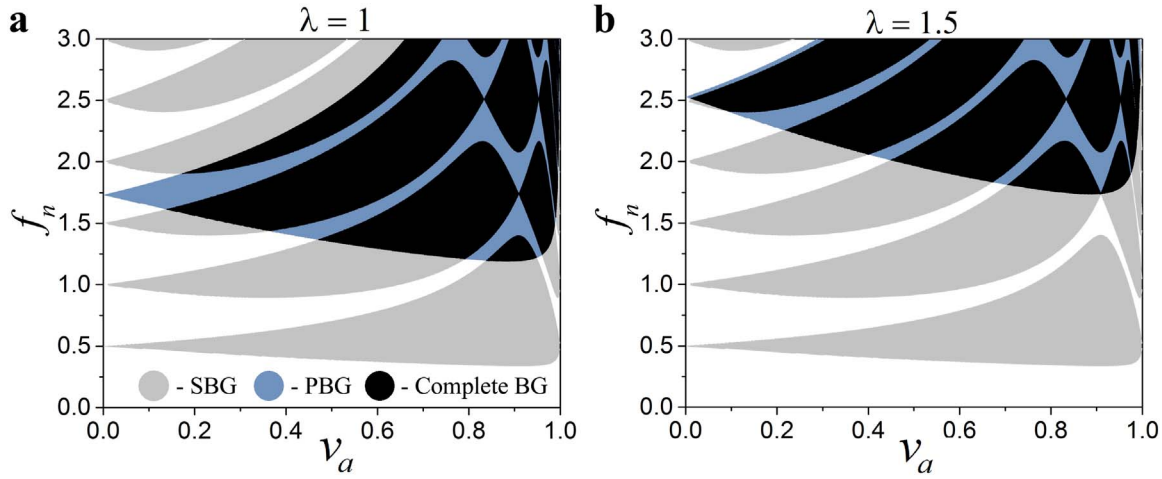

Fig. 11. Band gaps vs. volume fraction of the phase a in the undeformed laminate (a) and the one subjected to the in-plane tension of the magnitude $\lambda = 1.5$ (b) with $\mu_a/\mu_b = 100$, $\Lambda_a/\mu_a = 1000$, $\Lambda_b/\mu_b = 10$, and $\rho_{0a}/\rho_{0b} = 1$. The gray, blue, and black colors correspond to the shear wave, pressure wave, and complete BGs, respectively. (For interpretation of the references to color in this figure caption, the reader is referred to the web version of this paper.)

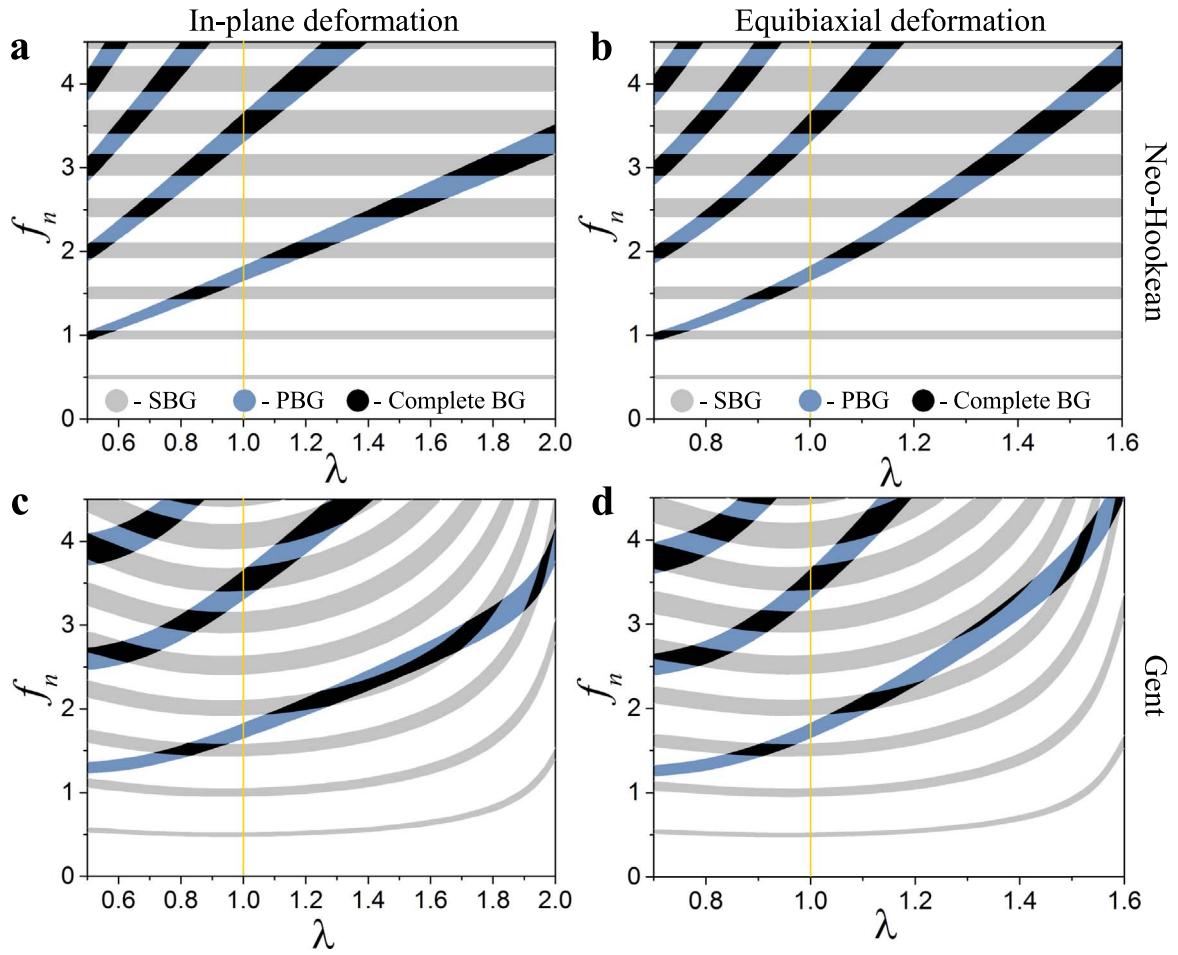

Fig. 12. Band gaps vs. in-plane ((a) and (c)) and equibiaxial ((b) and (d)) deformation for laminates with $v_a = 0.1$, $\mu_a/\mu_b = 100$, $\Lambda_a/\mu_a = 1000$, $\Lambda_b/\mu_b = 10$, and $\rho_{0a}/\rho_{0b} = 1$. (a) and (b) refer to the laminate with neo-Hookean phases and (c) and (d) refer to the laminate with Gent phases having $J_{ma} = 5$ and $J_{mb} = 2.5$.

and *complete* BGs, respectively. We refer to *complete* BGs when both pressure and shear waves cannot propagate. We find that the first PBG has a maximal width for a certain volume fraction v_a depending on the contrast in shear moduli and compressibility of each phase. Thus, different complete BGs can be tailored by varying the initial material properties and geometry.

In the case of shear waves, the ratio of acoustic impedances z_a/z_b is independent of deformation, although the acoustic impedances $z_\xi = \rho_\xi c_\xi$ for both phases are functions of the principal stretches. Substitution of the corresponding phase velocities $(57)_1$, geometry changes (12), and densities $\rho_\xi = J_\xi^{-1}\rho_{0\xi}$ into (23) together with the boundary conditions (25), producing relations $\lambda_{2a} = \lambda_{2b}$ and $\lambda_{3a} = \lambda_{3b}$, yields the dispersion relation (66). Consequently, the SBGs are not influenced by deformation in the laminates with compressible neo-Hookean phases. Similarly to the laminates with incompressible neo-Hookean phases, the deformation induced changes in the material properties are fully compensated by the changes in the geometry.

In the case of pressure waves, the dominant factor influencing PBGs is the deformation induced change in the geometry. This is due to the fact that the phase velocities of pressure waves in neo-Hookean materials change very slowly with the deformation; moreover, the change is negligible in the case of nearly incompressible materials (see Eq. $(57)_2$). A comparison of the BGs in the undeformed laminates (Fig. 11(a)) and the BGs in the laminates subjected to the in-plane tension, $\lambda = 1.5$ (Fig. 11(b)), shows that the applied deformation does not change the SBGs while it significantly influences the PBGs.

To clarify how the pressure wave and complete BGs depend on deformation in the laminates with compressible phases exhibiting weak and strong stiffening, we present these BGs as functions of the applied stretch ratio in Fig. 12. Fig. 12(a) and (b) illustrate how the in-plane (27) and equibiaxial deformations (28) of the layered material with neo-Hookean phases influence the BG structure. We observe that PBGs narrow and shift towards lower frequencies in the laminate undergoing contraction while extension of the laminate widens and shifts PBGs towards higher frequencies. In particular, the lower boundary of the first PBG shifts from $f_n = 1.65$ up to $f_n = 3.17$ and its width increases from $\Delta f_n = 0.18$ up to $\Delta f_n = 0.34$ in the laminate subjected to the in-plane extension of the magnitude $\lambda = 2$ (see Fig. 12(a)). The equibiaxial deformation has a more pronounced effect on the PBGs, in particular, the equibiaxial extension of the magnitude $\lambda = 1.6$ shifts the lower boundary of the first PBG from $f_n = 1.65$ up to $f_n = 4.04$ and widens it from $\Delta f_n = 0.18$ up to $\Delta f_n = 0.44$ (see Fig. 12(b)). Remarkably, complete BGs can be induced in a required frequency range by

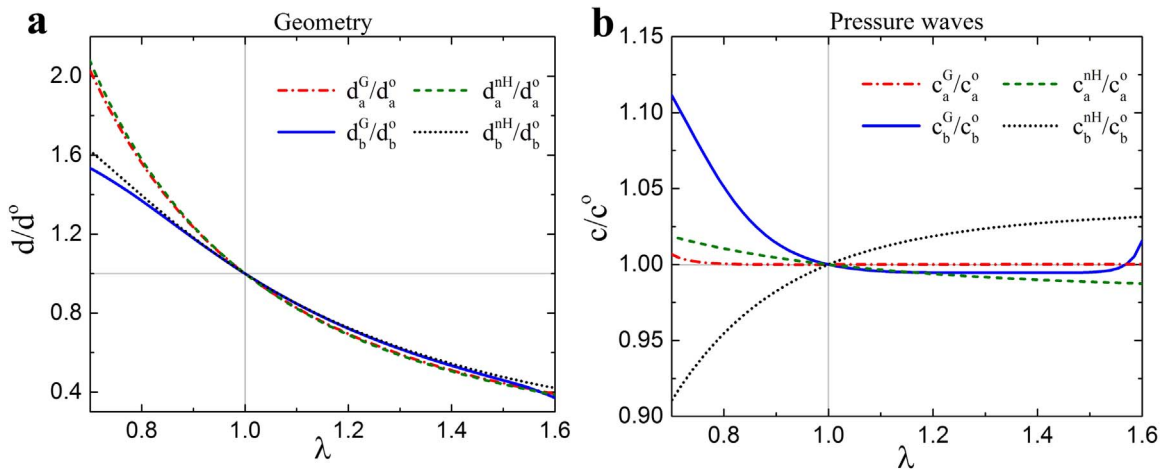

Fig. 13. Relative change in thicknesses of the layers (a) and phase velocities of pressure (b) waves as functions of equibiaxial deformation for the laminates with $\nu_a = 0.1$, $\mu_a/\mu_b = 100$, $\Lambda_a/\mu_a = 1000$, $\Lambda_b/\mu_b = 10$, $J_{ma} = 5$, $J_{mb} = 2.5$, and $\rho_{0a}/\rho_{0b} = 1$. (For interpretation of the references to color in this figure caption, the reader is referred to the web version of this paper.)

deformation while the undeformed laminates do not produce complete BGs in that range. For example, the laminate with $\nu_a = 0.1$, $\mu_a/\mu_b = 100$, $\Lambda_a/\mu_a = 1000$ and $\Lambda_b/\mu_b = 10$ has no complete BGs (in the considered frequency range) in the undeformed state while it has the complete BG of width $\Delta f_n = 0.15$ when subjected to the in-plane contraction of the stretch ratio magnitude $\lambda = 0.85$ (see Fig. 12(a)). In contrast to the in-plane tension, for the equibiaxial deformation we have more "islands" of the complete BGs in the same range of deformation, however, these "islands" are smaller (compare Fig. 12(a) and (b)).

Fig. 12(c) and (d) illustrate how the in-plane (27) and equibiaxial deformations (28) of the layered material with compressible Gent phases influence the BG structure. We observe that in the laminate undergoing in-plane contraction PBGs shift towards lower frequencies less than in laminates with neo-Hookean phases (compare Fig. 12(a) and (c)). In particular, the lower boundary of the first PBG shifts from $f_n = 0.94$ up to $f_n = 1.23$ due to the stiffening of the laminate induced by the in-plane contraction of the magnitude $\lambda = 0.5$. Analogously, the equibiaxial contraction of the laminate with Gent phases shifts PBGs towards lower frequencies less than in the laminate with neo-Hookean phases (compare Fig. 12(b) and (d)). Specifically, the lower boundary of the second PBG shifts from $f_n = 1.86$ up to $f_n = 2.39$ because the laminate under the equibiaxial contraction of the magnitude $\lambda = 0.7$ significantly stiffens. Similar to the effect of contraction in the laminate with Gent phases, the extension induced stiffening shifts PBGs towards higher frequencies compared to the laminates with neo-Hookean phases. In particular, the lower boundary of the first PBG shifts from $f_n = 3.17$ up to $f_n = 3.68$ in the laminate with Gent phases undergoing the in-plane extension of the magnitude $\lambda = 2$ (compare Fig. 12(a) and (c)).

Next, let us consider the mechanisms governing the PBGs in the finitely deformed compressible laminates exhibiting weak and strong stiffening. Fig. 13 presents the relative changes in the thicknesses of the layers (a), and the relative changes in the phase velocities of pressure waves (b) in each layer as functions of the stretch ratio. The example is given for the laminates with neo-Hookean and Gent phases subjected to equibiaxial deformation. The laminate parameters are $\nu_a = 0.1$, $\mu_a/\mu_b = 100$, $\Lambda_a/\mu_a = 1000$, $\Lambda_b/\mu_b = 10$, $J_{ma} = 5$, and $J_{mb} = 2.5$. The corresponding dependence of the BGs on deformation is presented in Fig. 12(b) and (d). A comparison of Fig. 12(b) and (d) together with Fig. 13 shows a correlation between the position of PBGs and changes in the geometry and phase velocities of the layers. In particular, we observe that in the laminate with Gent phases undergoing equibiaxial contraction, the phase velocity of the pressure wave in the highly compressible Gent phase increases while it decreases for the highly compressible neo-Hookean phase (compare continuous blue and dotted black curves in Fig. 13(b)). For example, for the equibiaxial contraction of the magnitude $\lambda = 0.7$ the changes in the pressure wave velocities are $c_b^G/c_b^o = 1.11$ and $c_b^{nH}/c_b^o = 0.91$ for the highly compressible Gent and neo-Hookean phases, respectively. On the other hand, the layer thickness of the highly compressible Gent phase increases less than for the neo-Hookean phase, namely $d_b^G/d_b^o = 1.53$ and $d_b^{nH}/d_b^o = 1.62$ for the laminate subjected to the equibiaxial contraction of $\lambda = 0.7$ (compare continuous blue and dotted black curves in Fig. 13(a)). As a result, the PBGs in the laminates with Gent phases shift towards lower frequencies less than in the laminate with neo-Hookean phases. For the equibiaxial extension of the magnitude $\lambda = 1.6$, the changes in the pressure wave velocities are $c_b^G/c_b^o = 1.02$ and $c_b^{nH}/c_b^o = 1.03$ for the highly compressible Gent and neo-Hookean phases, respectively (Fig. 13(b)); whereas the changes in the layer thicknesses are $d_b^G/d_b^o = 0.37$ and $d_b^{nH}/d_b^o = 0.42$ (Fig. 13(a)). Although the difference in the phase velocities and layer thicknesses between the Gent and neo-Hookean phases is relatively small, the lower boundary of the first PBG shifts from $f_n = 4.04$ in the laminate with neo-Hookean phases up to $f_n = 4.50$ in the laminate with Gent phases undergoing the equibiaxial extension of the magnitude $\lambda = 1.6$ (see Fig. 12(b) and (d)). This happens because of the nonlinear dependence of PBGs on the changes in the material properties and geometry induced by deformation, especially in the case of the extreme deformations approaching the lock-up state ($\lambda^{lock} = 1.64$).

Finally, we consider the influence of compressibility of the laminate constituents on the BGs. Fig. 14 shows BGs as a function of compressibility of the thin softer layers embedded in the nearly incompressible stiffer phase. The results for the undeformed laminate are presented in Fig. 14(a) while the response of the laminate subjected to the equibiaxial compression ($\lambda = 0.5$) is shown in

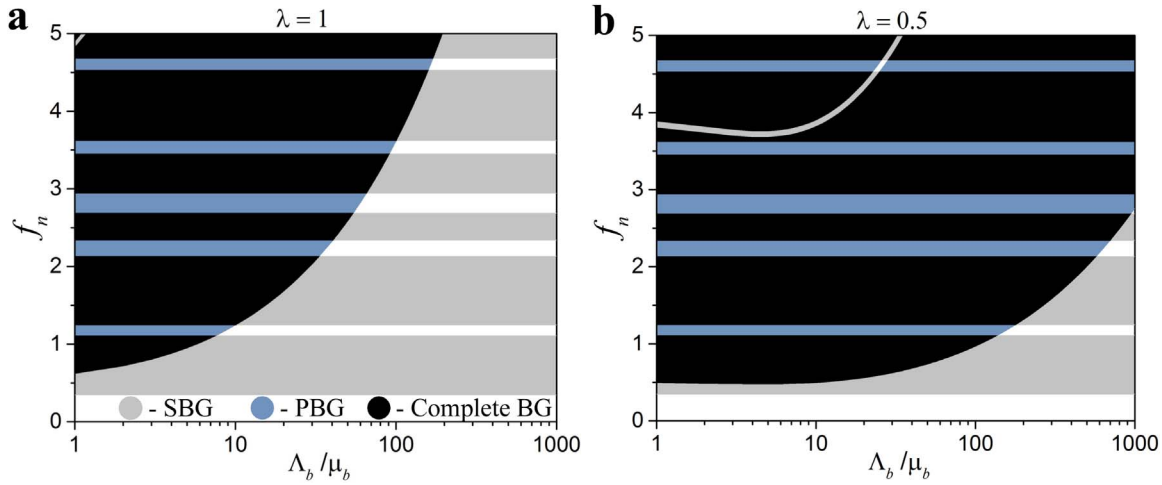

Fig. 14. Band gaps vs. compressibility of the phase b for the laminate with $v_a = 0.96$, $\mu_a/\mu_b = 100$, $\Lambda_a/\mu_a = 1000$, and $\rho_{0a}/\rho_{0b} = 1$ in the undeformed state (a) and the one subjected to the equibiaxial compression, $\lambda = 0.5$ (b).

Fig. 14(b). We observe complete BGs in low-frequency range when compressibility of softer phase increases (i.e. Λ_b/μ_b decreases). For example, for the undeformed laminate with $\Lambda_b/\mu_b = 10$ we observe the first complete BG of width $\Delta f_n = 0.89$ with the lower boundary at $f_n = 1.25$, while for $\Lambda_b/\mu_b > 35$ there are no complete BGs in the considered frequency range (see Fig. 14(a)). Furthermore, the maximal width and position of the lowest complete BG vary depending on the applied deformation; thus, for the laminate with $\Lambda_b/\mu_b = 10$ undergoing equibiaxial contraction ($\lambda = 0.5$), the lowest complete BG has width $\Delta f_n = 0.61$ with the lower boundary at $f_n = 0.50$ (see Fig. 14(b)). Note that an increase in compressibility of the thin layers results in a shift of PBGs towards lower frequencies, producing complete BGs at the low-frequency range. Thus, the wide complete BGs can be realized by composing laminates of a nearly incompressible matrix and highly compressible thin layers.

Fig. 15 shows BGs as functions of deformations for the laminates with both highly compressible phases exhibiting weak ((a) and (c)) and strong ((b) and (d)) stiffening effects. Consistent with the observations in Fig. 14, complete BGs shift down towards lower frequencies. Moreover, the position of complete BGs is highly tunable via deformation. In particular, in the undeformed laminate with $v_a = 0.95$, $\mu_a/\mu_b = 100$, $\Lambda_a/\mu_a = 10$, and $\Lambda_b/\mu_b = 5$, the lowest complete BG has the width $\Delta f_n = 0.29$ with the lower boundary at $f_n = 0.92$, while for the laminate under in-plane compression, $\lambda = 0.5$, the lowest complete BG has the width $\Delta f_n = 0.63$ with the lower boundary at $f_n = 0.57$ (see Fig. 15(a)). In case of the equibiaxial compression, $\lambda = 0.5$, the lowest complete BG has the width $\Delta f_n = 0.75$ with the lower boundary at $f_n = 0.46$ (see Fig. 15(c)). Consequently, the equibiaxial deformation has a more pronounced influence on the position of complete BGs as compared to the effect of the in-plane deformation.

A comparison of Fig. 15(a) and (b) (and also Fig. 15(c) and (d)) shows that in the laminate with Gent phases the PBGs are wider and they appear at higher frequencies compared to the PBGs in the laminates with neo-Hookean phases. This leads to the shifting of complete BGs towards higher frequencies. In particular, the lower boundary of the first complete BG in the laminate undergoing the in-plane contraction of the magnitude $\lambda = 0.5$ shifts from $f_n = 0.57$ up to $f_n = 0.71$ (compare Fig. 15(a) and (b)). In the case of the equibiaxial contraction of magnitude $\lambda = 0.7$, the lower boundary of the first complete BG shifts from $f_n = 0.57$ up to $f_n = 0.69$ (compare Fig. 15(c) and (d)). Similarly to the laminates considered in Fig. 12, the transformations of the BGs correlate with the changes in the thicknesses of the layers and phase velocities within each layer. In particular, an increase in the thicknesses of the layers ($d/d^o > 1$) shifts BGs towards lower frequencies whereas a decrease in the layer thicknesses ($d/d^o < 1$) shifts BGs towards higher frequencies. Once again, an increase in phase velocities ($c/c^o > 1$) shifts BGs towards higher frequencies, and a decrease in phase velocities ($c/c^o < 1$) shifts BGs towards lower frequencies.

3.2.3. An example of band gap structures for possible realistic layered materials

In this section, we provide a calculation of the BG structure for composites made of silicon rubber (Elite Double 32, Zhermarck) and one of a digital material used in multimaterial 3D printing (A85). Both of these materials can be described by the extended neo-Hookean strain energy function (30). Table 1 summarizes the corresponding parameters for these deformable materials. The phase a is made of the digital material A85, and the phase b is made of the silicon rubber Zhermarck Elite Double 32. Fig. 16 shows pressure and shear wave BGs as functions of the volume fraction of phase a in the undeformed and deformed laminates. We observe that the lowest complete BG has a maximal width for a certain volume fraction v_a in the undeformed laminate. In particular, for the laminate with $v_a = 0.87$ the lowest complete BG has width $\Delta f_n = 0.26$ with the lower boundary at $f_n = 2.50$, while for the laminate with $v_a = 0.1$ the lowest complete BG has width $\Delta f_n = 0.3$ with the lower boundary at $f_n = 3.4$. Consistent with previous observations in this paper, an extension of the laminate does not change the position of SBGs and shifts up PBGs towards higher frequencies. For example, the in-plane extension of the magnitude $\lambda = 1.3$ shifts the lower boundary of the first PBG from $f_n = 2.50$ up to $f_n = 3.23$ in the laminate with $v_a = 0.87$ (compare Fig. 16(a) and (b)).

To clarify how the pressure wave and complete BGs depend on deformation in the laminates made of silicon rubber (Elite Double

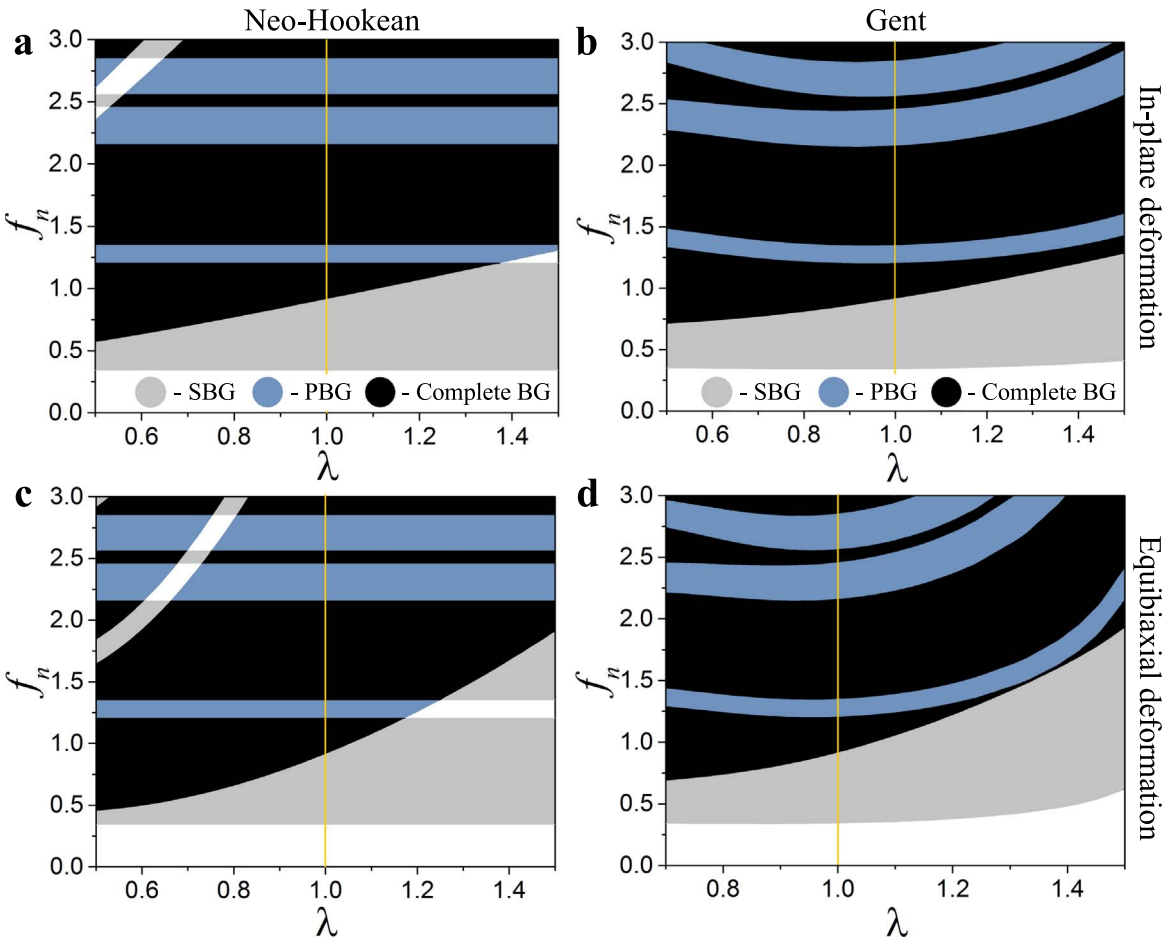

Fig. 15. Band gaps vs. stretch ratio for laminates subjected to ((a) and (b)) in-plane tension and ((c) and (d)) equibiaxial deformations. $\nu_a = 0.95$, $\mu_a/\mu_b = 100$, $\Lambda_a/\mu_a = 10$, $\Lambda_b/\mu_b = 5$, $\rho_{0a}/\rho_{0b} = 1$, and $J_{ma} = J_{mb} = 2.5$. (a) and (c) refer to laminate with neo-Hookean phases and (b) and (d) refer to laminate with Gent phases.

32, Zhermarck) and the digital material (A85), we present BGs as functions of the applied stretch ratio in Fig. 17. Fig. 17(a) and (b) illustrate how the in-plane (27) and equibiaxial deformations (28) of the layered material with $\nu_a = 0.3$ influence the BG structure. We observe that PBGs narrow and shift towards lower frequencies in the laminate undergoing contraction while an extension of the laminate widens and shifts PBGs towards higher frequencies. In particular, the lower boundary of the first PBG shifts from $f_n = 3.05$ down to $f_n = 2.45$ and its width decreases from $\Delta f_n = 1.33$ down to $\Delta f_n = 1.07$ in the laminate subjected to the in-plane contraction of the magnitude $\lambda = 0.8$ (see Fig. 17(a)). The equibiaxial deformation has a more pronounced effect on the PBGs; in particular, the equibiaxial contraction of the magnitude $\lambda = 0.8$ shifts the lower boundary of the first PBG from $f_n = 3.05$ down to $f_n = 1.98$ and narrows it from $\Delta f_n = 1.33$ down to $\Delta f_n = 0.86$ (see Fig. 17(b)). Remarkably, complete BGs can be induced in a required frequency range by deformation while the undeformed laminate does not produce complete BGs in that range. For example, the considered here laminate has no complete BGs (in the frequency range up to $f_n = 3$) in the undeformed state while it has the complete BG of width $\Delta f_n = 0.49$ when subjected to the in-plane contraction of the stretch ratio magnitude $\lambda = 0.83$ (see Fig. 17(a)).

Fig. 17 also shows the Bragg limit frequency, $f^{(BL)} = \bar{c}_{pw}/(2\pi d)$, and an estimate for the resonance frequency of stiffer layer, $f^{(R)} = \bar{c}_{pw}/(2\pi d_a)$. Clearly, the first complete BG occurs in the vicinity of the resonance frequency of the stiffer layer; moreover, it occurs above the Bragg limit. Hence, a composition of both Bragg scattering and inner resonance of stiffer layers participate in formation of complete BGs. In other words, in layered media the mechanism forming complete BGs is based on the destructive

Table 1
Material parameters.

Material	μ, MPa	Λ, MPa	ρ_0, kg/m^3
Elite Double 32	0.444	22.2	1050
Digital material (A85)	22	1100	1200

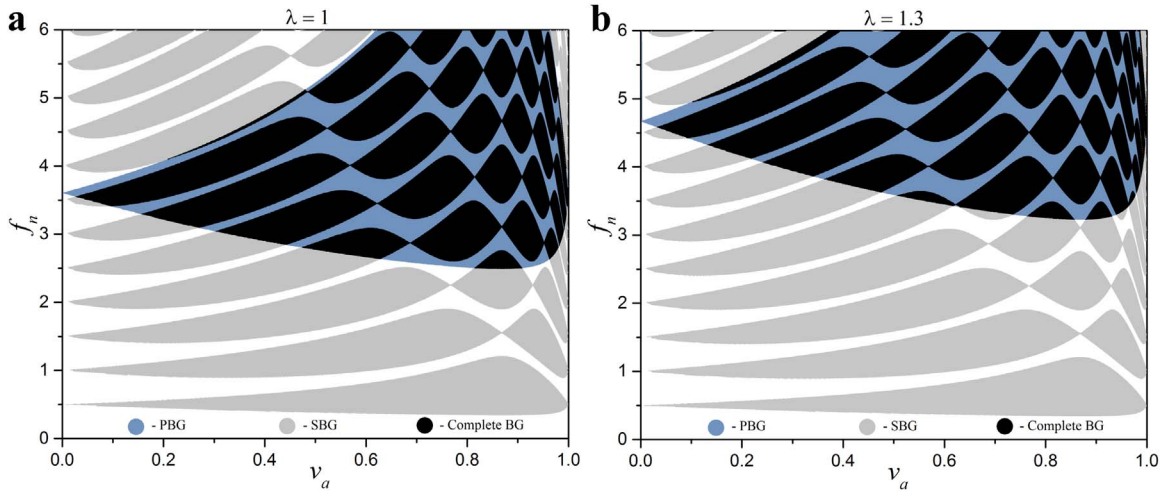

Fig. 16. Band gaps vs. volume fraction of the phase a in (a) the undeformed laminate and (b) the one subjected to the in-plane tension of the magnitude $\lambda = 1.3$ with $\mu_a/\mu_b = 50$, $\Lambda_a/\mu_a = 50$, $\Lambda_b/\mu_b = 50$, and $\rho_{0a}/\rho_{0b} = 1.14$. The gray, blue, and black colors correspond to the shear wave, pressure wave, and complete BGs, respectively. (For interpretation of the references to color in this figure caption, the reader is referred to the web version of this paper.)

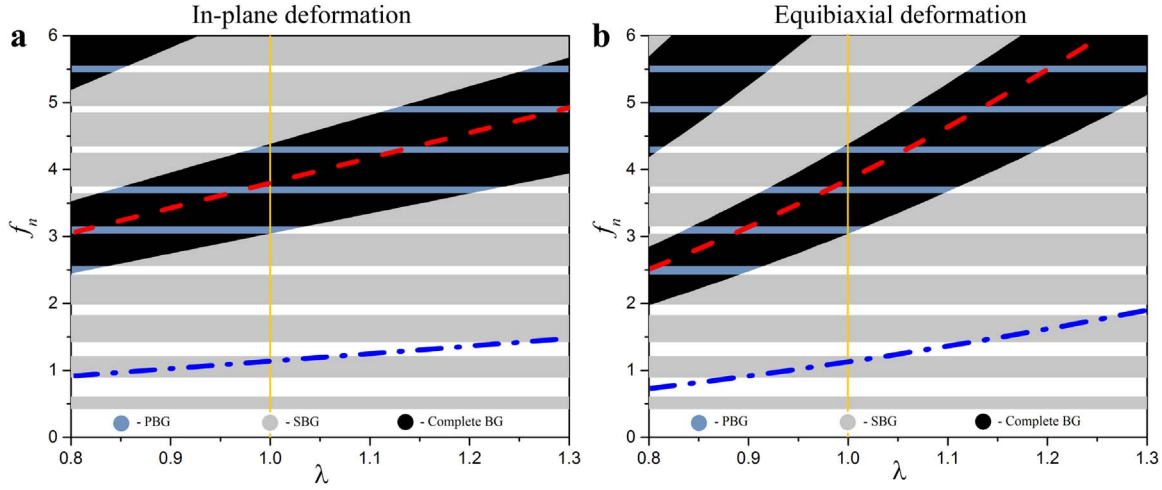

Fig. 17. Band gaps vs. in-plane (a) and equibiaxial (b) deformations for the laminate with $v_a = 0.3$, $\mu_a/\mu_b = 50$, $\Lambda_a/\mu_a = 50$, $\Lambda_b/\mu_b = 50$, and $\rho_{0a}/\rho_{0b} = 1.14$. The blue dash-dotted and red dashed curves correspond to estimates of the Bragg limit and the resonance frequency of stiffer layer, respectively. (For interpretation of the references to color in this figure caption, the reader is referred to the web version of this paper.)

interference of the scattered waves by the stiffer layers and inner resonances of these layers.

4. Conclusions

We considered elastic wave propagation in soft periodic layered media undergoing finite deformations. Firstly, based on an exact analytical solution for finitely deformed laminates with alternating neo-Hookean phases, we derived explicit relations for phase (41) and group velocities (55) and (56). Secondly, we obtained long wave estimates (59) and (63) for the phase velocities of pressure and shear waves propagating perpendicular to the layers in the finitely deformed *compressible* laminates with neo-Hookean and Gent phases. These estimates provide the important information on elastic wave propagation with wavelengths larger than microstructure size, namely $l \gtrsim \pi d$; moreover, these explicit expressions may provide estimates for transversely isotropic fiber composites. Thirdly, we provided a detailed analysis of the band gap structures for the waves propagating perpendicular to the layers in the incompressible and compressible layered materials. Specifically, we identified the key parameters and mechanisms influencing the shear wave, pressure wave, and complete BGs. Based on the analysis, we revealed the advantageous compositions of the laminates producing the wide BGs in the low-frequency range.

For *incompressible* laminates, we showed that (i) a small amount of a soft phase in a stiffer matrix produces wide SBGs; (ii) SBG structure in layered materials with phases exhibiting weak stiffening effects is not influenced by deformation because deformation induced changes in geometry and effective material properties compensate each other; (iii) contraction or extension of the laminate

with stiffening in phases widens and shifts up SBGs towards higher frequencies due to the stronger effect of deformation induced changes in the material properties (as compared to the geometry changes).

For *compressible* laminates, we showed that (i) wide complete BGs can be produced by composing periodic laminates with thin highly compressible layers embedded in a nearly incompressible matrix; (ii) the dominant mechanism influencing PBGs is the deformation induced change in the thicknesses of the layers; (iii) by application of deformation to the laminates with highly compressible phases, complete BGs in the low-frequency range can be produced. These low-frequency range BGs are not accessible for laminates with nearly incompressible phases.

In this work, we considered small amplitude motions (superimposed on finite deformations); therefore, the presented results cannot be fully applied for finite amplitude elastic waves propagating in soft microstructured materials. This can be potentially an interesting direction of future research. Another aspect is the influence of the direction of elastic wave propagation. We fully address this aspect in the analysis of long waves considering any direction of wave propagation and any applied deformations. However, our analysis of elastic wave band gaps focuses on the normal direction of wave propagation, and the consideration of oblique elastic waves would require different techniques such as Bloch–Floquet numerical analysis or transfer matrix methods. Finally, we note that a consideration of dissipation can potentially improve the accuracy of the predictions, especially for the composites with constituents characterized by strong damping effects (Babaee et al., 2015).

Acknowledgments

This work was supported by the BASF North American Center for Research of Advanced Materials. S.R. and P.G. gratefully acknowledge the support of the Israel Science Foundation (grant 1550/15 and 1973/15). S.R. thanks the support of Taub Foundation through the Horev Fellowship – Leaders in Science and Technology.

References

Arruda, E.M., Boyce, M.C., 1993. A three-dimensional constitutive model for the large stretch behavior of rubber elastic materials. J. Mech. Phys. Solids 41, 389–412.
Auld, B., 1990. Acoustic Fields and Waves in Solids. Krieger Publishing Company, Malabar, Fl.
Auriault, J.-L., 1994. Acoustics of heterogeneous media: macroscopic behavior by homogenization. Curr. Top. Acoust. Res. 1, 63–90.
Auriault, J.-L., Bonnet, G., 1985. Dynamique des composites lastiques priodiques. Arch Mech. 37 (4–5), 269–284.
Auriault, J.-L., Boutin, C., 2012. Long wavelength inner-resonance cut-off frequencies in elastic composite materials. Int. J. Solids Struct. 49, 3269–3281.
Babaee, S., Shim, J., Weaver, J., Chen, E., Patel, N., Bertoldi, K., 2013. 3D soft metamaterials with negative Poisson's ratio. Adv. Mater. 25 (36), 5044–5049.
Babaee, S., Viard, N., Wang, P., Fang, N.X., Bertoldi, K., 2016. Harnessing deformation to switch on and off the propagation of sound. Adv. Mater. 28 (8), 1631–1635.
Babaee, S., Wang, P., Bertoldi, K., 2015. Three-dimensional adaptive soft phononic crystals. J. Appl. Phys. 117, 244903.
Bedford, A., Drumheller, D., 1994. Elastic Wave Propagation. Wiley, Bedford.
Bertoldi, K., Boyce, M.C., 2008a. Mechanically triggered transformations of phononic band gaps in periodic elastomeric structures. Phys. Rev. B 77 (5), 052105.
Bertoldi, K., Boyce, M.C., 2008b. Wave propagation and instabilities in monolithic and periodically structured elastomeric materials undergoing large deformations. Phys. Rev. B 78, 184107.
Bertoldi, K., Boyce, M.C., Deschanel, S., Prange, S.M., Mullin, T., 2008. Mechanics of deformation-triggered pattern transformations and superelastic behavior in periodic elastomeric structures. J. Mech. Phys. Solids 56 (8), 2642–2668.
Boulanger, P., Hayes, M., Trimarco, C., 1994. Finite-amplitude plane waves in deformed Hadamard elastic materials. Geophys. J. Int. 118 (2), 447–458.
Brunet, T., Leng, J., Mondain-Monval, O., 2013. Soft acoustic metamaterials. Science 342 (6156), 323–324.
Crosby, A.J., 2010. Why should we care about buckling? Soft Matter 6, 5660.
deBotton, G., 2005. Transversely isotropic sequentially laminated composites in finite elasticity. J. Mech. Phys. Solids 53, 1334–1361.
Destrade, M., Ogden, R.W., 2011. On magneto-acoustic waves in finitely deformed elastic solids. Math. Mech. Solids 16, 594–604.
Galich, P.I., Rudykh, S., 2015a. Comment on Disentangling longitudinal and shear elastic waves by neo-Hookean soft devices [Appl. Phys. Lett. 106 (2015) 161903]. Appl. Phys. Lett. 107, 056101., http://dx.doi.org/10.1063/1.4928392.
Galich, P.I., Rudykh, S., 2015b. Influence of stiffening on elastic wave propagation in extremely deformed soft matter: from nearly incompressible to auxetic materials. Extreme Mech. Lett. 4, 156–161.
Galich, P.I., Rudykh, S., 2016. Manipulating pressure and shear elastic waves in dielectric elastomers via external electric stimuli. Int. J. Solids Struct. 91, 18–25.
Gei, M., Roccabianca, S., Bacca, M., 2011. Controlling bandgap in electroactive polymer-based structures. IEEE/ASME Trans. Mechatron. 16 (1), 102–107.
Gent, A.N., 1996. A new constitutive relation for rubber. Rubber Chem. Technol. 69, 59–61.
Horgan, C.O., Saccomandi, G., 2004. Compressible hyperelastic isotropic materials, constitutive models, limiting chain extensibility. J. Elast. 77 (2), 123–138.
Hussein, M.I., 2009. Reduced Bloch mode expansion for periodic media band structure calculations. Proc. R. Soc. Lond. Ser. A 465 (2109), 2825–2848.
Khelif, A., Adibi, A., 2016. Phononic Crystals. Springer, New York.
Kittel, C., 2004. Introduction to Solid State Physics 8th ed.. Wiley, Hoboken, N.J.
Kolle, M., Lethbridge, A., Kreysing, M., Baumberg, J., Aizenberg, J., Vukusic, P., 2013. Bio-inspired band-gap tunable elastic optical multilayer fibers. Adv. Mater. 25 (15), 2239–2245.
Kushwaha, M., Halevi, P., Dobrzynski, L., Djafari-Rouhani, B., 1993. Acoustic band structure of periodic elastic composites. Phys. Rev. Lett. 71 (13), 2022–2025.
Kushwaha, M., Halevi, P., Martinez, G., Dobrzynski, L., Djafari-Rouhani, B., 1994. Theory of acoustic band structure of periodic elastic composites. Phys. Rev. B 49 (4), 2313–2322.
Li, Y., Kaynia, N., Rudykh, S., Boyce, M.C., 2013. Wrinkling of interfacial layers in stratified composites. Adv. Eng. Mater. 15 (10), 921–926.
Liu, X.N., Hu, G.K., Huang, G.L., Sun, C.T., 2011. An elastic metamaterial with simultaneously negative mass density and bulk modulus. Appl. Phys. Lett. 98, 251907.
Liu, Z., Zhang, X., Mao, Y., Zhu, Y., Yang, Z., Chan, C., Sheng, P., 2000. Locally resonant sonic materials. Science 289 (5485), 1734–1736.
Mousanezhad, D., Babaee, S., Ghosh, R., Mahdi, E., Bertoldi, K., Vaziri, A., 2015. Honeycomb phononic crystals with self-similar hierarchy. Phys. Rev. B 92, 104304.
Nayfeh, A.H., 1995. Wave Propagation in Layered Anisotropic Media: With Applications to Composites. Elsevier Science, Amsterdam, New York.
Ogden, R.W., 1997. Non-Linear Elastic Deformations. Dover Publications, New York.
Rosen, B.W., 1965. Mechanics of composite strengthening. In: Fibre Composite Materials. American Society for Metals, Ohio, pp. 37–75.
Rudykh, S., Boyce, M., 2014a. Analysis of elasmoid fish imbricated layered scale-tissue systems and their bio-inspired analogues at finite strains and bending. IMA J. Appl. Math. 79, 830–847.
Rudykh, S., Boyce, M., 2014b. Transforming wave propagation in layered media via instability-induced interfacial wrinkling. Phys. Rev. Lett. 112, 034301.
Rudykh, S., deBotton, G., 2012. Instabilities of hyperelastic fiber composites: micromechanical versus numerical analyses. J. Elast. 106, 123–147.
Rudykh, S., Ortiz, C., Boyce, M., 2015. Flexibility and protection by design: imbricated hybrid microstructures of bio-inspired armor. Soft Matter 11, 2547–2554.
Rytov, S., 1956. Acoustical properties of a thinly laminated medium. Sov. Phys. Acoust. 2, 68–80.

Slesarenko, V., Rudykh, S., 2016. Harnessing viscoelasticity and instabilities for tuning wavy patterns in soft layered composites. Soft Matter 12, 3677–3682.
Spinelli, S.A., Lopez-Pamies, O., 2015. Some simple explicit results for the elastic dielectric properties and stability of layered composites. Int. J. Eng. Sci. 88, 15–28.
Tanaka, Y., Tomoyasu, Y., Tamura, S.-I., 2000. Band structure of acoustic waves in phononic lattices: two-dimensional composites with large acoustic mismatch. Phys. Rev. B 62 (11), 7387–7392.
Triantafyllidis, N., Maker, B.N., 1985. On the comparison between microscopic and macroscopic instability mechanisms in a class of fiber-reinforced composites. J. Appl. Mech. Trans. ASME 52, 794–800.
Tzianetopoulou, T., 2007. Micro-and Macromechanics of Single Crystal and Polygrannular Lamellar Block Copolymers (Ph.D. thesis). MIT.
Wang, P., Shim, J., Bertoldi, K., 2013. Effects of geometric and material non-linearities on the tunable response of phononic crystals. Phys. Rev. B 88, 014304.
Zhou, X.-Z., Wang, Y.-S., Zhang, C., 2009. Effects of material parameters on elastic band gaps of two-dimensional solid phononic crystals. J. Appl. Phys. 106, 1.

Shear Wave Propagation and Band Gaps in Finitely Deformed Dielectric Elastomer Laminates: Long Wave Estimates and Exact Solution

Pavel I. Galich
Department of Aerospace Engineering,
Technion—Israel Institute of Technology,
Haifa 32000, Israel

Stephan Rudykh
Department of Aerospace Engineering,
Technion—Israel Institute of Technology,
Haifa 32000, Israel
e-mail: rudykh@technion.ac.il

We analyze small amplitude shear waves (SWs) propagating in dielectric elastomer (DE) laminates subjected to finite deformations and electrostatic excitations. First, we derive long wave estimates for phase and group velocities of the shear waves propagating in any direction in DE laminates subjected to any homogenous deformation in the presence of an electric filed. To this end, we utilize a micromechanics-based energy potential for layered media with incompressible phases described by neo-Hookean ideal DE model. The long wave estimates reveal the significant influence of electric field on the shear wave propagation. However, there exists a configuration, for which electric field does not influence shear waves directly, and can only alter the shear waves through deformation. We study this specific configuration in detail, and derive an exact solution for the steady-state small amplitude waves propagating in the direction perpendicular to the finitely deformed DE layers subjected to electrostatic excitation. In agreement with the long wave estimate, the exact dispersion relation and the corresponding shear wave band gaps (SBGs)—forbidden frequency regions—are not influenced by electric field. However, SBGs in DE laminates with highly nonlinear electroelastic phases still can be manipulated by electric field through electrostatically induced deformation. In particular, SBGs in DE laminates with electroelastic Gent phases widen and shift toward higher frequencies under application of an electric field perpendicular to the layers. However, in laminates with neo-Hookean ideal DE phases, SBGs are not influenced either by electric field or by deformation. This is due to the competing mechanisms of two governing factors: changes in geometry and material properties induced by deformation. In this particular case, these two competing factors entirely cancel each other.
[DOI: 10.1115/1.4037159]

Keywords: dielectric elastomers, layered materials, wave propagation, finite deformations, band gaps

1 Introduction

Dielectric elastomers (DEs) can develop large deformations when excited by an external electric field [1]. Therefore, these artificial muscles are of great interest for various applications, such as soft robotics [2], various actuators [3,4], energy generators [5,6], to name a few. It has been recently shown that large deformations can significantly influence wave propagation even in relatively simple deformable materials without electromechanical coupling [7–10]. In turn, DEs offer a way to manipulate elastic waves via application of an external electric field. Thus, for example, the effect has been used to control wave propagation in homogenous DEs [11–13]. Moreover, microstructured DEs hold even greater potential for active control of elastic waves by an electric field [14,15]. Hence, investigation of wave propagation in composite DEs opens new possibilities in improving of small length-scale devices, for example, micro-electromechanical systems, where an electric field is the preferred operated variable.

Following the work of Toupin [16], the theory of nonlinear electroelasticity for homogeneous isotropic hyperelastic media has been revised recently by Dorfmann and Ogden [17], McMeeking and Landis [18], and Suo et al. [19]. More recently, Cohen et al. [20] proposed a model based on considerations of polymer networks under electromechanical loadings. Motivated by potential enhancement of electromechanical coupling, which is typically rather weak in DEs, microstructured DEs have been explored [21–23] showing significant potential of this approach. We note that microstructured DEs may develop instabilities at different length scales [24–28].

The analysis of small amplitude wave propagation in finitely deformed nonlinear electroelastic materials in the presence of an electric field in the frame of the quasi-electrostatic approximation was presented by Dorfmann and Ogden [29]. This paper has been followed by a number of works on elastic wave propagation in finitely deformed homogenous and composite DEs [11–13,30]. Note that layered DEs are of specific importance since they may be realized through various layer-by-layer material fabrication techniques, which already allow manufacturing of deformable layered materials across length scales [31–33]. However, the existing literature on elastic wave propagation in finitely deformed DE laminates in the presence of an electric field reports some contradictory results. In particular, Shmuel and deBotton [30] considered shear wave band gap (SBGs) structures in DE laminates with ideal dielectric neo-Hookean incompressible phases, and they

Contributed by the Applied Mechanics Division of ASME for publication in the Journal of Applied Mechanics. Manuscript received April 11, 2017; final manuscript received June 17, 2017; published online July 7, 2017. Assoc. Editor: Daining Fang.

reported that these SBGs alter under application of an external electric field. However, our results clearly show that the SBGs in the neo-Hookean DE laminates are not influenced either by electric field or by induced deformation. We note that our results agree with the exact solution for the long waves in DE laminates. Moreover, the derived dispersion relation reduces to the classical result for linear elastic layered media [34] in the absence of an electric field and deformation. We should note that Shmuel and deBotton [35] have just published the corrigendum reporting that the SBGs in the neo-Hookean DEs are shifted by electric field toward higher frequencies. However, these new results by Shmuel and deBotton [35] do not agree with the exact solution for long waves and with the exact solution for any wavelengths as detailed in the Appendix.

To shed light on the influence of electric field on shear waves in DE laminates, we analyze small amplitude shear wave propagating in DE layered media comprised of two alternating isotropic incompressible electroelastic phases. First, we derive the long wave estimates for phase and group velocities of shear waves propagating in any direction in DE laminates undergoing any homogenous deformation in the presence of an electric field. To this end, we make use of an exact solution for finitely deformed DE laminates allowing us to express an effective energy potential in terms of microstructure parameters and physical properties of the constituents. These estimates reveal the significant dependence of the shear wave characteristics on electric field and deformation. However, we found that there is a unique configuration—when elastic waves propagate perpendicular to the layers—for which phase and group velocities are independent of electric field, and these acoustic characteristics can be influenced only through electrostatically induced deformations. This holds true for any direction of an applied electric field. Again, for any other direction of propagation, the phase and group velocities explicitly depend on electric field. We further analyze this specific configuration and derive the dispersion relation for the small amplitude shear waves propagating perpendicular to finitely deformed layers with electric field applied perpendicular to the layers. The derived dispersion relation is shown to be of the same form as the relation for hyperelastic laminates [36] undergoing finite deformations in the absence of an electric field. Thus, shear waves propagating perpendicular to the layers in DE laminates are not affected by electric field directly, and they can be influenced by electric field only through induced deformations. Note that this result is in full agreement with the exact solution for long waves. Finally, we analyze SBGs in DE laminates by making use of the derived dispersion relation. In particular, we show that SBGs widen and shift up toward higher frequencies in DE laminates with ideal dielectric Gent phases subjected to an electric field through the thickness of the layers. Once again, SBGs in the DE laminates with neo-Hookean ideal dielectric phases do not depend on electric field.

2 Theoretical Background

To describe finite deformations of a continuous electroelastic body occupying Ω_0 and Ω_t domains in the reference and current configurations, respectively, we introduce the deformation gradient $\mathbf{F}(\mathbf{X},t)=\partial\mathbf{x}(\mathbf{X},t)/\partial\mathbf{X}$, where $\mathbf{X}$ and $\mathbf{x}$ are position vectors in the reference and current configurations, respectively. Then, the Jacobian $J\equiv \det\mathbf{F}>0$ defines the volume change of the body with respect to the reference state.

2.1 Electrostatics. In this work, we adopt the so-called quasi-electrostatic approximation assuming the absence of magnetic fields and neglecting electromagnetic interactions. Thus, in the absence of free body charges and currents, the equations of electrostatics in the current configuration read as

$$\mathrm{div}\mathbf{D}=0 \ \text{ and } \ \mathrm{curl}\mathbf{E}=\mathbf{0} \tag{1}$$

where $\mathbf{D}$ and $\mathbf{E}$ denote electric displacement and electric field applied in the current configuration, respectively. Here and thereafter, the differential operators with the first low-case letter refer to the current configuration, while the differential operators with the first upper-case letter refer to the reference configuration.

In the reference configuration, the equations of electrostatics read as

$$\mathrm{Div}\mathbf{D}_L=0 \ \text{ and } \ \mathrm{Curl}\mathbf{E}_L=\mathbf{0} \tag{2}$$

where

$$\mathbf{D}_L=J\mathbf{F}^{-1}\cdot\mathbf{D} \ \text{ and } \ \mathbf{E}_L=\mathbf{F}^T\cdot\mathbf{E} \tag{3}$$

are the Lagrangian counterparts of $\mathbf{D}$ and $\mathbf{E}$, respectively.

2.2 Mechanical Balance Laws. In the absence of body forces, the linear and angular momentum balance for an electroelastic material are

$$\mathrm{div}\boldsymbol{\tau}=\rho\mathbf{x}_{,tt} \ \text{ and } \ \boldsymbol{\tau}=\boldsymbol{\tau}^T \tag{4}$$

where $\boldsymbol{\tau}$ represents the *total* Cauchy stress tensor and ρ is the mass density of the material in the current configuration.

In Lagrangian description, the balance equations (4) read as

$$\mathrm{Div}\mathbf{P}=\rho_0\mathbf{x}_{,tt} \ \text{ and } \ \mathbf{P}\cdot\mathbf{F}^T=\mathbf{F}\cdot\mathbf{P}^T \tag{5}$$

where

$$\mathbf{P}=J\boldsymbol{\tau}\cdot\mathbf{F}^{-T} \ \text{ and } \ \rho_0=J\rho \tag{6}$$

are the first Piola–Kirchhoff *total* stress tensor and the mass density of the material in the reference configuration, respectively.

2.3 Constitutive Equations. To model nonlinear behavior of DEs, we consider an energy potential $\psi(\mathbf{F},\mathbf{D}_L)$, as introduced in Dorfmann and Ogden [17]. The strain energy-density potential is a function of deformation gradient $\mathbf{F}$ and Lagrangian counterpart of electric displacement $\mathbf{D}_L$. Then, for an electroelastic material, the first Piola–Kirchhoff total stress tensor and Lagrangian counterpart of electric field are given by

$$\mathbf{P}=\frac{\partial\psi}{\partial\mathbf{F}} \quad \text{and} \quad \mathbf{E}_L=\frac{\partial\psi}{\partial\mathbf{D}_L} \tag{7}$$

For an incompressible material, $J=1$, and the constitutive equations (7) modify as

$$\mathbf{P}=\frac{\partial\psi}{\partial\mathbf{F}}-p\mathbf{F}^{-T} \quad \text{and} \quad \mathbf{E}_L=\frac{\partial\psi}{\partial\mathbf{D}_L} \tag{8}$$

where p denotes an unknown Lagrange multiplier.

2.4 Incremental Equations. For an electroelastic material, the incremental constitutive equations for the first Piola–Kirchhoff stress and Lagrangian electric field read as

$$\dot{\mathbf{P}}=\mathbb{C}_0:\dot{\mathbf{F}}+\boldsymbol{\mathcal{M}}_0\cdot\dot{\mathbf{D}}_L \quad \text{and} \quad \dot{\mathbf{E}}_L=\dot{\mathbf{F}}:\boldsymbol{\mathcal{M}}_0+\mathbf{K}_0\cdot\dot{\mathbf{D}}_L \tag{9}$$

respectively. Here, the superposed dot represent incremental changes in the corresponding variables; $\mathbb{C}_0$, $\boldsymbol{\mathcal{M}}_0$, and $\mathbf{K}_0$ are the tensors of electroelastic moduli defined as

$$\mathbb{C}_0=\frac{\partial^2\psi}{\partial\mathbf{F}\partial\mathbf{F}}, \quad \boldsymbol{\mathcal{M}}_0=\frac{\partial^2\psi}{\partial\mathbf{F}\partial\mathbf{D}_L} \quad \text{and} \quad \mathbf{K}_0=\frac{\partial^2\psi}{\partial\mathbf{D}_L\partial\mathbf{D}_L} \tag{10}$$

For an incompressible material, the incremental equations (9) read as

$$\dot{\mathbf{P}} = \mathbb{C}_0 : \dot{\mathbf{F}} + p\mathbf{F}^{-T}\cdot\dot{\mathbf{F}}^{T}\cdot\mathbf{F}^{-T} - \dot{p}\mathbf{F}^{-T} + \boldsymbol{\mathcal{M}}_0\cdot\dot{\mathbf{D}}_L \quad \text{and} \quad \dot{\mathbf{E}}_L = \dot{\mathbf{F}} : \boldsymbol{\mathcal{M}}_0 + \mathbf{K}_0\cdot\dot{\mathbf{D}}_L \tag{11}$$

2.5 Incremental Motions Superimposed on Finite Deformation in the Presence of an Electric Field. In the frame of the updated Lagrangian formulation, the incremental forms of the governing Eqs. (2) and $(5)_1$, describing small motions superimposed on finite deformation, transform to

$$\mathrm{div}\dot{\mathbf{D}}_{L\star} = 0, \quad \mathrm{curl}\dot{\mathbf{E}}_{L\star} = \mathbf{0}, \text{ and } \mathrm{div}\dot{\mathbf{P}}_{\star} = \rho\ddot{\mathbf{x}}_{,tt} \tag{12}$$

where

$$\dot{\mathbf{D}}_{L\star} = J^{-1}\mathbf{F}\cdot\dot{\mathbf{D}}_L, \quad \dot{\mathbf{E}}_{L\star} = \mathbf{F}^{-T}\cdot\dot{\mathbf{E}}_L, \text{ and } \dot{\mathbf{P}}_{\star} = J^{-1}\dot{\mathbf{P}}\cdot\mathbf{F}^{T} \tag{13}$$

are the so-called push-forward versions of $\dot{\mathbf{D}}_L$, $\dot{\mathbf{E}}_L$, and $\dot{\mathbf{P}}$, respectively. Identifying the field of incremental displacements as $\mathbf{u} = \dot{\mathbf{x}}$ and then displacement gradient as $\mathbf{H} = \mathrm{grad}\mathbf{u} = \dot{\mathbf{F}}\cdot\mathbf{F}^{-1}$, we obtain the following updated incremental relations (9):

$$\dot{\mathbf{P}}_{\star} = \mathbb{C} : \mathbf{H} + \boldsymbol{\mathcal{M}}\cdot\dot{\mathbf{D}}_{L\star} \quad \text{and} \quad \dot{\mathbf{E}}_{L\star} = \mathbf{H} : \boldsymbol{\mathcal{M}} + \mathbf{K}\cdot\dot{\mathbf{D}}_{L\star} \tag{14}$$

where

$$\mathbb{C}_{irks} = J^{-1}\mathbb{C}_{0ijkl}F_{rj}F_{sl}, \quad \mathcal{M}_{irk} = \mathcal{M}_{0ijm}F_{rj}F^{-1}_{mk} \quad \text{and} \quad \mathbf{K} = J\mathbf{F}^{-T}\cdot\mathbf{K}_0\cdot\mathbf{F}^{-1} \tag{15}$$

are the updated tensors of electroelastic moduli, possessing the following symmetries:

$$\mathbb{C}_{irks} = \mathbb{C}_{ksir}, \quad \mathcal{M}_{irk} = \mathcal{M}_{rik}, \quad \text{and} \quad \mathbf{K} = \mathbf{K}^{T} \tag{16}$$

For an incompressible material, the incremental equations (14) read as

$$\dot{\mathbf{P}}_{\star} = \mathbb{C} : \mathbf{H} + p\mathbf{H}^{T} - \dot{p}\mathbf{I} + \boldsymbol{\mathcal{M}}\cdot\dot{\mathbf{D}}_{L\star} \quad \text{and} \quad \dot{\mathbf{E}}_{L\star} = \mathbf{H} : \boldsymbol{\mathcal{M}} + \mathbf{K}\cdot\dot{\mathbf{D}}_{L\star} \tag{17}$$

moreover, the incompressibility assumption implies

$$\mathrm{tr}\mathbf{H} \equiv \mathrm{div}\,\mathbf{u} = 0 \tag{18}$$

2.6 Plane Waves in Incompressible DEs Subjected to Electromechanical Loading. We seek for solution of Eq. (12) in the form of plane waves with constant polarizations [29]

$$\mathbf{u} = \mathbf{g}f(\mathbf{n}\cdot\mathbf{x} - ct), \quad \dot{\mathbf{D}}_{L\star} = \mathbf{d}g(\mathbf{n}\cdot\mathbf{x} - ct), \quad \text{and} \quad \dot{p} = \Pi(\mathbf{n}\cdot\mathbf{x} - ct) \tag{19}$$

where f, g, and Π are arbitrary twice continuously differentiable, continuously differentiable, and continuous functions, respectively; the unit vectors $\mathbf{g}$ and $\mathbf{d}$ represent polarization vectors of mechanical and electrical displacements, respectively; the unit vector $\mathbf{n}$ denotes the direction of wave propagation; and c is the phase velocity of the wave.

Substitution of Eqs. (17) and (19) into Eqs. (12) and (18) yields

$$\hat{\mathbf{A}}\cdot\mathbf{g} = \rho c^2\mathbf{g} \quad \text{and} \quad \mathbf{g}\cdot\mathbf{n} = 0 \tag{20}$$

where $\hat{\mathbf{A}}$ is the so-called generalized acoustic tensor defining the condition of propagation of plane elastic waves in an incompressible electroelastic solid. The generalized acoustic tensor for an electroelastic material with an arbitrary energy potential $\psi(\mathbf{F}, \mathbf{D}_L)$ can be calculated as follows [37]:

$$\hat{\mathbf{A}} = \hat{\mathbf{Q}} - \frac{2}{(\mathrm{tr}\hat{\mathbf{K}})^2 - \mathrm{tr}\hat{\mathbf{K}}^2}\hat{\mathbf{R}}\cdot((\mathrm{tr}\hat{\mathbf{K}})\hat{\mathbf{I}} - \hat{\mathbf{K}})\cdot\hat{\mathbf{R}}^{T} \tag{21}$$

where

$$\hat{\mathbf{I}} = \mathbf{I} - \mathbf{n}\otimes\mathbf{n} \tag{22}$$

is the projection on the plane normal to $\mathbf{n}$; $\hat{\mathbf{K}} = \hat{\mathbf{I}}\cdot\mathbf{K}\cdot\hat{\mathbf{I}}$, $\hat{\mathbf{Q}} = \hat{\mathbf{I}}\cdot\mathbf{Q}\cdot\hat{\mathbf{I}}$ and $\hat{\mathbf{R}} = \hat{\mathbf{I}}\cdot\mathbf{R}\cdot\hat{\mathbf{I}}$, where

$$Q_{ik} = \mathbb{C}_{ijkl}n_jn_l \quad \text{and} \quad \mathbf{R} = \mathbf{n}\cdot\boldsymbol{\mathcal{M}} \tag{23}$$

Note that the generalized acoustic tensor $\hat{\mathbf{A}}$ is symmetric. Recall that an incompressible electroelastic material is strongly elliptic (stable), if its generalized acoustic tensor $\hat{\mathbf{A}}$ is positively defined, i.e., $\mathbf{g}\cdot\hat{\mathbf{A}}\cdot\mathbf{g} > 0$ for any unit vectors $\mathbf{n}$ and $\mathbf{g}$ satisfying the incompressibility constraint $(J = 1)$ $\mathbf{n}\cdot\mathbf{g} = 0$ along an electromechanical loading path defined through a combination of $\mathbf{D}_L$ and $\mathbf{F}$.

3 Analysis and Results

Consider periodic laminates made out of two isotropic incompressible alternating ideal DE phases with volume fractions $v^{(a)}$ and $v^{(b)} = 1 - v^{(a)}$. Here and thereafter, the fields and parameters of the phases are denoted by superscripts $(\bullet)^{(a)}$ and $(\bullet)^{(b)}$, respectively. Geometrically, the layers are characterized by their thicknesses $H^{(a)} = v^{(a)}H$ and $H^{(b)} = v^{(b)}H$, where H is the period of the undeformed laminate (see Fig. 1(*a*)). In the deformed laminates (see Fig. 1(*b*)), the layer thicknesses change as follows:

$$h^{(a)} = \lambda_2^{(a)}H^{(a)}, \quad h^{(b)} = \lambda_2^{(b)}H^{(b)}, \text{ and } h = \bar{\lambda}_2 H \tag{24}$$

where $\bar{\lambda}_2 = v^{(a)}\lambda_2^{(a)} + v^{(b)}\lambda_2^{(b)}$ and $\lambda_2^{(a,b)}$ are the stretch ratios in the direction $\mathbf{e}_2$ for phases a and b, respectively.

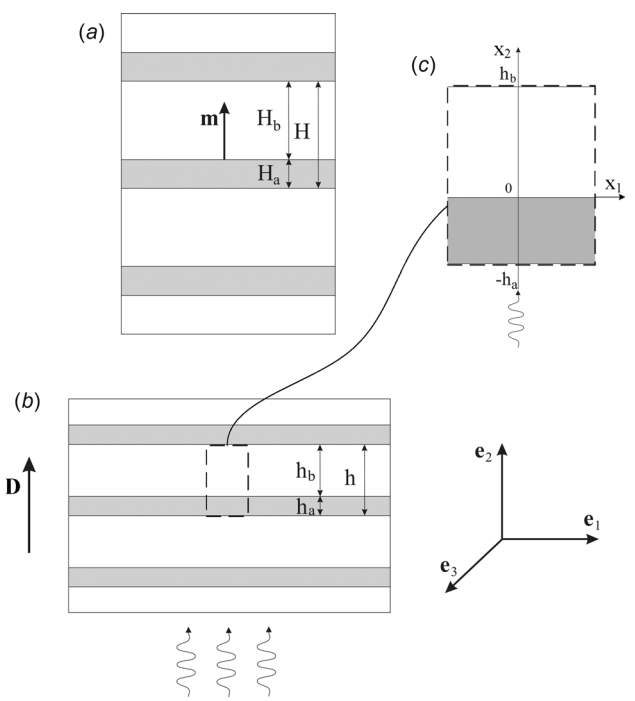

Fig. 1 Schematic representation of the undeformed (*a*) and subjected to the electromechanical load (*b*) periodic layered material with alternating phases *a* and *b*. A unit cell (*c*); $(\mathbf{e}_1, \mathbf{e}_2, \mathbf{e}_3)$ is the orthonormal basis.

The macroscopically applied electromechanical loads are expressed in terms of the average deformation gradient $\bar{\mathbf{F}}$ and Lagrangian electric displacement $\bar{\mathbf{D}}_L$, namely

$$\bar{\mathbf{F}} = v^{(a)}\mathbf{F}^{(a)} + v^{(b)}\mathbf{F}^{(b)} \quad \text{and} \quad \bar{\mathbf{D}}_L = v^{(a)}\mathbf{D}_L^{(a)} + v^{(b)}\mathbf{D}_L^{(b)} \tag{25}$$

The continuity of the displacements along the interface between the layers yields condition for the deformation gradients $\mathbf{F}^{(a)}$ and $\mathbf{F}^{(b)}$

$$(\mathbf{F}^{(a)} - \mathbf{F}^{(b)}) \cdot \mathbf{q} = \mathbf{0} \tag{26}$$

and the continuity of the tractions across the interface between the layers yields

$$(\mathbf{P}^{(a)} - \mathbf{P}^{(b)}) \cdot \mathbf{m} = \mathbf{0} \tag{27}$$

where unit vector $\mathbf{m}$ denotes the initial lamination direction (see Fig. 1(*a*)), and $\mathbf{q}$ is an arbitrary unit vector perpendicular to $\mathbf{m}$. In the absence of free charges at the interfaces, the jump conditions for Lagrangian electric displacement and electric field are

$$(\mathbf{D}_L^{(a)} - \mathbf{D}_L^{(b)}) \cdot \mathbf{m} = 0 \quad \text{and} \quad (\mathbf{E}_L^{(a)} - \mathbf{E}_L^{(b)}) \times \mathbf{m} = \mathbf{0} \tag{28}$$

In the current configuration, the interface jump conditions (27) and (28) read as

$$(\boldsymbol{\tau}^{(a)} - \boldsymbol{\tau}^{(b)}) \cdot \mathbf{m} = \mathbf{0}, \quad (\mathbf{D}^{(a)} - \mathbf{D}^{(b)}) \cdot \mathbf{m} = 0 \quad \text{and} \quad (\mathbf{E}^{(a)} - \mathbf{E}^{(b)}) \times \mathbf{m} = \mathbf{0} \tag{29}$$

3.1 Long Wave Estimates for DE Laminates Under Electromechanical Loads. Let us consider DE laminates with isotropic *incompressible* dielectric phases described by the neo-Hookean ideal dielectric model, namely

$$\psi^{(\xi)} = \frac{\mu^{(\xi)}}{2}(\mathbf{F}^{(\xi)} : \mathbf{F}^{(\xi)} - 3) + \frac{1}{2\varepsilon^{(\xi)}}\mathbf{D}_L^{(\xi)} \cdot \mathbf{C}^{(\xi)} \cdot \mathbf{D}_L^{(\xi)} \tag{30}$$

where $\mu^{(\xi)}$ and $\varepsilon^{(\xi)}$ are the shear modulus and the electric permittivity in the undeformed state, respectively; $\mathbf{C} = \mathbf{F}^T \cdot \mathbf{F}$ is the right Cauchy–Green tensor. Under the incompressibility assumption, a closed-form exact solution for finitely deformed periodic layered electroactive materials with neo-Hookean ideal dielectric phases can be derived [21,24–26]. By utilizing the exact analytical solution, an effective free energy function can be constructed [37]

$$\psi(\bar{\mathbf{F}}, \bar{\mathbf{D}}_L) = \frac{\bar{\mu}}{2}(\bar{\mathbf{F}} : \bar{\mathbf{F}} - 3) - \frac{\bar{\mu} - \breve{\mu}}{2}\left(\mathbf{m} \cdot \bar{\mathbf{C}} \cdot \mathbf{m} - \frac{1}{\mathbf{m} \cdot \bar{\mathbf{C}}^{-1} \cdot \mathbf{m}}\right) + \frac{1}{2\bar{\varepsilon}}\bar{\mathbf{D}}_L \cdot \bar{\mathbf{C}} \cdot \bar{\mathbf{D}}_L + \frac{1}{2}\left(\frac{1}{\breve{\varepsilon}} - \frac{1}{\bar{\varepsilon}}\right)\frac{(\bar{\mathbf{D}}_L \cdot \mathbf{m})^2}{\mathbf{m} \cdot \bar{\mathbf{C}}^{-1} \cdot \mathbf{m}} \tag{31}$$

where $\bar{\mathbf{C}} = \bar{\mathbf{F}}^T \cdot \bar{\mathbf{F}}$ is the average right Cauchy–Green tensor, and

$$\bar{\mu} = v^{(a)}\mu^{(a)} + v^{(b)}\mu^{(b)} \quad \text{and} \quad \breve{\mu} = \left(\frac{v^{(a)}}{\mu^{(a)}} + \frac{v^{(b)}}{\mu^{(b)}}\right)^{-1} \tag{32}$$

$$\bar{\varepsilon} = v^{(a)}\varepsilon^{(a)} + v^{(b)}\varepsilon^{(b)} \quad \text{and} \quad \breve{\varepsilon} = \left(\frac{v^{(a)}}{\varepsilon^{(a)}} + \frac{v^{(b)}}{\varepsilon^{(b)}}\right)^{-1} \tag{33}$$

The generalized acoustic tensor (21) corresponding to the free energy function (31) takes the form

$$\hat{\mathbf{A}}(\mathbf{n}, \bar{\mathbf{F}}, \bar{\mathbf{D}}_L) = A_1\hat{\mathbf{I}} + A_2(\hat{\mathbf{I}} \cdot \bar{\mathbf{F}}^{-T} \cdot \mathbf{m}) \otimes (\hat{\mathbf{I}} \cdot \bar{\mathbf{F}}^{-T} \cdot \mathbf{m}) \tag{34}$$

where

$$A_1 = \bar{\mu}(\mathbf{n} \cdot \bar{\mathbf{B}} \cdot \mathbf{n}) + (\breve{\mu} - \bar{\mu})(\mathbf{n} \cdot \bar{\mathbf{F}} \cdot \mathbf{m})^2 \tag{35}$$

and

$$A_2 = \frac{\bar{\mu} - \breve{\mu}}{\alpha^2}\left(\frac{4\beta^2}{\alpha} - 1\right) - \left(\frac{1}{\breve{\varepsilon}} - \frac{1}{\bar{\varepsilon}}\right) \times \left(\frac{(\bar{\mathbf{D}}_L \cdot \mathbf{m})^2}{\alpha^2} - \frac{4}{\gamma}\left(\frac{(\bar{\mathbf{D}}_L \cdot \mathbf{m})^2\beta^2}{\alpha^2} + \frac{1}{4}(\mathbf{n} \cdot \bar{\mathbf{F}} \cdot \bar{\mathbf{D}}_L)^2 - \frac{(\bar{\mathbf{D}}_L \cdot \mathbf{m})(\mathbf{n} \cdot \bar{\mathbf{F}} \cdot \bar{\mathbf{D}}_L)\beta}{\alpha}\right)\right) \tag{36}$$

where $\bar{\mathbf{B}} = \bar{\mathbf{F}} \cdot \bar{\mathbf{F}}^T$ is the average left Cauchy–Green tensor, $\alpha = \mathbf{m} \cdot \bar{\mathbf{C}}^{-1} \cdot \mathbf{m}$, $\beta = \mathbf{n} \cdot \bar{\mathbf{F}}^{-T} \cdot \mathbf{m}$, and $\gamma = \alpha\bar{\varepsilon}/\breve{\varepsilon} + \beta^2(1 - \bar{\varepsilon}/\breve{\varepsilon})$. One can show that the generalized acoustic tensor (34) has the following eigenvalues in the two-dimensional space normal to $\mathbf{n}$:

$$a_1 = A_1 \quad \text{and} \quad a_2 = A_1 + A_2(\alpha - \beta^2) \tag{37}$$

In general, we have two distinct shear waves propagating in finitely deformed DE laminates in the presence of an electric field. The corresponding phase velocities are

$$\bar{c}_{\text{sw}}^{(1)} = \sqrt{a_1/\bar{\rho}} \quad \text{and} \quad \bar{c}_{\text{sw}}^{(2)} = \sqrt{a_2/\bar{\rho}} \tag{38}$$

where $\bar{\rho} = v^{(a)}\rho^{(a)} + v^{(b)}\rho^{(b)}$ is the average density of the laminate. Remarkably, the first shear wave phase velocity $\bar{c}_{\text{sw}}^{(1)}$ is explicitly independent of the electric field; moreover, it coincides with the phase velocity of the corresponding shear wave propagating in finitely deformed laminate in the absence of an electric field [36]. However, the second shear wave phase velocity $\bar{c}_{\text{sw}}^{(2)}$ depends explicitly on electric field.

Let us consider some particular cases, where for simplicity, we set

$$\mathbf{m} = \mathbf{e}_2 \quad \text{and} \quad \bar{\mathbf{F}} = \bar{\lambda}_1\mathbf{e}_1 \otimes \mathbf{e}_1 + \bar{\lambda}_2\mathbf{e}_2 \otimes \mathbf{e}_2 + \bar{\lambda}_3\mathbf{e}_3 \otimes \mathbf{e}_3 \tag{39}$$

First, we study shear waves propagating perpendicular to layers, i.e., $\mathbf{n} = \mathbf{e}_2$. Regardless of the value and the direction of the applied electric displacement, the phase velocities of both shear waves are identical and independent of electric quantities, namely

$$\bar{c}_{\text{sw}} = \bar{c}_{\text{sw}}^{(1)} = \bar{c}_{\text{sw}}^{(2)} = \bar{\lambda}_2\sqrt{\breve{\mu}/\bar{\rho}} \tag{40}$$

Thus, the phase velocities (40) depend on electric field only if $\bar{\lambda}_2 = \bar{\lambda}_2(\bar{\mathbf{D}}_L)$.

Second, we apply an electric field along the layers, $\bar{\mathbf{D}}_L = \bar{D}_L\sqrt{\bar{\mu}\breve{\varepsilon}}\,\mathbf{e}_1$, and study shear waves propagating along the layers. Thus, for wave propagation in the same direction as the applied electric field ($\mathbf{n} = \mathbf{e}_1$), the phase velocities of the shear waves are distinct, and one of them depends on the electric field, namely

$$\bar{c}_{\text{sw}}^{(1)} = \bar{\lambda}_1\sqrt{\bar{\mu}/\bar{\rho}} \quad (\mathbf{g}^{(1)} = \mathbf{e}_3) \tag{41}$$

and

$$\bar{c}_{\text{sw}}^{(2)} = \sqrt{\left(\bar{\lambda}_2^2\left(\frac{\bar{\mu}}{\breve{\mu}} - 1\right) + \bar{\lambda}_1^2\left(1 + \bar{D}_L^2\frac{\breve{\varepsilon}}{\bar{\varepsilon}}\left(1 - \frac{\breve{\varepsilon}}{\bar{\varepsilon}}\right)\right)\right)\frac{\bar{\mu}}{\bar{\rho}}} \quad (\mathbf{g}^{(2)} = \mathbf{e}_2) \tag{42}$$

However, for wave propagation perpendicular to the electric field ($\mathbf{n} = \mathbf{e}_3$), the phase velocities of the shear waves are distinct and independent of electric field, namely

$$\bar{c}_{\mathrm{sw}}^{(1)} = \bar{\lambda}_3 \sqrt{\bar{\mu}/\bar{\rho}} \quad (\mathbf{g}^{(1)} = \mathbf{e}_1) \tag{43}$$

and

$$\bar{c}_{\mathrm{sw}}^{(2)} = \sqrt{\left(\bar{\lambda}_2^2\left(\frac{\breve{\mu}}{\bar{\mu}} - 1\right) + \bar{\lambda}_3^2\right)\frac{\bar{\mu}}{\bar{\rho}}} \quad \left(\mathbf{g}^{(2)} = \mathbf{e}_2\right) \tag{44}$$

Third, we apply an electric field perpendicular to the layers ($\bar{\mathbf{D}}_L = D_L\sqrt{\bar{\mu}\breve{\varepsilon}}\,\mathbf{e}_2$) and analyze shear wave propagation along the layers ($\mathbf{n} = \mathbf{e}_{1,3}$). In this case, the phase velocities of shear waves are different, and the phase velocity of the so-called in-plane shear wave (with polarization $\mathbf{g}^{(2)} = \mathbf{e}_2$) depends explicitly on electric field, i.e.,

$$\bar{c}_{\mathrm{sw}}^{(1)} = \bar{\lambda}_{1,3} \sqrt{\bar{\mu}/\bar{\rho}} \quad (\mathbf{g}^{(1)} = \mathbf{e}_{3,1}) \tag{45}$$

and

$$\bar{c}_{\mathrm{sw}}^{(2)} = \sqrt{\left(\bar{\lambda}_{1,3}^2 + \bar{\lambda}_2^2\left(\frac{\breve{\mu}}{\bar{\mu}} - 1 - D_L^2\left(1 - \frac{\breve{\varepsilon}}{\bar{\varepsilon}}\right)\right)\right)\frac{\bar{\mu}}{\bar{\rho}}} \quad \left(\mathbf{g}^{(2)} = \mathbf{e}_2\right) \tag{46}$$

Now, let us consider the example when deformation of DE laminates is induced by an electric field applied perpendicular to the layers, i.e.,

$$\begin{aligned} &\mathbf{m} = \mathbf{e}_2, \quad \bar{\mathbf{D}}_L = D_L\sqrt{\bar{\mu}\breve{\varepsilon}}\,\mathbf{e}_2, \ \text{and} \\ &\bar{\boldsymbol{\tau}} = v^{(a)}\boldsymbol{\tau}^{(a)} + v^{(b)}\boldsymbol{\tau}^{(b)} = \mathbf{0} \end{aligned} \tag{47}$$

Then, the symmetry of the problem in the plane $\langle \mathbf{e}_1, \mathbf{e}_3 \rangle$, the incompressibility assumption, and the continuity condition for displacements along interfaces between the layers (26) yield the average deformation gradient in the form

$$\bar{\mathbf{F}} = \lambda \mathbf{e}_2 \otimes \mathbf{e}_2 + \lambda^{-1/2}(\mathbf{I} - \mathbf{e}_2 \otimes \mathbf{e}_2) \tag{48}$$

The total Cauchy stress and electric field within each phase are

$$\boldsymbol{\tau}^{(\xi)} = \mu^{(\xi)}\mathbf{B}^{(\xi)} + (\varepsilon^{(\xi)})^{-1}\mathbf{D}^{(\xi)} \otimes \mathbf{D}^{(\xi)} - p^{(\xi)}\mathbf{I} \ \text{and} \ \mathbf{E}^{(\xi)} = \mathbf{D}^{(\xi)}/\varepsilon^{(\xi)} \tag{49}$$

where in our case, $\mathbf{D}^{(\xi)} = D_2\mathbf{e}_2 = \lambda D_L\sqrt{\bar{\mu}\breve{\varepsilon}}\,\mathbf{e}_2$ and $\mathbf{B}^{(\xi)} = \lambda^2\mathbf{e}_2 \otimes \mathbf{e}_2 + \lambda^{-1}(\mathbf{I} - \mathbf{e}_2 \otimes \mathbf{e}_2)$. Hence

$$\begin{aligned} &\tau_{11}^{(\xi)} = \tau_{33}^{(\xi)} = \mu^{(\xi)}\lambda^{-1} - p^{(\xi)} \ \text{and} \\ &\tau_{22}^{(\xi)} = \mu^{(\xi)}\lambda^2 + (\varepsilon^{(\xi)})^{-1}\bar{\mu}\breve{\varepsilon}\,\lambda^2 D_L^2 - p^{(\xi)} \end{aligned} \tag{50}$$

The continuity condition $(29)_1$ and $(47)_3$ yield

$$\tau_{22}^{(a)} = \tau_{22}^{(b)} = 0 \ \text{and} \ v^{(a)}\tau_{11}^{(a)} + v^{(b)}\tau_{11}^{(b)} = 0 \tag{51}$$

By solving the system of equations (51), we obtain an expression for the induced stretch

$$\lambda = (1 + D_L^2)^{-1/3} \tag{52}$$

In terms of the Lagrangian electric field

$$\bar{\mathbf{E}}_L = E_L\sqrt{\frac{\bar{\mu}}{\breve{\varepsilon}}}\mathbf{e}_2 \tag{53}$$

where $E_L = \lambda^2 D_L$. Equation (52) reads as

$$E_L^2 = \lambda(1 - \lambda^3) \tag{54}$$

Equation (54) yields only one physically relevant solution, namely

$$\lambda = \left(1 + \sqrt{12\eta^{-3} - 1}\right)\frac{\eta}{2\sqrt[3]{6}} \tag{55}$$

where

$$\eta = \sqrt{\frac{8\sqrt[3]{3}\mathrm{E}_\mathrm{L}^2}{\sqrt[3]{9 + \sqrt{3(27 - 256E_L^6)}}} + \sqrt[3]{2\left(9 + \sqrt{3(27 - 256E_L^6)}\right)}} \tag{56}$$

Note that Eq. (54) yields expressions for the so-called limiting electric field and the corresponding stretch induced by this field, namely

$$\begin{aligned} &E_L^{\lim} = \frac{\sqrt{3}}{2\sqrt[3]{2}} \simeq 0.687, \quad \lambda^{\lim} = 2^{-2/3} \simeq 0.63, \ \text{and} \\ &D_L^{\lim} = \sqrt{3} \simeq 1.732 \end{aligned} \tag{57}$$

Figure 2(*a*) shows the induced stretch (55) as the function of the dimensionless Lagrangian electric field. Remarkably, the limiting

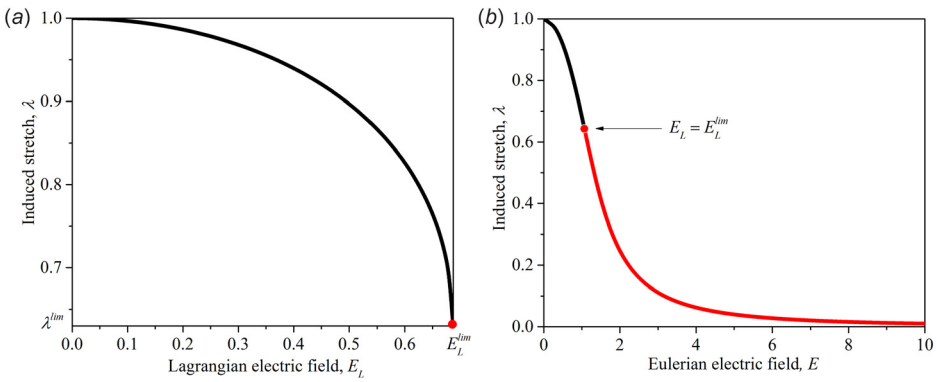

Fig. 2 Induced stretch as function of dimensionless Lagrangian (*a*) and Eulerian (*b*) electric fields

induced stretch $\lambda_{\lim} = 2^{-2/3}$ does not depend on composition of the laminate and coincides with the limiting stretch for homogeneous DEs [38]. The induced stretch can be expressed as a function of the Eulerian electric field, $\bar{\mathbf{E}} = \bar{\mathbf{F}}^{-T} \cdot \bar{\mathbf{E}}_L = E\sqrt{\bar{\mu}/\breve{\varepsilon}}\,\mathbf{e}_2$, where $E = \lambda^{-1}E_L$. Thus, Eq. (54) reads as

$$E^2 = \lambda^{-1} - \lambda^2 \tag{58}$$

Figure 2(*b*) shows the induced stretch as the function of the normalized true or Eulerian electric field as described by Eq. (58). Analogously to the case of homogeneous DEs [38], the limiting value of electric field may be interpreted as the starting point of thinning down without limit, after the critical value of electric field is reached, $E \geq E^{\lim} = 2^{-2/3}\sqrt{3}$. Hence, in the continuation, we present our examples for electric fields ranging from 0 up to $E^{\lim}$.

For the considered electrostatically induced deformations (48) and (52), the expressions for the phase velocities (40), (45), and (46) read as

(1) $\mathbf{n} = \mathbf{e}_2$

$$\bar{c}_{\mathrm{sw}} = \bar{c}_{\mathrm{sw}}^{(1)} = \bar{c}_{\mathrm{sw}}^{(2)} = (1 + D_L^2)^{-1/3}\sqrt{\breve{\mu}/\bar{\rho}} \tag{59}$$

(2) $\mathbf{n} = \mathbf{e}_{1,3}$

$$\bar{c}_{\mathrm{sw}}^{(1)} = (1 + D_L^2)^{1/6}\sqrt{\bar{\mu}/\bar{\rho}} \quad (\mathbf{g}^{(1)} = \mathbf{e}_{3,1}) \tag{60}$$

and

$$\bar{c}_{\mathrm{sw}}^{(2)} = \left(1 + D_L^2\right)^{-1/3}\sqrt{\left(1 + D_L^2\frac{\breve{\varepsilon}}{\bar{\varepsilon}}\frac{\bar{\mu}}{\breve{\mu}}\right)\frac{\breve{\mu}}{\bar{\rho}}} \quad \left(\mathbf{g}^{(2)} = \mathbf{e}_2\right) \tag{61}$$

Note that if $\mu^{(a)}/\mu^{(b)} = \varepsilon^{(a)}/\varepsilon^{(b)}$, then $\breve{\varepsilon}/\bar{\varepsilon} = \breve{\mu}/\bar{\mu}$; hence, for $\mu^{(a)}/\mu^{(b)} = \varepsilon^{(a)}/\varepsilon^{(b)}$, Eq. (61) reduces to

$$\bar{c}_{\mathrm{sw}}^{(2)} = (1 + D_L^2)^{1/6}\sqrt{\breve{\mu}/\bar{\rho}} \quad (\mathbf{g}^{(2)} = \mathbf{e}_2) \tag{62}$$

Figure 3 shows the normalized phase velocities of the shear waves (59)–(61) as functions of the dimensionless Lagrangian electric displacement. We normalize the phase velocities by the corresponding values in the absence of an electric field, i.e., $\bar{c}_0 = \bar{c}_{\mathrm{sw}}|_{D_L=0}$; therefore, all presented curves are valid for any density contrasts $\rho^{(a)}/\rho^{(b)}$ between the layers; moreover, thanks to the normalization the dash-dotted gray curve, corresponding to the wave propagating perpendicular to the layers, is valid for any composition of DE laminates. The phase velocities of both shear waves propagating perpendicular to the layers coincide and monotonically decrease with an increase in electric displacement; in particular, the phase velocities decrease by ~37 % for $D = D_{\lim}$ (see the dash-dotted gray curve in Fig. 3).

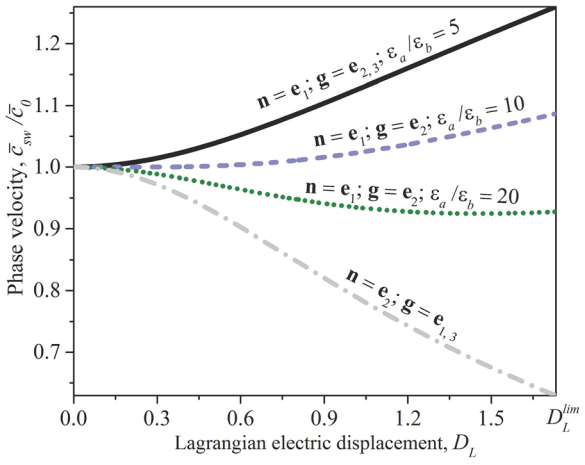

Fig. 3 The phase velocities of shear waves (59)–(61) as functions of the dimensionless electric displacement for laminates with $\nu^{(a)} = 0.2$ and $\mu^{(a)}/\mu^{(b)} = 5$. The phase velocities are normalized by the corresponding values in the absence of electric field.

To illustrate the influence of electric field and direction of wave propagation on the characteristics of elastic waves in the layered DEs, we consider wave propagation in the plane $\langle \mathbf{e}_1, \mathbf{e}_2 \rangle$, i.e., $\mathbf{n} = \cos\varphi\,\mathbf{e}_1 + \sin\varphi\,\mathbf{e}_2$. Thus, the expression for the phase velocities (38) together with Eqs. (48) and (52) reduces to

$$\bar{c}_{\mathrm{sw}}^{(1)}(\varphi) = \left(1 + D_L^2\right)^{-1/3}\sqrt{\left(\left(1 + D_L^2\right)\cos^2\varphi + \frac{\breve{\mu}}{\bar{\mu}}\sin^2\varphi\right)\frac{\bar{\mu}}{\bar{\rho}}} \tag{63}$$

and

$$\bar{c}_{\mathrm{sw}}^{(2)}(\varphi) = \left(1 + D_L^2\right)^{-1/3} \times \sqrt{\left(\frac{\breve{\mu}}{\bar{\mu}}\cos^2 2\varphi + \sin^2 2\varphi + D_L^2\cos^2\varphi\left(\frac{\bar{\varepsilon}}{\breve{\varepsilon}}\cos^2\varphi + \sin^2\varphi\right)^{-1}\right)\frac{\bar{\mu}}{\bar{\rho}}} \tag{64}$$

By making use of the explicit relations (63) and (64), we construct the polar diagrams of slownesses $\bar{s}_{\mathrm{sw}}(\varphi) = 1/\bar{c}_{\mathrm{sw}}(\varphi)$. Figure 4 shows an example of the slowness curves for the so-called out-of-plane (with polarization $\mathbf{g} = \mathbf{e}_3$) and in-plane (with polarization lying in the plane $\langle \mathbf{e}_1, \mathbf{e}_2 \rangle$) shear waves in the DE laminates subjected to an electric field applied perpendicular to the layers. Remarkably, the slownesses of the in-plane shear waves increase for any direction of wave propagation in DE laminates subjected to an electric field, if contrast in electric permittivities is larger than the contrast in shear moduli (see Fig. 4(*d*)).

The dispersion relations for long waves in the incompressible DE laminates are derived from Eq. (38), and have the following form:

$$\bar{\omega}_{\mathrm{sw}}^{(1)} = \sqrt{b_1/\bar{\rho}} \quad \text{and} \quad \bar{\omega}_{\mathrm{sw}}^{(2)} = \sqrt{b_2/\bar{\rho}} \tag{65}$$

where

$$b_1 = \bar{\mu}(\mathbf{k}\cdot\bar{\mathbf{B}}\cdot\mathbf{k}) + (\breve{\mu} - \bar{\mu})(\mathbf{k}\cdot\bar{\mathbf{F}}\cdot\mathbf{m})^2 \tag{66}$$

and

$$b_2 = b_1 + \left(\alpha k^2 - \beta_k^2\right)\left[\frac{\bar{\mu} - \breve{\mu}}{\alpha^2}\left(\frac{4\beta_k^2}{\alpha k^2} - 1\right) - \left(\frac{1}{\breve{\varepsilon}} - \frac{1}{\bar{\varepsilon}}\right) \times \left(\frac{(\bar{\mathbf{D}}_L\cdot\mathbf{m})^2}{\alpha^2} - \frac{4}{\gamma_k}\left(\frac{(\bar{\mathbf{D}}_L\cdot\mathbf{m})^2\beta_k^2}{\alpha^2} + \frac{1}{4}(\mathbf{k}\cdot\bar{\mathbf{F}}\cdot\bar{\mathbf{D}}_L)^2 - \frac{(\bar{\mathbf{D}}_L\cdot\mathbf{m})(\mathbf{k}\cdot\bar{\mathbf{F}}\cdot\bar{\mathbf{D}}_L)\beta_k}{\alpha}\right)\right)\right] \tag{67}$$

where $\mathbf{k}$ is the wave vector, $k = |\mathbf{k}|$ is the wave number, $\beta_k = \mathbf{k}\cdot\bar{\mathbf{F}}^{-T}\cdot\mathbf{m}$ and $\gamma_k = \alpha k^2\bar{\varepsilon}/\breve{\varepsilon} + \beta_k^2(1 - \bar{\varepsilon}/\breve{\varepsilon})$.

Now, group velocity can be calculated as

$$\mathbf{v}_g = \nabla_{\mathbf{k}}\bar{\omega} \tag{68}$$

From Eqs. (65) and (68), we obtain the explicit formulae for the shear wave group velocities in homogenized DE laminates

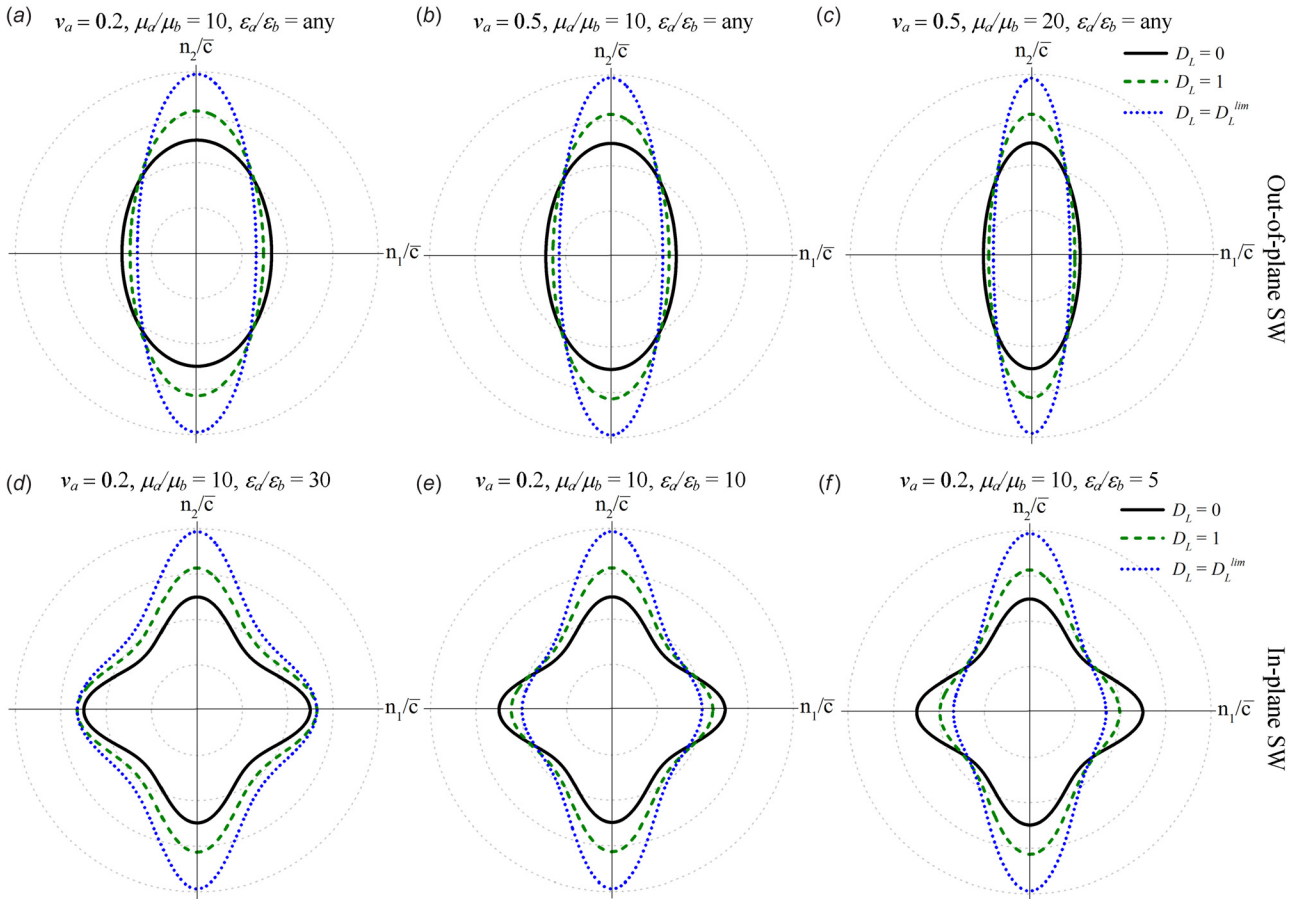

Fig. 4 Slowness curves for the out-of-plane (*a*)–(*c*) and in-plane (*d*)–(*f*) shear waves propagating in the DE laminates with different compositions subjected to electric field perpendicular to the layers. Scale is 0.4 per division, and slowness is normalized by $\sqrt{\bar{\mu}/\bar{\rho}}$. Note that the horizontal and vertical axes with the corresponding labels $n_1/\bar{c}$ and $n_2/\bar{c}$ serve for showing the principal directions and physical quantity presented on the polar plot only.

$$\mathbf{v}_{\mathrm{sw}}^{(1)} = \frac{\bar{\mu}\bar{\mathbf{B}}\cdot\mathbf{n} + (\breve{\mu} - \bar{\mu})(\mathbf{n}\cdot\bar{\mathbf{F}}\cdot\mathbf{m})\bar{\mathbf{F}}\cdot\mathbf{m}}{\sqrt{\bar{\rho}a_1}} \tag{69}$$

and

$$\begin{aligned}\mathbf{v}_{\mathrm{sw}}^{(2)} = {} & \frac{1}{\sqrt{\bar{\rho}a_2}}\left(\bar{\mu}\bar{\mathbf{B}}\cdot\mathbf{n} + (\breve{\mu} - \bar{\mu})(\mathbf{n}\cdot\bar{\mathbf{F}}\cdot\mathbf{m})\bar{\mathbf{F}}\cdot\mathbf{m}\right. \\ & + \frac{\bar{\mu}-\breve{\mu}}{\alpha^2}\left(\beta\left(5 - \frac{8\beta^2}{\alpha}\right)\bar{\mathbf{F}}^{-T}\cdot\mathbf{m} + \left(\frac{4\beta^4}{\alpha} - \alpha\right)\mathbf{n}\right) \\ & + \left(\frac{1}{\breve{\varepsilon}} - \frac{1}{\bar{\varepsilon}}\right)\left\{\frac{D_m^2}{\alpha^2}\left(\beta\bar{\mathbf{F}}^{-T}\cdot\mathbf{m} - \alpha\mathbf{n}\right)\right. \\ & + \frac{2}{\gamma^2}\left[2\beta^2\left(\beta D_m\left(\frac{\beta D_m}{\alpha} - F_{nD}\right) + \frac{\alpha}{4}F_{nD}^2\right)\mathbf{n}\right. \\ & + \gamma(\alpha-\beta^2)\left(\frac{1}{2}F_{nD} - \frac{D_m\beta}{\alpha}\right)\bar{\mathbf{F}}\cdot\bar{\mathbf{D}}_L \\ & + \left(\beta\left(D_m\beta\left(\frac{\beta^2}{\alpha}\left(F_{nD} - \frac{2D_m\beta}{\alpha}\right) + F_{nD}\right) - \frac{\alpha}{2}F_{nD}^2\right)\right. \\ & + \frac{\bar{\varepsilon}D_m}{\breve{\varepsilon}}\left(2D_m\beta\left(1 - \frac{2\beta^2}{\alpha}\right) + F_{nD}(2\beta^2 - \alpha)\right. \\ & \left.\left.\left.\left.\left. - \frac{\beta^4}{\alpha}\left(F_{nD} - \frac{2D_m\beta}{\alpha}\right)\right)\right)\bar{\mathbf{F}}^{-T}\cdot\mathbf{m}\right]\right\}\Bigg)\end{aligned} \tag{70}$$

where $D_m = \bar{\mathbf{D}}_L\cdot\mathbf{m}$ and $F_{nD} = \mathbf{n}\cdot\bar{\mathbf{F}}\cdot\bar{\mathbf{D}}_L$. We note that, for $\mathbf{m} = \mathbf{e}_2$ and $\bar{\mathbf{F}} = \bar{\lambda}_1\mathbf{e}_1\otimes\mathbf{e}_1 + \bar{\lambda}_2\mathbf{e}_2\otimes\mathbf{e}_2 + \bar{\lambda}_3\mathbf{e}_3\otimes\mathbf{e}_3$, the absolute values of the group velocities coincide with the phase velocities for the waves propagating along the principal directions in the DE laminates subjected to the electric field along or perpendicular to the layers.

To illustrate the influence of electric field and direction of wave propagation on the energy propagation in DE laminates, we consider wave propagation in the plane $\langle\mathbf{e}_1,\mathbf{e}_2\rangle$, i.e., $\mathbf{n} = \cos\varphi\,\mathbf{e}_1 + \sin\varphi\,\mathbf{e}_2$. Recall that the outer normal to the slowness curve defines the direction of the energy flow [39]. Thus, by assigning the absolute value of the group velocity (i.e., $|\mathbf{v}_{\mathrm{sw}}|$) to the normal to the slowness curve for all possible propagation directions, we construct the polar diagrams for the group velocity or the energy curves [39,40]. In particular, the expression for the group velocities (69) and (70) together with Eqs. (48) and (52) yields energy curves shown in Fig. 5. Clearly, the group velocities of shear waves (SWs) strongly depend on the propagation direction and applied electric field. Application of electric field perpendicular to the layers increases the group velocity of the out-of-plane SW propagating along the layers and decreases it for SW propagating perpendicular to the layers regardless of laminate composition (see Figs. 5(*a*)–5(*c*)). While the group velocity of the in-plane SW propagating along the layers can either decrease or increase with application of electric field depending on the laminate composition (compare Figs. 5(*d*)–5(*f*)). Moreover, the energy curves of the in-plane SWs have intersections, meaning that the absolute values and directions of the group velocities coincide for two distinct wave propagation directions. Remarkably, the position of these

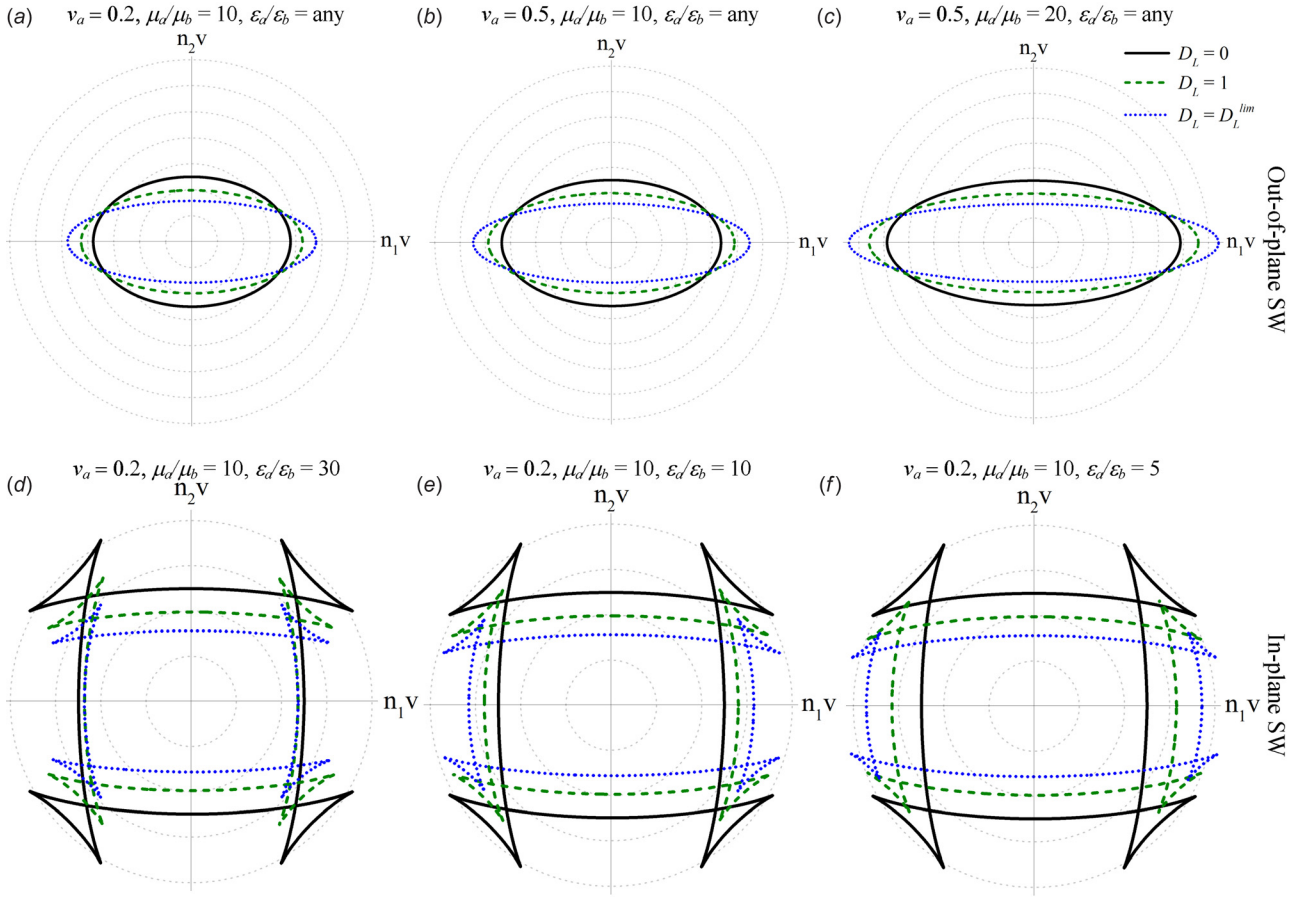

Fig. 5 Energy curves for the out-of-plane (*a*)–(*c*) and in-plane (*d*)–(*f*) shear waves propagating in the DE laminates with different compositions subjected to electric field perpendicular to the layers. Scale is 0.4 per division, where group velocity is normalized by $\sqrt{\bar{\rho}}/\bar{\mu}$. Note that the horizontal and vertical lines with the corresponding labels ($n_1 v$) and ($n_2 v$) serve for showing the principal directions and physical quantity presented on the polar plot only.

intersections changes with a change in the magnitude of the applied electric field. It is worth noting also that the energy curves of plane waves presented here may serve as a tool to define the wave fronts of impulsive point source excited waves in homogenized laminates [40,41]. In this case, the intersections of the energy curves correspond to the regions of null energy [40].

3.2 Band Gap Structure. In this section, we consider laminates with incompressible electroelastic phases describing by the following energy potential:

$$\psi^{(\xi)}\left(\mathbf{F}^{(\xi)}, \mathbf{D}_L^{(\xi)}\right) = \psi_{\text{elas}}^{(\xi)}\left(I_1^{(\xi)}\right) + \frac{1}{2\varepsilon^{(\xi)}} I_5^{(\xi)} \tag{71}$$

where $I_1 = \text{tr}\mathbf{C} = \mathbf{F} : \mathbf{F}$ is the first invariant of the right Cauchy–Green deformation tensor $\mathbf{C} = \mathbf{F}^T \cdot \mathbf{F}$, and $I_5 = \mathbf{D}_L \cdot \mathbf{C} \cdot \mathbf{D}_L$ is the additional invariant accounting for the electromechanical coupling. The tensors of electroelastic moduli (15) for energy potential (71) are

$$\begin{aligned} \mathbb{C}_{ijkl}^{(\xi)} &= 2\left(\delta_{ik} B_{lj}^{(\xi)} \psi_1^{(\xi)} + 2B_{ij}^{(\xi)} B_{kl}^{(\xi)} \psi_{11}^{(\xi)}\right) + \frac{1}{\varepsilon^{(\xi)}} \delta_{ik} D_l^{(\xi)} D_j^{(\xi)}, \\ \boldsymbol{\mathcal{M}}_{ijk}^{(\xi)} &= \frac{1}{\varepsilon^{(\xi)}}\left(\delta_{ik} D_j^{(\xi)} + \delta_{jk} D_i^{(\xi)}\right), \quad K_{ij}^{(\xi)} = \frac{1}{\varepsilon^{(\xi)}} \delta_{ij} \end{aligned} \tag{72}$$

where $\psi_1^{(\xi)} = \partial\psi^{(\xi)}/\partial I_1^{(\xi)}$ and $\psi_{11}^{(\xi)} = \partial\psi_1^{(\xi)}/\partial I_1^{(\xi)}$.

We consider steady-state transversal small amplitude excitations propagating perpendicular to the interface between the layers (along the x_2 direction, see Fig. 1(*c*)) in the laminate subjected to macroscopically applied electromechanical loads

$$\bar{\mathbf{F}} = \lambda_1 \mathbf{e}_1 \otimes \mathbf{e}_1 + \lambda_2 \mathbf{e}_2 \otimes \mathbf{e}_2 + \lambda_3 \mathbf{e}_3 \otimes \mathbf{e}_3 \quad \text{and} \quad \bar{\mathbf{D}}_L = D_L \sqrt{\bar{\mu}\bar{\varepsilon}}\, \mathbf{e}_2 \tag{73}$$

Here, we use the displacement continuity along the interface between the layers (26) producing $\lambda_1^{(a)} = \lambda_1^{(b)} \equiv \lambda_1$ and $\lambda_3^{(a)} = \lambda_3^{(b)} \equiv \lambda_3$, and the incompressibility assumption yielding $\lambda_2^{(a)} = \lambda_2^{(b)} \equiv \lambda_2$. Following Tiersten [42], we assume that the incremental fields $\mathbf{u}^{(\xi)}$, $\dot{\mathbf{D}}_{L\star}^{(\xi)}$, and $\dot{p}^{(\xi)}$ depend on the coordinate x_2 and time t only. Under these assumptions, substitution of Eqs. (17), (18), and (72) into Eq. (12) yields

$$\frac{\partial^2 u_1^{(\xi)}}{\partial t^2} = \left(c_{\text{sw}}^{(\xi)}\right)^2 \frac{\partial^2 u_1^{(\xi)}}{\partial x_2^2}, \quad \frac{\partial \dot{p}^{(\xi)}}{\partial x_2} = 0, \text{ and } \frac{\partial^2 u_3^{(\xi)}}{\partial t^2} = \left(c_{\text{sw}}^{(\xi)}\right)^2 \frac{\partial^2 u_3^{(\xi)}}{\partial x_2^2} \tag{74}$$

where

$$c_{\text{sw}}^{(\xi)} = \lambda_2 \sqrt{2\psi_1^{(\xi)} \Big/ \rho^{(\xi)}} \tag{75}$$

Next, substitution of Eqs. (18), (72), and (73) into Eq. (17) yields

$$
\begin{aligned}
\dot{P}^{(\xi)}_{\star 12} &= 2\lambda_2^2\psi_1^{(\xi)}\frac{\partial u_1^{(\xi)}}{\partial x_2}+\frac{D_2^{(\xi)}}{\varepsilon^{(\xi)}}\left(D_2^{(\xi)}\frac{\partial u_1^{(\xi)}}{\partial x_2}+\dot{D}^{(\xi)}_{L\star 1}\right),\\
\dot{E}^{(\xi)}_{L\star 1} &= \frac{1}{\varepsilon^{(\xi)}}\left(D_2^{(\xi)}\frac{\partial u_1^{(\xi)}}{\partial x_2}+\dot{D}^{(\xi)}_{L\star 1}\right)\\
\dot{P}^{(\xi)}_{\star 22} &= \frac{2}{\varepsilon^{(\xi)}}D_2^{(\xi)}\dot{D}^{(\xi)}_{L\star 2}-\dot{p}^{(\xi)}\\
\dot{P}^{(\xi)}_{\star 32} &= 2\lambda_2^2\psi_1^{(\xi)}\frac{\partial u_3^{(\xi)}}{\partial x_2}+\frac{D_2^{(\xi)}}{\varepsilon^{(\xi)}}\left(D_2^{(\xi)}\frac{\partial u_3^{(\xi)}}{\partial x_2}+\dot{D}^{(\xi)}_{L\star 3}\right),\\
\dot{E}^{(\xi)}_{L\star 3} &= \frac{1}{\varepsilon^{(\xi)}}\left(D_2^{(\xi)}\frac{\partial u_3^{(\xi)}}{\partial x_2}+\dot{D}^{(\xi)}_{L\star 3}\right)
\end{aligned}
\tag{76}
$$

where $D_2^{(\xi)}=D_2$ according to Eq. $(29)_2$.

The incremental jump conditions across the interface between the layers ($x_2=0$) are

$$
\begin{aligned}
&\dot{P}^{(a)}_{\star 12}=\dot{P}^{(b)}_{\star 12},\quad \dot{P}^{(a)}_{\star 22}=\dot{P}^{(b)}_{\star 22},\quad \dot{P}^{(a)}_{\star 32}=\dot{P}^{(b)}_{\star 32},\\
&\dot{E}^{(a)}_{L\star 1}=\dot{E}^{(b)}_{L\star 1},\quad \dot{E}^{(a)}_{L\star 3}=\dot{E}^{(b)}_{L\star 3},\quad \dot{D}^{(a)}_{L\star 2}=\dot{D}^{(b)}_{L\star 2}
\end{aligned}
\tag{77}
$$

Hence, substitution of Eq. (76) into Eq. (77) yields

$$
\begin{aligned}
\psi_1^{(a)}\frac{\partial u_1^{(a)}}{\partial x_2}\bigg|_{x_2=0} &= \psi_1^{(b)}\frac{\partial u_1^{(b)}}{\partial x_2}\bigg|_{x_2=0},\\
\psi_1^{(a)}\frac{\partial u_3^{(a)}}{\partial x_2}\bigg|_{x_2=0} &= \psi_1^{(b)}\frac{\partial u_3^{(b)}}{\partial x_2}\bigg|_{x_2=0},\\
\dot{p}^{(b)}-\dot{p}^{(a)} &= D_2\dot{D}_{L\star 2}\left(\frac{1}{\varepsilon^{(b)}}-\frac{1}{\varepsilon^{(a)}}\right)
\end{aligned}
\tag{78}
$$

We seek solution for Eq. $(74)_1$ in the form

$$
u_1^{(\xi)}=A^{(\xi)}e^{i(k^{(\xi)}x_2-\omega t)}+B^{(\xi)}e^{i(-k^{(\xi)}x_2-\omega t)} \tag{79}
$$

where ω represents the angular frequency, and $k^{(\xi)}=\omega/c^{(\xi)}$ is the wave number. The perfect bonding between the layers implies

$$
u_1^{(a)}|_{x_2=0}=u_1^{(b)}|_{x_2=0} \tag{80}
$$

Then, the substitution of Eq. (79) into Eq. (80) yields

$$
A^{(a)}+B^{(a)}-A^{(b)}-B^{(b)}=0 \tag{81}
$$

Next, the substitution of Eq. (79) into Eq. $(78)_1$ yields

$$
\frac{\psi_1^{(a)}}{c^{(a)}}A^{(a)}-\frac{\psi_1^{(a)}}{c^{(a)}}B^{(a)}-\frac{\psi_1^{(b)}}{c^{(b)}}A^{(b)}+\frac{\psi_1^{(b)}}{c^{(b)}}B^{(b)}=0 \tag{82}
$$

Two additional conditions for constants $A^{(a)}$, $B^{(a)}$, $A^{(b)}$, and $B^{(b)}$ are obtained from the periodicity consideration. Hence, we adjust the form of the solution (79) to be the steady-state wave expression with the same wave number k for both phases

$$
u_1^{(\xi)}=U_1^{(\xi)}(x_2)e^{i(kx_2-\omega t)} \tag{83}
$$

where

$$
U_1^{(\xi)}(x_2)=A^{(\xi)}e^{iK_-^{(\xi)}x_2}+B^{(\xi)}e^{-iK_+^{(\xi)}x_2}\quad\text{and}\quad K_\pm^{(\xi)}=k^{(\xi)}\pm k \tag{84}
$$

According to Floquet theorem, functions $U_1^{(\xi)}(x_2)$ must be periodic with the period equal to the length of the unit cell (see Fig. 1(*c*)), namely $h=h^{(a)}+h^{(b)}$

$$
U_1^{(a)}(-h^{(a)})=U_1^{(b)}(h^{(b)}) \tag{85}
$$

Thus, substitution of Eq. (84) into Eq. (85) yields

$$
e^{-iK_-^{(a)}h^{(a)}}A^{(a)}+e^{iK_+^{(a)}h^{(a)}}B^{(a)}-e^{iK_-^{(b)}h^{(b)}}A^{(b)}-e^{-iK_+^{(b)}h^{(b)}}B^{(b)}=0 \tag{86}
$$

Next, substituting Eq. (83) and $\dot{D}^{(\xi)}_{L\star 1}=d_1^{(\xi)}(x_2)e^{i(kx_2-\omega t)}$ into Eq. $(76)_1$, we obtain

$$
\begin{aligned}
&\dot{E}^{(\xi)}_{L\star 1}(x_2,t)=\mathcal{E}_1^{(\xi)}(x_2)e^{i(kx_2-\omega t)},\\
&\mathcal{E}_1^{(\xi)}(x_2)=\frac{1}{\varepsilon^{(\xi)}}\left(D_2\frac{i\omega}{c^{(\xi)}}\left(A^{(\xi)}e^{iK_-^{(\xi)}x_2}-B^{(\xi)}e^{-iK_+^{(\xi)}x_2}\right)+d_1^{(\xi)}(x_2)\right)
\end{aligned}
\tag{87}
$$

and

$$
\begin{aligned}
&\dot{P}^{(\xi)}_{\star 12}(x_2,t)=\mathcal{P}_1^{(\xi)}(x_2)e^{i(kx_2-\omega t)},\\
&\mathcal{P}_1^{(\xi)}(x_2)=2\lambda_2^2\psi_1^{(\xi)}\frac{i\omega}{c^{(\xi)}}\left(A^{(\xi)}e^{iK_-^{(\xi)}x_2}-B^{(\xi)}e^{-iK_+^{(\xi)}x_2}\right)+D_2\mathcal{E}_1^{(\xi)}(x_2)
\end{aligned}
\tag{88}
$$

where according to Floquet theorem

$$
\begin{aligned}
&\mathcal{P}_1^{(a)}(-h^{(a)})=\mathcal{P}_1^{(b)}(h^{(b)}),\quad \mathcal{E}_1^{(a)}(-h^{(a)})=\mathcal{E}_1^{(b)}(h^{(b)}),\\
&d_1^{(a)}(-h^{(a)})=d_1^{(b)}(h^{(b)})
\end{aligned}
\tag{89}
$$

Finally, substitution of Eq. (88) into Eq. (89) yields

$$
\begin{aligned}
&\frac{\psi_1^{(a)}}{c^{(a)}}e^{-iK_-^{(a)}h^{(a)}}A^{(a)}-\frac{\psi_1^{(a)}}{c^{(a)}}e^{iK_+^{(a)}h^{(a)}}B^{(a)}-\frac{\psi_1^{(b)}}{c^{(b)}}e^{iK_-^{(b)}h^{(b)}}A^{(b)}\\
&\quad+\frac{\psi_1^{(b)}}{c^{(b)}}e^{-iK_+^{(b)}h^{(b)}}B^{(b)}=0
\end{aligned}
\tag{90}
$$

System of equations (81), (82), (86), and (90) has a nontrivial solution if

$$
\det\begin{bmatrix}
1 & 1 & -1 & -1\\
\dfrac{\psi_1^{(a)}}{c^{(a)}} & -\dfrac{\psi_1^{(a)}}{c^{(a)}} & -\dfrac{\psi_1^{(b)}}{c^{(b)}} & \dfrac{\psi_1^{(b)}}{c^{(b)}}\\
e^{-iK_-^{(a)}h^{(a)}} & e^{iK_+^{(a)}h^{(a)}} & -e^{iK_-^{(b)}h^{(b)}} & -e^{-iK_+^{(b)}h^{(b)}}\\
\dfrac{\psi_1^{(a)}}{c^{(a)}}e^{-iK_-^{(a)}h^{(a)}} & -\dfrac{\psi_1^{(a)}}{c^{(a)}}e^{iK_+^{(a)}h^{(a)}} & -\dfrac{\psi_1^{(b)}}{c^{(b)}}e^{iK_-^{(b)}h^{(b)}} & \dfrac{\psi_1^{(b)}}{c^{(b)}}e^{-iK_+^{(b)}h^{(b)}}
\end{bmatrix}=0
\tag{91}
$$

One can show that Eq. (91) together with Eq. (75) reduces to

$$
\begin{aligned}
\cos kh &= \cos\left(\frac{\omega h^{(a)}}{c^{(a)}}\right)\cos\left(\frac{\omega h^{(b)}}{c^{(b)}}\right)\\
&\quad-\frac{1}{2}\left(\frac{\rho^{(a)}c^{(a)}}{\rho^{(b)}c^{(b)}}+\frac{\rho^{(b)}c^{(b)}}{\rho^{(a)}c^{(a)}}\right)\sin\left(\frac{\omega h^{(a)}}{c^{(a)}}\right)\sin\left(\frac{\omega h^{(b)}}{c^{(b)}}\right)
\end{aligned}
\tag{92}
$$

describing the dispersion relation $\omega=\omega(k)$ with $c^{(\xi)}$ and $h^{(\xi)}$ being functions of deformation, which can be induced by electric field or otherwise, for example, purely mechanically. The obtained dispersion relation fully agrees with the exact solution for long waves (40) propagating perpendicular to the layers in electroelastic laminates, clearly showing that shear wave propagation is independent of electric field for this configuration. We note that the dispersion relation (92) is different from those presented

by Shmuel and deBotton [30,35] as detailed in the Appendix. Moreover, the dispersion relation (92) has the same form as the classical result for purely elastic laminates [34], if no deformation is applied. Recently, the dispersion relation by Rytov [34] has been extended to account for finite deformations in purely mechanical hyperelastic laminates [36]. Remarkably, the dispersion relation (92) is identical to the one considered in Galich et al. [36] for the purely mechanical problem; the only difference, which, however, does not affect the way how SBGs change, is that here the deformation is induced by an electric field. Thus, the analysis and conclusions of Galich et al. [36] can be fully applied here. In particular, Galich et al. [36] showed that SBGs do not depend on deformation in laminates with neo-Hookean phases. This is due to the fact that the two main factors—changes in the geometry and phase velocity induced by deformation—completely cancel each other [36]. This is again in contradiction with the conclusions of Shmuel and deBotton [30,35], and Shmuel and Band [43]; these works utilized different dispersion relations, but all arrived at the conclusions that SBGs are tunable by an electric field [30,35] or by deformation [43] in neo-Hookean ideal dielectric or purely mechanical neo-Hookean laminates, respectively. Once again, the SBGs do not depend either on deformation or on electric field in the neo-Hookean ideal dielectric or purely mechanical neo-Hookean laminates.

To achieve electric field (or deformation)-induced tunability of the SBGs, one should consider laminates with phases exhibiting stronger stiffening, for example, Arruda–Boyce [44] or Gent [45] phases. To illustrate this, we consider laminates with electroelastic phases describing by the energy potential (71) with Gent elastic part [45]

$$\psi_{\text{elas}}^{(\xi)}(\mathbf{F}^{(\xi)}) = -\frac{\mu^{(\xi)} J_m^{(\xi)}}{2} \ln\left(1 - \frac{I_1^{(\xi)} - 3}{J_m^{(\xi)}}\right) \tag{93}$$

where $J_m^{(\xi)}$ is the dimensionless parameter defining the lock-up stretch ratio, such that in the limit $(I_1^{(\xi)} - 3) \to J_m^{(\xi)}$, the strain energy becomes unbounded. Recall that the stiffening effects describing by the Gent model, which is an approximation of the Arruda–Boyce model [44], refer to finite extensibility of polymer chains. For DE laminates with electroelastic Gent phases subjected to the electric field perpendicular to the layers (as defined in Eq. (47)), the relation between the induced stretch and Lagrangian electric displacement is

$$D_L = \lambda^{-1} \sqrt{\frac{\lambda^3 - 1}{\bar{\mu}} \left(\frac{J_m^{(a)} \nu^{(a)} \mu^{(a)}}{2 - \left(3 + J_m^{(a)}\right)\lambda + \lambda^3} + \frac{J_m^{(b)} \nu^{(b)} \mu^{(b)}}{2 - \left(3 + J_m^{(b)}\right)\lambda + \lambda^3} \right)} \tag{94}$$

Substitution of Eq. (93) into Eq. (75) yields [8]

$$c_G^{(\xi)} = \lambda \sqrt{\frac{J_m^{(\xi)}}{3 + J_m^{(\xi)} - \lambda^2 - 2\lambda^{-1}} \frac{\mu^{(\xi)}}{\rho^{(\xi)}}} \tag{95}$$

Next, by making use of Eqs. (94), (95), (24), and (92), SBG structures can be constructed for electroelastic laminates subjected to the electric field perpendicular to the layers. Figures 6(*a*)–6(*c*) show the SBGs as functions of the Lagrangian electric displacement applied perpendicular to the layers for wave propagating perpendicular to the layers in the DE laminates with the Gent electroelastic phases. Thanks to the specific normalization of the Lagrangian electric displacement, namely $\bar{\mathbf{D}}_L = D_L \sqrt{\bar{\mu}\bar{\varepsilon}}\, \mathbf{e}_2$, the presented band gaps correspond to DE laminates with any contrast in electric permittivities $\varepsilon^{(a)}/\varepsilon^{(b)}$ between the layers. The lock-up stretch for $J_m = 0.5$ is $\lambda_{\text{lock}} \simeq 0.65$. Application of $D_L = 3.5$ leads the contraction of the considered DE laminates down to $\lambda \simeq 0.68$. Clearly, the application of the electric field perpendicular to the layers widens and shifts SBGs up to the higher frequencies. In particular, the application of the Lagrangian electric displacement of $D_L = 3.5$ to the laminate with $\nu^{(a)} = 0.5$ and $\mu^{(a)}/\mu^{(b)} = 10$ shifts the lower boundary of the first SBG from $f_n = 0.41$ up to

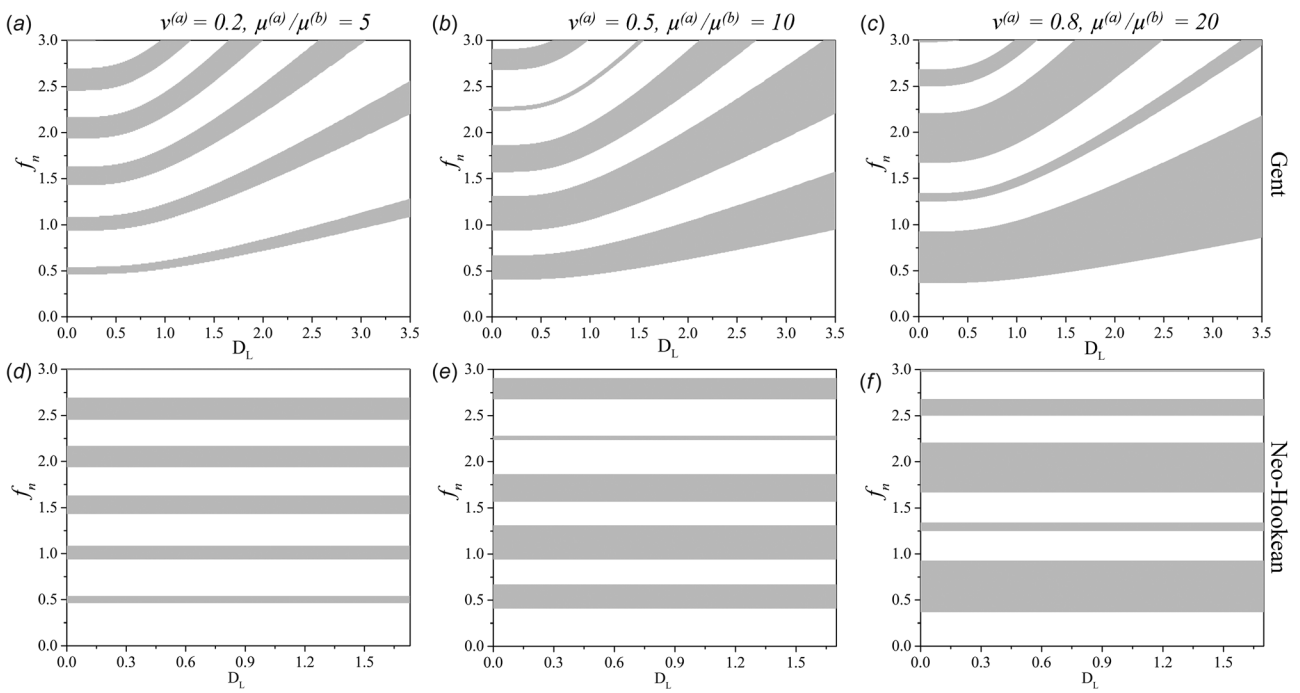

Fig. 6 Shear wave band gaps as functions of dimensionless Lagrangian electric displacement for waves propagating perpendicular to the layers. The band gap structures are true for any contrast in electric permittivities $\varepsilon^{(a)}/\varepsilon^{(b)}$ between the layers. The locking parameters for Gent phases are $J_m^{(a)} = J_m^{(b)} = 0.5$. The densities of the layers are identical, i.e., $\rho^{(a)}/\rho^{(b)} = 1$. Frequency is normalized as $f_n = (\omega H/2\pi)\sqrt{\bar{\rho}/\bar{\mu}}$.

$f_n = 0.95$ and widens it from $\Delta f_n = 0.26$ up to $\Delta f_n = 0.62$ (see Fig. 6(*b*)). Once again, these changes in SBGs occur due to electrostatically induced deformation. As a comparison, Figs. 6(*d*)–6(*f*) show the SBGs as functions of the Lagrangian electric displacement applied perpendicular to the layers for the waves propagating perpendicular to the layers in the DE laminates with the neo-Hookean electroelastic phases. Recall that for the neo-Hookean dielectric elastomer laminates, the normalized limiting electric displacement is constant, i.e., $D_L^{\lim} = \sqrt{3}$, while for the Gent dielectric elastomer laminates, the limiting electric field depends on the on the locking parameter J_m. Note that for the Gent DE laminates discussed in Fig. 6, the limiting electric fields are higher than the ones needed to reach the lock-up stretches. Finally, we note that the influence of stiffening effects on band gap structures in finitely deformed incompressible and compressible layered materials was thoroughly analyzed by Galich et al. [36]. The only difference is that here we induce deformation by application of an electric field.

4 Conclusion

We considered shear wave propagation in electroelastic layered media subjected to finite deformations and electric fields. First, we derived the long wave estimates—the exact solution for the long waves—for phase and group velocities of shear waves propagating in the laminates with electroelastic neo-Hookean phases. The derived formulae are expressed in terms of the volume fractions and electroelastic constants of the phases. Moreover, these long wave estimates are given for any direction of wave propagation, and for any applied electric field and homogenous finite deformations. Furthermore, we have found that the shear wave propagation perpendicular to the layers depends on electric field only though the induced deformation.

Second, we derived the dispersion relations for the shear waves propagating perpendicular to the layers in the laminates with incompressible hyperelastic ideal dielectric phases, described by the energy potential (71). Consistently with the long wave estimates, the derived dispersion relation is independent of electric field, and the dispersion relation has the same form as its analog for the purely elastic laminates. The dispersion relation shows that SBGs in the electroelastic laminates are tunable by an electric field only through induced deformation. In particular, the application of an electric field to the DE laminates with electroelastic Gent phases widens and shifts SBGs toward higher frequencies. However, SBGs do not depend on deformation (induced by an electric field or mechanically) in DE laminates with electroelastic neo-Hookean phases. Finally, we emphasize that consideration of dissipation can potentially improve the accuracy of the predictions, especially for the composites with constituents characterized by strong damping effects [46].

Acknowledgment

S.R. thanks the support of Taub Foundation through the Horev Fellowship—Leaders in Science and Technology. P.G. thanks the support through the Jacobs Fellowship.

Funding Data

- Israel Science Foundation (1550/15).

Appendix: Comparison of Dispersion Relation, Exact Solution for Long Waves, and Results by Shmuel and deBotton

Figure 7 shows a comparison of the exact solution for long waves (59), dispersion relation (92), and the results reported by Shmuel and deBotton [30,35]. For clarity, we normalize the wave vector and frequency as in Shmuel and deBotton [30]. The DE laminate is subjected to the electrostatic excitation of $D_L = 1.27$ (corresponding to $\hat{D} = 1.5$ in Shmuel and deBotton [30,35]). The continuous black and dotted blue curves correspond to the exact solution for long waves (59) and dispersion relation (92), respectively. The dotted and dashed red curves refer to the results reported by Shmuel and deBotton [30] (see Fig. 8(*a*) therein) and the results presented in Shmuel and deBotton [35] (see Fig. 7(*b*) therein), respectively. We observe that the curves for dispersion relation (92) and exact solution for long waves (59) overlap, while the dispersion curves from Shmuel and deBotton [30,35] significantly differ from the exact solution for long waves.

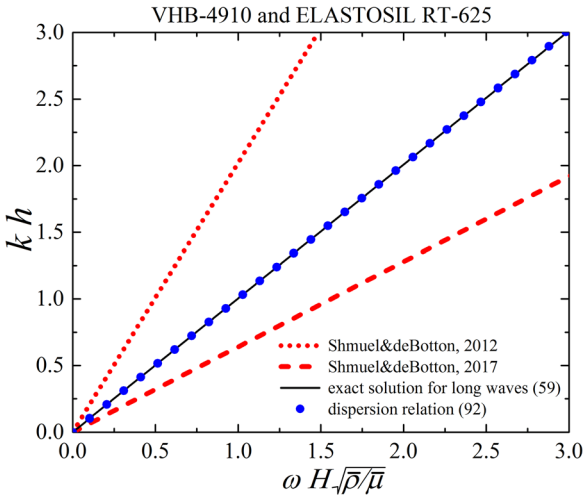

Fig. 7 Comparison of the exact solution for long waves (59), dispersion relation (92), and results reported by Shmuel and deBotton [30,35] for the shear waves propagating perpendicular to the layers in the laminates with incompressible ideal DE neo-Hookean phases subjected to electric field perpendicular to layers, namely $D_L = 1.27$. The laminate is made of VHB-4910 and ELASTOSIL RT-625: $\nu^{(a)} = 0.5$, $\mu^{(a)}/\mu^{(b)} = 1.19$, $\varepsilon^{(a)}/\varepsilon^{(b)} = 1.74$, and $\rho^{(a)}/\rho^{(b)} = 0.94$, where $\mu^{(b)} = 342$ kPa, $\varepsilon^{(b)} = 2.7$, and $\rho^{(b)} = 1020$ kg/m^3.

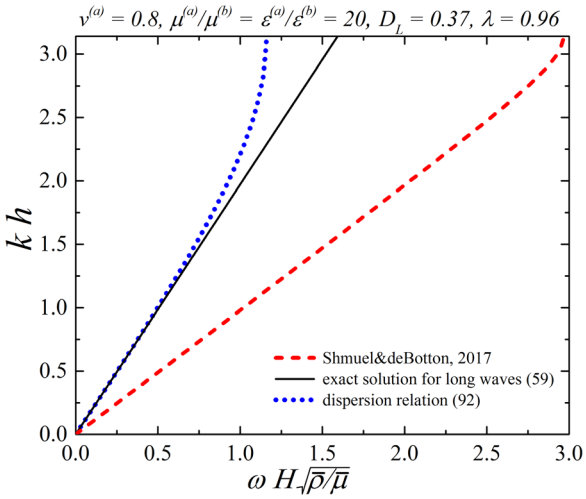

Fig. 8 Comparison of the exact solution for long waves (59), dispersion relation (92), and dispersion relation by Shmuel and deBotton [35] for the waves propagating perpendicular to the layers in the laminates with incompressible neo-Hookean phases subjected to electric field perpendicular to layers, namely, $D_L = 0.37$, $\nu^{(a)} = 0.8$, $\mu^{(a)}/\mu^{(b)} = \varepsilon^{(a)}/\varepsilon^{(b)} = 20$, and $\rho^{(a)}/\rho^{(b)} = 1$

For completeness, we show a comparison of the exact solution for long waves (59), dispersion relation (92), and dispersion relation reported by Shmuel and deBotton [35] for the DE laminates with a more pronounced dispersion. In particular, the comparison is shown for the DE laminates with incompressible neo-Hookean phases with $\nu^{(a)} = 0.8$, $\mu^{(a)}/\mu^{(b)} = \varepsilon^{(a)}/\varepsilon^{(b)} = 20$, and $\rho^{(a)}/\rho^{(b)} = 1$ in Fig. 8. The laminate is subjected to the electric field perpendicular to the layers, namely, $D_L = 0.37$ (corresponding to $\hat{D} = 3$ in the notation of Shmuel and deBotton [35]). We observe that dispersion relation (92) and the exact solution for long waves (59) are in excellent agreement for the corresponding wavelengths, whereas the results reported by Shmuel and deBotton [35] produce significantly different results from the exact solution for long waves (59) even in the long wave limit of $kh \to 0$. In particular, for this case, the phase velocity predicted by the exact solution (59) significantly differs from the phase velocity calculated from the dispersion relation by Shmuel and deBotton [35] by a factor of 2, namely, $\bar{c}^{(\mathrm{SD})} \simeq 2\bar{c}_{\mathrm{sw}}$.

References

[1] Pelrine, R., Kornbluh, R., Pei, Q.-B., and Joseph, J., 2000, "High-Speed Electrically Actuated Elastomers With Strain Greater Than 100%," Science, **287**(5454), pp. 836–839.

[2] Bar-Cohen, Y., 2004, *Electroactive Polymer (EAP) Actuators as Artificial Muscles: Reality, Potential, and Challenges*, Vol. 136, SPIE Press, Bellingham, WA.

[3] Rudykh, S., Bhattacharya, K., and deBotton, G., 2012, "Snap-Through Actuation of Thick-Wall Electroactive Balloons," Int. J. Nonlinear Mech., **47**(2), pp. 206–209.

[4] Li, T., Keplinger, C., Baumgartner, R., Bauer, S., Yang, W., and Suo, Z., 2013, "Giant Voltage-Induced Deformation in Dielectric Elastomers Near the Verge of Snap-Through Instability," J. Mech. Phys. Solids, **61**(2), pp. 611–628.

[5] McKay, T., O'Brien, B., Calius, E., and Anderson, I., 2010, "An Integrated, Self-Priming Dielectric Elastomer Generator," Appl. Phys. Lett., **97**(6), p. 062911.

[6] Kornbluh, R. D., Pelrine, R., Prahlad, H., Wong-Foy, A., McCoy, B., Kim, S., Eckerle, J., and Low, T., 2012, "From Boots to Buoys: Promises and Challenges of Dielectric Elastomer Energy Harvesting," *Electroactivity in Polymeric Materials*, Springer, Berlin, pp. 67–93.

[7] Rudykh, S., and Boyce, M., 2014, "Transforming Wave Propagation in Layered Media Via Instability-Induced Interfacial Wrinkling," Phys. Rev. Lett., **112**(3), p. 034301.

[8] Galich, P. I., and Rudykh, S., 2015, "Influence of Stiffening on Elastic Wave Propagation in Extremely Deformed Soft Matter: From Nearly Incompressible to Auxetic Materials," Extreme Mech. Lett., **4**, pp. 156–161.

[9] Galich, P. I., and Rudykh, S., 2015, "Comment on "Disentangling Longitudinal and Shear Elastic Waves by neo-Hookean Soft Devices" [Appl. Phys. Lett., 106, 161903 (2015)]," Appl. Phys. Lett., **107**(5), p. 056101.

[10] Galich, P. I., Slesarenko, V., and Rudykh, S., 2017, "Shear Wave Propagation in Finitely Deformed 3D Fiber-Reinforced Composites," Int. J. Solids Struct., **110–111**, pp. 294–304.

[11] Gei, M., Roccabianca, S., and Bacca, M., 2011, "Controlling Bandgap in Electroactive Polymer-Based Structures," IEEE/ASME Trans. Mechatronics, **16**(1), pp. 102–107.

[12] Galich, P. I., and Rudykh, S., 2016, "Manipulating Pressure and Shear Elastic Waves in Dielectric Elastomers Via External Electric Stimuli," Int. J. Solids Struct., **91**, pp. 18–25.

[13] Wu, B., Su, Y., Chen, W., and Zhang, C., 2017, "On Guided Circumferential Waves in Soft Electroactive Tubes Under Radially Inhomogeneous Biasing Fields," J. Mech. Phys. Solids, **99**, pp. 116–145.

[14] Yang, W.-P., and Chen, L.-W., 2008, "The Tunable Acoustic Band Gaps of Two-Dimensional Phononic Crystals With a Dielectric Elastomer Cylindrical Actuator," Smart Mater. Struct., **17**(1), p. 015011.

[15] Celli, P., Gonella, S., Tajeddini, V., Muliana, A., Ahmed, S., and Ounaies, Z., 2017, "Wave Control Through Soft Microstructural Curling: Bandgap Shifting, Reconfigurable Anisotropy and Switchable Chirality," Smart Mater. Struct., **26**(3), p. 035001.

[16] Toupin, R. A., 1956, "The Elastic Dielectric," Arch. Ration. Mech. Anal., **5**, pp. 849–915.

[17] Dorfmann, A., and Ogden, R. W., 2005, "Nonlinear Electroelasticity," Acta. Mech., **174**(3–4), pp. 167–183.

[18] McMeeking, R. M., and Landis, C. M., 2005, "Electrostatic Forces and Stored Energy for Deformable Dielectric Materials," ASME J. Appl. Mech., **72**(4), pp. 581–590.

[19] Suo, Z., Zhao, X., and Greene, W. H., 2008, "A Nonlinear Field Theory of Deformable Dielectrics," J. Mech. Phys. Solids, **56**(2), pp. 467–486.

[20] Cohen, N., Dayal, K., and deBotton, G., 2016, "Electroelasticity of Polymer Networks," J. Mech. Phys. Solids, **92**, pp. 105–126.

[21] deBotton, G., Tevet-Deree, L., and Socolsky, E. A., 2007, "Electroactive Heterogeneous Polymers: Analysis and Applications to Laminated Composites," Mech. Adv. Mater. Struct., **14**(1), pp. 13–22.

[22] Tian, L., Tevet-Deree, L., deBotton, G., and Bhattacharya, K., 2012, "Dielectric Elastomer Composites," J. Mech. Phys. Solids, **60**(1), pp. 181–198.

[23] Rudykh, S., Lewinstein, A., Uner, G., and deBotton, G., 2013, "Analysis of Microstructural Induced Enhancement of Electromechanical Coupling in Soft Dielectrics," Appl. Phys. Lett., **102**(15), p. 151905.

[24] Rudykh, S., and deBotton, G., 2011, "Stability of Anisotropic Electroactive Polymers With Application to Layered Media," Z. Angew. Math. Phys., **62**(6), pp. 1131–1142.

[25] Bertoldi, K., and Gei, M., 2011, "Instabilities in Multilayered Soft Dielectrics," J. Mech. Phys. Solids, **59**(1), pp. 18–42.

[26] Rudykh, S., Bhattacharya, K., and deBotton, G., 2014, "Multiscale Instabilities in Soft Heterogeneous Dielectric Elastomers," Proc. R. Soc. A, **470**(2162), p. 20130618.

[27] Abu-Salih, S., 2017, "Analytical Study of Electromechanical Buckling of a Micro Spherical Elastic Film on a Compliant Substrate—Part I: Formulation and Linear Buckling of Periodic Patterns," Int. J. Solids Struct., **109**, pp. 180–188.

[28] Goshkoderia, A., and Rudykh, S., 2017, "Electromechanical Macroscopic Instabilities in Soft Dielectric Elastomer Composites With Periodic Microstructures," Eur. J. Mech. A, **65**, pp. 243–256.

[29] Dorfmann, A., and Ogden, R. W., 2010, "Electroelastic Waves in a Finitely Deformed Electroactive Material," IMA J. Appl. Math., **75**(4), pp. 603–636.

[30] Shmuel, G., and deBotton, G., 2012, "Band-Gaps in Electrostatically Controlled Dielectric Laminates Subjected to Incremental Shear Motions," J. Mech. Phys. Solids, **60**(11), pp. 1970–1981.

[31] Kolle, M., Lethbridge, A., Kreysing, M., Baumberg, J., Aizenberg, J., and Vukusic, P., 2013, "Bio-Inspired Band-Gap Tunable Elastic Optical Multilayer Fibers," Adv. Mater., **25**(15), pp. 2239–2245.

[32] Rudykh, S., Ortiz, C., and Boyce, M., 2015, "Flexibility and Protection by Design: Imbricated Hybrid Microstructures of Bio-Inspired Armor," Soft Matter, **11**(13), pp. 2547–2554.

[33] Slesarenko, V., and Rudykh, S., 2016, "Harnessing Viscoelasticity and Instabilities for Tuning Wavy Patterns in Soft Layered Composites," Soft Matter, **12**(16), pp. 3677–3682.

[34] Rytov, S., 1956, "Acoustical Properties of a Thinly Laminated Medium," Sov. Phys. Acoust., **2**, pp. 68–80.

[35] Shmuel, G., and deBotton, G., 2017, "Corrigendum to 'Band-Gaps in Electrostatically Controlled Dielectric Laminates Subjected to Incremental Shear Motions' [J. Mech. Phys. Solids, 60 (2012) 1970–1981]," J. Mech. Phys. Solids, **105**, pp. 21–24.

[36] Galich, P. I., Fang, N. X., Boyce, M. C., and Rudykh, S., 2017, "Elastic Wave Propagation in Finitely Deformed Layered Materials," J. Mech. Phys. Solids, **98**, pp. 390–410.

[37] Spinelli, S. A., and Lopez-Pamies, O., 2015, "Some Simple Explicit Results for the Elastic Dielectric Properties and Stability of Layered Composites," Int. J. Eng. Sci., **88**, pp. 15–28.

[38] Zhao, X., Hong, W., and Suo, Z., 2007, "Electromechanical Hysteresis and Coexistent States in Dielectric Elastomers," Phys. Rev. B, **76**(13), p. 134113.

[39] Musgrave, M., 1970, *Crystal Acoustics: Introduction to the Study of Elastic Waves and Vibrations in Crystals*, Holden-Day, San Francisco, CA.

[40] Nayfeh, A. H., 1995, *Wave Propagation in Layered Anisotropic Media: With Applications to Composites*, Elsevier Science, New York.

[41] Langenberg, K. J., Marklein, R., and Mayer, K., 2010, "Energy vs. Group Velocity for Elastic Waves in Homogeneous Anisotropic Solid Media," IEEE URSI International Symposium on Electromagnetic Theory (EMTS), Berlin, Aug. 16–19, pp. 733–736.

[42] Tiersten, H. F., 1963, "Thickness Vibrations of Piezoelectric Plates," J. Acoust. Soc. Am., **35**(1), pp. 53–58.

[43] Shmuel, G., and Band, R., 2016, "Universality of the Frequency Spectrum of Laminates," J. Mech. Phys. Solids, **92**, pp. 127–136.

[44] Arruda, E. M., and Boyce, M. C., 1993, "A Three-Dimensional Constitutive Model for the Large Stretch Behavior of Rubber Elastic Materials," J. Mech. Phys. Solids, **41**(2), pp. 389–412.

[45] Gent, A. N., 1996, "A New Constitutive Relation for Rubber," Rubber Chem. Technol., **69**(1), pp. 59–61.

[46] Babaee, S., Wang, P., and Bertoldi, K., 2015, "Three-Dimensional Adaptive Soft Phononic Crystals," J. Appl. Phys., **117**(24), p. 244903.

International Journal of Solids and Structures 110–111 (2017) 294–304

Contents lists available at ScienceDirect

International Journal of Solids and Structures

journal homepage: www.elsevier.com/locate/ijsolstr

Shear wave propagation in finitely deformed 3D fiber-reinforced composites

Pavel I. Galich, Viacheslav Slesarenko, Stephan Rudykh*

Department of Aerospace Engineering, Technion – Israel Institute of Technology, Haifa 32000, Israel

ARTICLE INFO

Article history:
Received 19 September 2016
Revised 19 November 2016
Available online 13 December 2016

Keywords:
Fiber-reinforced composites
Wave propagation
Finite deformations
Dispersion
Transversely isotropic
Micromechanics

ABSTRACT

We investigate the propagation of shear waves in finitely deformed 3D fiber-reinforced composites. We employ a micromechanics based approach and derive explicit expressions for the phase and group velocities of the shear waves in the long wave limit. Thus, we obtain the important characteristics of the shear waves in terms of the volume fractions and material properties of the constituents. We find that the phase and group velocities significantly depend on the applied deformation and direction of wave propagation. To account for interactions between the elastic waves and microstructure in finitely deformed 3D periodic fiber-reinforced materials, we employ the Bloch wave analysis superimposed on large macroscopically applied homogeneous deformations, and we implement the technique into a finite element code. The Bloch wave numerical analysis reveals the essential dispersion phenomenon for the shear waves propagating along the fibers in the finitely deformed 3D periodic fiber-reinforced materials. We find that the appearance of the dispersion phenomenon and the corresponding wavelengths can be tuned by material composition and deformation.

1. Introduction

Nature actively exploits sophisticated microstructures to achieve remarkable material properties and functionalities. In particular, the fiber-reinforced deformable composites, possessing a light weight, high strength and flexibility at the same time, are widely present in nature (Saheb and Jog, 1999). However, natural materials are biodegradable and poorly resistant to moisture, and not always they can provide desirable properties; therefore, synthetic composite materials are of a great interest. The mechanical performance of composite materials can be tailored by designing microstructures combining soft and stiff constituents. Recent advances in the material fabrication techniques and 3D-printing already allow realization of microstructured metamaterials with various properties and functionalities (Babaee et al., 2013; Kolle et al., 2013; Rudykh and Boyce, 2014a; Lin et al., 2014; Ge et al., 2013; Bafekrpour et al., 2014; Rudykh et al., 2015; Celli and Gonella, 2015; Srivastava, 2016; Golub et al., 2012; Fomenko et al., 2014). Moreover, *soft* metamaterials can be reversibly deformed, and, thus, enabling us to manipulate their effective properties via deformation (Li et al., 2013; Slesarenko and Rudykh, 2016). Thus, for example, elastic wave propagation in soft composite materials can be controlled by deformation (Bertoldi and Boyce, 2008b; Bertoldi et al., 2008; Gei, 2008; Rudykh and Boyce, 2014b; Galich et al., 2017; Babaee et al., 2016; Chen and Elbanna, 2016). Even in relatively simple homogeneous hyperelastic materials, elastic wave characteristics can be significantly transformed via deformation (Dorfmann and Ogden, 2010; Galich and Rudykh, 2015b; 2015a; 2016). It is worth noting that many soft biological tissues are found to possess fiber-matrix microstructures (Humphrey, 2002), and the soft tissues frequently experience large deformations due to growth or other physiological processes. Hence, investigation of elastic wave propagation in 3D fiber composites (FCs) undergoing finite deformations can be beneficial for biomedical applications such as ultrasound testing.

Small amplitude elastic wave propagation in finitely deformed homogeneous isotropic materials was pioneered by Biot (1940) on the basis of the static nonlinear theory (Biot, 1939). Waves of a finite amplitude propagating in a pre-stressed elastic medium were investigated by John (1966), and Currie and Hayes (1969). Boulanger and Hayes (1992) considered wave propagation in finitely deformed incompressible Mooney–Rivlin materials and derived explicit relations for wave velocities. Boulanger et al. (1994) extended this work to a broader class of finitely deformed compressible Hadamard materials and first obtained the explicit expressions for the phase velocities of longitudinal and transversal waves. Recently, Destrade and Ogden (2013) have revised and generalized the problem of an infinitesimal wave propagation in

* Corresponding author.
E-mail address: rudykh@technion.ac.il (S. Rudykh).

http://dx.doi.org/10.1016/j.ijsolstr.2016.12.007
0020-7683/

the finitely deformed hyperelastic materials by application of the invariant theory. More recently, Galich and Rudykh (2015b) have investigated infinitesimal wave propagation in finitely deformed compressible Gent materials, exhibiting pronounced stiffening effects, and obtained closed form expressions for the phase velocities of longitudinal and transversal waves.

By employing the nonlinear elastic theory (Truesdell and Noll, 1965) and a phenomenological approach, Scott and Hayes (1976) considered small amplitude plane waves superimposed on a homogeneous deformation in the so-called idealized fiber-reinforced materials, assuming an incompressible matrix and inextensible fibers. Later, Scott (1991, 1992) extended this analysis and considered infinitesimal vibrations of an arbitrary form superimposed on a finite deformation for a broad class of elastic anisotropic materials. The infinitesimal elastic wave propagation in nearly incompressible and nearly inextensible fiber-reinforced materials with unidirectional and orthogonal fibers was examined by Rogerson and Scott (1994). More recently, Ogden and Singh (2011) revisited the problem of infinitesimal wave propagation in an incompressible transversely isotropic elastic solid in the presence of an initial stress. In their work, Ogden and Singh (2011) exploited the phenomenological theory of invariants and presented a more general and transparent formulation of the theory for small amplitude waves propagating in a deformed transversely isotropic hyperelastic solid.

In this work, we employ a *micromechanics* based approach accounting for the phase properties and their spatial distribution to analyze the wave propagation in finitely deformed 3D FCs, as opposite to previous works that employ phenomenological approach (Scott and Hayes, 1976; Scott, 1991, 1992; Rogerson and Scott, 1994; Ogden and Singh, 2011), or numerically model the composites in 2D settings (Rudykh and Boyce, 2014b; Bertoldi and Boyce, 2008b), or do not consider finite deformations (Aberg and Gudmundson, 1997; Kushwaha et al., 1993). Here, we derive explicit closed form expressions for phase and group velocities of the shear waves for any direction of wave propagation in finitely deformed 3D fiber-reinforced materials with neo-Hookean phases. These explicit expressions provide important information on the elastic wave propagation in the long wave limit. To account for the interaction of the elastic waves with the composite microstructure, the Bloch wave analysis is implemented in the finite element code, allowing us to analyze small amplitude motions superimposed on finite macroscopically applied homogeneous deformations. It should be noted that we analyze the finitely deformed fibrous materials in fully 3D settings – both the deformation and the direction of the wave propagation – which, to the best of our knowledge, is not covered in the existing literature. We investigate the role of the material composition and phase properties in the dispersion of shear waves. We specifically focus on the influence of deformation on the dispersion of the shear waves. By considering the waves propagating in the direction of fibers, we find that the applied deformation strongly affects the long waves; whereas the influence of the deformation is weaker for the ranges of short wavelengths. The effect of deformation is found to be more pronounced in FCs with moderate and large shear modulus contrasts between the phases and with large volume fractions of fibers. Finally, we compare the micromechanics based homogenization technique and the numerical Bloch wave analysis, thus, bringing together the different length-scale analyses, and showing the equivalence of these distinct approaches at certain ranges of wavelengths.

2. Theoretical background

Consider a continuum body and identify each point in the undeformed configuration with its vector $\mathbf{X}$. In the deformed body, the new location of the corresponding points is defined by mapping function $\mathbf{x} = \boldsymbol{\chi}(\mathbf{X}, t)$. Hence, the deformation gradient is $\mathbf{F} = \partial\mathbf{x}/\partial\mathbf{X}$, and its determinant $J \equiv \det\mathbf{F} > 0$. For a hyperelastic material described by a strain energy function $\psi(\mathbf{F})$, the first Piola–Kirchhoff stress tensor can be calculated as follows

$$\mathbf{P} = \frac{\partial\psi(\mathbf{F})}{\partial\mathbf{F}}. \tag{1}$$

For an incompressible material, $J = 1$ and Eq. (1) modifies as

$$\mathbf{P} = \frac{\partial\psi(\mathbf{F})}{\partial\mathbf{F}} - p\mathbf{F}^{-T}, \tag{2}$$

where p represents an unknown Lagrange multiplier. The corresponding Cauchy stress tensor is related to the first Piola-Kirchhoff stress tensor via the relation $\boldsymbol{\sigma} = J^{-1}\mathbf{P}\cdot\mathbf{F}^T$.

In the absence of body forces the equations of motion can be written in the undeformed configuration as

$$\mathrm{Div}\mathbf{P} = \rho_0\frac{D^2\boldsymbol{\chi}}{Dt^2}, \tag{3}$$

where ρ_0 is the initial density of the material and the operator $D^2(\bullet)/Dt^2$ represents the material time derivative. If the deformation is applied quasi-statically, the right hand part of Eq. (3) can be assumed to be zero, and the equilibrium equation is obtained as

$$\mathrm{Div}\mathbf{P} = \mathbf{0}. \tag{4}$$

Consider next infinitesimal motions superimposed on the equilibrium state. The equations of the incremental motions are

$$\mathrm{Div}\dot{\mathbf{P}} = \rho_0\frac{D^2\mathbf{u}}{Dt^2}, \tag{5}$$

where $\dot{\mathbf{P}}$ is the incremental change in the first Piola–Kirchhoff stress tensor and $\mathbf{u}$ is the incremental displacement.

The linearized constitutive law can be written as

$$\dot{P}_{ij} = \mathcal{A}_{0ijkl}\dot{F}_{kl}, \tag{6}$$

where $\dot{\mathbf{F}} = \mathrm{Grad}\,\mathbf{u}$ is the incremental change in the deformation gradient, and the tensor of elastic moduli is defined as $\mathcal{A}_{0i\alpha k\beta} = \partial^2\psi/\partial F_{i\alpha}\partial F_{k\beta}$. Under substitution of Eq. (6) into Eq. (5) the incremental motion equation takes the form

$$\mathcal{A}_{0ijkl}u_{k,lj} = \rho_0\frac{D^2u_i}{Dt^2}. \tag{7}$$

3. Long wave estimates for finitely deformed incompressible fiber composites

To analyze small amplitude motions superimposed on a finite deformation, we present equation of motion (7) in the updated Lagrangian formulation

$$\mathcal{A}_{ijkl}u_{k,lj} = \rho\frac{\partial^2u_i}{\partial t^2}, \tag{8}$$

where $\mathcal{A}_{iqkp} = J^{-1}\mathcal{A}_{0ijkl}F_{pl}F_{qj}$ and $\rho = J^{-1}\rho_0$ is the density of the deformed material.

We seek a solution for Eq. (8) in the form of plane waves with constant polarization

$$\mathbf{u} = \mathbf{g}h(\mathbf{n}\cdot\mathbf{x} - ct), \tag{9}$$

where h is a twice continuously differentiable function and unit vector $\mathbf{g}$ denotes the polarization; the unit vector $\mathbf{n}$ defines the direction of wave propagation, and c is the phase velocity of the wave.

Substituting (9) into (8), we obtain

$$\mathbf{Q}(\mathbf{n})\cdot\mathbf{g} = \rho c^2\mathbf{g}, \tag{10}$$

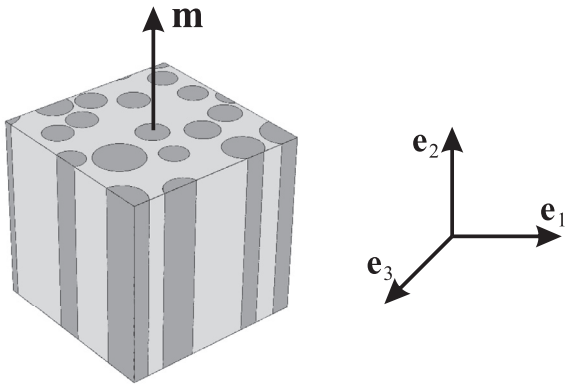

Fig. 1. Schematic representation of the FC with random distribution of fibers. ($\mathbf{e}_1$, $\mathbf{e}_2$, $\mathbf{e}_3$) is the orthonormal basis.

where

$$Q_{ij} = \mathcal{A}_{ijkl} n_j n_l \tag{11}$$

is the acoustic tensor defining the condition of propagation of the infinitesimal plane waves.

For incompressible materials Eq. (8) modifies as

$$\mathcal{A}_{ijkl} u_{k,lj} + \dot{p}_{,i} = \rho \frac{\partial^2 u_i}{\partial t^2}, \tag{12}$$

together with the incompressibility constraint

$$u_{i,i} = 0. \tag{13}$$

Substitution of (9) and $\dot{p} = p_0 h'(\mathbf{n}\cdot\mathbf{x} - ct)$, where p_0 is a scalar, into (12) and (13) yields

$$\hat{\mathbf{Q}}(\mathbf{n})\cdot\mathbf{g} = \rho c^2 \mathbf{g} \quad \text{and} \quad \mathbf{g}\cdot\mathbf{n} = 0, \tag{14}$$

where $\hat{\mathbf{Q}} = \hat{\mathbf{I}}\cdot\mathbf{Q}\cdot\hat{\mathbf{I}}$ and $\hat{\mathbf{I}} = \mathbf{I} - \mathbf{n}\otimes\mathbf{n}$ is the projection onto the plane normal to $\mathbf{n}$.

Next, let us consider a FC made out of aligned fibers embedded in a softer matrix with the volume fractions v_f and $v_m = 1 - v_f$. Here and thereafter, the fields and parameters of the constituents are denoted by the subscripts $(\bullet)_f$ and $(\bullet)_m$ for fibers and matrix, respectively. In the reference configuration the volume fractions of the phases can be calculated as

$$v_f = 1/\Omega \int_\Omega \eta_f(\mathbf{X}) d\mathbf{X} \quad \text{and} \quad v_m = 1/\Omega \int_\Omega \big(1 - \eta_f(\mathbf{X})\big) d\mathbf{X}, \tag{15}$$

where $\eta_f = 1$ if $\mathbf{X}$ is within the fiber phase and $\eta_f = 0$ otherwise; Ω is the volume occupied by the composite in the reference state. The macroscopic deformation gradient is defined as

$$\bar{\mathbf{F}} = 1/\Omega \int_\Omega \mathbf{F}(\mathbf{X}) d\mathbf{X}. \tag{16}$$

The *boundary conditions* for $\mathbf{F}_f$ and $\mathbf{F}_m$, and for $\mathbf{P}_f$ and $\mathbf{P}_m$ at the interfaces between the fibers and matrix are

$$\big(\mathbf{F}_f - \mathbf{F}_m\big)\cdot\mathbf{m} = \mathbf{0} \quad \text{and} \quad \big(\mathbf{P}_f - \mathbf{P}_m\big)\cdot\mathbf{w} = \mathbf{0}, \tag{17}$$

where the unit vector $\mathbf{m}$ denotes the initial fiber directions (see Fig. 1), and $\mathbf{w}$ is the arbitrary unit vector orthogonal to $\mathbf{m}$.

In this work, we consider fiber-reinforced materials with *incompressible* phases described by a neo-Hookean strain energy function (Ogden, 1997)

$$\psi_\xi^{inc} = \frac{\mu_\xi}{2}(\mathbf{F}_\xi : \mathbf{F}_\xi - 3), \tag{18}$$

where μ_ξ is the initial shear modulus. For a FC with incompressible neo-Hookean phases, an effective strain energy density function can be constructed (deBotton et al., 2006)

$$\psi(\bar{\mathbf{F}}) = \frac{\tilde{\mu}}{2}\big(\bar{\mathbf{F}} : \bar{\mathbf{F}} - 3\big) + \frac{\bar{\mu} - \tilde{\mu}}{2}\big(I_4 + 2I_4^{-1/2} - 3\big), \tag{19}$$

where $I_4 = \mathbf{m}\cdot\bar{\mathbf{C}}\cdot\mathbf{m}$, and $\bar{\mathbf{C}} = \bar{\mathbf{F}}^T\cdot\bar{\mathbf{F}}$ is the average right Cauchy-Green deformation tensor;

$$\bar{\mu} = v_f\mu_f + v_m\mu_m \quad \text{and} \quad \tilde{\mu} = \mu_m \frac{\big(1+v_f\big)\mu_f + v_m\mu_m}{v_m\mu_f + \big(1+v_f\big)\mu_m} \tag{20}$$

are the homogenized elastic moduli.

The acoustic tensor (14) corresponding to the strain energy function (19) takes the form

$$\hat{\mathbf{Q}}(\mathbf{n}, \bar{\mathbf{F}}) = q_1\hat{\mathbf{I}} + q_2\big(\hat{\mathbf{I}}\cdot\bar{\mathbf{F}}\cdot\mathbf{m}\big)\otimes\big(\hat{\mathbf{I}}\cdot\bar{\mathbf{F}}\cdot\mathbf{m}\big), \tag{21}$$

where

$$q_1 = \tilde{\mu}\big(\mathbf{n}\cdot\bar{\mathbf{B}}\cdot\mathbf{n}\big) + (\bar{\mu} - \tilde{\mu})\big(1 - I_4^{-3/2}\big)\big(\mathbf{n}\cdot\bar{\mathbf{F}}\cdot\mathbf{m}\big)^2 \tag{22}$$

and

$$q_2 = 3I_4^{-5/2}(\bar{\mu} - \tilde{\mu})\big(\mathbf{n}\cdot\bar{\mathbf{F}}\cdot\mathbf{m}\big)^2, \tag{23}$$

where $\bar{\mathbf{B}} = \bar{\mathbf{F}}\cdot\bar{\mathbf{F}}^T$ is the average left Cauchy–Green deformation tensor. The acoustic tensor (21) has the following nontrivial eigenvalues with the eigenvectors lying in the plane normal to $\mathbf{n}$

$$a_1 = q_1 \quad \text{and} \quad a_2 = q_1 + q_2\Big(I_4 - \big(\mathbf{n}\cdot\bar{\mathbf{F}}\cdot\mathbf{m}\big)^2\Big). \tag{24}$$

Thus, we have two distinct shear waves propagating in a finitely deformed incompressible FC with the corresponding phase velocities

$$\bar{c}_{sw}^{(1)} = \sqrt{\frac{a_1}{\bar{\rho}_0}} \quad \text{and} \quad \bar{c}_{sw}^{(2)} = \sqrt{\frac{a_2}{\bar{\rho}_0}}, \tag{25}$$

where $\bar{\rho}_0 = v_f\rho_{0f} + v_m\rho_{0m}$ is the average initial density of the FC.

The phase velocities of the shear waves (25) coincide only for special cases of applied deformations and directions of wave propagation. For instance, let us consider a uniaxially deformed FC with the corresponding macroscopic deformation gradient

$$\bar{\mathbf{F}} = \lambda\mathbf{e}_2\otimes\mathbf{e}_2 + \lambda^{-1/2}(\mathbf{I} - \mathbf{e}_2\otimes\mathbf{e}_2), \tag{26}$$

where λ is the applied macroscopic stretch ratio. Then, for waves propagating perpendicular to the fibers, i.e. $\mathbf{m} = \mathbf{e}_2$ and $\mathbf{n} = \mathbf{e}_1$, the phase velocities of the shear waves coincide

$$\bar{c}_{sw} = \bar{c}_{sw}^{(1)} = \bar{c}_{sw}^{(2)} = \sqrt{\frac{\tilde{\mu}}{\lambda\bar{\rho}_0}}. \tag{27}$$

The phase velocities also coincide for the waves propagating along the fibers, i.e. $\mathbf{n} = \mathbf{m} = \mathbf{e}_2$,

$$\bar{c}_{sw} = \bar{c}_{sw}^{(1)} = \bar{c}_{sw}^{(2)} = \lambda\sqrt{\frac{\bar{\mu} + (\tilde{\mu} - \bar{\mu})\lambda^{-3}}{\bar{\rho}_0}}. \tag{28}$$

However, for an oblique propagation of the waves relative to the fiber direction, for example, $\mathbf{m} = \mathbf{e}_2$ and $\mathbf{n} = (\mathbf{e}_1 + \mathbf{e}_2)/\sqrt{2}$, the phase velocities of the shear waves are distinct

$$\bar{c}_{sw}^{(1)} = \sqrt{\frac{2\tilde{\mu} + \big(\lambda^3 - 1\big)\bar{\mu}}{2\lambda\bar{\rho}_0}} \quad (\mathbf{g} = \mathbf{e}_3) \tag{29}$$

and

$$\bar{c}_{sw}^{(2)} = \sqrt{\frac{\tilde{\mu} + \bar{\mu}\big(1 + 2\lambda^3\big)}{4\lambda\bar{\rho}_0}} \quad \big(\mathbf{g} = (\mathbf{e}_2 - \mathbf{e}_1)/\sqrt{2}\big). \tag{30}$$

Note that (28) yields an explicit expression for the critical stretch ratio corresponding to the onset of macroscopic instability under uniaxial contraction (Rudykh and deBotton, 2012), namely

$$\lambda_{cr} = \left(1 - \frac{\tilde{\mu}}{\bar{\mu}}\right)^{1/3}. \tag{31}$$

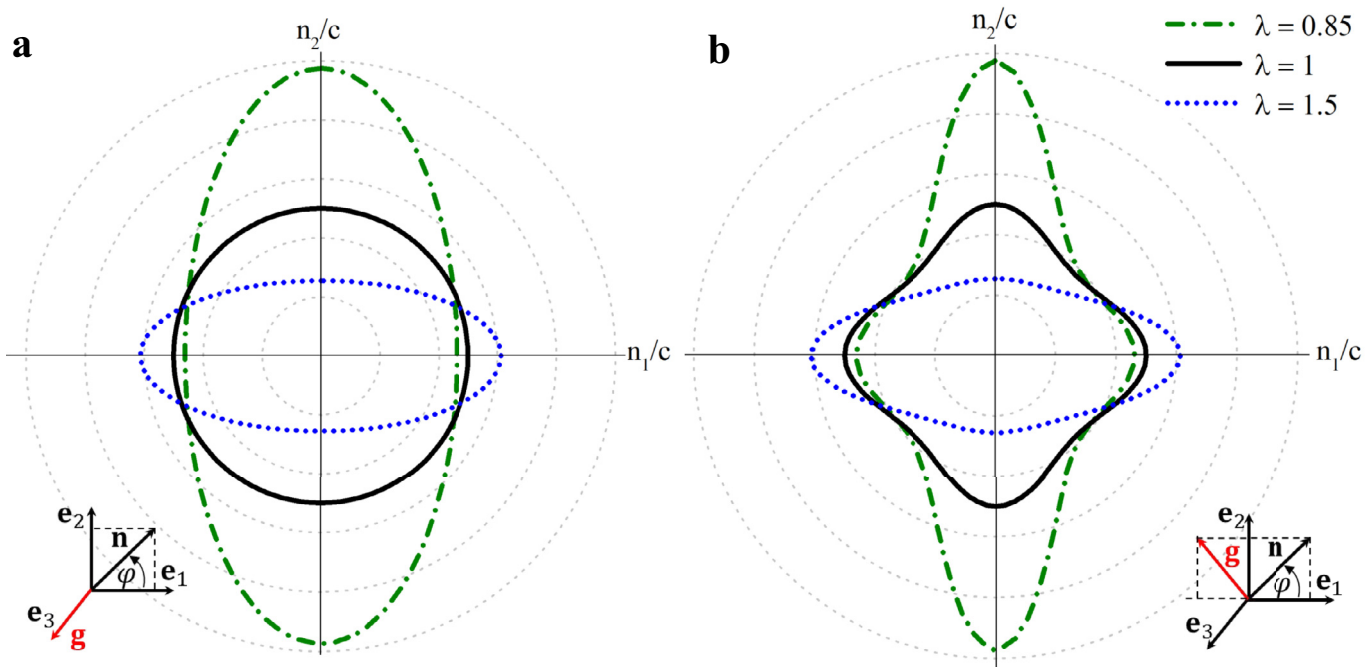

Fig. 2. Slowness curves for the out-of-plane (a) and in-plane (b) shear waves propagating in the FC with $\nu_f = 0.2$, $\mu_f/\mu_m = 10$, and $\rho_{0f}/\rho_{0m} = 1$ under uniaxial tension (26). Scale is 0.4 per division, and slowness is normalized by $\sqrt{\bar{\mu}/\bar{\rho}_0}$. Note that the horizontal and vertical axes with the corresponding labels n_1/c and n_2/c serve for showing the principal directions and physical quantity presented on the polar plot only.

To illustrate the influence of the deformation and direction of wave propagation on the characteristics of elastic waves in the FCs, we consider wave propagation in the plane $\langle \mathbf{e}_1, \mathbf{e}_2 \rangle$, i.e. $\mathbf{n} = \cos\varphi\ \mathbf{e}_1 + \sin\varphi\ \mathbf{e}_2$. By the use of the explicit relations (25) we construct the polar diagrams of slowness $\bar{s}_{sw}(\varphi) = 1/\bar{c}_{sw}(\varphi)$, also known in literature as slowness curves (Musgrave, 1970; Nayfeh, 1995). Fig. 2 shows an example of the slowness curves for the so-called out-of-plane (with polarization $\mathbf{g} = \mathbf{e}_3$) and in-plane (with polarization lying in plane $\langle \mathbf{e}_1, \mathbf{e}_2 \rangle$) shear waves in the FC undergoing uniaxial tension along the fibers. The examples are given for the FC with $\nu_f = 0.2$, $\mu_f/\mu_m = 10$, and the fiber direction $\mathbf{m} = \mathbf{e}_2$. The continuous black curves correspond to the undeformed FC, while the dash-dotted green and dotted blue curves are for the FC under the uniaxial contraction ($\lambda = 0.85$) and extension ($\lambda = 1.5$), respectively. Note that the critical stretch ratio for the considered FC undergoing uniaxial contraction is $\lambda_{cr} = 0.80$; therefore, the presented slowness curves for the compressed ($\lambda = 0.85$) FC correspond to a macroscopically stable state. The slowness curves clearly indicate the significant influence of the applied deformation on the shear wave propagation. Specifically, the contraction along the fibers results in a significant decrease of the phase velocities of the shear waves propagating in the direction of fibers; while the phase velocities increase for the waves propagating perpendicular to the fibers since these directions experience extension. Note that the phase velocity of the in-plane shear wave in the uniaxially deformed FC is maximal for certain directions of wave propagation $\mathbf{n}_0$. To find these directions, we substitute (26), $\mathbf{n}_0 = \cos\varphi_0\ \mathbf{e}_1 + \sin\varphi_0\ \mathbf{e}_2$, and $\mathbf{m} = \mathbf{e}_2$ into $(25)_2$, and then solve the extreme value problem for the phase velocity $\bar{c}^{(2)}_{sw}$ as a function of φ_0:

$$\varphi_0 = \pm\frac{1}{2}\arccos\left(\frac{1-\lambda^3}{3\left(1-\frac{\bar{\mu}}{\tilde{\mu}}\right)}\right) + \pi z,\ z = 0, 1. \tag{32}$$

In the undeformed state $\varphi_0 = \pm\frac{\pi}{4}, \pm\frac{3\pi}{4}$. Moreover, these directions differ from the principal directions in contrast to the out-of-plane shear wave – the phase velocity of which has the maxima in the directions of the principal axes. For example, in the uniaxially stretched FC the phase velocity of the out-of-plane shear wave is maximal for the wave propagation along the fibers, i.e. for $\mathbf{n} = \pm\mathbf{e}_2$ (see Fig. 2 (a)).

The dispersion relations for the long waves in an incompressible neo-Hookean FC are derived from (25) and have the following form

$$\bar{\omega}^{(1)}_{sw} = \sqrt{\frac{b_1}{\bar{\rho}_0}} \quad \text{and} \quad \bar{\omega}^{(2)}_{sw} = \sqrt{\frac{b_2}{\bar{\rho}_0}} \tag{33}$$

where

$$b_1 = \tilde{\mu}(\mathbf{k}\cdot\bar{\mathbf{B}}\cdot\mathbf{k}) + (\bar{\mu}-\tilde{\mu})\left(1-I_4^{-3/2}\right)\left(\mathbf{k}\cdot\bar{\mathbf{F}}\cdot\mathbf{m}\right)^2 \tag{34}$$

and

$$b_2 = b_1 + 3I_4^{-5/2}(\bar{\mu}-\tilde{\mu})\left(\mathbf{k}\cdot\bar{\mathbf{F}}\cdot\mathbf{m}\right)^2\left(I_4 - k^{-2}\left(\mathbf{k}\cdot\bar{\mathbf{F}}\cdot\mathbf{m}\right)^2\right), \tag{35}$$

where $\mathbf{k}$ is the wave vector and $k = |\mathbf{k}|$ is the wave number.

Hence, we can find the corresponding group velocity defined as

$$\mathbf{v}_g = \nabla_{\mathbf{k}}\omega. \tag{36}$$

Substitution of (33) into (36) yields explicit expressions for the group velocities of the long waves propagating in the finitely deformed FC

$$\mathbf{v}^{(1)}_{sw} = \frac{\left(\tilde{\mu}\bar{\mathbf{B}}\cdot\mathbf{n} + (\bar{\mu}-\tilde{\mu})\left(1-I_4^{-3/2}\right)\left(\mathbf{n}\cdot\bar{\mathbf{F}}\cdot\mathbf{m}\right)\bar{\mathbf{F}}\cdot\mathbf{m}\right)}{\sqrt{\bar{\rho}_0 a_1}} \tag{37}$$

and

$$\begin{aligned}\mathbf{v}^{(2)}_{sw} = \frac{1}{\sqrt{\bar{\rho}_0 a_2}}\Big(&\tilde{\mu}\bar{\mathbf{B}}\cdot\mathbf{n} + \\ &(\bar{\mu}-\tilde{\mu})\left(\mathbf{n}\cdot\bar{\mathbf{F}}\cdot\mathbf{m}\right)\Big[3I_4^{-5/2}\left(\mathbf{n}\cdot\bar{\mathbf{F}}\cdot\mathbf{m}\right)^3\mathbf{n} + \\ &\left(1+2I_4^{-3/2}\left(1-3I_4^{-1}\left(\mathbf{n}\cdot\bar{\mathbf{F}}\cdot\mathbf{m}\right)^2\right)\right)\bar{\mathbf{F}}\cdot\mathbf{m}\Big]\Big).\end{aligned} \tag{38}$$

In particular, the group velocities of the shear waves coincide for waves propagating perpendicular to the fibers (i.e. $\mathbf{m} = \mathbf{e}_2$ and $\mathbf{n} = \mathbf{e}_1$) in the uniaxially deformed FC

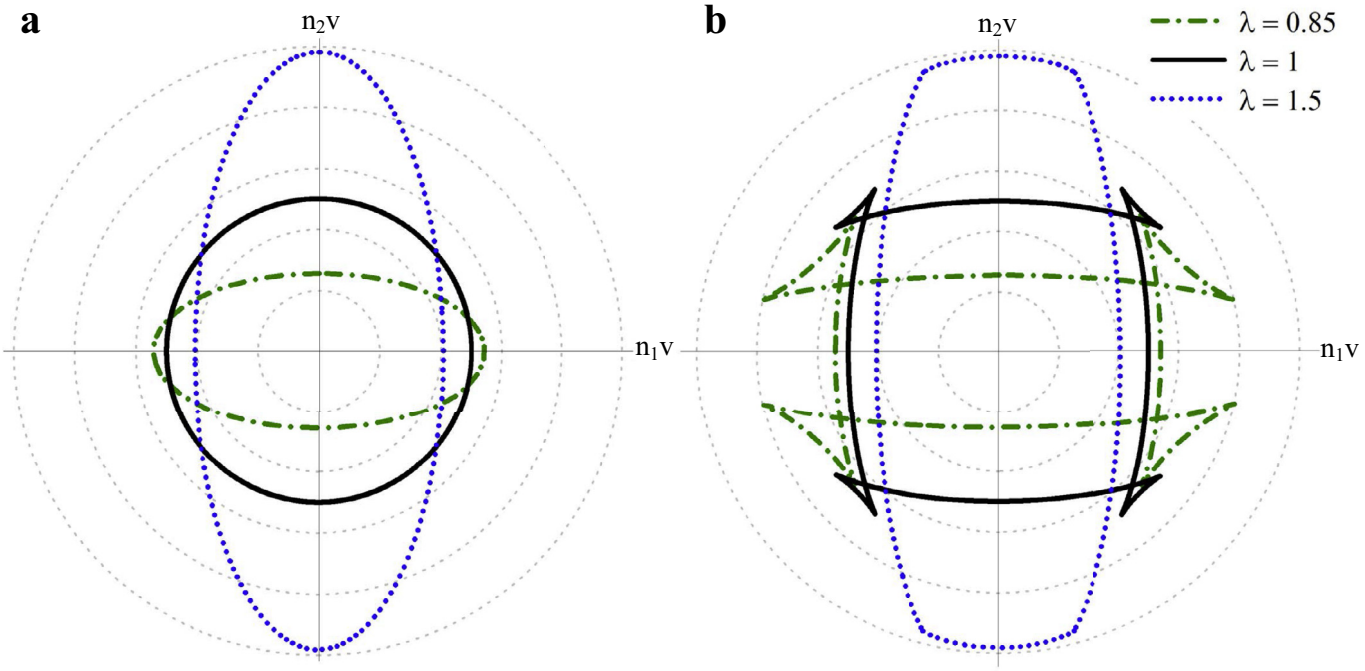

Fig. 3. Energy curves for (a) – out-of-plane and (b) – in-plane shear waves propagating in the FC with $\nu_f = 0.2$, $\mu_f/\mu_m = 10$, and $\rho_{0f}/\rho_{0m} = 1$ under uniaxial tension. Scale is 0.4 per division, where group velocity is normalized by $\sqrt{\bar{\rho}_0/\tilde{\mu}}$. Note that the horizontal and vertical axes with the corresponding labels (n_1v) and (n_2v) serve for showing the principal directions and physical quantity presented on the polar plot only.

$$\mathbf{v}_{sw}^{(1)} = \mathbf{v}_{sw}^{(2)} = \sqrt{\frac{\tilde{\mu}}{\lambda\bar{\rho}_0}}\,\mathbf{e}_1. \tag{39}$$

The group velocities also coincide for the waves propagating along the fibers, i.e. $\mathbf{n} = \mathbf{m} = \mathbf{e}_2$,

$$\mathbf{v}_{sw}^{(1)} = \mathbf{v}_{sw}^{(2)} = \lambda\sqrt{\frac{\bar{\mu} + (\tilde{\mu} - \bar{\mu})\lambda^{-3}}{\bar{\rho}_0}}\,\mathbf{e}_2. \tag{40}$$

To illustrate the derived results (37) and (38), we consider wave propagation in the plane $\langle \mathbf{e}_1, \mathbf{e}_2 \rangle$, i.e. $\mathbf{n} = \cos\varphi\ \mathbf{e}_1 + \sin\varphi\ \mathbf{e}_2$. Recall that the outer normal to the slowness curve shows the direction of the energy flow (Musgrave, 1970; Nayfeh, 1995). Hence, by assigning the absolute value of the group velocity (i.e. $|\mathbf{v}_{sw}|$) to the normal to the slowness curve for all possible propagation directions, the polar diagrams of group velocity or the energy curves (Musgrave, 1970; Nayfeh, 1995) are constructed. Fig. 3 shows an example of the energy curves for (a) out-of-plane and (b) in-plane shear waves propagating in the uniaxially deformed FC with $\nu_f = 0.2$, $\mu_f/\mu_m = 10$, and $\rho_{0f}/\rho_{0m} = 1$. The continuous black curves correspond to the undeformed FC while the dash-dotted green and dotted blue curves refer to the uniaxial contraction ($\lambda = 0.85$) and extension ($\lambda = 1.5$), respectively. Clearly, the group velocities of the shear waves strongly depend on the applied deformation and direction of wave propagation. Moreover, the energy curve of the in-plane shear wave has intersections, and their position can be manipulated by deformation (see Fig. 3 (b)). These intersections of the energy curves mean that the absolute values and directions of group velocity coincide for two different directions of wave propagation. For the out-of-plane shear wave the intersections are not observed (see Fig. 3 (a)). It is worth mentioning also that the energy curves of plane waves coincide with the wave fronts of impulsive point source excited waves in homogeneous anisotropic materials (Langenberg et al., 2010; Nayfeh, 1995). In this case, these cusps of energy curves will correspond to the regions of null energy (Nayfeh, 1995).

Next, let us consider slowness and energy curves near to, and at the onset of instability point. Fig. 4 shows the slowness curves of the shear waves propagating in the FC subjected to the uniaxial contraction of $\lambda = 0.81$ (dash-dotted green) and $\lambda = 0.80$ (dotted red), while $\lambda_{cr} = 0.80$. A comparison of Figs. 2 and 4 shows that the slowness of both shear waves propagating along the fibers dramatically increases (or phase velocity decreases) when the critical stretch is approached. In particular, in the FC contracted to $\lambda = 0.81$, the slownesses of shear waves propagating in the direction of fibers are 3.8 times larger than in the undeformed FC. Eventually, the slownesses tend to infinity in the FC contracted to the critical stretch ratio, i.e. at $\lambda = 0.80$. This is due to the fact that the phase velocities of the shear waves propagating along the fibers attain zero value in the FC subjected to $\lambda = \lambda_{cr}$ (see (28)). Lastly, Fig. 5 shows the energy curves of the shear waves propagating in the FC subjected to the uniaxial contraction of $\lambda = 0.81$ ((a) and (b)) and $\lambda = 0.80$ ((c) and (d)). We observe that the energy curve of the out-of-plane shear wave for the FC subjected to λ_{cr} degenerates into the three dots (see Fig. 5 (c)). The dot in the center means that the absolute value of the group velocity is zero for the wave propagating in direction of fibers (see (40)); the other two dots mean that the absolute value and direction of the group velocity do not change with the wave propagation direction. For the in-plane shear wave, the energy curve degenerates into the dot and two curved triangles (see Fig. 5 (d)). The dot in the center corresponds to the zero group velocity of the wave propagating along the fibers, while the curved triangles refer to the curvature of the corresponding slowness curve (see Fig. 4 (b)) in the vicinity of the wave propagation directions perpendicular to the fibers (i.e. $\mathbf{n} = \pm\mathbf{e}_1$).

4. Bloch wave analysis for wave propagation in 3D periodic FCs

To obtain the dispersion relations for finitely deformed 3D periodic FCs, we employ the Bloch wave analysis superimposed on a finite deformation (Aberg and Gudmundson, 1997; Bertoldi and Boyce, 2008b; 2008a; Rudykh and Boyce, 2014b). We implement

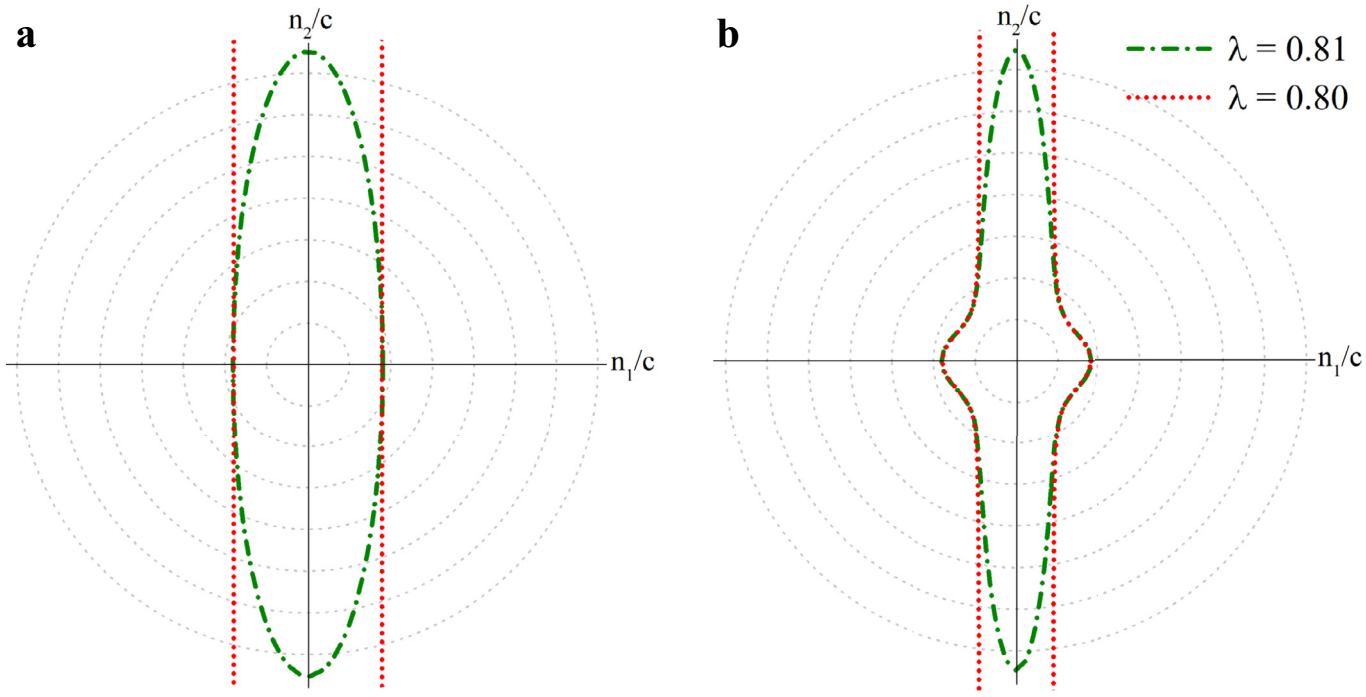

Fig. 4. Slowness curves for the out-of-plane (a) and in-plane (b) shear waves propagating in the FC with $\nu_f = 0.2$, $\mu_f/\mu_m = 10$, and $\rho_{0f}/\rho_{0m} = 1$ under uniaxial tension (26) near the instability. Scale is 0.5 per division, and slowness is normalized by $\sqrt{\tilde{\mu}/\tilde{\rho}_0}$.

the analysis in the finite element code. Fig. 6 shows an example of the corresponding representative volume element (RVE) for a FC with a square periodic unit cell. Geometrically, the fibers are characterized by their diameters, namely $d = 2a\sqrt{\nu_f/\pi}$, where a is the period of the FC (see Fig. 6). The periodic unit cell occupies a domain Ω in the undeformed configuration, namely

$$-a/2 \le x_1 \le a/2, \quad -h/2 \le x_2 \le h/2, \quad \text{and} \quad -a/2 \le x_3 \le a/2. \tag{41}$$

First, a solution for a finitely deformed state is obtained. The macroscopic deformation gradient $\bar{\mathbf{F}} = 1/\Omega \int_\Omega \mathbf{F} dV$ is applied through periodic boundary conditions imposed on the displacements of the RVE faces such that

$$\mathbf{U}_B - \mathbf{U}_A = \left(\bar{\mathbf{F}} - \mathbf{I}\right) \cdot (\mathbf{X}_B - \mathbf{X}_A) = \bar{\mathbf{H}} \cdot (\mathbf{X}_B - \mathbf{X}_A), \tag{42}$$

where A and B are the nodes on the opposite faces of the RVE boundary, $\bar{\mathbf{H}}$ is the average displacement gradient tensor, and $\mathbf{U} = \mathbf{x}(\mathbf{X}) - \mathbf{X}$ is the displacement field. The macroscopic first Piola–Kirchhoff stress tensor and the corresponding Cauchy stress tensor are calculated as $\bar{\mathbf{P}} = 1/\Omega \int_\Omega \mathbf{P} dV$ and $\bar{\boldsymbol{\sigma}} = 1/\Omega \int_\Omega \boldsymbol{\sigma} dV$, respectively. Rigid body motions are prevented by fixing the displacements of a single node. Although the analysis is general and it can be applied for materials subjected to any macroscopically applied homogeneous deformation $\bar{\mathbf{F}}$, here the examples are given for a uniaxial loading (26).

Second, the Bloch wave analysis is performed for the finitely deformed state. The corresponding incremental change in the displacement and the first Piola–Kirchhoff stress tensor can be expressed as

$$\mathbf{u}(\mathbf{X}, t) = \dot{\boldsymbol{\kappa}}(\mathbf{X}) e^{-i\omega t} \quad \text{and} \quad \dot{\mathbf{P}} = \dot{\mathcal{P}} e^{-i\omega t}, \tag{43}$$

where ω is the angular frequency. By substitution (43) in (5), we obtain

$$\mathrm{Div}\dot{\mathcal{P}} + \rho_0 \omega^2 \dot{\boldsymbol{\kappa}} = \mathbf{0}. \tag{44}$$

According to the Floquet theorem (Kittel, 2004)

$$\dot{\boldsymbol{\kappa}}(\mathbf{X} + \mathbf{R}) = \dot{\boldsymbol{\kappa}}(\mathbf{X}) e^{-i\mathbf{K}^0 \cdot \mathbf{R}}, \tag{45}$$

where $\mathbf{R}$ defines the distance between the nodes on the opposite faces of the RVE in the reference configuration. The periodicity conditions (45) are imposed in the finite element code through the corresponding boundary conditions for the displacements of the opposite faces (Slesarenko and Rudykh, 2017; Bertoldi and Boyce, 2008a; 2008b; Wang and Bertoldi, 2012). The dispersion relations are obtained by solving the eigenvalue problem stemming from Eqs. (43)–(45) for a range of the wave vectors $\mathbf{K}^0$.

We start from comparing the results of the Bloch wave numerical analysis and the analytical estimates (33) for the long wave limit. Fig. 7 presents the comparisons for the wave propagating in the direction of fibers. The FCs are subjected to the uniaxial tension (26) along the fiber direction of the magnitude $\lambda = 1.25$. Fig. 7 (a) and (b) show the comparison for FCs with $\nu_f = 0.25$, $\mu_f/\mu_m = 10$ and $\mu_f/\mu_m = 1000$, respectively; while Fig. 7 (c) and (d) show the comparison for FCs with $\nu_f = 0.01$, $\mu_f/\mu_m = 10$ and $\mu_f/\mu_m = 1000$, respectively. The continuous black curves refer to the numerical simulations while the dashed red curves correspond to the long wave estimates (33). Here and thereafter, we consider FCs with constituents having identical densities (i.e. $\rho_{0f}/\rho_{0m} = 1$), and frequency is normalized as $f_n = fa\sqrt{\tilde{\rho}_0/\tilde{\mu}}$, where $f = \omega/(2\pi)$. Fig. 7 (a) and (c) show that the long wave estimates are in excellent agreement with the results of numerical simulations up to the wavelengths comparable with the period a of the unit cell for FCs possessing a small amount of fibers and a moderate contrast in the shear modulus between the constituents. However, for larger contrasts in the shear moduli, the long wave estimates are in good agreement with the Bloch wave analysis only for wavelengths significantly exceeding the period of the unit cell, namely $l \gtrsim \pi^2 a$ (see Fig. 7 (b) and (d)). Thus, the difference between the long wave estimates (33) and Bloch wave analysis increases with an increase in the volume fraction and shear modulus of fibers (i.e. the role of the fibers becomes more significant).

Fig. 8 presents the dispersion curves for the periodic FCs with $\nu_f = 0.25$ and (a) $\mu_f/\mu_m = 10$, (b) $\mu_f/\mu_m = 100$, and (c) $\mu_f/\mu_m = 1000$ undergoing uniaxial deformations along the fibers.

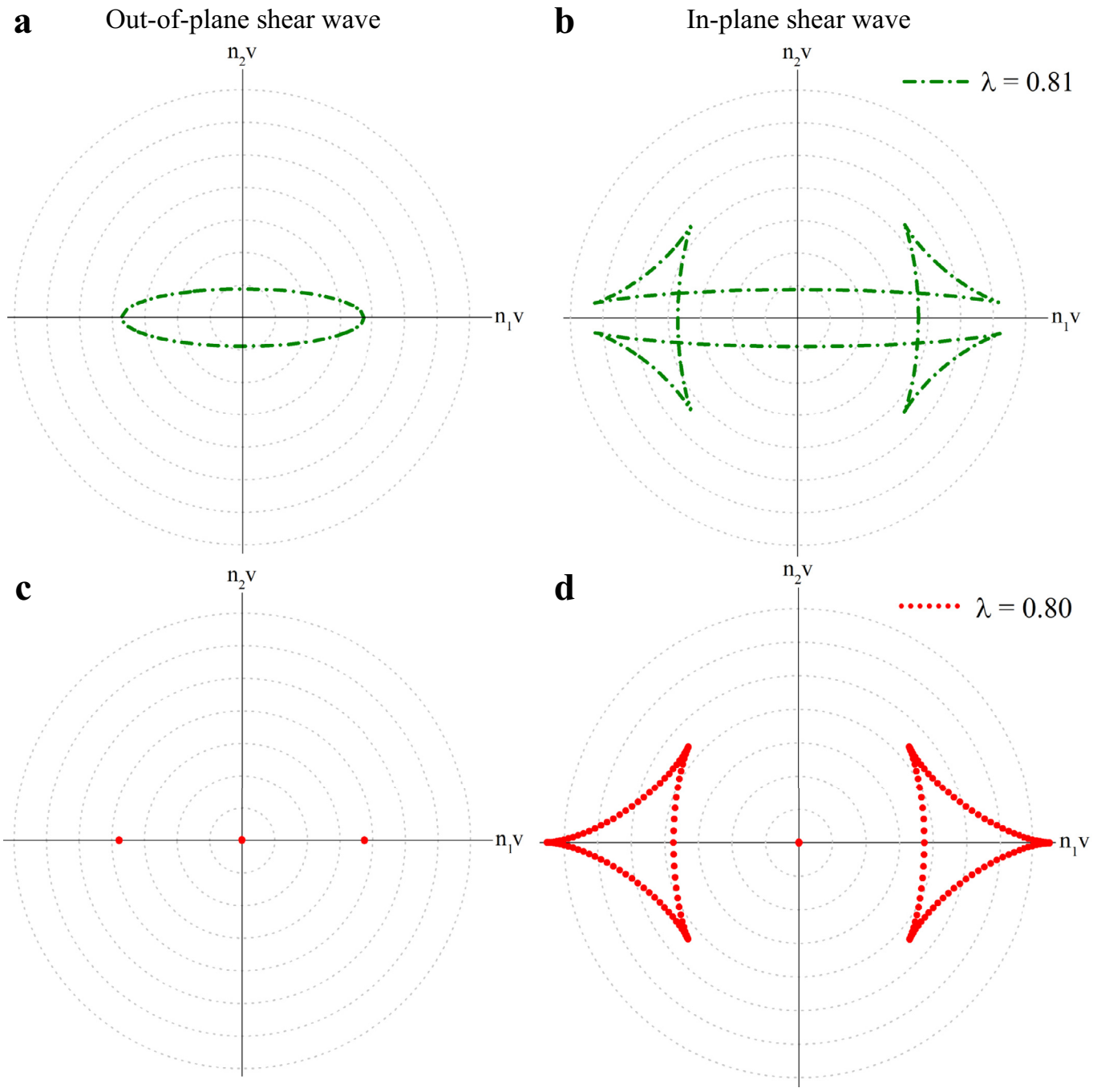

Fig. 5. Energy curves for the out-of-plane (a, c) and in-plane (b, d) shear waves propagating in the FC with $\nu_f = 0.2$, $\mu_f/\mu_m = 10$, and $\rho_{0f}/\rho_{0m} = 1$ under uniaxial tension (26) near the instability. Scale is 0.3 per division, and group velocity is normalized by $\sqrt{\tilde{\rho}_0/\tilde{\mu}}$.

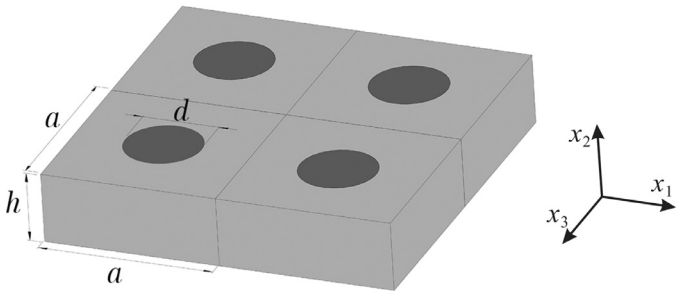

Fig. 6. RVE for a 3D periodic FC with a square arrangement of fibers.

The dispersion curves presented in Fig. 8 (and also in Fig. 9) are obtained by utilizing the Bloch wave analysis implemented in the finite element code. Clearly, for the FC with the low shear modulus contrast between the fibers and matrix (e.g., $\mu_f/\mu_m = 10$), the deformation slightly influences dispersion curves (Fig. 8 (a)). However, the influence of deformation increases for the FCs with moderate and high shear modulus contrasts (e.g., $\mu_f/\mu_m = 100$ and $\mu_f/\mu_m = 1000$). Specifically, deformation considerably influences the dispersion of the waves with wavelengths exceeding the characteristic length-scale of the FC (Fig. 8 (b) and (c)). For example, for the wavenumber $ka/(2\pi) = 0.2$, the uniaxial tension of the magnitude $\lambda = 1.5$ shifts the dispersion curve from $f_n = 0.29$ up to

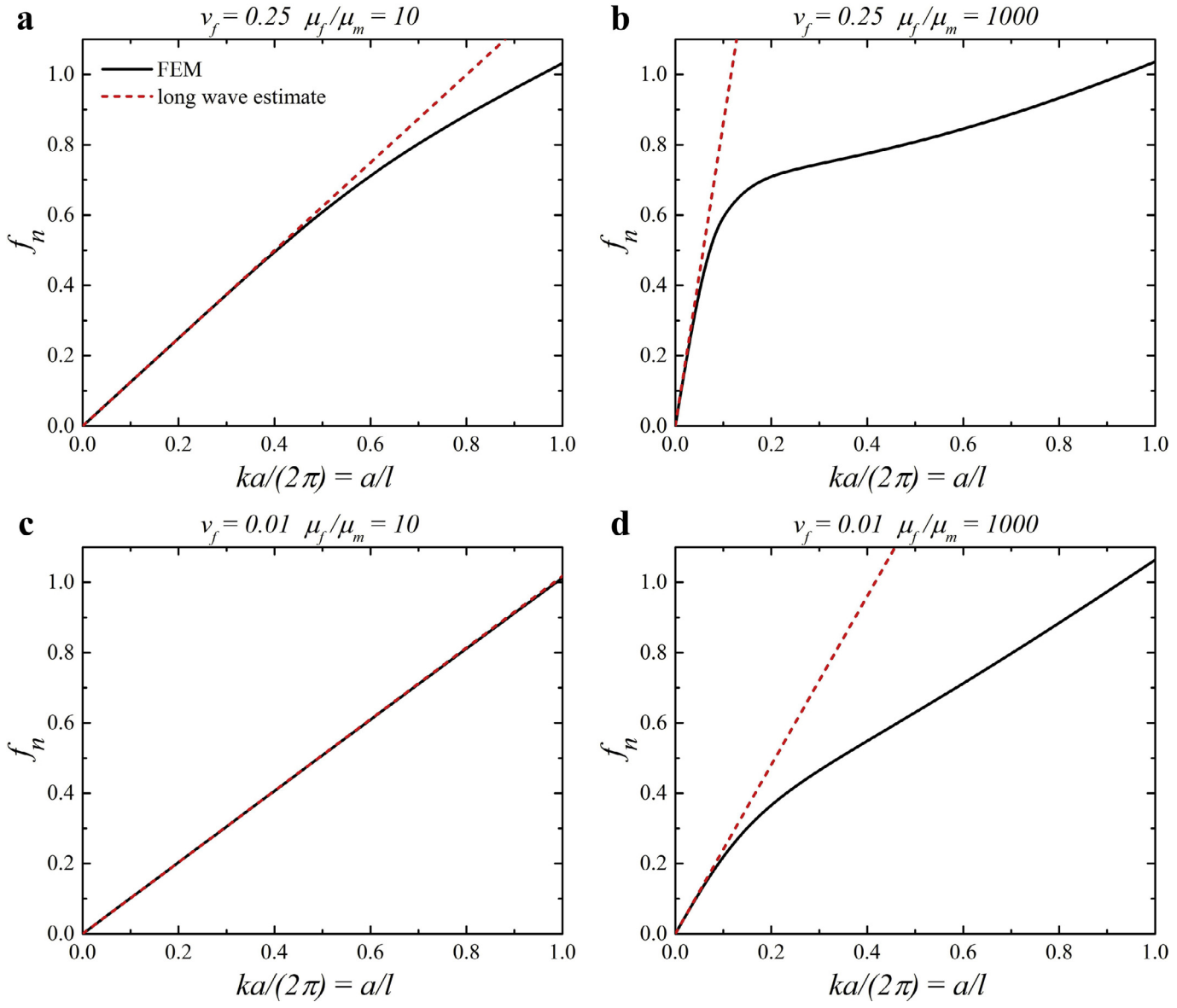

Fig. 7. Comparison of the long wave estimates (33) and the Bloch wave numerical analysis for the shear waves propagating in the direction of fibers. Periodic FCs with $v_f = 0.25$ and (a) $\mu_f/\mu_m = 10$, (b) $\mu_f/\mu_m = 1000$, and $v_f = 0.01$ and (c) $\mu_f/\mu_m = 10$, (d) $\mu_f/\mu_m = 1000$ are subjected to the uniaxial tension along the fiber direction, $\lambda = 1.25$. Frequency is normalized as $f_n = \frac{\omega a}{2\pi}\sqrt{\tilde{\rho}_0/\tilde{\mu}}$.

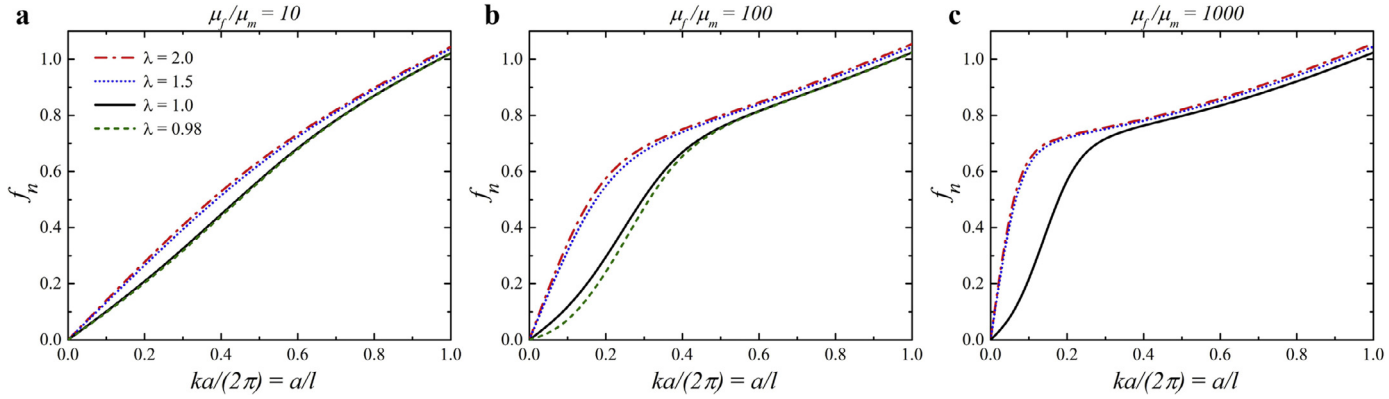

Fig. 8. Dispersion curves for the shear waves propagating in the direction of fibers in FCs with $v_f = 0.25$ and (a) $\mu_f/\mu_m = 10$, (b) $\mu_f/\mu_m = 100$, and (c) $\mu_f/\mu_m = 1000$. The FCs are subjected to the uniaxial tension of the magnitude $\lambda = 0.98$ (dashed green curves), $\lambda = 1$ (continuous black curves), $\lambda = 1.5$ (dotted blue curves), and $\lambda = 2$ (dash-dotted red curves). Frequency is normalized as $f_n = \frac{\omega a}{2\pi}\sqrt{\tilde{\rho}_0/\tilde{\mu}}$. (For interpretation of the references to colour in this figure legend, the reader is referred to the web version of this article.)

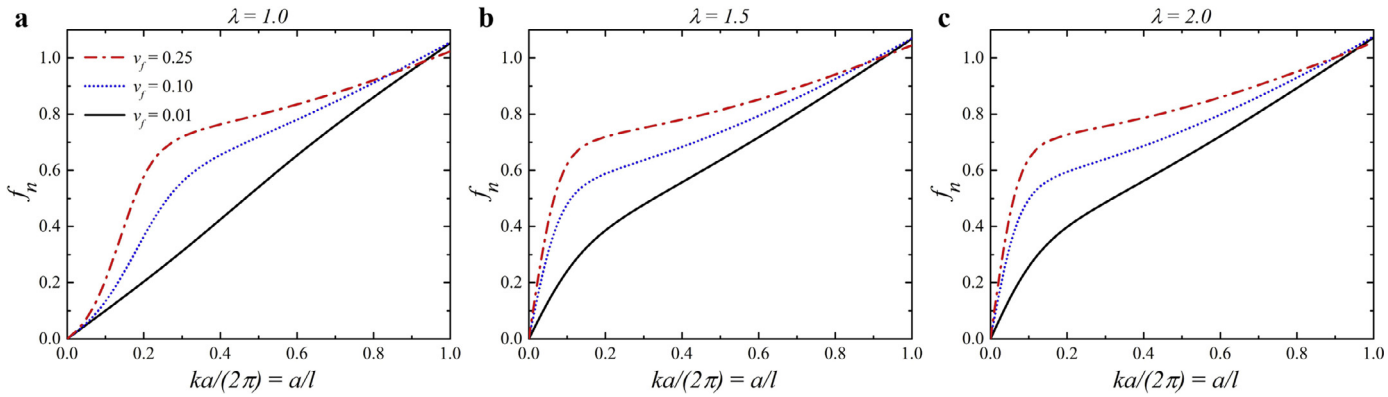

Fig. 9. Dispersion curves for shear waves propagating in the direction of fibers in FCs with $\mu_f/\mu_m = 1000$ in the undeformed state (a) and for the FCs subjected to the uniaxial tension of magnitude $\lambda = 1.5$ (b) and $\lambda = 2$ (c).

$f_n = 0.55$ as compared to the response of the undeformed FC with $v_f = 0.25$ and $\mu_f/\mu_m = 100$ (Fig. 8 (b)). Remarkably, the dispersion curves for the short waves (i.e. $l \lesssim 2a$) are barely affected by the uniaxial deformation (Fig. 8 (b) and (c)). Moreover, the dispersion curves change more slowly with deformation after a certain level of stretch is reached (compare dash-dotted red and dotted blue curves in Fig. 8). This happens because the phase velocities (28) of the long shear waves start to change slowly when a certain level of deformation is achieved.

To clarify the influence of the deformation on the dispersion phenomenon in FCs with various volume fractions of the fibers, we present dispersion curves for FCs with $\mu_f/\mu_m = 1000$ in the undeformed state (a) and for the FCs subjected to the uniaxial tension of magnitude $\lambda = 1.5$ (b) and $\lambda = 2$ (c) in Fig. 9. The continuous black, dotted blue, and dashed-dotted red curves correspond to $v_f = 0.01$, $v_f = 0.10$, and $v_f = 0.25$, respectively. We observe that the dispersion of shear waves in the fiber direction is more pronounced for the periodic FCs with large volume fractions of fibers (compare continuous black and dash-dotted red curves in Fig. 9 (a)). Moreover, a uniaxial extension of the periodic FCs along the fibers significantly affects dispersion curves (Fig. 9 (b) and (c)); however, an increase in the loading leads to a moderate change in the dispersion curve after a certain level of deformation (compare Fig. 9 (b) and (c)). For example, the frequency of the shear wave with $ka/(2\pi) = 0.1$ propagating in the FC with $v_f = 0.25$ and $\mu_f/\mu_m = 1000$ increases from $f_n = 0.21$ in the undeformed FC up to $f_n = 0.64$ in the FC subjected to the uniaxial tension of the magnitude $\lambda = 1.5$ while it increases only up to $f_n = 0.66$ in the FC subjected to the uniaxial tension of the magnitude $\lambda = 2$ (compare dash-dotted red curves in Fig. 9). This is due to the fact that the phase velocities (28) of long shear waves change more slowly after a certain level of deformation is reached.

Finally, we consider the influence of the fiber arrangement on the shear wave propagation in the direction of fibers. Fig. 10 shows an example of RVE for a FC with a rectangular periodic unit cell. Geometrically, the fibers are characterized by their diameters, namely $d = 2\sqrt{abv_f/\pi}$ (see Fig. 10). The periodic unit cell occupies a domain Ω in the undeformed configuration, namely

$$-a/2 \le x_1 \le a/2, \quad -h/2 \le x_2 \le h/2, \quad \text{and} \quad -b/2 \le x_3 \le b/2. \tag{46}$$

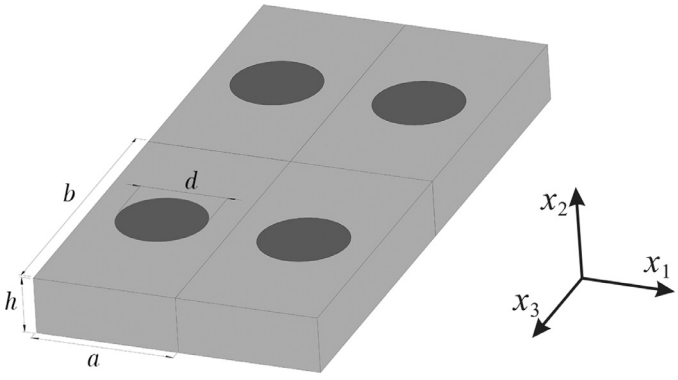

Fig. 10. RVE for a 3D periodic FC with a rectangular arrangement of fibers.

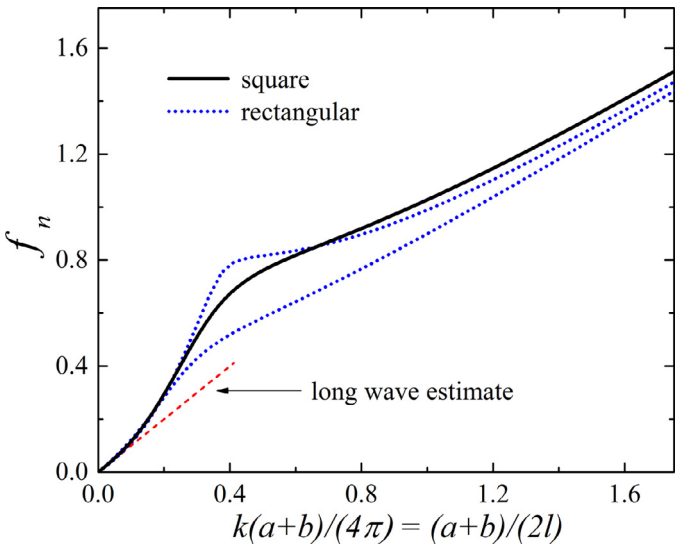

Fig. 11. Dispersion curves for shear waves propagating in the direction of fibers in FCs with $v_f = 0.25$ and $\mu_f/\mu_m = 100$ in the undeformed state with square and rectangular ($b = 2a$) arrangements of fibers.

Fig. 11 presents a comparison of the dispersion curves for shear waves propagating along the fibers in the FC with the square and rectangular ($b = 2a$) arrangements of the fibers. The dispersion curves of the shear waves vary in the FC with rectangular arrangement of fibers, because we have two distinct characteristic lengths, namely a and b, as opposite to the square arrangement. We compare FCs with the same volume fractions of fibers (i.e. $v_f = 0.25$); as a result, the dispersion curves of the long shear waves (i.e. $l \gtrsim 5(a+b)/2$) coincide for both square and rectangular periodic FCs. Consistently with the previous observations, a significant nonlinearity of dispersion curves is observed for the shear waves with wavelengths being comparable to the characteristic lengths of the

FC, namely $l \sim (a+b)$. The dispersion curves for shorter waves (i.e. $l \lesssim (a+b)/3$) are affected only slightly by the fiber arrangement.

5. Concluding remarks

We considered the shear wave propagation in the 3D fiber-reinforced composites undergoing finite deformations. First, we derived the explicit closed form expressions for the phase and group velocities of the shear waves propagating in the finitely deformed 3D FCs on the basis of a micromechanical approach accounting for the material properties and distribution of the phases. Hence, the derived explicit relations for the phase and group velocities were expressed in terms of the actual mechanical properties of composite constituents and their volume fractions. By utilizing these expressions, we constructed the slowness and energy curves revealing the strong influence of deformation on the propagation of shear waves. In particular, the shear wave velocities were shown to vary considerably with the deformation and direction of wave propagation. Moreover, the energy curve of the in-plane shear wave was shown to have deformation tunable intersections, meaning that the absolute values and directions of the group velocities coincide for the different directions of wave propagation. Thus, we are able to estimate characteristics of wave and energy propagation in the finitely deformed 3D fiber composites employing these explicit relations, which are applicable for any direction of wave propagation and for any macroscopically applied homogeneous pre-deformation. These important characteristics are expressed in terms of the actual microstructure parameters, such as volume fractions and phase material properties. This important feature distinguishes our results from those derived from phenomenological models, where the material parameters need to be fitted, and they are not directly related to the microstructure parameters and material properties of the constituents.

Second, we examined the shear wave propagation in the finitely deformed 3D periodic FCs by application of the Bloch wave approach in the finite element code. This allowed us to account for the interactions of the elastic waves with the material microstructure. As a result, we found the dispersion phenomenon manifesting in the strongly nonlinear dependence of the wave frequencies on wavenumber. The dispersion and the corresponding wavelengths of the shear waves in the 3D periodic FCs were found to be tunable by the change in the shear modulus contrast between the constituents and volume fraction of the fibers. Specifically, an increase in the shear modulus contrast and amount of fibers leads to a more pronounced dispersion of shear waves propagating in the direction of fibers, i.e. the dispersion curves exhibit a significant nonlinearity. Moreover, the dispersion of shear waves is highly sensitive to deformation. In particular, a moderate deformation significantly increases the frequency of the long waves. However, the influence of deformation for the short waves is relatively weak. We found that the influence of deformation on the dispersion of shear waves is more pronounced at the beginning of the loading due to the fact that the phase velocities (28) of the long shear waves change quickly up to a certain level of deformation and then the phase velocities vary slowly with a further loading. Next, we compared the results of the Bloch wave analysis and the long wave estimates. We found that the long wave estimates for the phase velocities (25) of shear waves accurately describe the dispersion relations for the finitely deformed FCs with low shear modulus contrast between the fibers and matrix (i.e. $\mu_f/\mu_m \lesssim 10$) and small volume fractions of the fibers (i.e. $v_f \lesssim 0.25$).

Finally, we analyzed the influence of the fiber arrangement on the propagation of shear waves along the fibers. In particular, by comparing dispersion curves of shear waves for FCs with square and rectangular arrangements of fibers, we observed that (i) long shear waves are independent of the fiber arrangement, (ii) shear waves with wavelengths being comparable to the characteristic lengths of the FC are significantly affected by the fiber arrangement, and (iii) short shear waves are affected only slightly by the fiber arrangement.

Acknowledgments

This work was supported by the Israel Science Foundation (grant №1550/15 and 1973/15). Stephan Rudykh gratefully acknowledges the support of Taub Foundation through the Horev Fellowship – Leaders in Science and Technology. Viacheslav Slesarenko thanks the support through the Technion Postdoctoral Fellowship.

References

Aberg, M., Gudmundson, P., 1997. The usage of standard finite element codes for computation of dispersion relations in materials with periodic microstructure. J. Acoust. Soc. Am. 102, 2007–2013.
Babaee, S., Shim, J., Weaver, J., Chen, E., Patel, N., Bertoldi, K., 2013. 3D soft metamaterials with negative poisson's ratio. Adv. Mater. 25 (36), 5044–5049.
Babaee, S., Viard, N., Wang, P., Fang, N.X., Bertoldi, K., 2016. Harnessing deformation to switch on and off the propagation of sound. Adv. Mater. 28 (8), 1631–1635.
Bafekrpour, E., Molotnikov, A., Weaver, J.C., Brechet, Y., Estrin, Y., 2014. Responsive materials: a novel design for enhanced machine-augmented composites. Sci. Rep. 4, 5801–5821.
Bertoldi, K., Boyce, M.C., 2008a. Mechanically triggered transformations of phononic band gaps in periodic elastomeric structures. Phys. Rev. B 77 (5), 052105.
Bertoldi, K., Boyce, M.C., 2008b. Wave propagation and instabilities in monolithic and periodically structured elastomeric materials undergoing large deformations. Phys. Rev. B 78, 184107.
Bertoldi, K., Boyce, M.C., Deschanel, S., Prange, S., Mullin, T., 2008. Mechanics of deformation-triggered pattern transformations and superelastic behavior in periodic elastomeric structures. J. Mech. Phys. Solids 56 (8), 2642–2668.
Biot, M.A., 1939. Non Linear Theory of Elasticity and the linearized case for a body under initial stress. Philos. Mag. XXVII, 468–489.
Biot, M.A., 1940. The influence of initial stress on elastic waves. J. Appl. Phys. 11 (8), 522.
Boulanger, P., Hayes, M., 1992. Finite-amplitude waves in deformed mooney-rivlin materials. Q. J. Mech. Appl. Math. 45 (4), 575–593.
Boulanger, P., Hayes, M., Trimarco, C., 1994. Finite-amplitude plane waves in deformed hadamard elastic materials. Geophys. J. Int. 118 (2), 447–458.
Celli, P., Gonella, S., 2015. Manipulating waves with LEGO® bricks: a versatile experimental platform for metamaterial architectures. Appl. Phys. Lett. 107, 081901.
Chen, Q., Elbanna, A., 2016. Modulating elastic band gap structure in layered soft composites using sacrificial interfaces. J. Appl. Mech. 83, 111009.
Currie, P., Hayes, M., 1969. Longitudinal and transverse waves in finite elastic strain. hadamard and green materials. IMA J. Appl. Math. 5 (2), 140–161.
deBotton, G., Hariton, I., Socolsky, E.A., 2006. Neo-Hookean fiber-reinforced composites in finite elasticity. J. Mech. Phys. Solids 54, 533–559.
Destrade, M., Ogden, R.W., 2013. On stress-dependent elastic moduli and wave speeds. J. Appl. Math. 78 (5), 965–997.
Dorfmann, A., Ogden, R.W., 2010. Electroelastic waves in a finitely deformed electroactive material. IMA J. Appl. Math. 75 (4), 603–636.
Fomenko, S.I., Golub, M.V., Zhang, C., Bui, T.Q., Wang, Y.-S., 2014. In-plane elastic wave propagation and band-gaps in layered functionally graded phononic crystals. Int. J. Solids Struct. 51, 2491–2503.
Galich, P.I., Fang, N.X., Boyce, M.C., Rudykh, S., 2017. Elastic wave propagation in finitely deformed layered materials. J. Mech. Phys. Solids 98, 390–410.
Galich, P.I., Rudykh, S., 2015a. Comment on "Disentangling longitudinal and shear elastic waves by neo-Hookean soft devices". Appl. Phys. Lett. 107, 056101. 106, 161903.
Galich, P.I., Rudykh, S., 2015b. Influence of stiffening on elastic wave propagation in extremely deformed soft matter: from nearly incompressible to auxetic materials. Extreme Mech. Lett. 4, 156–161.
Galich, P.I., Rudykh, S., 2016. Manipulating pressure and shear elastic waves in dielectric elastomers via external electric stimuli. Int. J. Solids Struct. 91, 18–25.
Ge, Q., Qi, H.J., Dunn, M.L., 2013. Active materials by four-dimension printing. Appl. Phys. Lett. 103 (13), 131901.
Gei, M., 2008. Elastic waves guided by a material interface. Eur. J. Mech. 27 (3), 328–345.
Golub, M.V., Fomenko, S.I., Bui, T.Q., Zhang, C., Wang, Y.-S., 2012. Transmission and band gaps of elastic SH waves in functionally graded periodic laminates. Int. J. Solids Struct. 49, 344–354.
Humphrey, J.D., 2002. Cardiovascular Solid Mechanics: Cells, Tissues, and Organs. Springer-Verlag, New York.
John, F., 1966. Plane elastic waves of finite amplitude. hadamard materials and harmonic materials. Commun. Pure Appl. Math. 19 (3), 309–341.
Kittel, C., 2004. Introduction to Solid State Physics. Wiley, Hoboken, N.J.
Kolle, M., Lethbridge, A., Kreysing, M., Baumberg, J., Aizenberg, J., Vukusic, P., 2013. Bio-inspired band-gap tunable elastic optical multilayer fibers. Adv. Mater. 25 (15), 2239–2245.

Kushwaha, M., Halevi, P., Dobrzynski, L., Djafari-Rouhani, B., 1993. Acoustic band structure of periodic elastic composites. Phys. Rev. Lett. 71 (13), 2022–2025.
Langenberg, K.J., Marklein, R., Mayer, K., 2010. Energy vs. group velocity for elastic waves in homogeneous anisotropic solid media. In: Proceedings of 2010 URSI International Symposium on Electromagnetic Theory, pp. 733–736.
Li, Y., Kaynia, N., Rudykh, S., Boyce, M.C., 2013. Wrinkling of interfacial layers in stratified composites. Adv. Eng. Mater. 15 (10), 921–926.
Lin, E., Li, Y., Ortiz, C., Boyce, M.C., 2014. 3D printed, bio-inspired prototypes and analytical models for structured suture interfaces with geometrically-tuned deformation and failure behavior. J. Mech. Phys. Solids 73, 166–182.
Musgrave, M.J.P., 1970. Crystal Acoustics: Introduction to the Study of Elastic Waves and Vibrations in Crystals. Holden-day, San Francisco.
Nayfeh, A.H., 1995. Wave Propagation in Layered Anisotropic Media: With Applications to Composites. Elsevier Science, Amsterdam.
Ogden, R., Singh, B., 2011. Propagation of waves in an incompressible transversely isotropic elastic solid with initial stress: biot revisited. J. Mech. Mater. Struct. 6 (1–4), 453–477.
Ogden, R.W., 1997. Non-linear Elastic Deformations. Dover Publications, New York.
Rogerson, G., Scott, N., 1994. Doubly constrained elastic wave propagation. Int. J. Solids Struct. 31 (20), 2769–2792.
Rudykh, S., Boyce, M., 2014a. Transforming small localized loading into large rotational motion in soft anisotropically-structured materials. Adv. Eng. Mater. 16 (11), 1311–1317.
Rudykh, S., Boyce, M., 2014b. Transforming wave propagation in layered media via instability-induced interfacial wrinkling. Phys. Rev. Lett. 112, 034301.
Rudykh, S., deBotton, G., 2012. Instabilities of hyperelastic fiber composites: micromechanical versus numerical analyses. J. Elasticity 106, 123–147.
Rudykh, S., Ortiz, C., Boyce, M., 2015. Flexibility and protection by design: imbricated hybrid microstructures of bio-inspired armor. Soft Matter 11, 2547–2554.
Saheb, D.N., Jog, J.P., 1999. Natural fiber polymer composites: a review. Adv. Polym. Technol. 18 (4), 351–363.
Scott, N., 1991. Small vibrations of prestrained constrained elastic materials: the idealized fibre-reinforced material. Int. J. Solids Struct. 27 (15), 1969–1980.
Scott, N., 1992. Waves in a homogeneously prestrained incompressible, almost inextensible, fibre-reinforced elastic material. Proc. R. Irish Acad. Sect. A 92A (1), 9–36.
Scott, N., Hayes, M., 1976. Small vibrations of a fibre-reinforced composite. Q. J. Mech. Appl. Math. 29 (4), 467–486.
Slesarenko, V., Rudykh, S., 2016. Harnessing viscoelasticity and instabilities for tuning wavy patterns in soft layered composites. Soft Matter 12, 3677–3682.
Slesarenko, V., Rudykh, S., 2017. Microscopic and macroscopic instabilities in hyperelastic fiber composites. J. Mech. Phys. Solids doi:10.1016/j.jmps.2016.11.002.
Srivastava, A., 2016. Metamaterial properties of periodic laminates. J. Mech. Phys. Solids 96, 252–263.
Truesdell, C., Noll, W., 1965. The Non-Linear Field Theories of Mechanics. Springer.
Wang, L., Bertoldi, K., 2012. Mechanically tunable phononic band gaps in three-dimensional periodic elastomeric structures. Int. J. Solids Struct. 49 (19–20), 2881–2885.

International Journal of Solids and Structures 135 (2018) 303–304

Contents lists available at ScienceDirect

International Journal of Solids and Structures

journal homepage: www.elsevier.com/locate/ijsolstr

Corrigendum to "Shear wave propagation in finitely deformed 3D fiber-reinforced composites" [Int. J. Solids Struct. 110–111 (2017) 294–304]

Pavel I. Galich, Viacheslav Slesarenko, Stephan Rudykh*

Department of Aerospace Engineering, Technion – Israel Institute of Technology, Haifa 32000, Israel

In our paper (Galich et al., 2017), Figs. 7–9 show frequencies as functions of wavenumber K^0 (in the undeformed configuration); thus, in Figs. 7–9, $K^0 = |\mathbf{K}^0|$ must replace $k = |\mathbf{k}|$ (in the deformed configuration). Recall that the corresponding wave vectors in the undeformed

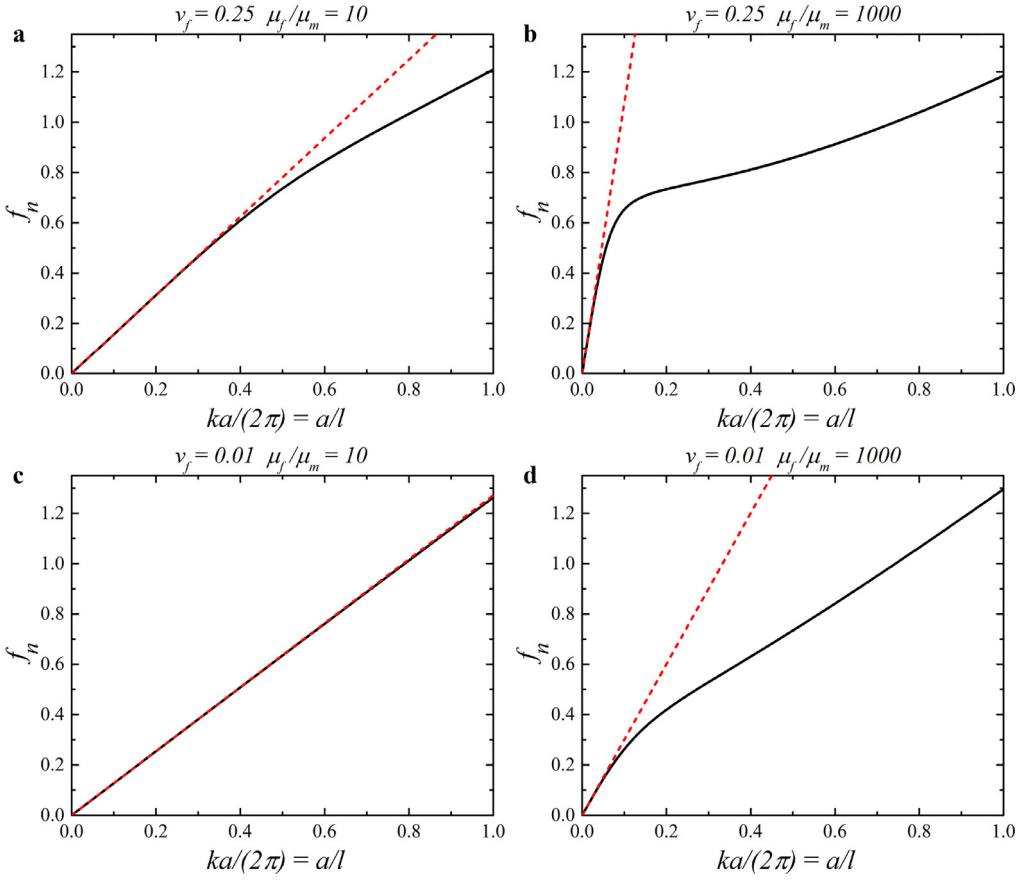

Fig. 1. Comparison of the long wave estimates (33) and the Bloch wave numerical analysis for the shear waves propagating in the direction of fibers. Periodic FCs with $v_f = 0.25$ and (a) $\mu_f/\mu_m = 10$, (b) $\mu_f/\mu_m = 1000$, and $v_f = 0.01$ and (c) $\mu_f/\mu_m = 10$, (d) $\mu_f/\mu_m = 1000$ are subjected to the uniaxial tension along the fiber direction, $\lambda = 1.25$. Frequency is normalized as $f_n = \frac{\omega a}{2\pi}\sqrt{\tilde{\rho}_0/\tilde{\mu}}$.

DOI of original article: 10.1016/j.ijsolstr.2016.12.007

* Corresponding author.
E-mail address: rudykh@technion.ac.il (S. Rudykh).

https://doi.org/10.1016/j.ijsolstr.2017.12.027
0020-7683

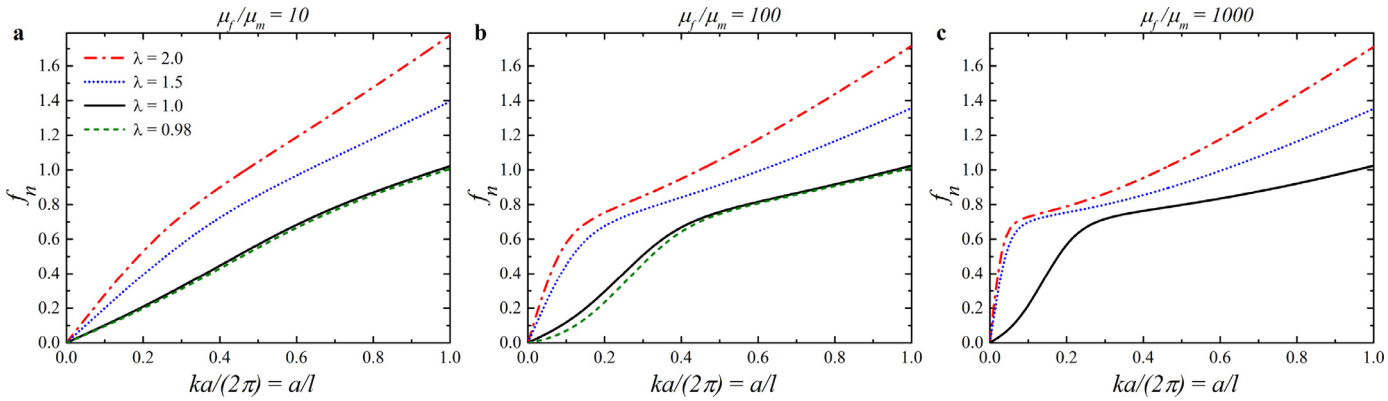

Fig. 2. Dispersion curves for the shear waves propagating in the direction of fibers in FCs with $v_f = 0.25$ and (a) $\mu_f/\mu_m = 10$, (b) $\mu_f/\mu_m = 100$, and (c) $\mu_f/\mu_m = 1000$. The FCs are subjected to the uniaxial tension of the magnitude $\lambda = 0.98$ (dashed green curves), $\lambda = 1$ (continuous black curves), $\lambda = 1.5$ (dotted blue curves), and $\lambda = 2$ (dash-dotted red curves). (For interpretation of the references to colour in this figure legend, the reader is referred to the web version of this article.)

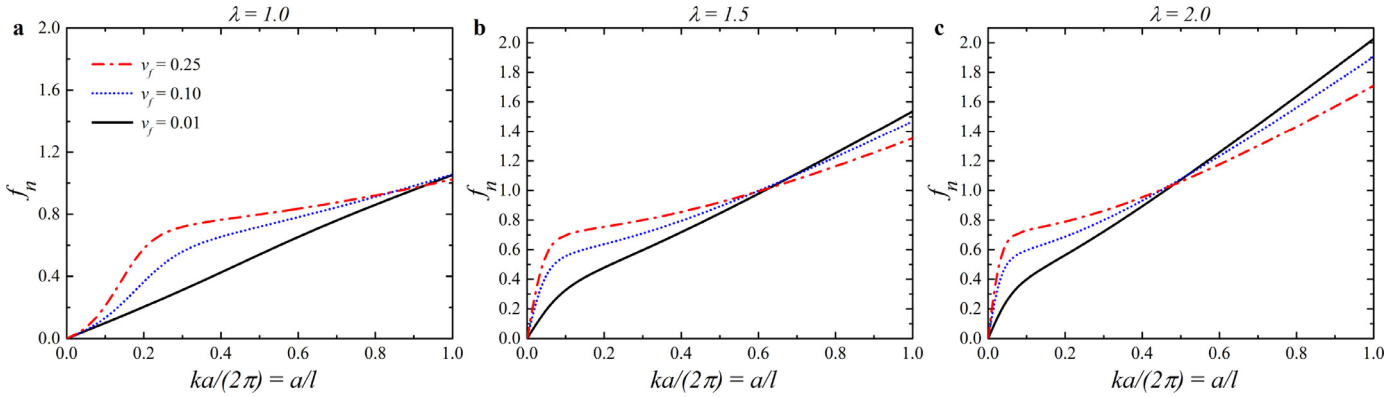

Fig. 3. Dispersion curves for shear waves propagating in the direction of fibers in FCs with $\mu_f/\mu_m = 1000$ in the undeformed state (a) and for the FCs subjected to the uniaxial tension of magnitude $\lambda = 1.5$ (b) and $\lambda = 2$ (c).

and deformed configurations are related via $\mathbf{K}^0 = \mathbf{F}^T \cdot \mathbf{k}$. Here, we present frequencies as functions of wavenumber k in the deformed configuration. Figs. 1–3 correspond to Figs. 7, 8 and 9, respectively, in the original paper (Galich et al., 2017). Thus, the conclusion in Galich et al. (2017) about the weak influence of the applied deformation on short shear waves (with wavelength $l \lesssim 2a$) needs to be corrected. As can be seen from Fig. 2, the applied uniaxial deformation influence shear waves in both long and short wave ranges. All other conclusions in Galich et al. (2017) agree with the dispersion curves presented in Figs. 1–3.

Reference

Galich, P.I., Slesarenko, V., Rudykh, S., 2017. Shear wave propagation in finitely deformed 3D fiber-reinforced composites. Int. J. Solids Struct. 110–111, 294–304.

Chapter 4

Conclusions and discussion

By employing rigorous analytical methods of non-linear mechanics (see Section 2.1), I derived long wave estimates for important characteristics of elastic waves – phase and group velocities – propagating in non-linear layered [19] and fibrous [25] composites. Next, by combining Bloch-Floquet approach (see Section 2.2) and non-linear constitutive models for each layer, I derived closed-form dispersion relations for P- and S-waves propagating perpendicularly to the layers in the non-linear periodic laminates and found that BGs (forbidden frequency ranges, where waves cannot propagate) can be initiated and shifted towards desirable low frequencies in non-linear elastic laminates by mechanical loading [19]. In parallel, I explored the influence of material stiffening on elastic wave propagation in the non-linear isotropic materials [21] and laminates [19] comprised of these materials. Then, I extended my analysis to the problem of wave propagation in non-linear electroelastic isotropic materials [22] and laminates [23] composed of these materials.

4.1 Influence of stiffening on elastic wave propagation in extremely deformed soft matter: from nearly incompressible to auxetic materials

In this paper, I derived closed-form expressions for phase velocities of elastic waves propagating in the finitely deformed materials with pronounced stiffening effects. I demonstrated that finite deformation can significantly influence elastic waves in nearly incompressible, highly compressible and auxetic (with negative Poisson's ratio) materials. Moreover, I studied influence of propagation direction on the phase velocities of elastic waves. I found that for nearly incompressible materials S-wave velocities exhibit strong dependence on the direction of propagation and pre-strain, whereas the P-wave velocity is barely affected until extreme levels of deformation are reached. For highly compressible materials, I showed that both P- and S-wave velocities significantly depend on applied deformation and propagation direction. Furthermore, the dependence becomes stronger when the stiffening effects become more pronounced. My findings can help to design or better understand mechanics of deformation-tunable elastic metamaterials comprised of materials with strong stiffening effects.

4.2 Manipulating pressure and shear waves in dielectric elastomers via external electric stimuli

In this manuscript, I considered P- and S- elastic waves propagating in finitely deformed DEs in the presence of an electric field. To allow consideration of P-waves, I utilized the ideal and enriched material models accounting for the volumetric changes. I derived closed-form expressions for the phase velocities of elastic waves propagating in DEs subjected to an electric field. I found that, for the ideal DE model, the elastic wave propagation is explicitly independent of an applied electric field, while it can be influenced through the deformation induced via an electric field. However, characteristics of elastic waves explicitly depend on the applied electric field in case of the proposed enriched material model. Specifically, the phase velocity of the in-plane S-wave decreases upon application of an electric field. Then, I applied my findings to explore the phenomenon of disentangling (decoupling) P- and S-waves in DEs by an electric field (see Fig. 1 in [22]). I showed that the divergence angle between P- and S-waves strongly depends on the value of the applied electric field and propagation direction. Moreover, I found that an increase in the material compressibility weakens the decoupling of P- and S-waves (see Fig. 4 in [22]). This is because the P-wave refracts in the same direction as the S-wave from the initial propagation direction, while for nearly incompressible materials the change in the P-wave direction is negligible. The phenomenon can be used to manipulate elastic waves by a bias electrostatic field, which can be beneficial for small length-scale devices, such as micro-electromechanical systems, where an electric field is the preferred control parameter.

4.3 Elastic wave propagation in finitely deformed layered materials

In this work, I studied elastic wave propagation in finitely deformed bi-laminates. Firstly, based on an exact analytical solution for finitely deformed laminates with alternating neo-Hookean phases, I derived closed-form expressions for the phase and group velocities of S-waves propagating in any direction in these laminates. Secondly, I obtained long wave estimates and for the phase velocities of P- and S-waves propagating perpendicularly to the layers in the finitely deformed compressible bi-laminates with neo-Hookean and Gent layers. These estimates provide the important information on elastic wave propagation with wavelengths sufficiently larger than period of the laminate, namely $l \gtrsim 3d$. Thirdly, I performed a detailed analysis of the BG structures for the waves propagating perpendicularly to the layers in the incompressible and compressible laminates. Specifically, I identified the key parameters and mechanisms influencing the S-wave, P-wave, and complete BGs and then revealed the advantageous compositions of the laminates having the wide BGs in the low-frequency range.

Finally, I rigorously showed that SBGs in laminates comprised of layers exhibiting weak stiffening effects (neo-Hookean) are independent of the applied deformation because deformation induced changes in geometry and effective material properties fully compensate each other. However, contraction or extension of the laminate made of layers with strong stiffening effects (e.g., Gent) widens and shifts SBGs towards higher frequencies due to the stronger effect of deformation induced changes in the material properties (as compared to the geometry changes). Fur-

thermore, I found that laminates with thin highly compressible layers embedded in a nearly incompressible matrix possess wide complete BGs, and the dominant mechanism influencing PBGs is the deformation induced change in the thicknesses of the layers.

4.4 Shear wave propagation and band gaps in finitely deformed dielectric elastomer laminates: long wave estimates and exact solution

In this article, I investigated S-wave propagation in electroelastic bi-laminates subjected to finite deformations and electric fields. I obtained the long wave estimates – the exact solution for the waves with wavelength sufficiently larger than period of the laminate – for phase and group velocities of S-waves propagating in the bi-laminates with electroelastic ideal (neo-Hookean) layers. The derived closed-form formulas are expressed in terms of the volume fractions and electroelastic constants of the layers. Moreover, these long wave estimates can be used for any direction of wave propagation, for any applied electric field, and for any homogeneous finite pre-deformations. Remarkably, the S-wave propagation perpendicular to the layers depends on electric field only though the induced deformation.

Next, I derived the dispersion relations for the S-waves propagating perpendicular to the layers in the laminates with incompressible hyperelastic ideal dielectric layers and general elastic part (that is function of the first strain invariant only, e.g., neo-Hookean, Gent, Arruda-Boyce, Yeoh, to name a few). Consistently with

the exact solution for long waves, the derived dispersion relation is independent of electric field, and it coincides with its analogue for the purely elastic laminates. This dispersion relation shows that SBGs in the electroelastic laminates are tunable by an electric field only through induced deformation. In particular, the application of an electric field to the DE laminates with electroelastic Gent phases widens and shifts SBGs towards higher frequencies. However, SBGs are independent of deformation (either it is induced by electrical or mechanical stimuli) in DE laminates with electroelastic neo-Hookean layers.

4.5 Shear wave propagation in finitely deformed 3D fiber-reinforced composites

In this paper, I considered the S-wave propagation in the finitely deformed 3D FCs. Based on a micromechanical approach accounting for the constituent properties and their distribution in the composite, I derived the closed-form expressions for the phase and group velocities of the S-waves propagating in the finitely deformed 3D FCs. Hence, the expressions for the phase and group velocities are presented in terms of the actual mechanical properties of composite constituents and their volume fractions. Next, I constructed the slowness and energy curves revealing the significant influence of deformation on the propagation of S-waves. In particular, the S-wave velocities were shown to vary considerably with the deformation and propagation direction. Moreover, the energy curve of the in-plane S-wave was shown to have deformation tunable intersections, meaning that the absolute values

and directions of the group velocities coincide for the different directions of wave propagation. Thus, characteristics of wave and energy propagation in the finitely deformed 3D FCs can be estimated via employing the derived relations, which are applicable for any direction of wave propagation and for any macroscopically applied homogeneous pre-deformation.

Finally, I examined the S-wave propagation in the finitely deformed 3D periodic FCs by application of the Bloch-Floquet approach in the finite element code (see Section 2.2). This allowed me to account for the interactions of the S-waves with the composite microstructure, i.e. to calculate dispersion relations for S-waves propagating along fibers. The dispersion and the corresponding wavelengths of the S-waves in the 3D periodic FCs were found to be tunable by the change in the shear modulus contrast between the fibers and matrix and volume fraction of the fibers. Specifically, an increase in the shear modulus contrast and amount of fibers leads to a more pronounced dispersion of S-waves propagating in the direction of fibers, i.e. the dispersion curves exhibit a significant nonlinearity (highly sensitive to pre-deformation). Additionally, I analyzed the influence of the fiber periodicity on the propagation of S-waves along the fibers. In particular, by comparing dispersion curves of S-waves for FCs with square and rectangular arrays of fibers, I observed that long S-waves are independent of the fiber distribution, while S-waves with wavelengths being comparable to the characteristic lengths of the FC are significantly affected by the spacial distribution of fibers.

Bibliography

[1] M. Aberg and P. Gudmundson. The usage of standard finite element codes for computation of dispersion relations in materials with periodic microstructure. *J. Acoust. Soc. Am.*, 102:2007–2013, 1997.

[2] M. Agoras, O. Lopez-Pamies, and P. Ponte Castañeda. Onset of macroscopic instabilities in fiber-reinforced elastomers at finite strain. *J. Mech. Phys. Solids*, 57:1828–1850, 2009.

[3] K. Bertoldi and M. C. Boyce. Wave propagation and instabilities in monolithic and periodically structured elastomeric materials undergoing large deformations. *Phys. Rev. B*, 78:184107, 2008.

[4] K. Bertoldi and M. Gei. Instabilities in multilayered soft dielectrics. *J. Mech. Phys. Solids*, 59:18–42, 2011.

[5] M. A. Biot. The Influence of Initial Stress on Elastic Waves. *J. Appl. Phys.*, 11(8):522, 1940.

[6] P. Boulanger and M. Hayes. Finite-amplitude waves in deformed mooney-rivlin materials. *Q. J. Mech. Appl. Math.*, 45(4):575–593, 1992.

[7] P. Boulanger, M. Hayes, and C. Trimarco. Finite-amplitude plane waves in deformed hadamard elastic materials. *Geophys. J. Int.*, 118(2):447–458, 1994.

[8] B. Cantor, H. Assender, and P. Grant. *Lightweight materials*, chapter 9-16, pages 89–226. Taylor & Francis Group, Boca Raton, FL, 2001.

[9] Z. Chang, H.-Y. Guo, B. Li, and X.-Q. Feng. Disentangling longitudinal and shear elastic waves by neo-Hookean soft devices. *Appl. Phys. Lett.*, 106(16):161903, 2015.

[10] N. Cohen, K. Dayal, and G. deBotton. Electroelasticity of polymer networks. *J. Mech. Phys. Solids*, 92:105–126, 2016.

[11] G. deBotton, I. Hariton, and E. A. Socolsky. Neo-Hookean fiber-reinforced composites in finite elasticity. *J. Mech. Phys. Solids*, 54:533–559, 2006.

[12] G. deBotton, L. Tevet-Deree, and E. A. Socolsky. Electroactive heterogeneous polymers: analysis and applications to laminated composites. *Mech. Adv. Mater. Struct.*, 14:13–22, 2007.

[13] A. Demcenko, M. Mazilu, R. Wilson, A. W. F. Volker, and J. M. Cooper. Hyperelastic Tuning of One-Dimensional Phononic Band Gaps Using Directional Stress. *IEEE Transactions on Ultrasonics, Ferroelectrics, and Frequency Control*, 65(6):1056–1061, 2018.

[14] A. Demčenko, R. Wilson, J. M. Cooper, M. Mazilu, and A. W. F. Volker. Ultrasonic waves in uniaxially stressed multilayered and one-dimensional

phononic structures: Guided and Floquet wave analysis. *J. Acoust. Soc. Am.*, 144(1):81–91, 2018.

[15] M. Destrade and R. W. Ogden. On stress-dependent elastic moduli and wave speeds. *J. Appl. Math.*, 78(5):965–997, 2013.

[16] A. Dorfmann and R. W. Ogden. Nonlinear electroelasticity. *Acta. Mech.*, 174:167–183, 2005.

[17] A. Dorfmann and R. W. Ogden. Electroelastic waves in a finitely deformed electroactive material. *IMA J. Appl. Math.*, 75(4):604–636, 2010.

[18] L. Dorfmann and R. W. Ogden. *Nonlinear Theory of Electroelastic and Magnetoelastic Interactions*, volume 9781461495. Springer US, Boston, MA, 2014.

[19] P. I. Galich, N. X. Fang, M. C. Boyce, and S. Rudykh. Elastic wave propagation in finitely deformed layered materials. *J. Mech. Phys. Solids*, 98:390–410, 2017.

[20] P. I. Galich and S. Rudykh. Comment on "Disentangling longitudinal and shear elastic waves by neo-Hookean soft devices" [Appl. Phys. Lett. 106, 161903 (2015)]. *Appl. Phys. Lett.*, 107:056101, 2015.

[21] P. I. Galich and S. Rudykh. Influence of stiffening on elastic wave propagation in extremely deformed soft matter: from nearly incompressible to auxetic materials. *Extreme Mech. Lett.*, 4:156–161, 2015.

[22] P. I. Galich and S. Rudykh. Manipulating pressure and shear elastic waves in dielectric elastomers via external electric stimuli. *Int. J. Solids Struct.*, 91:18–25, 2016.

[23] P. I. Galich and S. Rudykh. Shear Wave Propagation and Band Gaps in Finitely Deformed Dielectric Elastomer Laminates: Long Wave Estimates and Exact Solution. *J. Appl. Mech.*, 84(9):091002, 2017.

[24] P. I. Galich, V. Slesarenko, J. Li, and S. Rudykh. Elastic instabilities and shear waves in hyperelastic composites with various periodic fiber arrangements. *International Journal of Engineering Science*, 130:51–61, 2018.

[25] P. I. Galich, V. Slesarenko, and S. Rudykh. Shear wave propagation in finitely deformed 3D fiber-reinforced composites. *Int. J. Solids Struct.*, 110-111:294–304, 2017.

[26] M. Gei, S. Roccabianca, and M. Bacca. Controlling bandgap in electroactive polymer-based structures. *Mechatronics, IEEE/ASME Transactions*, 16(1):102–107, 2011.

[27] A. Goshkoderia and S. Rudykh. Electromechanical macroscopic instabilities in soft dielectric elastomer composites with periodic microstructures. *Eur. J. Mech. - A/Solids*, 65:243–256, 2017.

[28] M. Jandron and D. L. Henann. A numerical simulation capability for electroelastic wave propagation in dielectric elastomer composites: Application to tunable soft phononic crystals. *International Journal of Solids and Structures*, In press, 2018.

[29] D. T. Kuhnel, J. M. Rossiter, and C. F. J. Faul. 3D printing with light: towards additive manufacturing of soft, electroactive structures. In Y. Bar-Cohen, ed-

itor, *Electroactive Polymer Actuators and Devices (EAPAD) XX*, volume 10594, page 34. SPIE, mar 2018.

[30] M. Kushwaha, P. Halevi, L. Dobrzynski, and B. Djafari-Rouhani. Acoustic band structure of periodic elastic composites. *Phys. Rev. Lett.*, 71(13):2022–2025, 1993.

[31] J. Li, V. Slesarenko, P. I. Galich, and S. Rudykh. Instabilities and pattern formations in 3D-printed deformable fiber composites. *Composites Part B: Engineering*, 148:114–122, 2018.

[32] J. Li, V. Slesarenko, P. I. Galich, and S. Rudykh. Oblique shear wave propagation in finitely deformed layered composites. *Mech. Res. Commun.*, 2018.

[33] J. Li, V. Slesarenko, and S. Rudykh. Microscopic instabilities and elastic wave propagation in finitely deformed laminates with compressible hyperelastic phases. *Eur. J. Mech. - A/Solids*, 73:126–136, 2019.

[34] O. Lopez-Pamies and P. Ponte Castañeda. On the overall behavior, microstructure evolution, and macroscopic stability in reinforced rubbers at large deformations: I—theory. *J. Mech. Phys. Solids*, 54:807–830, 2006.

[35] O. Lopez-Pamies and P. Ponte Castañeda. On the overall behavior, microstructure evolution, and macroscopic stability in reinforced rubbers at large deformations: II—application to cylindrical fibers. *J. Mech. Phys. Solids*, 54:831–863, 2006.

[36] R. M. McMeeking and C. M. Landis. Electrostatic forces and stored energy for deformable dielectric materials. *J. Appl. Mech., Trans. ASME*, 72:581–590, 2005.

[37] R. Ogden and B. Singh. Propagation of waves in an incompressible transversely isotropic elastic solid with initial stress: Biot revisited. *J. Mech. Mater. Struct.*, 6(1-4):453–477, 2011.

[38] G. Rogerson and N. Scott. Doubly constrained elastic wave propagation. *Int. J. Solids Struct.*, 31(20):2769–2792, 1994.

[39] J. Rossiter, P. Walters, and B. Stoimenov. Printing 3D dielectric elastomer actuators for soft robotics. volume 7287, page 72870H. International Society for Optics and Photonics, 2009.

[40] S. Rudykh and G. deBotton. Stability of anisotropic electroactive polymers with application to layered media. *Z. Angew. Math. Phys.*, 62:1131–1142, 2011.

[41] S. Rudykh and G. deBotton. Instabilities of hyperelastic fiber composites: micromechanical versus numerical analyses. *J. Elasticity*, 106:123–147, 2012.

[42] S. Rudykh, A. Lewinstein, G. Uner, and G. deBotton. Analysis of microstructural induced enhancement of electromechanical coupling in soft dielectrics. *Appl. Phys. Lett.*, 102:151905, 2013.

[43] S. Rytov. Acoustical properties of a thinly laminated medium. *Sov. Phys. Acoust*, 2:68–80, 1956.

[44] N. Scott. Small vibrations of prestrained constrained elastic materials: The idealized fibre-reinforced material. *Int. J. Solids Struct.*, 27(15):1969–1980, 1991.

[45] N. Scott. Waves in a homogeneously prestrained incompressible, almost inextensible, fibre-reinforced elastic material. *Proc. R. Irish Acad. Sect. A*, 92A(1):9–36, 1992.

[46] N. Scott and M. Hayes. Small vibrations of a fibre-reinforced composite. *Q. J. Mech. Appl. Math.*, 29(4):467–486, 1976.

[47] G. Shmuel and R. Band. Universality of the frequency spectrum of laminates. *J. Mech. Phys. Solids*, 92:127–136, 2016.

[48] G. Shmuel and G. deBotton. Band-gaps in electrostatically controlled dielectric laminates subjected to incremental shear motions. *J. Mech. Phys. Solids*, 60(11):1970–1981, 2012.

[49] G. Shmuel and G. deBotton. Corrigendum to "Band-gaps in electrostatically controlled dielectric laminates subjected to incremental shear motions" [J. Mech. Phys. Solids 60 (2012) 19701981]. *J. Mech. Phys. Solids*, 105:21–24, 2017.

[50] V. Slesarenko, P. I. Galich, J. Li, N. X. Fang, and S. Rudykh. Foreshadowing elastic instabilities by negative group velocity in soft composites. *Appl. Phys. Lett.*, 113(3):031901, 2018.

[51] V. Slesarenko and S. Rudykh. Microscopic and macroscopic instabilities in hyperelastic fiber composites. *J. Mech. Phys. Solids*, 99:471–482, 2017.

[52] S. A. Spinelli and O. Lopez-Pamies. Some simple explicit results for the elastic dielectric properties and stability of layered composites. *Int. J. Eng. Sci.*, 88:15–28, 2015.

[53] A. Srivastava. Metamaterial properties of periodic laminates. *J. Mech. Phys. Solids*, 96:252–263, 2016.

[54] Z. Suo, X. Zhao, and W. H. Greene. A nonlinear field theory of deformable dielectrics. *J. Mech. Phys. Solids*, 56(2):467–486, 2008.

[55] L. Tian, L. Tevet-Deree, G. deBotton, and K. Bhattacharya. Dielectric elastomer composites. *J. Mech. Phys. Solids*, 60:181–198, 2012.

[56] R. A. Toupin. The elastic dielectric. *Arch. Rational. Mech. Anal.*, 5(6):849–915, 1956.

[57] C. Truesdell and W. Noll. *The non-linear field theories of mechanics*. Springer, 1965.

[58] K. Volokh. *Mechanics of Soft Materials*. Springer Singapore, Singapore, 2016.

[59] J. Willis. Negative refraction in a laminate. *J. Mech. Phys. Solids*, 97:10–18, 2016.

[60] B. Wu, Y. Su, W. Chen, and C. Zhang. On guided circumferential waves in soft electroactive tubes under radially inhomogeneous biasing fields. *J. Mech. Phys. Solids*, 99:116–145, 2017.

[61] W.-P. Yang and L.-W. Chen. The tunable acoustic band gaps of two-dimensional phononic crystals with a dielectric elastomer cylindrical actuator. *Smart Mater. Struct.*, 17(1):015011, 2008.

מניפולציית התקדמות
גל אלסטי בחומרים גמישים
לא ליניאריים באמצעות גירויים חיצוניים

חיבור על מחקר

לשם מילוי חלקי של הדרישות לקבלת התואר
דוקטור לפילוסופיה

פבל גליץ'

הוגש לסנט הטכניון — מכון טכנולוגי לישראל
אלול תשע"ח חיפה אוגוסט 2018

מניפולציית התקדמות
גל אלסטי בחומרים גמישים
לא ליניאריים באמצעות גירויים חיצוניים

פבל גליץ'